

THE FORMATION OF PLASMA BEAMS CONTAINING IONIC SPECIES

Stanley Singer, N. G. Kim, A. W. Merkl, L. B. Marantz
and C. Bodai

Research and Development Laboratories · RPI

Pasadena, California

The preparation of a plasma from substances stable under ordinary conditions can provide a steady state mixture of many reactive species. Neutral and ionic fragments are formed from the original reagent as a result of the high temperature and electron impact processes. The plasma involves a complex mixture of free radicals and ions in different levels of excitation. The formation of different species at different excitation levels in the plasma presents the possibility of different chemical reactions and products from a single reagent (c.f., for example, ref. 1). A study was made to devise a preparation of relatively pure reagents such as might be found in a plasma. A method in which the identity and excitation level of the reagent could be well known was desired. Ionic species have proven to be effective reagents, particularly in liquid phase organic reactions.

Many ionic species are readily formed by electron impact. The magnetron ion source is particularly suited for the formation of ions in large quantities with low energy electrons.^{2,3} Specific methods have been required for large currents of particular ionic species. For example, a beam of protons has been prepared from hydrogen-saturated titanium by using an electrical discharge along the surface of the metal.⁴ Ions have been made from the alkali metals by thermionic emission from a hot surface with a suitable work function such as tungsten.⁵ The preparation of polyatomic ions has been carried out in ion sources similar to those used in mass spectrometers by electron impact. Electron energies most effective for ionization are used, usually from 70-100 electron volts. Such energies are much greater than the threshold required for ionization of most organic molecules and fragmentation results, providing a mixture of many different ions. The magnetron ion source provides a large current of ionizing electrons at low energies, and the resultant controlled ionization permits formation of plasmas containing selected ionic species.

1. K. R. Kopecky, G. S. Hammond, and P. A. Leermakers, *J. Am. Chem. Soc.* **83**, 2397 (1961).
2. B.G. Perovic, "Proceedings of the Third International Congress on Ionization Phenomena in Gases (Venice, June 1957)," Italian Society of Physics, Milan, October 1957, p. 813.
3. H.R. Kaufman, "An Ion Rocket with an Electron-Bombardment Ion Source, National Aeronautics and Space Administration, Technical Note D-585, Washington D.C., January, 1961.
4. K. W. Ehlers et al., *Rev. Sci. Instr.* **29**, 614 (1958).
5. M. von Ardenne, "Tabellen der Elektronenphysik, Ionenphysik, und Ultramikroskopie," Deutscher Verlag der Wissenschaften, Berlin, 1956, Vol. I, p. 498.

EXPERIMENTAL

A dual-anode magnetron has been used for preparation of the ionic plasmas by electron impact. The usual magnetron configuration was modified, as shown in Fig. 1, by the addition of a central anode. A heated tungsten filament, used as the electron source, is placed between the two anodes also in a cylindrical surface. Electrons falling from this filament to the two anodes are provided with carefully controlled energies by placing the anodes at potentials only slightly above the appearance potential of the ion of interest. A magnetic field of approximately 500 gauss is applied along the axis of the source.

The outer cylinder of this source, which provides a plasma consisting largely of single ionic species and electrons, is a copper tube 7.5 cm. in diameter and 10 cm. in length as shown in Fig. 1. An orifice 1.9 cm. in diameter in the cylinder allows the extraction and study of the ions. The gas to be subjected to electron impact is passed into the magnetron through a 3 mm. tube on the opposite side from this orifice. Copper cooling coils through which water circulates are wrapped around the outside of the cylinder. The central anode is a 1 cm. steel rod. The heated cathode is a tungsten filament 66 cm. in length and 0.76 mm. (0.030 inches) in diameter, and is drawn through insulated supports from one end to the other of the cylinder in alternating strands so as to be midway between the concentric anodes. The tungsten cathode was heated with approximately 30 amperes of 60 volt a.c. current.

In forming the desired plasma the ionizing gas is passed into the source at pressures of 5×10^{-4} to 1×10^{-3} Torr. If the electron energy required to ionize the gas is known, the anodes are placed a few volts above the necessary ionization potential, and the filament temperature is gradually increased until a collector placed a short distance outside the orifice indicates extraction of a strong current. Currents obtained with different anode potentials have been studied. If the ionization energy involved is unknown, the above procedure may be followed to determine effective conditions for generation of the desired plasma. Filament current, gas pressure, and anode potentials all affect ionization of a specific gas strongly, and these parameters interact strongly during operation of the magnetron. The ions formed were identified in this work by mass spectrometric analysis with a radio frequency quadrupole mass spectrometer.⁶ The ionization of three gases was studied in this way, nitrogen dioxide (Matheson, 99.5%), tetrafluorohydrazine (Air Products and Chemical Co., Research Grade, 99+%), and oxygen difluoride (General Chemical Div. of Allied Chemical Co.).

Extraction of the positive ion current when nitrogen dioxide was ionized in the magnetron with anode potentials of 12.5 volts showed that more than 99% of the ions formed were NO_2^+ . Less than 1% of the ions in the extracted current were NO^+ . With increasing anode potentials the amount of NO^+ increased. At 15 volts the beam contained approximately 5% of NO^+ ; and at 30 volts it contained 27% of NO^+ . With tetrafluorohydrazine ionization at anode potentials of 12 volts gave a plasma containing largely NF_2^+ , indicated by mass spectrometric analysis of the extracted ion beam in which 93% of the ions were NF_2^+ . The remaining species were NF^+ , and possibly a small quantity of NO^+ from impurities in the initial material. With increase in anode potentials the quantity of NF^+ in the extracted

6. W. Paul, H. P. Reinhard, and U. Von Zahn, *Z. Phys.* **152**, 143 (1958).

current increased, similar to the effect observed with nitrogen dioxide. Ionization of oxygen difluoride was studied at anode potentials of 13 volts. The only positive ion detected was OF^+ which made up 76% of the ionic current extracted. Fluoride ion was also found; the negative ion was ca. 24% of the total extracted beam.

DISCUSSION

Magnetron Characteristics. - The concentric anode configuration of the magnetron used in these studies results in a markedly different electric field from that in the standard magnetrons. The strong axial magnetic field aids in efficient use of electrons for ionization, necessary in view of the low electric fields present. Ion currents on the order of 1 milliampere can be extracted from the magnetron by potentials of 1 to 10 volts, and if desired the flow of gas into the magnetron can be adjusted so that the extracted current corresponds to almost complete ionization of the entering gas. The anode potentials correspond to the maximum energy available from the ionizing electrons. With energies very close to the appearance potential of the desired ion the cross section for ionization is very low. This obstacle in forming a high concentration of ions is overcome in part by using a large electron current. Under typical operating conditions electron flow of 1 1/2 to 5 amperes to the anodes has been observed. Use of an oscilloscope to observe the currents flowing in the magnetron has shown that large 60-cycle electron pulses flow to the anodes. At typical pressures (0.5 - 1.5 microns) the pulse duration is 1-10 milliseconds; the pulse length increases with increasing pressure. These pulses briefly lower the anode potentials approximately 1/2 volt.

Formation of NO_2^+ Plasma. - Previous studies of the ionization of nitrogen dioxide by electron impact, aside from determinations of the ionization potential, showed that NO^+ was the predominant ion formed when electron energies of 40-70 volts were employed.^{7,8} Although the possibility of forming a plasma containing almost 90% of NO^+ was shown,⁷ NO_2^+ varied from less than 10% to perhaps 20% of the total ionic species, as estimated from the mass spectrometric peak intensities. Monatomic and diatomic positive ions of both nitrogen and oxygen were also present. Eight different ionization potentials varying from 9.78 electron volts up to 18.87 electron volts have been reported for nitrogen dioxide.⁹⁻¹⁵ The higher ionization potentials reported have been attributed to formation of the ion in excited electronic states.

The use of lower energy electrons for ionization in this work evidently prevented formation of significant quantities of NO^+ . Reduction of magnetron anode potentials

-
7. E. G. C. Stueckelberg, and H. D. Smyth, *Phys. Rev.* **36**, 478 (1930).
 8. R. A. Friedel, A. G. Sharkey, Jr., J. L. Schultz and C. R. Howard, *Anal. Chem.* **25**, 1314 (1953).
 9. T. Nakayama, M. Y. Kitamura, and K. Watanabe, *J. Chem. Phys.* **30**, 1180 (1959).
 10. D. C. Frost, D. Mak, and C. A. McDowell, *Can. J. Chem.* **40**, 1064 (1962).
 11. R. J. Kandel, *J. Chem. Phys.* **23**, 84 (1955).
 12. K. Watanabe, *J. Chem. Phys.* **26**, 542 (1957).
 13. W. C. Price and D. M. Simpson, *Trans. Faraday Soc.* **37**, 106 (1941).
 14. J. Collin and F. P. Lossing, *J. Chem. Phys.* **28**, 900 (1958).
 15. Y. Tanaka and A. S. Jursa, *J. Chem. Phys.* **36**, 2493 (1962).

from 12.5 to 11.0 volts gave no further decrease in NO^+ concentration noted in ions extracted. The presence of some 6 reported ionization potentials lying between 9.78 and 12.3 electron volts, however, indicates that several electronic states may be present.

In previous investigations the formation of fragment ions was attributed, at least in part, to thermal dissociation as a result of the hot cathode. The present results show that ionization in the magnetron occurs prior to dissociation and that higher electron energies can cause fragmentation.

Formation of NF_2^+ Plasma. - The use of tetrafluorohydrazine in preparation of the NF_2^+ plasma demonstrates how the ionizing gas can be selected to avoid the formation of undesired ions in certain cases. Ionization of ammonium trifluoride has been reported to give NF_2^+ as the major product.¹⁶ The parent ion, NF_3^+ and the fragment NF^+ were also formed in significant quantities, however. If lower electron energies, slightly above the appearance potential of NF_2^+ from nitrogen trifluoride, were used it appears likely that significant, possibly greater, quantities of NF_3^+ would be formed because of the lower appearance potential of the latter ion and the rapid increase of ionization efficiency with electron energy near the appearance potential. In addition, fluorine atoms or possibly fluoride ions accompany the formation of NF_2^+ from nitrogen trifluoride. The symmetrical structure of tetrafluorohydrazine indicates the possibility of preparation of a plasma containing only NF_2^+ ions. The appearance potentials of ions from tetrafluorohydrazine have been determined, and mass spectroscopic studies have been made showing the ionic composition obtained by ionization with electrons of moderate energy.^{17,18,19,20}

The formation of NF_2^+ with magnetron anode potentials of 12 volts, slightly below the published appearance potentials of this ion from tetrafluorohydrazine, 12.5 to 12.7 volts,^{18,20} may indicate either the spread of electron energies in the magnetron or ionization of NF_2 radicals, which may form by dissociation of parent molecules and which have ionization potential below 12 volts.²⁰

Preparation of OF^+ Plasma. - Mass spectrometric studies of the ionization of oxygen difluoride with 70 volt electrons showed the formation of the parent peak for OF_2^+ in greater quantities than OF^+ .²¹ The appearance potential of OF^+ from the neutral fragment OF was estimated at 13.0 electron volts, from the parent molecule, 15.8 volts. The magnetron anodes were therefore placed at 13 volts, below the appearance potential reported for OF_2^+ , 13.7 volts. Extraction of ion current from the magnetron by means of external potentials and mass spectrometric analysis of the ions showed the presence of OF^+ and no other positive ions. The negative ion F^- was also observed, in quantities less than 1/3 the OF^+ current. Thus, attempts to ionize oxygen difluoride may provide a plasma containing large quantities of fluorine atoms in addition to the OF^+ and F^- ions.

ACKNOWLEDGMENT

The encouragement of Dr. J. F. Masi and the support of the Air Force Office of Scientific Research are gratefully acknowledged.

16. R. M. Reese, and V. H. Dibeler, *J. Chem. Phys.* 24, 1175 (1956).
17. C. B. Colburn and A. Kennedy, *J. Am. Chem. Soc.* 80, 5004 (1958).
18. J. T. Herron and V. H. Dibeler, *J. Chem. Phys.* 33, 1595 (1960).
19. C. B. Colburn and F. A. Johnson, *J. Chem. Phys.* 33, 1869 (1960).
20. A. Kennedy and C. B. Colburn, *J. Chem. Phys.* 35, 1892 (1961).
21. V. H. Dibeler, R. N. Reese and J. L. Franklin, *J. Chem. Phys.* 27, 1296 (1957).

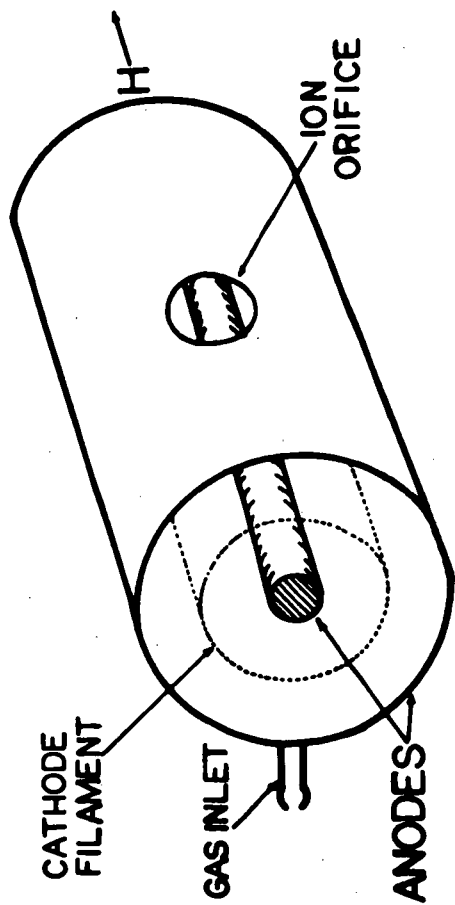


Fig. 1. Concentric Dual-Anode Magnetron

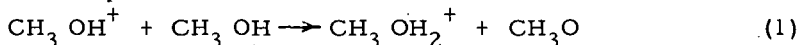
Ion-Molecule Reactions in Methanol and Ethanol

Keith R. Ryan⁽¹⁾, L. Wayne Sieck, and Jean H. Futrell

Aerospace Research Laboratories
Office of Aerospace Research
Wright-Patterson Air Force Base, Ohio

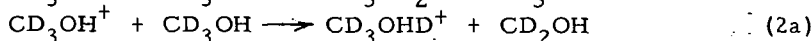
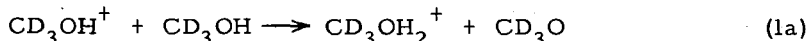
INTRODUCTION

The very large cross section observed for proton transfer ion-molecule reactions in alcohol has prompted a number of workers to investigate these systems in some detail. Theard and Hamill investigated the dependence of the cross section for proton transfer on the field strength in the ion source for 70 volt electrons (1), while Moran and Hamill have shown that the total cross section for these reactions changes significantly with the energy of the ionizing electrons. (2) Recently extensive studies on ethanol and methanol by the method of charge exchange have been reported by Lindholm et al. (3, 4, 5) In addition, these workers determined relative cross sections for the two possible proton transfer reactions between the parent methanol ion and methanol molecules

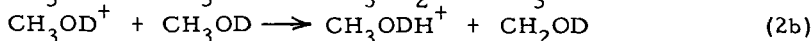


The use of the isotopically labeled methanol (CD_3OH) established the mechanism of formation of the product ion.

In Lindholm's apparatus the secondary ion beam is extracted in a direction perpendicular to the direction of the primary ion beam. This procedure is certainly suitable for the study of dissociative charge transfer but severe discrimination occurs against the extraction of secondary ions formed by processes involving momentum transfer. This discrimination is sufficient to preclude the observation of ion-molecule interactions in which entities other than the isotopes of hydrogen are transferred. Furthermore, in the reactions



the observed relative rate constants will be greater than for the equivalent reactions in methanol because of both this discrimination and the deuterium isotope effect. An indication of the magnitude of these effects can be obtained from the parallel reactions with CH_3OD



which have also been reported by Lindholm and Wilmenius. (5)

An examination of recorded appearance potential data for methanol reveals that at least one volt separates the onset of the parent ion and the process of next lowest energy (6). Consequently a study of proton transfer in the electron energy region below the onset of the CH_2OH^+ ion should yield information on the required

(1) Visiting Research Associate

cross sections. Once these are known a study of proton transfer as a function of electron energy should allow the elucidation of additional proton transfer reactions in the methanol system. These results, using the older techniques of ion molecule studies, are essentially free of momentum discrimination effects.

Until now the proton transfer reaction in ethanol has been assumed to involve the parent ion exclusively (7). By analogy with methanol it appeared that this reaction might also occur with the $\text{CH}_3\text{CH}_2\text{OH}^+$ ion. Accordingly an examination of the possible proton transfer reactions in ethanol was also undertaken.

Experimental

The instrument used in this study, a modified Consolidated Model 21-103C, has been described recently (8). The Bendix model M.306 electron multiplier was replaced by a Consolidated electron multiplier while the Wien filter was retained.

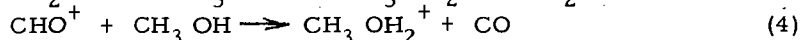
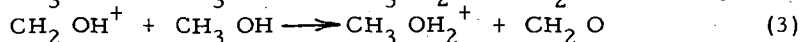
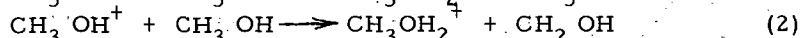
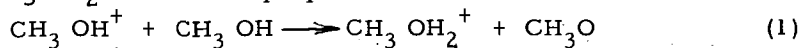
Appearance potentials were measured in the following manner: Magnetic scanning was used to bring the ions of interest to focus at 500 volts. Electric fields in the ionization region were reduced by operating the electron trap at 10 volts and both ion repellers at 4.5 volts. In order to compare the appearance potentials of two ions the sensitivity of the ion detector was adjusted so that the apparent abundances of both ions were the same at 50 electron volts. The appearance potential of an ion was arbitrarily taken to be the electron energy at which the ion current had fallen to 0.3 per cent of its value at 50 electron volts. Because of the similarity in shape of the curves being compared this technique was considered to be satisfactory. Furthermore, the difference in appearance potential between any two ions studied was constant irrespective of whether of the onset was chosen as the energy where the ion current had reached 0.1, 0.2 or 0.3 per cent of its value at 50 volts. In subsequent sections of this paper we are concerned only with the difference in energy for the onset of several processes. Accordingly we have used an uncorrected electron energy scale.

To facilitate the determination of appearance potentials, the ionization efficiency curves were displayed directly on an Electro Instrument Inc. model 300 X-Y recorder. Since the ion source of the mass spectrometer is always at acceleration potential (relative to ground) a signal from the helipot used to control the electron energy could not be fed directly to the recorder. Accordingly the output of the electron energy helipot was transmitted mechanically by means of an insulating shaft to a second helipot. A constant one volt signal was placed across this second potentiometer causing an electrical signal proportional to the electron energy to be developed between one end of the helipot and the moving contact. This signal was transmitted to the recorder and, suitably attenuated, was applied to the x-axis.

The relationship between reservoir pressure and ion source concentration was determined after the method described by Stevenson and Schissler, (9) using the ionization cross section of argon and the dimensions of the source. In this calibration reservoir pressures were read directly from the micromanometer provided with the instrument. In the methanol investigation reservoir pressures greater than 584 microns were sometimes employed. Since this pressure is the upper limit of reading of the micromanometer range all ion source concentrations corresponding to higher reservoir pressures than this were measured directly in the source by the method of total ionization. To convert total ion current to units of concentration it is only necessary to know the ionization cross section of methanol relative to argon. This was determined at lower ion source concentrations where the reservoir pressures of the gases could be measured.

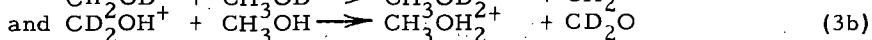
Formation of $\text{CH}_3\text{CH}_2\text{OH}_2^+$

The CH_3OH_2^+ ion has been observed in the high pressure mass spectrum of methanol, (1, 2, 9, 10) in the mass spectrum of mixtures of methanol and water (11) and in the experiments of Lindholm et al. (3-5) Mechanisms for the formation of CH_3OH_2^+ have been proposed as follows:



Using isotopically substituted methanols Theard and Hamill (1) found the appearance potentials for mechanisms (1) and (2) to be the same within experimental error.

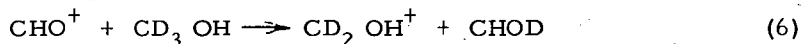
The importance of reaction (3) involving proton transfer from the hydroxyl position has been demonstrated by Lindholm and Wilmenius (5), who observed the reactions



in their tandem instrument. They also postulated mechanism (4) followed by the subsequent dissociation of some of the product ion (2)

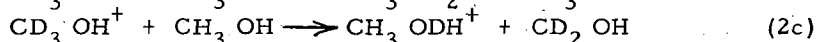
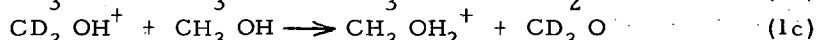
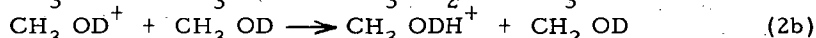
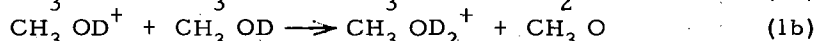
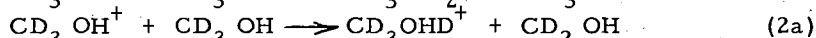
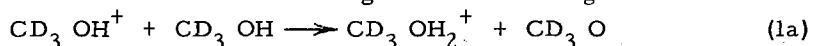


However, in a later publication (3) the same authors appear to favor the following hydride ion transfer reaction



over reaction (4).

In order to determine the relative cross sections of reactions (1) and (2) Lindholm and Wilmenius investigated the following reactions



In these three sets of reactions the ratios of product ion by mechanism (1) to product ion by mechanism (2) were 2:3, 1:3 and 2:3 respectively.

We have studied proton transfer using the techniques outlined by Lampe, Franklin and Field. (12) Since in our ion source secondary ions formed along the path of the primary ion beam are extracted in the same direction as the primary ion beam, discrimination because of momentum transfer should be minimized.

Figure 1 shows a plot of $\frac{\text{CD}_3\text{OH}_2^+}{\text{CD}_3\text{ODH}^+}$

against nominal electron energy over an eight volt range near threshold in the high pressure mass spectrum of CD_3OH . The curve has three distinct regions; A.

and C. In the low energy region one can detect only those secondary ions which have the parent ion as their precursor. As the electron energy is increased the curve breaks steadily upward along B. This is interpreted as the appearance of $CD_3OH_2^+$ ions from reaction of CD_2OH^+ with CD_3OH analogous to reaction (3). Eventually an electron energy is reached above which the ratio of product of CD_3CHD^+ relative to the rate of production of $CD_3OH_2^+$ is again constant. The establishment of this plateau C demonstrates that the only two ions which contribute significantly to proton transfer in this region of electron energy are CD_3OH^+ and CD_2OH^+ . It may be noted that this second plateau occurs in the same region of nominal ionizing voltage where the ionization efficiency curves for CH_2OH^+ and CH_3OH^+ from methanol are parallel.

The mean ratio in the plateau region A is about 0.92:1 whereas the ratio in the second plateau region is approximately 1.75:1. A parallel set of measurements using CH_3OD resulted in a value of 0.71 for the ratio $\frac{CH_3OD_2^+}{CH_3ODH^+}$ in plateau region A.

Under the source conditions employed it is apparent that the ratio of product from reaction (1) to product from reaction (2) must lie between 0.92:1 and 0.71:1. In order to estimate the true ratio one may proceed as follows: Let α be the ratio of the probability of transferring H^+ to that of transferring D^+ from any position on the molecule. Further let β be the ratio of the probability of collecting an ion to which H^+ been transferred to that of collecting an ion to which D^+ has been transferred. Clearly β is a measure of the momentum discrimination against D^+ transfer. If R is the true ratio for the transfer then

$$R = \frac{0.92}{\alpha\beta} \quad \text{from reactions 1a and 2a.}$$

$$R = 0.71 \alpha \beta \quad \text{from reactions 1b and 2b.}$$

Hence, $\beta = 1.14$ and a value of $R = 0.81$ may be deduced from our measurements.

Similar treatment of the results of Lindholm and Wilmenius gives $\beta' = 1.4$ and $R = .475$. If we assume α to be the same in both sets of results one obtains $\beta' = 1.24$. This leads to the expected result that discrimination against momentum transfer is considerably greater in the collision chamber used by Lindholm and Wilmenius.

It is not clear why the values of R calculated from our results and those of Lindholm and Wilmenius should be so different. One experimental uncertainty is the energy of the impacting ion beam. Since it is well known that cross sections for ion-molecule reactions are strongly dependent on the velocities of the primary ions, the measured ratio may depend on the ion velocity. Lindholm and Wilmenius report their measurements for ions of about 5 e.v. impacting energy. Our results in Figure 1 are reported for a repeller value of 4.5 volts. The geometry of the C. E. C. 103 ion source is such that the maximum energy an ion can acquire before arriving at the ion exit slit is about half the repeller voltage. This maximum energy of about 2.3 volts is somewhat lower than the energy of the ions used by Lindholm. However, we found no significant change in the measured ratio when the field strength was varied from 4 to 40 volts/cm. From our results we therefore, conclude that the relative probability of proton transfer from the two positions is independent of ion energy over this range.

From the results of Theard and Hamill (4) in their study with CD_3OH it is clear that the ratio $\frac{CD_3OH_2^+}{CD_3ODH^+}$ at an electron impacting energy of 70 volts remained

unchanged as the field strength was varied from 12 to 80 volts/cm. Since this ratio reflects the contribution of several independent proton transfer processes it can be assumed that the ratio of the reaction rates of any two of these processes is independent of field strength.

Once the ratio of proton transfer from reactions (1) and (2) is established the relative importance of processes such as (3) and (4) at higher electron energies can be determined. As shown in Table 1 the ratio $\frac{CD_3ODH^+}{CD_3OH^+}$ is independent of

electron energy for some seven volts above the ionization potential. Combining this result with the fact that the ratio $\frac{CD_3OH_2^+}{CD_3OHD^+}$ from reactions involving the parent

ion is 0.92:1 it is possible to calculate the amount of $CD_3OH_2^+$ formed by reactions involving ions other than the parent ion. Also shown in Table 1 is the ratio $\frac{\Delta CD_3OH_2^+}{CD_2OH^+}$ where $\Delta CD_3OH_2^+$ represents the increase in $CD_3OH_2^+$ due to ions

other than the parent. Because $\frac{\Delta CD_3OH_2^+}{CD_2OH^+}$ is constant for at least 10 volts above the onset of CD_2OH^+ we conclude that CD_2OH^+ is the only ion apart from the

parent ion which contributes significantly to the formation of $CD_3OH_2^+$ in this energy range. The increase at 14 volts indicates the onset of additional deuteron transfer processes.

As would be expected, the formation of $CH_3OH_2^+$ from methanol by processes not involving the parent ion is reflected in the appearance potential curve of the secondary ion. We have already mentioned the appearance potentials were obtained by comparing the ionization efficiency curves for two ions after arbitrarily making their sensitivities equal at 50 electron volts. However, this procedure is only satisfactory when each of the ions is formed by only one process. When more than one process contributes to the formation of a given ion this fact must be considered. This is illustrated in Figure 2. In 2a we compare the ionization efficiency curves of CH_3OH^+ with $CH_3OH_2^+$ by adjusting the ion detector to indicate equal sensitivities for both ions at 50 electron volts. It can be seen that the apparent onset of $CH_3OH_2^+$ is higher than the onset of CH_3OH^+ .

In Figure 2b we again compare the ionization efficiency curve of $CH_3OH_2^+$ with that of CH_3OH^+ . In this case we have taken into account the observation that only 46% of the $CH_3OH_2^+$ ions are formed from the parent ion when making the sensitivity adjustment at 50 electron volts. When this is done it can be seen that both ions have the same apparent onset. The upward break in the $CH_3OH_2^+$ curve corresponds to the formation of significant amounts of $CH_3OH_2^+$ from CH_2OH^+ .

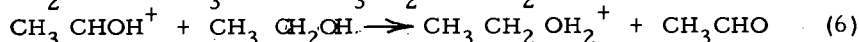
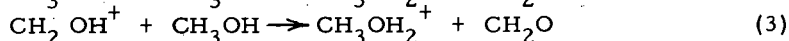
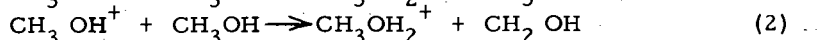
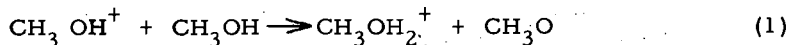
Formation of $C_2H_5OH_2^+$ in Ethanol

Several workers have observed the formation of $C_2H_5OH_2^+$ in the high pressure mass spectrum of ethanol. Tal'roze compared the appearance potential curves of $C_2H_5OH_2^+$ and $C_2H_5OH^+$ and concluded that $C_2H_5OH^+$ was a precursor for the formation of $C_2H_5OH_2^+$. (7) No other ions have previously been associated with the formation of $C_2H_5OH_2^+$.

In Figure 3 we show our ionization efficiency curves for the ions CH_3CHOH^+ , $\text{CH}_3\text{CH}_2\text{OH}^+$ and $\text{CH}_3\text{CH}_2\text{OH}_2^+$. From these results it is clear that CH_3CHOH^+ is the only important precursor for the formation of $\text{CH}_3\text{CH}_2\text{OH}_2^+$ for at least ten volts above the onset of $\text{CH}_3\text{CH}_2\text{OH}^+$. Furthermore, the same cross section is obtained for this reaction in the energy range of Figure 3 and at 70 ev. In sharp contrast to methanol the ethanol molecular ion plays no significant part in the formation of $\text{CH}_3\text{CH}_2\text{OH}_2^+$. This difference between the two molecules does not seem explicable in terms of the energetics of the corresponding reactions. Tal'roze and Frankevich have established lower limits and tentative upper limits to the proton affinities of the alcohols as 177-183 kcal/mole for methanol and 185-202 kcal/mole for ethanol. (11) From the work of D'or and Collin (12) and tabulated heats of formation in Field and Franklin (6) one can estimate the proton affinity of the methanol radical CH_2OH as 153 kcal/mole and of the ethanol radical CH_3CHOH as 159 kcal/mole. We are unable to suggest an alternate explanation.

Rate Constants for Proton Transfer Reactions

Having established the relative rates of proton transfer in the case of methanol and having shown that CH_3CHOH^+ , not $\text{CH}_3\text{CH}_2\text{OH}^+$, is the precursor for $\text{CH}_3\text{CH}_2\text{OH}_2^+$ formation it is possible to determine the rate constants for the following reactions



Consistent with recently tabulated values (13) we have determined rate constants and reaction cross sections at an ion repeller field of 10 volts/cm. Rate constants for all these reactions were observed to rise sharply at low field strength and to decrease at higher values, as is normally observed for ion-molecule reactions involving complex molecules. However, no attempt to extrapolate these results to zero field strength in order to obtain rate constants for thermal ions has been made.

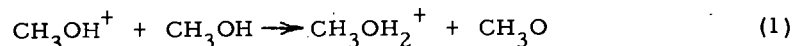
For any given secondary reaction, a plot of the ratio of secondary ions to the sum of precursor ions and secondary ions against ion source concentration is a straight line. As shown by Lampe and Field the slope S of this line can be expressed as

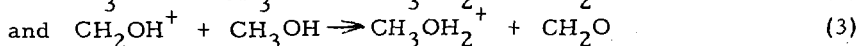
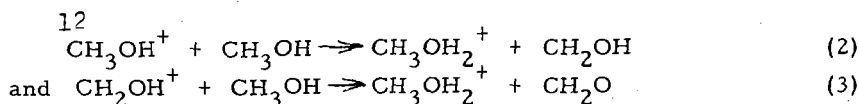
$$S = k\tau \quad (a)$$

$$S = l\sigma \quad (b)$$

Where k is the specific reaction rate, τ is the source residence time of the primary ion, l is the path length from the point of formation of the primary ions to the ion exit slit and σ is the reaction cross section. (14)

Reported in Table 2 are the reaction cross sections and rate constants for the reactions discussed. Also shown are results for methane from this study compared with earlier work. In this compilation we have corrected for the observation that 71% of the proton transfer product ion at a nominal electron impacting energy of 15 electron volts is produced by the parent ion. Since at this energy the remaining 29% of proton transfer product can be attributed to the CH_2OH^+ ion, the rate constants for

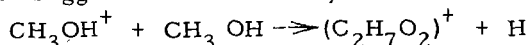




can be calculated by measuring the amount of proton transfer product at 15 volts and using the observed relative rates of reactions (1) and (2).

Ions with higher mass-to-charge ratios than those involving proton transfer

During this study we observed ions in the high pressure mass spectra of methanol and ethanol that had masses greater than those corresponding to proton transfer. In methanol the ions 73, 72, 63 and 45 were all observed. Of these only the 63 ion consistently exhibited a square law dependence on pressure. We are not sure of the mechanism of formation of these ions, but it is clear that 73 and 72 cannot be formed by second order ion molecule reactions involving only pure methanol. The appearance potential for 63 agrees well with that for CH_3OH^+ which suggests it is formed by the reaction.



In any event the abundance of these ions is less than 0.5 per cent of those produced by proton transfer.

In the high pressure mass spectrum of ethanol ions of mass-to-charge ratio 77 and 73 were both observed to follow a square law dependence with pressure. The relative abundance of these ions was less than 0.5 per cent of the secondary ions produced by proton transfer.

References

1. Theard, L. P. and Hamill, W. H., J. Amer. Chem. Soc. 84, 1134, (1962).
2. Moran, T. F. and Hamill, W. H., J. Chem. Phys. 39, 1413, (1963).
3. von Koch, H. and Lindholm, E., Arkiv For Fysik 19, 123, (1961).
4. Wilmenius, P. and Lindholm, E., Arkiv For Fysik 21, 97, (1962).
5. Lindholm, E. and Wilmenius, P., Arkiv For Kimi 20, 255, (1963).
6. Field, F. H. and Franklin, J. F., "Electron Impact Phenomena and the Properties of Gaseous Ions", Academic Press Inc., New York (1957).
7. Tal'roze, V. L., Pure and Appl. Chem. 5, 455, (1962).
8. Futrell, J. H. and Tiernan, T. O., J. Chem. Phys. 39, 2539, (1963).
9. Schissler, D. O. and Stevenson, D. P., J. Chem. Phys. 24, 926, (1956).
10. Stevenson, D. P., J. Phys. Chem. 61, 1453, (1957).
11. Tal'roze, V. L. and Frankevich, J., J. Amer. Chem. Soc. 80, 2344, (1958).
12. D'Or, L. and Collin, J., Bull. Roy. Soc. Liege 22, 285, (1956).
13. Lampe, F. W., Franklin, J. L. and Field, F. H., "Progress in Reaction Kinetics", G. Porter Ed. Pergamon Press 1961, pages 67 ff.
14. Lampe, F. W. and Field, F. H., Tetrahedron 7, 189, (1959).

TABLE 1

Nominal Energy E.V.	$\frac{CD_3ODH^+}{CD_3OH^+}$	$\frac{CD_3OH_2^+}{CD_2OH^+}$
5.6	.15	
6.0	.15	
6.4	.15	
6.8	.16	
7.2	.16	0
7.6	.16	0
8.0	.16	.08
8.4	.16	.12
8.8	.16	.14
9.2	.16	.14
9.6	.16	.13
10.0	.16	.14
10.4	.16	.13
10.8	.16	.14
12.0	.16	.14
13.0	.16	.14
14.0	.17	.14
15.0	.18	.132

TABLE 2

Reaction	σ , cm ² molecule ⁻¹ x 10 ¹⁶	k, cm ³ sec ⁻¹ molecule ⁻¹ x 10 ¹⁰
CH ₃ OH ⁺ + CH ₃ OH → CH ₃ OH ₂ ⁺ + CH ₃ O	79	11.0
CH ₃ OH ⁺ + CH ₃ OH → CH ₃ OH ₂ ⁺ + CH ₂ OH	97	13.5
CH ₂ OH ⁺ + CH ₃ OH → CH ₃ OH ₂ ⁺ + CH ₂ O	48	6.8
CH ₃ CHOH ⁺ + CH ₃ CH ₂ OH → CH ₃ CH ₂ OH ₂ ⁺ + CH ₃ CHO	531	60
CH ₄ ⁺ + CH ₄ ⁺ → CH ₅ ⁺ + CH ₃	{ 54	10.7
	{ 61 (a)	8.5 (a)

(a) Field, F. H., Franklin, J. L. and Lampe, F. W., J. Amer. Chem. Soc. 79, 2419, (1957)

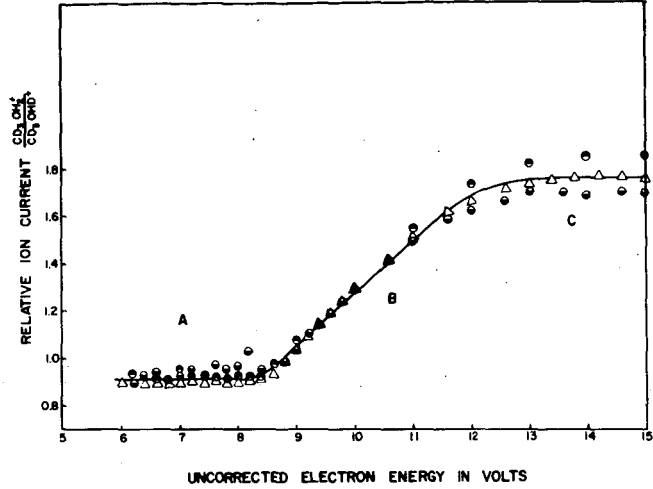


FIGURE 1 $\frac{CD_3OH_2^+}{CD_3OHD^+}$ current versus uncorrected electron energy (3 expts. at 3 different pressures in 3 different sources).

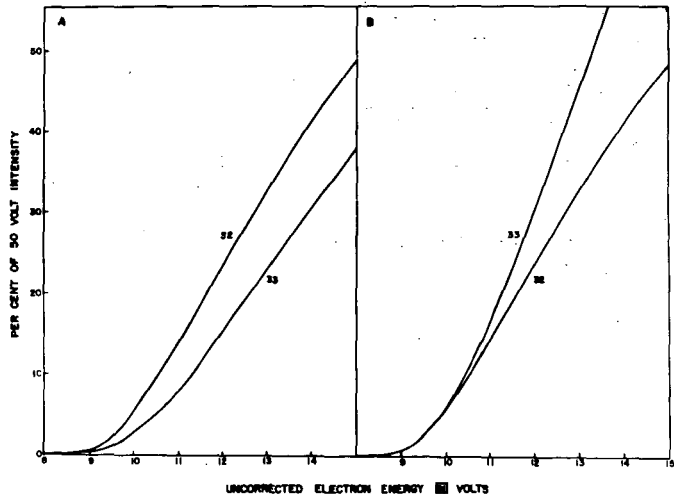
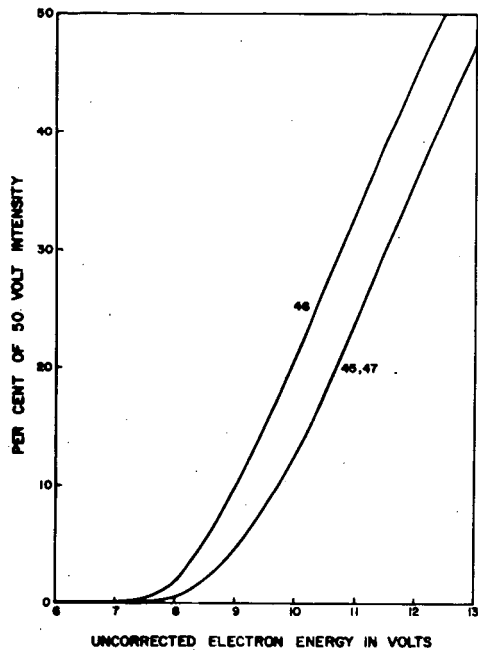


FIGURE 2 Uncorrected ionization efficiency curves for m/e 32 and 33 from methanol normalized to 50 volts and same curves corrected for $CH_3OH_2^+$ from CH_2OH^+ , respectively.



Normalized ionization efficiency curves for m/e 45, 46, and 47 from ethanol.

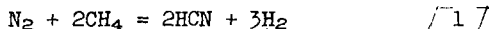
FIGURE 3

THE NATURE AND QUANTITATIVE DETERMINATION OF THE
REACTIVE SPECIES IN A NITROGEN PLASMA JET

Mark P. Freeman
Central Research Division
American Cyanamid Company
Stamford, Connecticut

INTRODUCTION

One of the "natural" reactions found to proceed in a plasma-jet reactor is the formation of hydrocyanic acid by the introduction of methane into a nitrogen jet:



The reaction can be made to proceed in good yield (based on methane consumption) and, furthermore, the main by-products, acetylene and hydrogen, are of considerable chemical significance. This reaction therefore, has received more than passing interest from various investigators purely as a production possibility.

In an ever widening circle of plasma-jet applications this reaction is almost unique in that it is almost certain that the chemistry must proceed via thermally produced intermediate species of a sort unknown at ordinary temperatures. This is the interesting sort of process one would like to contemplate when considering possibilities for plasma jet chemistry. One feels that if insight can be gained into the detailed mechanism for this key reaction, then it is quite possible that avenues will open to exploit other high temperature species in chemical synthesis or, indeed, to use the active species of a nitrogen jet in other reactions.

In the "active nitrogen" research (1,2,3) that has persisted in vigorous

-
- (1) K. R. Jennings and J. W. Linnett, *Quart. Rev.* 12, 116 (1958).
 (2) G. G. Mannella, *Chem. Rev.* 63, 1 (1963).
 (3) N. E. V. Evans, G. R. Freeman and C. A. Winkler, *Can. J. Chem.* 34, 1271 (1956).

activity for more than half a century, HCN plays an equally important role. In fact when cold methane is added to nitrogen at low pressure that has been recently passed through a high-voltage electric discharge, one gets exactly the stoichiometry of [1]. That the experimental systems themselves are different is apparent for the high-voltage discharge is a high-excitation device whereas the plasma jet is thought to be nearly in thermal equilibrium and hence a low-excitation device (spectroscopically speaking (

-
- (4) F. A. Kovolev and Yu. K. Kvaratskheli, *Optics & Spectroscopy*, 10, 200 (1961).

intermediate between arc and spark). Furthermore the plasma jet experiments reported here were performed at one-half atmosphere (as opposed to ~1 torr) and at a temperature twenty times as high on the absolute scale as room temperature, where the bulk of active nitrogen experiments have been performed. Finally, the reactive carbon-containing species evidently does not contact the active nitrogenous species as methane. That is, the products other than HCN are mainly acetylene and higher acetylenes with various degrees of saturation. These are the same products that would form if the jet were, say, argon. It has been shown elsewhere (5) that the precursors

(5) M. P. Freeman and J. F. Skrivan, *AIChE Journal*, 8, 450 (1962).

For these products form rapidly compared to the time for mixing of the methane with the jet.

In spite of these differences it nevertheless does not seem reasonable to say the two systems are only superficially related for the chemistry seems too specific and unique to permit one to accept this interpretation lightly. If one is willing to accept the fact of the chemistry given in equation [1] ... perhaps modified by an asterisk to indicate the nitrogen has been subjected to an excitation of some kind ... as an operational definition for active nitrogen then this study is in a true sense a study of active nitrogen. It is true that the plasma jet provides a difficult environment in which to do precise work. On the other hand this difficulty would seem to be offset by the fact that the relative concentration of active species is observed to be as high as 12% which is two orders of magnitude higher than the (at most) tenths of a percent quoted in conventional research (6).

(6) J. M. Benson, *J. App. Phys.* 23, 759 (1952).

Furthermore, whereas in conventional research on active nitrogen the partial pressure of the active species itself is on the order of hundredths of a torr, it is here observed to be in the tens of torrs. Naturally, this high concentration promotes a considerable simplification in the recovery and analysis of products. Perhaps most significant is the fact that owing to the high temperatures available in a plasma jet atomic nitrogen can be produced in large amount as an equilibrium constituent of the stream and hence serves as an important new variable.

The procedure followed was to add methane through an annular slot to a confined nitrogen jet of precisely defined average enthalpy. It has been shown that under these conditions mixing is very rapid as is the drop in temperature (5). After about 1 millisecond the resulting flow of high temperature species was further chilled by the entrainment of cold product gas .. (the fastest quench known) ... and the flow of HCN in the product gas relative to the effluent nitrogen flow chemically determined. Data were taken at about 350 torr reactor pressure in two reactors that differed in a significant way. In one reactor the methane mixes with the jet as it emerges from the head into a water cooled channel the same size as the front electrode orifice. In the other reactor, the jet enters a plenum chamber, with an exit orifice, and then expands to more than twice the original diameter. Only after the jet has persisted outside the head for more than a millisecond, during which it has lost about half of its enthalpy, is the methane added.

As the methane is added at various flow rates the corresponding rate of production of HCN relative to the effluent nitrogen flow is noted. Just as in Winkler's (7) work with active nitrogen, a plateau is observed which indicates that some active species is indeed determined. Because of equipment availability work was done with the second of the two reactors described above several months in advance of the first, a reactor that is both hotter and more amenable to an enthalpy-dependence study. Because the data from the earlier study indicated an HCN flow rate within a factor two of the nitrogen atom flow rate for a nitrogen stream of enthalpy equal to the average enthalpy (7) it was tentatively concluded (8) that the reagent

(7) F. Martinek, *Thermodynamic and Transport Properties of Gases, Liquid and Solids* (McGraw-Hill, New York, 1959), p. 130.

(8) H. M. Hulburt and M. P. Freeman, *Trans. N. Y. Acad. Sci.*, II, 25, 770 (1963).

species is the nitrogen atom. It is clear from the more complete study reported here

that this conclusion is, in fact, erroneous and that the apparent agreement was fortuitous, a consequence of the choice of power level used in that part of the study.

In order not to confuse what is observed with the immediately apparent interpretation, these factors are separated in the following presentation: After a reasonably complete presentation of the experimental procedure and details (EXPERIMENTAL) sample data are presented together with such generalizations about the data as seem warranted from simple inspection (RESULTS). Following this section, an attempt is made to discuss each of the observations in terms of the various interpretations they would seem to warrant (DISCUSSION). Included in this section is a brief discussion of the principal questions remaining unresolved. Finally, (SUMMARY) those interpretations that would seem most probable are collected together to present a plausible sequence for the observed reaction.

EXPERIMENTAL

Apparatus. Plasma-jet reactors consist of three parts, head or arc unit, intermediate section, and quenching section. The plasma-jet head used for this study is a Thermal-Dynamics L-40 Plasma-jet with "turbulent nitrogen" electrodes and it is powered by two 12 kw welding power supplies open circuit voltage 160 volts connected with their outputs in parallel, but with opposite phase rotations on the input so as to minimize power supply ripple in the output. The intermediate sections (Figures 1 and 2) are made of copper and fully water-cooled as is the head. The SOR (local designation) shown in Figure 2 has ducts and thermometers located so that heat lost to the cooling water upstream of the slot is determined independently from that lost downstream. The quenching section where the hot stream of plasma and reaction products is quenched by entrainment of cold product gas is simply a heat exchanger, i.e., it is a stainless steel pot 11 inches in diameter and 11 inches long sparsely wound with soldered copper tubing. Between the windings it gets hot enough to cause flesh burns but all parts subject to heat damage, such as seals, are well cooled. At the outlet of the quenching section is six feet of 1 inch I.D. thick-walled rubberized fabric acid tubing. This in turn is attached to the bottom of a 3 foot vertical mixing section of 2 inch stainless steel tubing loosely packed with glass wool. At the bottom of this mixing section carbon dioxide is mixed with the now cold discharge from the plasma-jet reactor. The top of the mixing section is connected to a high capacity steam jet vacuum pump with an automatic controller for maintaining desired pressures.

A Toeppler pump is arranged to withdraw 522 ml. of gas from the top of the mixing section at room temperature and at the reactor pressure. This aliquot may then be collected for analysis in a suitable gas collection system.

Gas flows, except for methane, are metered by orifice gages calibrated to within 1% for CO₂ and N₂ respectively by water displacement. Methane flow, much less critical, is determined by a rotameter calibrated by calculation. All cooling water flows are determined by experimentally calibrated rotameters. Cooling water temperature rise is determined by suitably graduated interconsistent mercury thermometers.

Procedure. Heat flow in the nitrogen plasma at the point of methane introduction is determined by subtracting from the voltage-current product in the arc the heat lost to all cooling-water supplies up to that point. (In the case of the TR reactor, a local designation for the reactor configuration of Figure 1, this is just the head cooling water.) For data taken at a particular heat flow (and hence average enthalpy) an attempt was made to keep this heat flow constant. In this endeavor the relatively great intrinsic stability of plasma jets made by this manufacturer

helped, but because data for a typical run extended over several hours there was an appreciable drift with occasional overcorrection (about 15%). This is undoubtedly the principal source of scatter in the data; note that the methane flow rates were set in random order so that trends in the data due to net power drift would not be observed except as scatter.

Except where noted, in all systems the pressure at the sampling tap (called reactor pressure was 350 ± 20 torr. The actual pressure of each sample was known to ± 1 torr but this is not a significant datum in the data analysis. Reactor pressure does not directly measure pressure in the head because of the pressure drop through the arc, which is quite large when the head is operating. Although this unit is not instrumented for an in-head static pressure measurement, some exploratory pressure measurements were run with a tap at the inlet to the head. It was found that pressure changes at this point at the standard flow rate were fairly insensitive to power level, as well as to reactor pressure in the range covered in these experiments. At 350 torr with a gas flow of $0.0171 \text{ gm. mole sec.}^{-1}$ the inlet pressure was observed to be 710 torr. No condition realized in this experiment at this flow rate altered this pressure by more than 10%. Lowering the gas flow rate by 27% reduced the pressure to about 600 torr, a change still less than 20%.

Whenever methane, power and/or pressure conditions were changed the system was operated for eight minutes before taking a sample. This was found to be sufficient time to establish a constant composition.

The collected gas aliquot was slowly sparged through 100 ml. of ice-cold caustic containing 12.50 millimoles of base. The half-liter space over the caustic was initially evacuated so that the entire sample, together with the air used to flush out residual product gas from the lines, might be collected in the caustic and the space over it. This was followed by one minute of vigorous shaking. This procedure has been found satisfactory for the quantitative recovery of CO_2 and HCN. Total acid in the aqueous solution was then determined by titration with 0.500 N HCl until all of the carbonate had been converted to bicarbonate (pH 8.3). Ammoniacal KI was then added as an indicator and cyanide determined alone by precipitometric titration with 0.0100 N silver ion. This permits the initial ratio of partial pressures and hence relative flow rates of HCN and CO_2 to be determined. But the ratio of the flow rates of N_2 (effluent) and CO_2 is known both from the calibrated gages and to similar precision from titration of a blank run done without power or methane. Consequently the ratio of HCN to effluent N_2 follows immediately.

Accounting for the various sources of uncertainty the actual ratio of HCN to N_2 is estimated to be within about 10% of the reported value and the heat flow to within about 5%. Air leakage into the system, a potential source of error, was between 0.1 and 0.01% of the total gas flow.

The quenching section is mounted with a window through which, for a time after each cleaning, the exhaust of the intermediate section can be observed. Under some conditions (notably high enthalpy and low gas flows) rapid solids formation occurred leading, indeed, to plugging at the highest heat flow. It is, therefore, of some interest that when totaled over all runs an inconsequential amount of solid product formed. More than 3 Kg of methane was used in the course of these experiments, resulting in less than 6 g. of recovered solid. This very bulky solid was found on Kjeldahl analysis to contain about 5% nitrogen by weight; it is apparently a mixture of HCN polymer and carbon.

Although temperatures are not quoted (and as will be shown below, cannot be meaningfully quoted because of a substantial departure from equilibrium) it is instructive to note that the eight-fold range of average enthalpy covered in this experiment,

would, on the assumption of equilibrium, correspond to temperatures from 3250°K. to 7000°K.

RESULTS

Yield. In Figure 3 typical results for the yield of hydrocyanic acid as a function of methane feed rate is shown for the TR reactor at a nitrogen flow of 0.0171 g. mole sec.⁻¹, at three widely different enthalpy levels. Several important observations may be made immediately:

- a. At every enthalpy level a limiting value of HCN production is achieved, as observed by Winkler, et al. (3)
- b. After the limiting or saturation value is reached a further excess of methane does not decrease the yield, suggesting a condition of frozen equilibrium.
- c. Before saturation is reached all of the yield curves coincide with each other and with a line slope of 1/3. That is when insufficient methane is added to reach the limiting production, only one carbon atom in three is converted to HCN.

The thing that strikes the investigator is the stability and reproducibility of these effects despite the difficulties inherent in keeping a plasma-jet system operating at precisely defined conditions for several hours. Figure 4 shows a yield curve as in Figure 3 for the highest enthalpy run done in the TR reactor at substantially reduced gas flow. Although this run was plagued by plugging and unstable operation it is clear that no qualitative difference in behavior is to be observed. Also shown in this figure is the initial run done in the SOR reactor at a single enthalpy. Again, essentially the same behavior occurs.

Variation with enthalpy. Because the yield varies rapidly with enthalpy, the enthalpy variations encountered during runs of several hours duration make average values determined from full yield curves such as those of Figures 3 and 4 no more precise than single points using methane flows corresponding to the plateau regions of the curve. At all available enthalpy levels a methane flow rate equal to one-half the nitrogen flow is seen to give the limiting yield of HCN and much of the data describing enthalpy dependence was taken at this feed ratio.

In Figure 5 the logarithm of the flow rate of active species (as measured by the saturation HCN production) is plotted vs reciprocal enthalpy. The open points represent "one point" data; the filled points were determined by a full yield curve of the sort shown in Figure 3. Circular points represent data from the TR reactor, at a nitrogen flow of 0.0171 g. moles sec.⁻¹ while triangular points represent data from the same reactor at 0.0125 g. moles sec.⁻¹. The square point represents data taken on the SOR reactor using average enthalpy determined at the slot. Also shown in this figure is a line segment representing the population of atomic nitrogen at 0.46 atmospheres as a function of enthalpy as calculated from equilibrium considerations (7). Two important conclusions can be drawn from this figure:

- d. The production of active species appears to be a smooth and reproducible function of enthalpy for a particular reactor regardless of flow rate.

- e. The population of active species correlates very poorly with nitrogen atom population based on average enthalpy, being many orders of magnitude too high at low enthalpy and a factor of 10 low at high enthalpy.

Pressure dependence. Although the experiment was principally run at a nominal reactor pressure of 350 torr some indication of sensitivity to pressure is necessary to assess the importance of the small pressure variations encountered. At a net power of 7000 ± 100 watts and a nitrogen flow of 0.0171 g. moles sec.^{-1} , the data of Table I were taken.

TABLE I

Relative Yield of HCN as a Function of Reactor
Pressure at Moderate Power

Total Reactor Pressure (torr)	195	350	484
n HCN/G	0.052	0.074	0.078
Heat Flow (watts)	6991	6992 (avg.)	7216
Conductance (mhos.)	1.27	0.58	0.68

Note that at 195 torr an appreciable fraction of the total enthalpy is tied up in directed kinetic energy so the free stream enthalpy is substantially lower than the heat flow would indicate. This leads to the further rather surprising observation:

- f. The fraction of nitrogen capable of ultimate reaction with the carbon containing species to HCN is nearly independent of reactor pressure.

Methane Utilization. Four gas samples were taken for mass spectrometric analysis at the 7000 watt level, corresponding to four points on the center curve of Figure 3, two below saturation and two above. Unreacted methane accounts for 10% of the methane flow at the highest flow rate ($\text{CH}_4/\text{H}_2 \approx 0.6$) but at all lower flows the conversion was found to be complete. In every case acetylene was found to be by far the major product, although for the points above the saturation value some carbon (a few percent) is found as other C_2 , C_4 and C_6 unsaturated hydrocarbons. If HCN production is estimated from Figure 3, the observed carbon balance is satisfactory to within the limited precision of the mass spectrometric analysis. This leads to the final observation:

- g. When the nitrogen is in excess all of the methane reacts to make for each molecule of HCN one of acetylene. When the methane is in excess, the excess methane that reacts forms chiefly acetylene, with minor amounts of C_4 and C_6 species.

DISCUSSION

General

In light of the observations a. and b. above, there would appear to be little question that the earlier interpretation (7) of the data taken on the SOR reactor was correct to the extent that a nitrogen plasma jet evidently contains some active species,

perhaps more than one, capable of reacting with the immediate decomposition products of methane to make HCN or its precursor. It seems equally clear that the procedure employed here quantitatively determines the flow rate of this (these) species.

Reactive Nitrogen Species

Atomic Nitrogen. From the welter of confusing evidence, and conflicting views that have accumulated over the decades of "active nitrogen" research, a sort of general agreement has recently been reached that at least the most important constituent must be atomic nitrogen in its ground state (1). With the high temperature thermal plasma investigated here it would seem that this possibility can be immediately excluded by observation. Taking into account all the known characteristics of a plasma-jet reactor, one can not account for the very low production rate of active species at high enthalpy. That is, on account of the intrinsic steep temperature gradient near the walls of a contained plasma-jet, one must always consider the possibility that the non-uniform radial temperature profile might cause observed effects. Furthermore, the enthalpy fluctuations to which a plasma jet is subject (9)

(9) M. P. Freeman, S. U. Li and W. vonJaskowsky, J. App. Phys. 33, 2845 (1962).

are not to be ignored. However, by actual computation one may very quickly satisfy himself that while a non-uniform temperature distribution might account for a total nitrogen atom population somewhat in excess of the average concentration calculated, no reasonable distribution of enthalpies could account for the observed dearth at high enthalpy.

Ionic Nitrogen. One of the theories of active nitrogen that has in the past enjoyed some popularity is that of Mitra (1). This theory invokes the molecular ion N_2^+ as the active species. This suggests attempting to correlate the production of active species with the rate of production of positive ions in the arc process. (The equilibrium population of ions at reactor conditions is much too small to be interesting.) This is, of course, just the rate of production of electrons, since the plasma remains electrically neutral. Note that at the higher power levels, even allowing for the considerable amount of heat involved in non-equilibrium ionization this implies, the temperature should still be high enough that the principal positively charged species is the atomic ion rather than the molecular ion. Since there is no reason to suppose that their ultimate products should be any different, this presents no difficulty.

A number proportional to the rate of production of electrons, and hence of positive ions, may be estimated in the following way: The conductivity, σ , in the actual arc discharge path is proportional to the density of electrons, n_e , and their mean free path (10). On allowing for the pressure dependence of the mean free path:

(10) H. O. G. Alfven, Cosmical Electrodynamics (Oxford, Clarendon Press, 1950) p. 47.

$$\sigma \propto n_e/P \quad [2]$$

There is also a weak temperature dependence, but this may be ignored as the temperature in the actual discharge path probably does not change much. If the discharge path occupies a fractional area, γ , of the total plasma-jet channel then the conductance M is proportional to:

$$M \propto \sigma \gamma \quad [3]$$

Now we make the assumption that the ion production rate, R , is just equal to the ion (and hence electron) population density in the discharge path times the velocity (proportional to $1/P$) of that part, γG , of the total flow, G , that flows through the discharge column:

$$R \propto n_e \gamma G/P \quad [4]$$

Combining [2], [3] and [4] we obtain the simple result that the conductance is proportional to the flow rate of ions out of the discharge path divided by the effluent flow rate:

$$M \propto R/G \quad [5]$$

Assuming that the heat flow, W , leaving the head is proportional to the energy actually dissipated in the arc (as opposed to energy dissipated to the cooling water in electrode processes) then from Watt's law:

$$R/G \propto I^2/W = M \text{ (mhos)} \quad [6]$$

Where I is the measured current through the head.

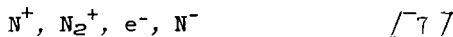
Figure 6 is a plot of conductance vs. relative rate of HCN production for all the data taken at 350 torr. Considering the crudeness of the derivation of [6] the agreement would seem to be extraordinarily good. It is fortunate that the analysis turns out to show little dependence on the reactor pressure as this variable was not held precisely constant for all the runs. Furthermore, this would seem to be consistent with observation elsewhere, despite the widely disparate reactor pressures employed, the active species production in the derivation of [6] now become apparent when one considers the conductance for it changes appreciably for the low pressure run. The points from the data of Table I are represented by asterisks on Figure 6. One might suppose the obvious disparity to be due to the arc length or mode of operation changing at low reactor pressure. As explained above, much larger changes in pressure are produced in the arc chamber by changing the flow rate than by changing the reactor pressure. Yet, if there is any real discrepancy between data taken at 0.0125 (Δ) and 0.0171 g. moles sec.⁻¹ (o) it is small.

Equilibrium Considerations. Apparently a charged specie (s) that persists in the jet is responsible for the observed HCN production rate. But now the question arises as to whether that species is present because of a slow recombination reaction and, hence large departures from local thermodynamic equilibrium (LTE) or whether it is due to the radial temperature profile discussed above. The square point in Figure 6, the datum for the SOR reactor, contributes a very direct answer to this question. For this reactor the methane is added only after the jet has been fired into a plenum, choked and then expanded. In the process it has lost nearly half the enthalpy it had on leaving the head: and yet it still agrees well with the correlation between HCN production and head conductivity exhibited by the TR reactor. Since even the maximum radial temperature in this case is well below that at which ions could exist at equilibrium, one must conclude that the back reaction destroying charged species in the jet is very slow compared to jet residence times (on the order of milliseconds for this reactor).

Another question that should be considered is whether so much enthalpy is tied up in non-equilibrium ionization that, assuming all other degrees of freedom to be equilibrated, the resulting temperatures are too low to allow an appreciable amount of atomic nitrogen. This could account for the unexpected lack of HCN generated by this species. However, in the worst possible case, subtracting from the

total enthalpy the heat of formation of a nitrogen ion for each HCN molecule formed, one finds that in the runs at highest heat flow there is still sufficient enthalpy to provide as much as 35% atomic nitrogen. Clearly one must look elsewhere to explain the inactivity of this species.

Unresolved Questions. It remains to identify, if possible the actual ionic species involved in the reaction from among the four likely candidates:



These may be quickly reduced to three by the following reasoning. If one positive ion is the reactive species then they both must be reactive since no difference is observed in Figure 6 between data taken at high power and at low. They must, in fact, be indistinguishable as reagents in this reaction. As a matter of convenience we may denote them both by the low temperature species, the molecular ion. Because the atomic ion is always surrounded by atoms and chilling is very rapid in the mixing zone of the reactor, it may be that the molecular ion is in fact the actual reagent.

The negative species presents more of a difficulty. It is certain that if charged particles of one sign are involved in the chemistry, so must particles of the opposite for the product emerges electrically neutral. The likely species to be involved, the electron gas, has certain drawbacks. Foremost among the drawbacks, it is hard to accept the slow recombination rate between electrons and positive ions implied. This would furthermore represent a disappointing departure from conventional active nitrogen research for by the use of microwave techniques Benson (6) has shown the concentration of electrons to be orders of magnitude too small to be paired in one-to-one correspondence with the active species (although the long persistence of conductivity could indicate the electrons were in equilibrium with some other species).

It has, to be sure, been almost axiomatic for three decades that the negative nitrogen ion can not form because in its ground state it is unstable, or nearly unstable, with respect to dissociation to the atom. However, Boldt (11) has recently

(11) G. Boldt, Z. f. Physik 154 330 (1959).

shown through spectroscopic evidence that a metastable nitride ion forms and persists in appreciable concentration in an arc discharge that is not appreciably different from the plasma generating arc employed here so that this possibility may not be lightly disregarded. The transition of this metastable ion to the ground state is spin forbidden. Its ionization potential is 1.1 ev to an excited metastable atomic state that lies 2.38 ev above the ground atomic state.

There would seem to be no good way to determine within the context of the present experiment whether the positive or negative species is involved in the reaction in a path determining way. More important perhaps within the context of active nitrogen research is the manifest inactivity of atomic nitrogen ... even under conditions of heavy methane flow.

Reactive Carbon Species

As a completely unexpected by-product of this work. observations c and g would seem to give interesting confirmation to the work of Skell and Wescott (12).

(12) P. S. Skell and L. D. Wescott, J. Am. Chem. Soc. 85, 1023 (1963).

These investigators have identified the principle species in carbon vapor at low pressures as a dicarbene:



[8]

by the chemical identification of its addition products with olefins when they are sublimed together onto a cold surface.

Observation c., that only one carbon atom in three may react to make HCN when the nitrogenous reactive species is in excess, the other two going to acetylene, is quite reasonably explained if in the principle step a nitrogen kernel is attached to a dicarbene which then subsequently forms one HCN and C_2H_2 . Observation g. follows equally well by postulating that when the dicarbene is in excess it dimerizes and then forms mono-, di-, and tri-acetylene units on subsequent attack by atomic hydrogen; partial hydrogenation of the higher acetylenes by atomic or molecular hydrogen to make vinyl- and divinyl-acetylene then completes the reaction sequence.

SUMMARY

This experiment, simple in concept and interpretation, would appear to shed considerable light on the details of the reaction of methane with a nitrogen plasma-jet. Although there are still many details requiring further work, at the present time we can propose the following simple concept for the reaction sequence:

1. A part of the nitrogen as it passes through the arc head unit, passes through the arc column or discharge path. There it is completely dissociated and ionized to the extent required by the arc process.
2. As the fresh gas enters the discharge column, atoms, atomic ions, and electrons are swept out where they mix with the relatively cold gas that is bypassing the discharge column.
3. The mixture equilibrates in most degrees of freedom to some reproducible steady state consisting of a mixture of at least atoms, molecules, atomic and molecular ions and electrons.
4. Some process leading to equilibration of that degree of freedom of the mixture involving the existence of the active species is effectively "frozen" or nearly so; the flow of active species in the stream is equal, or almost equal to the rate at which it or its precursor is displaced from the arc zone.
5. The rate at which the active species or its precursor is blown out of the arc zone is proportional to the rate at which charged particles of either sign are blown out, which is presumed to indicate that the active species or its precursor is charged.
6. As the end products are necessarily electrically neutral, ions of both polarities are required in the chemistry. Those with positive charge are probably an equilibrium mixture of the molecular and atomic ions, presumed to be chemically indistinguishable, while the negative charge carrier could be electrons, free nitride ion gas, or possibly some equilibrium mixture. From the present experiment there is no indication of the sign of the ions which initiate and determine the path of the reaction.
7. As the methane enters the reactor it rapidly mixes into the hot plasma and is converted to C_3 dicarbene molecules. The nitrogen containing active species

reacts with it to form one molecule of HCN and one of C_2H_2 on subsequent cooling and attack by atomic hydrogen. When the C_3 is in excess, the excess dimerizes; on subsequent cooling and attack by atomic hydrogen it goes mainly to acetylene with small amounts of C_4 and C_6 molecules with varying degrees of unsaturation.

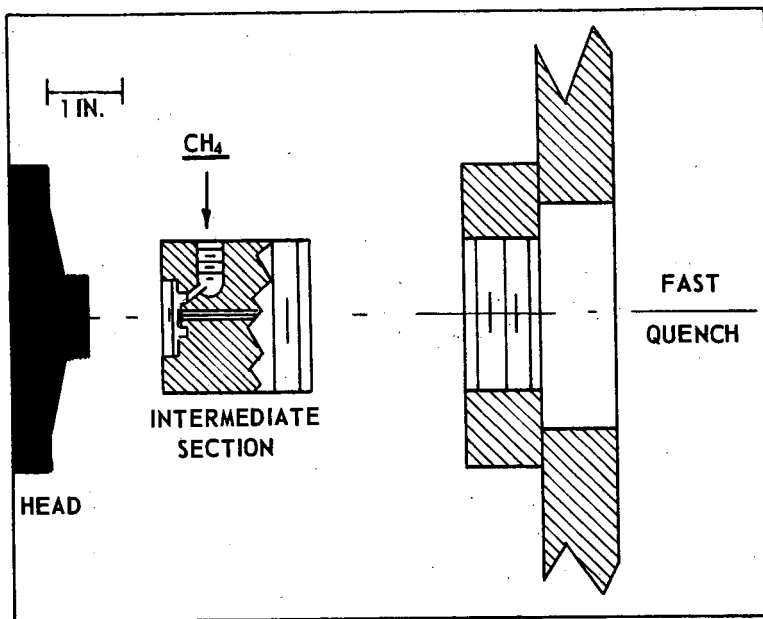
This reaction sequence is of course only appropriate to the plasma jet situation; however, the outstanding factor emerging from this study that one should keep in mind when considering the greater relevance of this work is that an active species has been found that has chemical properties generally attributed to ground state atomic nitrogen in conventional active nitrogen research. This species has been shown to be:

- a) Not atomic nitrogen in the ground state.
- b) In direct proportion to the number of charged particles produced in the arc process.

ACKNOWLEDGEMENT

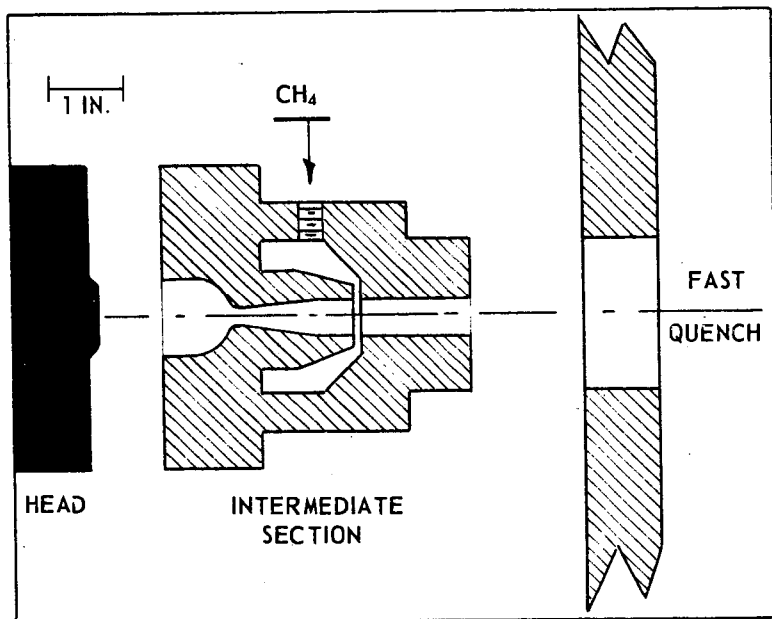
Among the numerous people who have contributed in some way to the conception and performance of the research the author must especially acknowledge the encouragement and helpful discussions of Drs. A. K. Hoffmann, H. M. Hulburt, J. E. Longfield and J. F. Skrivan, all of this organization. He wishes furthermore to acknowledge the considerable technical assistance of Mr. C. W. Beville.

Figure 1



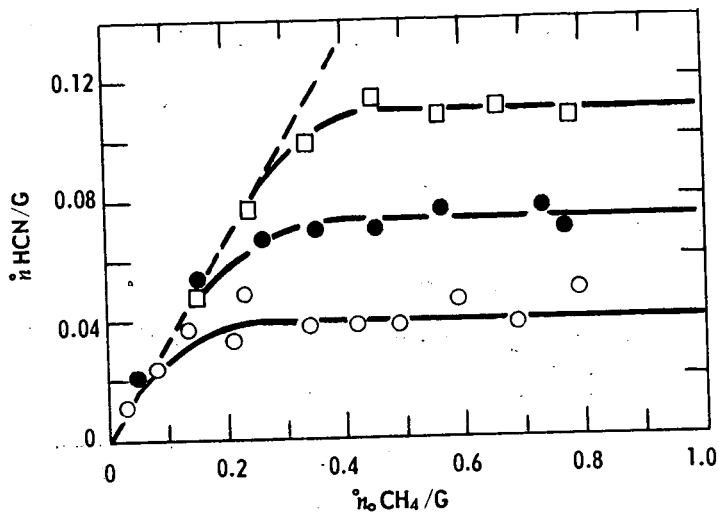
Exploded view of TR reactor. Intermediate section shown in simplified cross section. Material: Copper

Figure 2



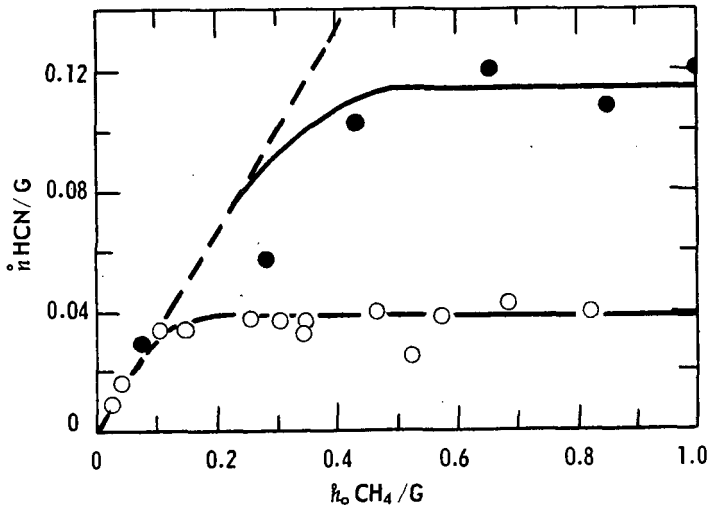
Exploded view of SOR reactor.
Intermediate section shown in simplified cross section.
Material: Copper

Figure 3



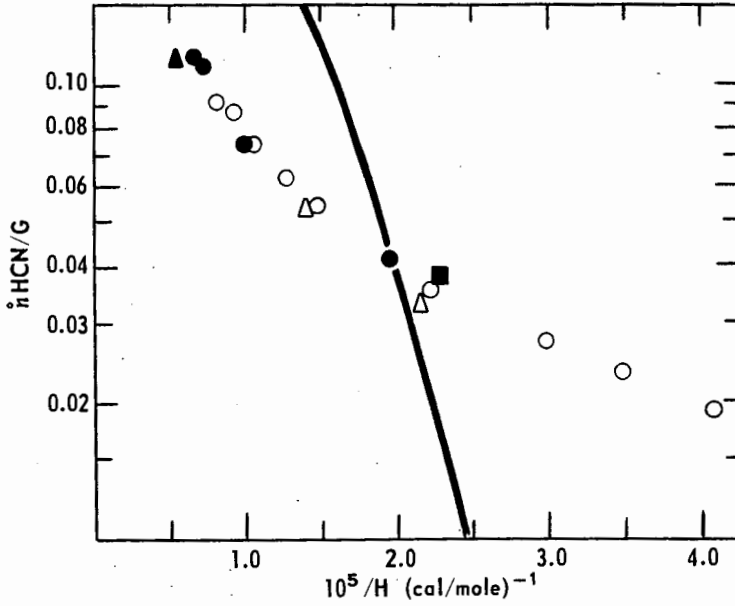
Rate of production of HCN vs. feed rate of methane (both relative to effluent nitrogen flow, G, of 0.0171 gram moles sec. $^{-1}$) at three net power levels: 3522 watts - \circ ; 6992 watts - \bullet ; and 9782 watts - \square TR reactor. Dashed line has slope of one-third.

Figure 4



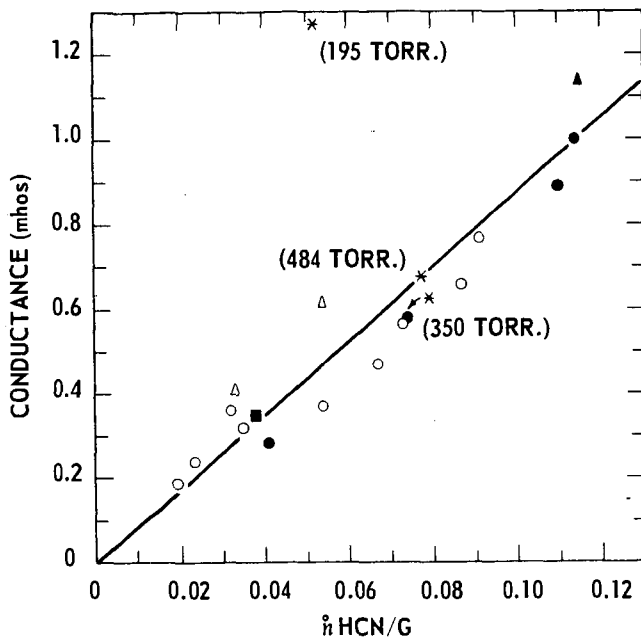
Same plot as Figure 3. ●-TR reactor at 9506 watts net power with reduced nitrogen flow ($G = 0.0125$ gram moles sec.^{-1}); highest enthalpy run. ○-SOR reactor at 2989 watts net power at feed slot ... power leaving head in gas was 5517 watts ... nitrogen feed rate 0.171 gram moles sec.^{-1} . Dashed line of slope one-third again shown.

Figure 5



Logarithmic plot of the flow rate of HCN (assumed equal to the flow rate of active species) relative to the flow rate of effluent nitrogen as a function of reciprocal average enthalpy at the point of introduction of methane. Point legend given in text. Line shown represents expected nitrogen atom population based on average enthalpy as calculated from equilibrium considerations.

Figure 6



Conductance (proportional to the fraction of nitrogen molecules ionized) vs. active species flow rate relative to effluent nitrogen. Legend of points corresponds to that of Figure 5. Points marked with asterisks correspond to the data of Table I.

HYDROCARBON REACTION IN CORONA DISCHARGE¹

M. Kawahata, J.C. Fraser, and J.A. Coffman

Advanced Technology Laboratories
General Electric Company
Schenectady, New York

-
1. This paper includes part of an investigation on "the coal hydrogenation by electric corona discharge", under the contract with the Office of Coal Research, Department of Interior.
-

INTRODUCTION

When an electric field (a-c in this paper) is applied to the series combination of a gaseous gap and a dielectric solid, the gas will break down and conduct at an applied voltage much lower than that required to break down the solid. The current increases rapidly with an increase in voltage. The dielectric barrier acts as a series ballast to stabilize the corona discharge, which appears as a "soft" glow electrical discharge. THIS FORM OF GLOW DISCHARGE AT ATMOSPHERIC PRESSURE IS DEFINED AS "CORONA"² in this paper. The dominant mechanism in corona

-
2. As contrasted with corona, the spark is a form of unstable discharge. Intense ionization along a definite path for a greater part of the electrode distance is a characteristic of spark. The arc is a form of concentrated spark characterized by a high current density at a relatively low voltage.
-

is ionization by electron impact. The free electrons in the gas acquire energy from the applied field, and, colliding with the gas molecules, create additional free electrons and positively charged ions.

Under stable corona electrical discharge in an electric field containing solid dielectric barriers, chemical reactions which only proceed with difficulty by conventional means may take place with reasonable efficiency. The chemical reactions caused by electric discharge are essentially those involving active species, like excited molecules, free radicals and ions, formed by inelastic collisions between accelerated electrons and molecules.

Extensive studies on the chemical reactions of aliphatic hydrocarbons under the electrical discharge were conducted in 1930's by Lind et al (3,4,5). Using methane as a reactant, the

-
3. S.C. Lind and G. Glockler, *J. Am. Chem. Soc.*, **51**, 2811 (1931).
4. S.C. Lind and G.R. Schultze, *ibid.*, **53**, 3355 (1931).
5. S.C. Lind and G.R. Schultze, *Trans. Electrochem. Soc.*, **59**, 165 (1931).
-

formation of free radicals followed by production of molecular hydrogen, and also condensation to higher paraffins was the essential process. Also, the reaction scheme and the reaction products of α -radiolysis were studied. A similarity between reactions in the electric discharge and radiolysis, was postulated by Lind et al (6,7).

-
6. S.C. Lind and G. Glockler, J. Am. Chem. Soc., 52, 4450 (1930).
 7. S.C. Lind and D.C. Bardwell, J. Am. Chem. Soc., 48, 2335 (1926).
-

The radiolysis of methane was investigated more recently in detail, especially to clarify the reaction mechanisms, including the primary and the secondary reaction processes (8,9,10,11,12,13).

-
8. F.W. Lampe, J. Am. Chem. Soc., 79, 1055 (1957).
 9. K. Yang and P.J. Manno, J. Am. Chem. Soc., 81, 3507 (1959).
 10. G.G. Meisels, W.H. Hamill and R.R. Williams, J. Phys. Chem., 60, 790 (1956).
 11. G.G. Meisels, W.H. Hamill and R.R. Williams, J. Phys. Chem., 61, 1456 (1957).
 12. G.J. Mains and A.S. Newton, J. Phys. Chem. 64, 511 (1960).
 13. R.R. Williams, Jr., J. Phys. Chem. 66, 372 (1962).
-

High energy electrons, low energy electrons, γ -ray and x-ray irradiations were employed for decomposition of methane, producing mainly H_2 , C_2H_6 , C_3H_8 , C_4H_{10} , and C_5H_{12} . It was found that the energy yield of the reactions were essentially independent of the radiation source, dosage, and the system pressure (6,7,8,9,10,11,12,13,14). However, because of the extreme complexity of the reaction processes, the mechanism is not yet completely understood.

-
14. S. Shida, Hoshasen Kagaku (Radiation Chemistry), Nikkan-Kogyosha, Tokyo, Japan (1960).
-

Electrical discharge chemistry has not yet studied intensively from the standpoint of chemical engineering except for a few processes (15,16,17). In order to achieve the technical progress in this field,

-
15. T. Rummel, Hochspannungs Entladungsschemie und Ihre Industrielle Anwendung, Munchen, Germany (1951).
 16. G. Glockler, and S.C. Lind, The Electrochemistry of Gases and Other Dielectrics, New York (1939).
 17. Electric Engineering Soc. Ozonizer Committee, Japan, edited by Suzuki Corona-sha, Tokyo, Japan (1960).
-

according to Suzuki et al, it is highly important to investigate the correlation between electric discharge phenomena and the chemical reactions caused by discharge. This includes: (1) clarification of the concentration and energy distribution of ions and electrons in the discharge space, (2) understanding of the probability of excitation and dissociation caused by collisions of molecules with slow electrons, and (3) clarification of the complete energy balance in the discharge reaction.

Recently in this laboratory, studies on hydrocracking of coal, tar, and related hydrocarbons, using an electric discharge system have been undertaken. This work was primarily intended to obtain chemical engineering knowledge of electric discharge chemical processes. As part of the program, decomposition of methane was studied, since this gas is likely to be used as one of the reactants for cracking of hydrocarbons, and further its simple chemical structure is well suited to definitive studies. Similar studies using aliphatic hydrocarbons other than methane were also conducted but they will be reported elsewhere.

EXPERIMENTAL

Apparatus The experimental apparatus is shown schematically in Figure 1-a. Methane was fed to the reactor with a definite flow rate determined by a rotameter. Then, the product gases were passed through a sampling bottle and a dry testmeter. The reactors employed in this investigation were essentially concentric electric discharge tube similar to ozonizers. The dimensions and the materials of the electrodes were varied, as summarized in Table 1. In Table 1, the discharge space, V , in cc., total surface area, S , in cm^2 , and the logarithmic average of the outside and inside electrode area, A , in cm^2 are listed together. On one side of the quartz electrode, a silver or tin oxide coating served as the electrically conductive surface. In order to determine the reactor temperature, thermistors were attached to the outside electrode and a thermometer was placed in the inside electrode. The electrical system is shown schematically in Figure 1-b.

The corona generating equipment used in these experiments consists of a high voltage, high frequency power supply, with associated instrumentation to control and measure the corona power generated. The output of a 10,000 cycle, 30 KW, inductor-alternator is fed to the primary of a 50 KV, high voltage transformer and, in turn, to a tuned circuit, to a corona cell, and to the high voltage instrumentation. The Basic Power and Instrumentation Circuit is shown on Figure 1-b.

Inductor-alternator output voltage and subsequently, transformer high voltage, are controlled from zero to maximum output by varying the alternator field current.

Since the corona cell itself represents a capacitive load on the inductor-alternator and the transformer, a tuning circuit is provided for power factor correction, so that the high voltage transformer sees only the resistive load represented by the corona power dissipated in the corona cell. This tuning circuit consists of an air-core, foil wound choke and a vacuum-capacitor bank, connected as a parallel resonant circuit across the transformer secondary.

High voltage instrumentation includes a vacuum tube voltmeter operating from a capacitance voltage divider, for reading the peak voltage applied to the corona cell, and a bridge circuit for determining corona power by means of the parallelogram-oscilloscope technique. This technique shows the relationship between the voltage on the cell electrodes at any instant and the charge flow in the circuit up to that instant. Using the area of parallelogram on the oscilloscope, the power input (18) to the reactor was computed.

-
18. The power dissipated in a concentric cylinder corona cell consisting of a gaseous gap in series with solid dielectric barriers can also be calculated from the expression:

$$P = 4fC_b V_g (V_m - V_t)$$

where P is power in watts,
 f is power supply frequency, c.p.s.,
 C_b is capacitance of the dielectric barriers,
 V_g is voltage across gaseous gap at the instant of corona initiation
 V_t is total voltage applied to the corona cell at the instant of corona initiation, and
 V_m is corona cell operating voltage, at some value greater than V_t .

In the above calculation, peak voltage values are used.

Procedures The entire system was first evacuated and methane was introduced to the reactor with a definite flow rate. The voltage applied to the reactor was gradually increased to the gas-space breakdown voltage, at which the electric discharge was initiated. Then, the voltage was adjusted until the parallelogram on the oscilloscope showed the desired discharge wattage. The discharge power was maintained constant during the run. The reaction was usually continued at least for 30 minutes before samples were taken. If there was liquid product in the condenser-I, it was weighed but no attempt was made to analyze it. The gaseous samples were analyzed by mass spectrometer. For reaction at higher temperatures, the methane was heated to the desired temperature in a preheater which was equipped with a temperature controller (West Co.).

EXPERIMENTAL RESULTS

Variation of the Composition with Residence Time The principal reaction products were hydrogen, ethane, propane, butane, pentane and further higher paraffins. In some experimental runs, a small amount of ethylene and propylene was found. In Figure 2 and 3, the variation of the composition with residence time is shown. These two sets of runs were conducted at temperatures between 200 and 230°C under a pressure of 760 mm Hg. The model III reactor was employed, and the current density levels were 0.13 and 0.15 ma./cm.². The current density was computed by using the voltage in the discharge space calculated from the total voltage applied, the discharge wattage and the logarithmic average area of the electrodes A, listed in Table 1. In these figures, the fraction C_2 and C_3 include ethylene and propylene, respectively, and the fraction $+C_4$ includes all the higher paraffin homologues.

It was observed that the disappearance of methane and the formation of H_2 , C_2 , C_3 and $+C_4$ were more rapid at the higher current density. In the initial period methane was consumed almost proportionally to time. This fact agrees to the results reported by Lind and Schultze(3) After this period, methane disappeared exponentially with time. It must be noted that in each of three runs having residence time longer than 100 seconds produced a small amount of liquid which was of amber color.

Effect of Temperature on the Initial Rate of Reaction Using the Model II and IV-C reactor, the initial rate of methane disappearance was investigated varying the reaction temperature. The reaction temperature was determined by taking the average of the inside and outside electrode temperatures. In Figure 4, is shown the Arrhenius plot of the initial rate of CH_4 disappearance in atm./sec. Two lines, AA and

BB, could be drawn, and the apparent activation energy of the overall reaction was calculated to be 4 Kcal./mol. The points along the line AA were determined at a current density of 0.095 ma./cm.² and an applied potential of 5 to 5.2 KV. across the discharge space using the model III reactor. The points along the line BB were determined at a current density of 0.15 to 0.17 ma./cm.² using the model IV-C reactor at 4.5 to 5.0 KV. across the discharge space. Both series were made under a pressure of one atmosphere.

Effect of Current Density on the Initial Rate of Reaction In order to correlate the initial rate of methane disappearance with current density, the rate of reaction at 200°C was computed from each rate obtained at various reaction temperatures by using the activation energy of 4 Kcal./mol. (The temperature, 200°C, is just an arbitrary temperature.) The computed rates of reaction are plotted against current density in Figure 5. The rate of reaction increased as the current density increased, following a relationship,

$$-\frac{d(\text{CH}_4)}{dt} = k(j) \quad (1)$$

where the rate is in atm./sec., the current density, j , is in ma./cm.², and k is 0.075 in average.

Electric Discharge in Space Packed with Alundum Grains and Effect of Pressure on the Rate of Reaction The discharge space of the model IV-B reactor was packed with alundum grains having a particle size of 10 x 15 Tyler mesh, to determine any consequent effect on the reaction rate. The total pressure of the system was also varied in two experimental runs. The experimental results are summarized in Table II. For this packed space reactor, the applied voltage required to initiate the discharge was greater and the discharge wattage was smaller than for the reactor without packing. For the packed discharge space reactor, the apparent current density and the apparent reaction rate are listed in Table II. The apparent dielectric constant of the space packed with alundum grains was calculated using Kamiyoshi's correlation (19), and

-
19. K. Kamiyoshi, Science Reports, Res. Inst. Tohoku Univ. Ser.A, 1, 305 (1949), C.A. 45, 5991
-

then the voltage applied to the packed discharge space and the apparent current density were estimated. For better comparison, the reaction rate at 200°C. was calculated for each run and listed in Table II. Since the rate increases with power density, it is seen that the reaction rate is considerably higher in the packed space reactor, and lower at reduced pressure.

Effect of the Uniformity of the Field on the Reaction Rate Using the several reactors having different diameter ratio, D_i/D_o , (the ratio between the inside diameter of the outside-electrode and the outside diameter of the inside-electrode), the possible effect of non-uniformity of the field on the reaction rate was investigated. It must be noted that for the model IV-D and the IV-E reactor, the inside electrode was tungsten rod or wire. (This type of reactor was called a semi-corona reactor by Lind et al.) The catalytic effect of the tungsten surface was assumed insignificant. It was observed that for these two reactors, discharge streamers were formed only around the center electrode, whereas in the other model reactors, numerous fine blueish streamers extended

from the inside electrode to the outside electrode resulting in formation of blue glow in all the discharge space.

The experimental results are listed in Table III. In the second experimental run, the IV-D reactor failed by arcing between the electrodes. Similarly, the experiment using the IV-E reactor was hindered by the formation of several hot spots on the tungsten electrode which resulted in arc-over between the electrodes. For better comparison, the reaction rates at 200°C were calculated using an activation energy of 4 Kcal/mol. and they are also listed in Table III. Taking into account the difference in current density, the reaction rate seemed lower in the reactor having larger D_i/d_o .

DISCUSSIONS

Based on studies of the radiolysis of methane, the following four steps may be considered to be of primary importance in the decomposition of methane by electric discharge:

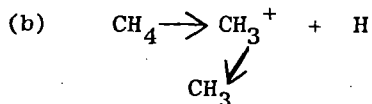
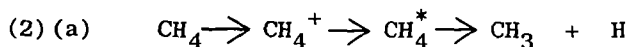
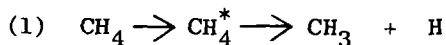
- (1) Formation of excited molecules by inelastic collisions with electrons having sufficiently high energy, and subsequent decomposition to free radicals and/or atoms.
- (2) Ionization of molecules and subsequent neutralization of ions, resulting in formation of free radicals.
- (3) Ion-molecule reactions (20), forming larger ions, and subsequent neutralization leading to formation of neutral molecules and free radicals.

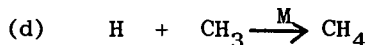
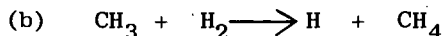
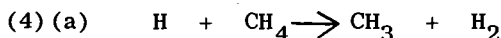
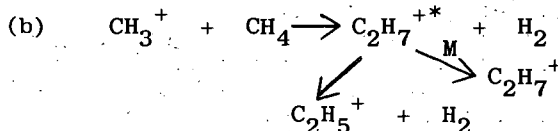
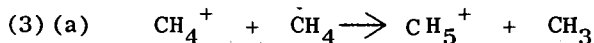
20. F.W. Lampe, J.L. Franklin, and F.H. Field, Kinetics of the Reactions of Ions with Molecules, in Progress in Reaction Kinetics, Vol. I, 67, Pergamon Press, New York, (1961).

-
- (4) Combination of free radicals or reaction of free radicals with molecules (21).

21. E.W.R. Steacie, Atomic and Free Radical Reactions, Reinhold Publishing Corp., New York (1954).

Thus, for example, the formation of ethane could be explained by the following steps:





Any attempt to explain the formation of higher paraffins leads to extremely complex reaction mechanisms involving successive ionizations or excitations of products by the electric discharge.

In this investigation, as noted earlier, the apparent activation energy of 4 Kcal/mol. was obtained for the overall rate of methane disappearance. For electric discharge reaction, it is reasonable to assume that the rate of reactions (1), (2) and (3) are essentially independent of temperature. The ion-molecule reactions, step (3), have also high specific rate of reaction. According to Steacie (21), for the free radical reactions, the activation energy is 6 Kcal/mol. for 4-(a), 10 Kcal/mol. for 4-(b) and 0 for 4-(c) and (d). There are other possible free radical reactions which could form ethane, but they have activation energies too high to be of importance here. For this reaction system, the concentration of high energy electrons produced by the electric discharge seems to be fairly low and, consequently, the concentration of free radicals formed may be low. Thus, it is probable that the role of free radical-molecule reactions could play an important role in the rate controlling sense. Further work is needed to clarify the mechanism.

The rate of the electron collision process in a positive column can be expressed by the following equation (22).

22. R.W. Lunt, The Mechanism of Ozone Formation in Electrical Discharges, in Ozone Chemistry and Technology, Advances in Chemistry Series (1959).

$$R = K \frac{(j)(p)}{(W)} \int_{V_e}^{\infty} v^{0.5} Q(v) f(v) dv \quad (2)$$

where, j is current density,
 W is electron drift velocity
 p is partial pressure of the reactant,
 $Q(v)$ is cross section for the reaction affect by electrons of energy v ,
 $f(v)$ is electron energy distribution function,
 V_e is critical energy, and
 R is rate of reaction.

If more than one kind of electron-reactant reaction is involved simultaneously, integral must be replaced by the sum of the integrals. In this investigation, the initial rate of methane consumption was found to be proportional to the current density when other factors are kept constant. Except for the initial time period, proportionality of the rate to the partial pressure of the reactant was also found as shown in Figure 2 and 3 which show the variation of methane concentration exponential to time. Taking into account the difference in current density, it is seen that proportionality between the rate and the pressure somewhat deviates for the packed bed reactor shown in Table II. This may be due to an uncertainty in estimation of the apparent dielectric constant of the alundum grains packed space and, therefore, in current density. However, as a first approximation, equation (2) seems to apply to this work.

Before corona is initiated the total applied voltage is distributed across the cell components inversely as their capacitance. Then, the voltage and gradients in a concentric cylinder reactor, just before the start of corona, can be expressed by the following expression:

$$E = \frac{V}{r k_g} \left[\frac{1}{\ln \left[\frac{(D_o/D_i)(d_o/d_i)}{k_b} \right] + \frac{\ln(D_i/d_o)}{k_g}} \right] \quad (3)$$

where, E is the field at any point in radius, r ,
 V is the total applied voltage,
 k_g and k_b are the dielectric constant for gas and barrier,
 respectively,
 D_o and D_i are the outside and inside diameter of the outside
 electrode, and
 d_o and d_i are the outside and inside diameter of the inside
 electrode.

After corona is initiated, the total applied voltage is distributed across the cell components directly as their impedance. However, this does not alter the equation (3) greatly.

Since,

$$\left(\frac{D_o}{D_i} \right) \left(\frac{d_o}{d_i} \right) \sim 1.0, \quad (4)$$

the equation (3) becomes

$$E \sim \frac{(1)}{(r)} \left[\frac{V}{\ln(D_i/d_o)} \right] \quad (5)$$

The drift velocity, W , and the integral term in equation (2) are a function of E/p , where p is the pressure. Thus, the overall rate of reaction becomes the integral of the equation (2) with respect to radial distance. Increasing the diameter ratio, D_i/d_o , appeared to cause a decrease in the overall rate of reaction. Since the exact expressions of $Q(V)$, $f(V)$, and W are not available, the analysis of the data is qualitative. Nevertheless, for the reactor having larger D_i/d_o , apparently a possible faster reaction rate in the strong field near the center electrode was overbalanced by the slower rate in the weak field portion of the reactor.

The rate of reaction was significantly increased, when the reactor discharge space was packed with alundum grains. This increase in the

rate cannot be explained clearly. Higher field in the packed space, surface reaction effects, if any, or higher concentration of high energy electrons in a smoothly diffused discharge formed in a packed space could be the reasons.

The energy yield of the process is shown in Figure 6, where energy introduced per unit mol. is plotted against methane consumption in per cent. The calculated reaction rates at 200°C were used for the plot. The slope, that is, the average energy spent per mol. of methane consumed was 1980 Kcal/mol. at 200°C for the initial period. The best result was obtained for the alundum grain packed reactor at 267°C. and the energy yields were 740, 1090, 3000, and 9000 Kcal per mol. of CH₄ disappearance, and H₂, C₂H₆ and +C₃ formation, respectively. The corresponding G values were 3.1 (-CH₄), 2.1 (H₂), 0.77 (C₂H₆) and 0.26 (+C₃). These values are about one-half of the values obtained by radiolysis (6,7,8,9,10,11,12,13,14).

ACKNOWLEDGEMENTS

The authors wish to thank T. H. Phoenix and G.A. Techy for their assistance in this experimental work, G. P. Schacher for mass spectrographic analysis, and N. R. Dibelius and C. D. Doyle for valuable discussions.

TABLE I
DIMENSIONS OF THE REACTORS

Reactor	Outside Electrode			Material	Inside Electrode		I.D. d_i mm
	Material	O.D. D_o mm	I.D. D_i mm		O.D. d_o mm	I.D. d_i mm	
II	quartz	19.0	17.0	quartz	11.0	9.0	9.0
III	quartz	45.7	42.4	quartz	35.3	32.0	32.0
IV-A	quartz	45.7	42.4	quartz	35.3	32.0	32.0
IV-B	quartz	20.0	18.0	quartz	12.0	10.0	10.0
IV-C	quartz	12.1	10.0	quartz	4.0	3.0	3.0
IV-D	quartz	9.5	7.3	tungsten	1.05	---	---
IV-E	quartz	8.5	8.3	tungsten	0.33	---	---

Reactor	Electrode Length L mm.	Discharge Space V cc.	Total Area S cm. ²	Average Cylindrical Area A cm. ²	Diameter Ratio D_i/d_o
II	78	10.3	71.7	34.0	1.5
III	400	168.0	975.0	488.0	1.2
IV-A	200	84.0	488.0	244.0	1.2
IV-B	200	29.0	188.0	93.0	1.5
IV-C	200	13.2	87.5	41.0	2.5
IV-D	200	8.2	52.5	20.4	7.0
IV-E	200	6.2	41.5	12.7	19.0

TABLE II

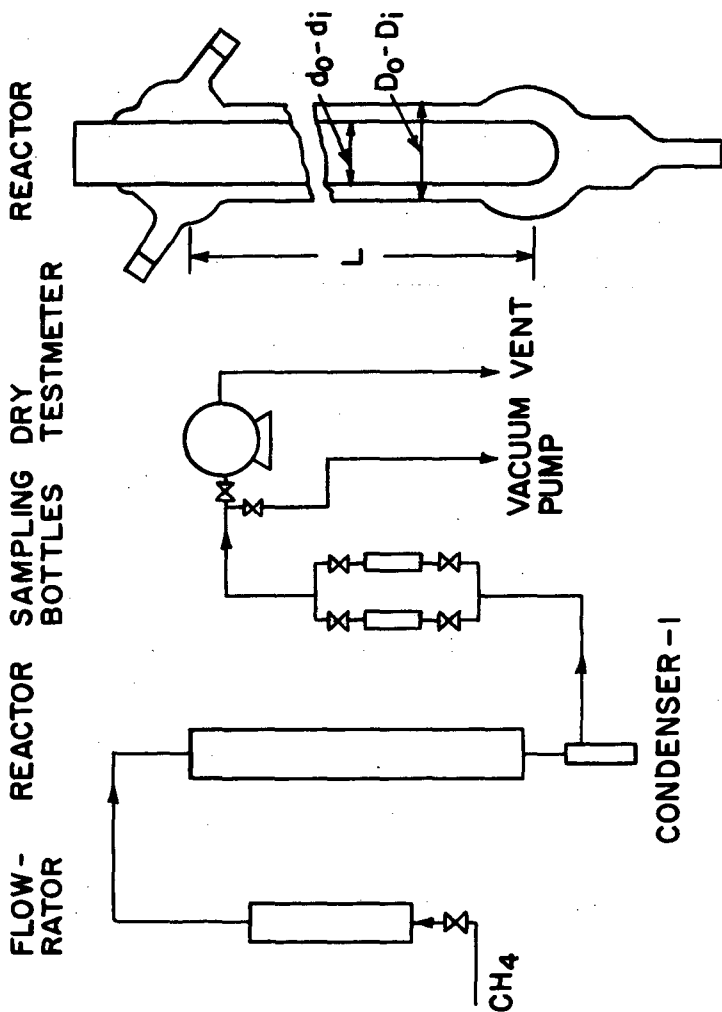
EFFECT OF THE REACTOR SPACE PACKED WITH ALUNDUM
GRAINS AND OF PRESSURES ON THE REACTION RATE
(IV-B REACTOR)

Exp. No.	Reactor Packing	Pressure mm.Hg	Temp. °C.	KV kv. g	Current Density, $2j$ ma./cm. ²	Rate (atm./sec.) $\times 10^2$	Computed Rate at 200°C (atm./sec.) $\times 10^2$
9-24-3-1	no	760	280	5.1	0.17	2.7	1.5
9-24-3-2	Al ₂ O ₃ grains	760	267	5.8	0.083	2.1	1.3
9-25-3-1	Al ₂ O ₃ grains	238	225	4.1	0.13	1.6	1.3
9-25-3-2	Al ₂ O ₃ grains	280	325	4.0	0.12	2.2	0.87

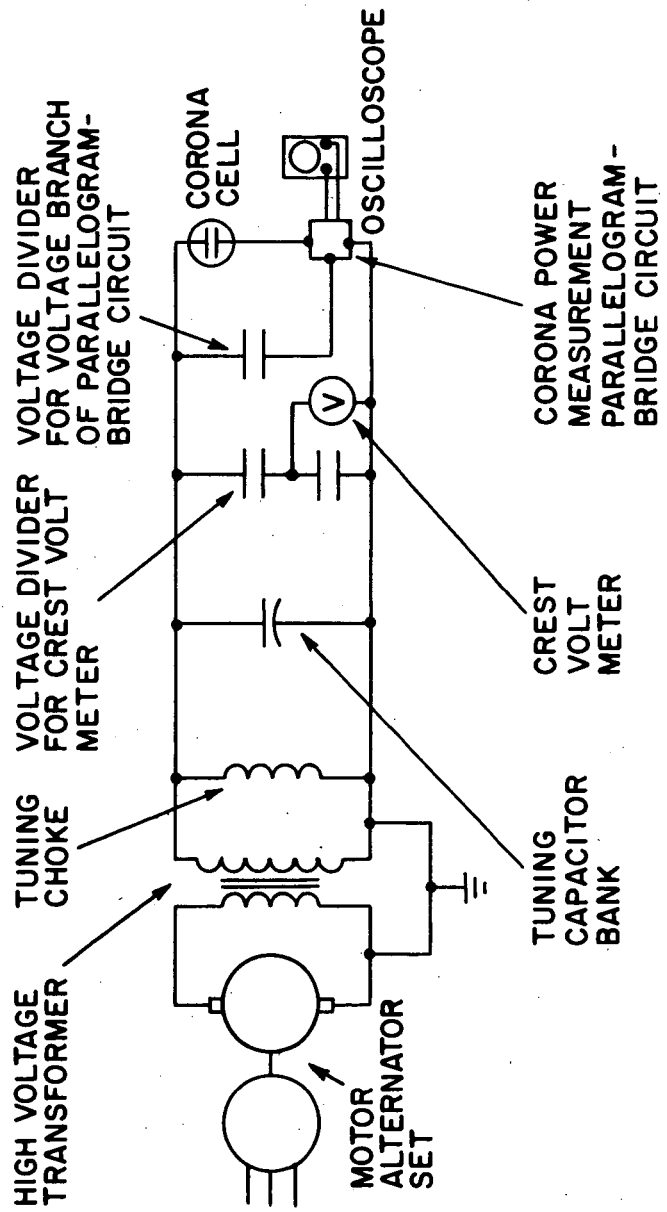
TABLE III

EFFECT OF UNIFORMITY OF THE FIELD ON THE REACTION RATE

Exp. No.	Reactor	D_1/d_0	Temp. °C.	KV kv. g	Current Density, $2j$ ma./cm. ²	Rate (atm./sec.) $\times 10^2$	Computed Rate at 200°C (atm./sec.) $\times 10^2$
9-24-3-1	IV-B	1.5	280	5.1	0.17	2.7	1.5
9-9-3	IV-C	2.5	215	5.0	0.15	1.1	1.0
9-11-31-1	IV-C	2.5	318	4.5	0.18	2.7	1.2
9-6-3	IV-D	7.0	217	4.8	0.32	1.9	1.7
9-16-3-1	IV-E	19.0	80	3.9	0.33	0.33	1.4
9-16-3-2	IV-E	19.0	110	4.4	0.32	0.48	1.3

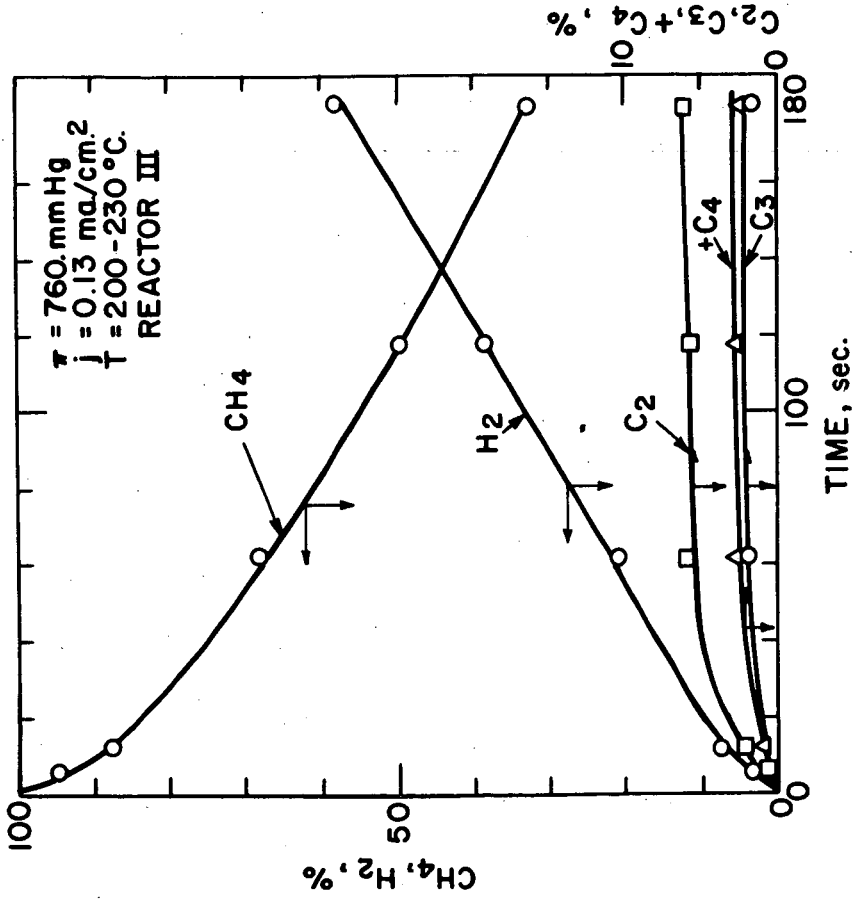


FLOW DIAGRAM OF THE APPARATUS
AND THE REACTOR
FIGURE 1-a

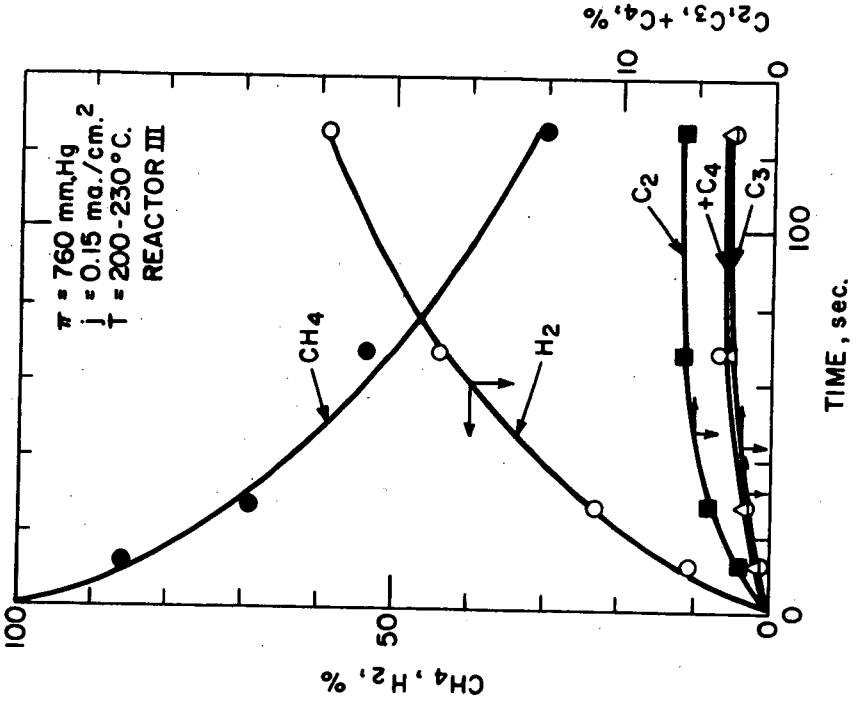


BASIC POWER AND INSTRUMENTATION CIRCUIT

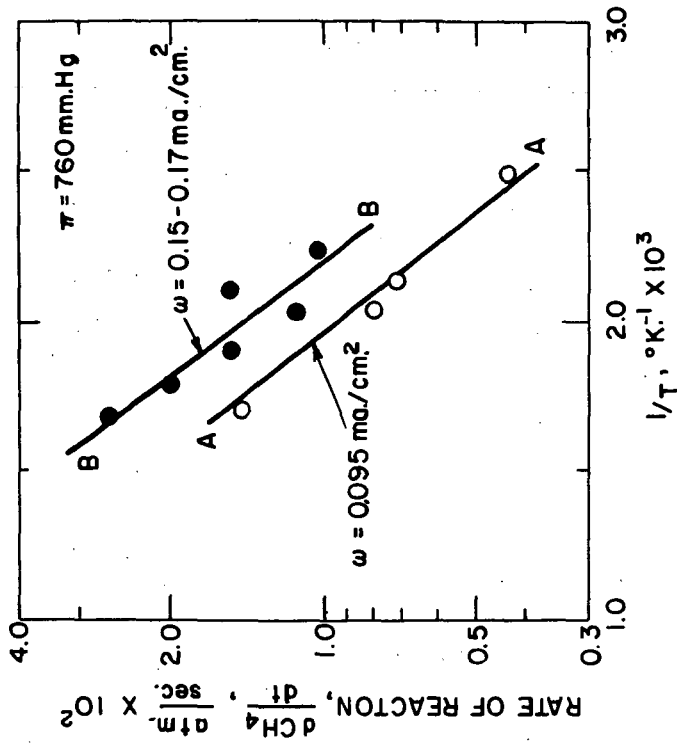
FIGURE 1-b



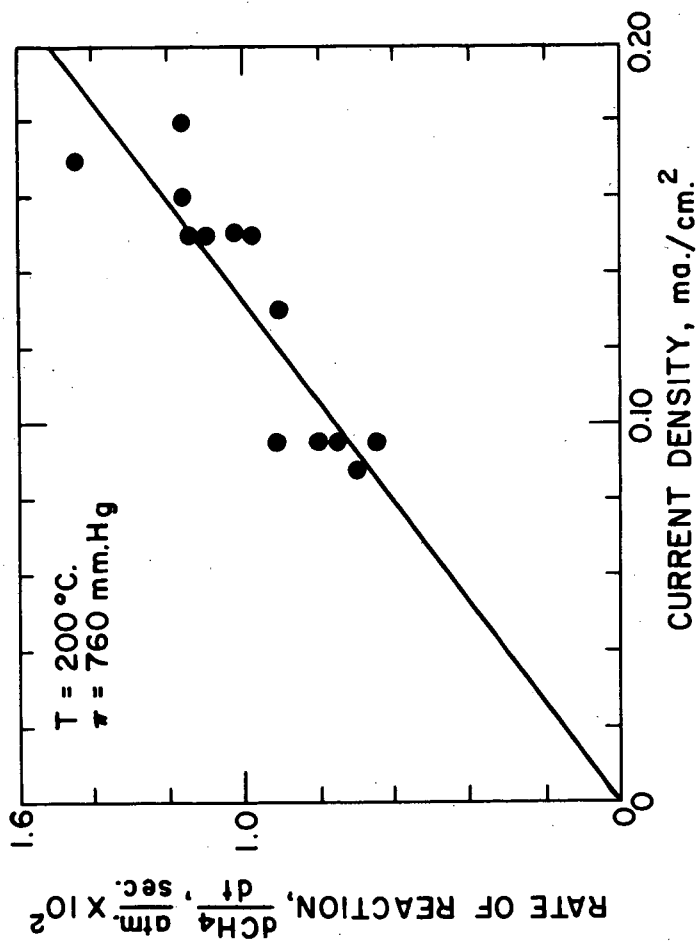
VARIATION OF COMPOSITION OF PRODUCT GASES WITH TIME
FIGURE 2



VARIATION OF COMPOSITION OF PRODUCT GASES WITH TIME
FIGURE 3

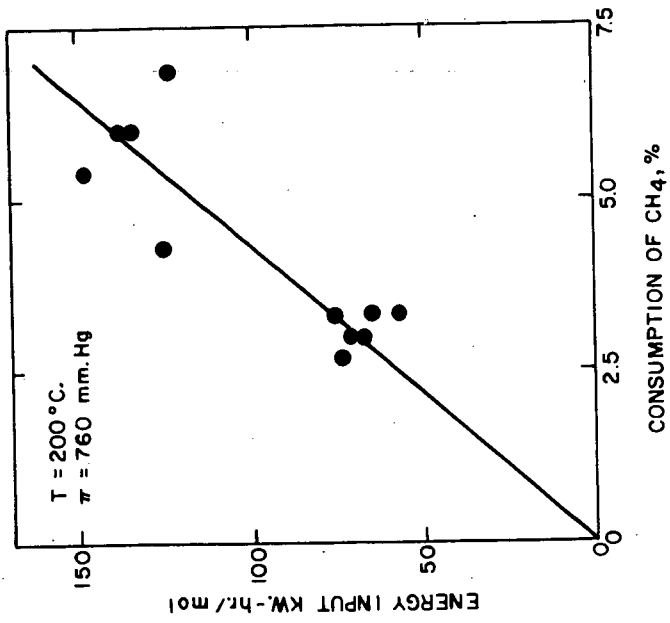


ARRHENIUS PLOT OF THE OVERALL
 RATE OF REACTION
 FIGURE 4



VARIATION OF RATE OF REACTION
WITH CURRENT DENSITY

FIGURE 5



VARIATION OF CH₄ CONSUMPTION
WITH ENERGY INPUT
FIGURE 6

PLASMA POLYMERIZATION

F. J. Vastola and B. Greco

Department of Fuel Technology, The Pennsylvania State University,
University Park, Pennsylvania

INTRODUCTION

Previous work with plasmas produced from hydrocarbons (1) demonstrated that both gaseous and solid plasma rearrangement products are produced. The distribution of these products depends upon the atomic hydrogen to carbon ratio of the reacting material. A limiting H/C ratio of approximately 1.6 was found for the solid. If the atomic H/C ratio of the starting material was greater than 1.6 both solid and gaseous products were formed, if the ratio was less than 1.6 only solid material was formed. With reacting gas ratios of less than 1.6 the solid would tend to have the same H/C ratio as the reacting gas.

The polymers produced by this process only depend upon the H/C ratio of the plasma and are independent of the molecular structure of the original reactants. With plasmas produced from single gases only a limited number of H/C ratios are available. However, by copolymerization of multicomponent mixtures solids of varying H/C ratio (max.=1.6) can be produced.

EXPERIMENTAL

Materials - Hydrogen (extra dry), acetylene (prepurified) and methane (CP) were obtained from the Matheson Co. The diacetylene was prepared according to the method described by Armitage, et al., (2) and purified by distillation.

Apparatus - The plasma generator consisted of a Raytheon* Diatherm unit (Model CMD 10) coupled to an Ophthos** cylindrical cavity. The frequency of the plasma generator was 2450 Mc. and the maximum output was 85 watts. The plasma reactions were carried out in a Pyrex bulb (vol.=150cc.) with a Vycor finger (OD=13mm).

Procedure - The experimental procedure consisted of filling the reaction bulbs with the reacting gas and analyzing the mixture mass spectrometrically before and after discharge; the H/C ratio of the solid produced is determined by making a material balance. The actual discharge takes place in the Vycor finger of the reaction bulb. The Vycor finger is positioned along the central axis of the cylindrical microwave cavity.

* Raytheon Co., Burlington, Mass.

** Ophthos Instrument Co., Rockville, Md.

RESULTS

Table I illustrates the relationship between the H/C ratio of the starting material and the H/C ratio of the solid produced.

Table I
DISCHARGE CHARACTERISTICS OF VARIOUS HYDROCARBONS

Mixture	H/C		Pressure, torr		Polymer Appearance
	Before Discharge	After Discharge	Before Discharge	After Discharge	
CH ₄	4.00	1.60	3.49	3.86	Clear
C ₄ H ₂ -H ₂	2.37	1.60	5.08	1.79	"
C ₂ H ₂ -H ₂	1.59	1.48	5.40	0.53	"
C ₂ H ₂ -H ₂	1.45	1.38	4.70	0.25	Very light brown
C ₄ H ₂ -CH ₄	1.38	1.28	3.75	0.67	"
C ₄ H ₂ -CH ₄	1.31	1.26	2.50	0.10	Light brown
C ₄ H ₂ -H ₂	1.23	1.20	2.70	0.05	"
C ₂ H ₂ -H ₂	1.20	1.20	4.10	0.02	"
C ₄ H ₂ -H ₂	1.20	1.19	5.42	0.15	"
C ₂ H ₂	1.00	1.00	5.02	0.03	Brown
C ₂ H ₂	1.00	1.00	4.90	0.03	"
C ₄ H ₂ -CH ₄	0.80	0.80	4.85	0.08	Dark brown
C ₄ H ₂ -H ₂	0.80	0.80	5.32	0.02	"
C ₄ H ₂	0.50	0.50	2.72	0.06	Very dark brown
C ₄ H ₂	0.50	0.50	3.35	0.02	"

If the initial H/C ratio is greater than 1.6 the solid will have a limiting H/C ratio of 1.6 and the remainder of the hydrogen and carbon in the system will be in the gas phase. Table II gives the composition of the gases remaining after a discharge lasting 120 seconds for a plasma produced from methane (H/C=4) and one produced from a diacetylene-hydrogen mixture (H/C=2.37).

Table II
Analysis, mole %

	CH ₄		C ₄ H ₂ -H ₂	
	Before Discharge	After Discharge	Before Discharge	After Discharge
H ₂	---	49	79	89
CH ₄	100	50	--	3
C ₂ H ₂	---	1	--	--
C ₄ H ₂	---	--	21	8

With a H/C ratio of less than 1.6 most of the starting material will be incorporated in the solid, and the discharge will be extinguished when the pressure remaining in the reactor reaches the lower pressure limit of the plasma generator.

Table III gives the time elapsed before a discharge will be extinguished for a series of diacetylene-hydrogen mixtures of constant total pressure and varying H/C ratio.

Table III
Plasma Extinction Time for $C_2H_4-H_2$ Mixtures

Total Pressure, torr	Ratio	Discharge Time, sec.
2.0	1.22	15
2.0	1.41	22
2.0	1.53	31
2.0	1.66	> 120

DISCUSSION

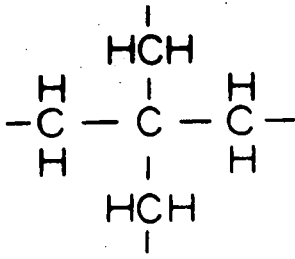
A hydrocarbon solid is one of the stable products formed by a hydrogen-carbon plasma. The maximum H/C ratio of this solid is approximately 1.6. This value cannot be exceeded even in cases where the H/C ratio of the plasma is greater than 1.6. The minimum H/C ratio of the solid is determined by the minimum H/C ratio of the hydrocarbon that is used for the plasma discharge, in this work the minimum H/C was 0.5 (diacetylene, C_4H_2). Table III illustrates that it is more difficult to produce solids as the H/C ratio approaches 1.6.

The physical appearance of the solids varied in a continuous manner from a clear, flexible film of H/C=1.6 to a very dark brown, brittle film of H/C=0.5. Infrared absorption analysis indicated no measureable aromatic structure even with a H/C ratio of 0.5. Absorption in the wave length regions 6.2 and 3.0-3.15 microns increased as the H/C ratio approached 0.5 indicating an increase in the degree of unsaturation. The decomposition products resulting from vacuum pyrolysis of the polymers were primarily hydrogen with a lesser amount of hydrocarbon gases ranging up to C_{10} . The majority of the C_4 to C_{10} hydrocarbons were highly branched compounds. No solvent was found for any of the polymers.

A possible structure for an insoluble, saturated aliphatic polymer with a H/C ratio of 1.6 is shown in Figure 1(a). This tetrahedral monomeric unit would form a three dimensional highly branched polymer; further hydrogenation would tend to destroy the polymeric structure. Since the polymers produced with H/C ratios varying from 0.5 to 1.6 seem to be part of a series, the structures shown in Figure 1(b) and 1(c) are possibilities of varying degrees of saturation of the basic monomer unit.

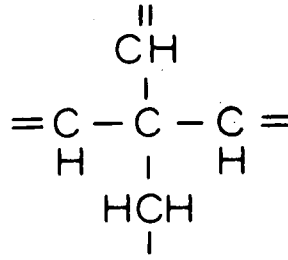
REFERENCES

1. F. J. Vastola and J. P. Wightman, *J. Appl. Chem.*, in press.
2. J. B. Armitage, E. R. H. Jones, and N. C. Whiting, *J. Chem. Soc.*, (1951), 44.



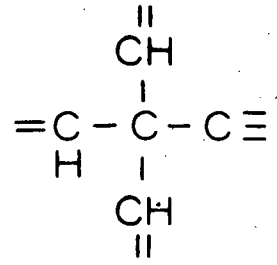
$$\text{H/C} = 1.6$$

(a)



$$\text{H/C} = 1.0$$

(b)



$$\text{H/C} = 0.6$$

(c)

MONOMER STRUCTURE FOR VARIOUS H/C RATIOS

FIGURE 1

Activation of Plastic Surfaces in a Plasmajet

Russell M. Mantell and William L. Ormand

AeroChem Research Laboratories, Inc.
Princeton, New Jersey

INTRODUCTION

The surface of a polymer such as polyethylene is difficult to paint, print, dye or laminate, unless previously prepared.¹ Methods of activating polymer surfaces may be conveniently divided into chemical, thermal, corona discharge, and the described non-equilibrium plasmajet types.

Typical chemical methods employ chromic acid solutions² or a combination of ozone and hydrogen halide.³ They do not appear to be of commercial importance.

Thermal methods which have been utilized industrially impinge heated air upon the surface⁴ while cooling the bulk of the plastic. The air is either preheated⁴ or a direct flame⁵ may be played on the surface.

Corona discharge methods, of recent industrial importance, pass polyethylene film over a rotating drum electrode while discharging a high frequency alternating current to the drum through a small air gap from a knife-edge electrode.⁶ Disadvantages of this process include puncturing of the polymer, inapplicability to inert, polar or readily-degraded polymers, and difficulties encountered in the treatment of irregularly-shaped or partly-conducting objects.

All of the above methods appear to involve some form of oxidation of the surface polymer while minimizing degradation of the bulk polymer. It is a convenient oversimplification to assume the thermal methods utilize diatomic oxygen, the corona discharge methods utilize triatomic oxygen, and a nonequilibrium

plasmajet method would utilize monoatomic oxygen. The latter was presumed to be the most reactive of the three oxygen species at low temperatures. Therefore, the oxygen plasmajet process was investigated in the hope of obtaining a novel,⁸ rapid and economical process for surface treatment capable of application to a variety of polymer surfaces.

The proposed plasmajet process described below utilizes a stream of oxygen which is partially dissociated by a glow discharge, expanded at high velocity through an orifice into a region of lower pressure, and then impinged upon the surface.

EXPERIMENTAL

Apparatus. The nonequilibrium plasmajet equipment utilized for the research is described elsewhere.^{9,10} It was modified by insertion, 12 inches downstream from the nozzle electrode, of a quick-opening Pyrex port of 4 inch I.D. by 12 inch length (measured at 90° from the axial reactor center). The port was closed by a 3/4 inch thick "Lucite" sheet, centrally drilled and tapped for a brass sleeve through which was loosely fitted a 1/4 inch diameter metal rod terminating in a 3 inch diameter by 1/4 inch thick brass target. The target was mounted so that the gas flow was parallel to the sample surface. Covering the target was a detachable metal hood into which the target and sample fit snugly to prevent exposure while operating conditions were being established. A thin Teflon sheet, cemented within the hood, contacted the plastic surface to be treated, to minimize abrasion. The hood and target arrangement was such that the specimen could be exposed at any desired distance from the jet axis. Vacuum-tight sliding seals were obtained by means of lubricated rubber couplings. The port permitted removal of the target and specimen within seconds after specimen exposure to permit an estimation by the use of a surface thermocouple of the film temperature attained. Insertion of the port into the apparatus was possible at various distances downstream from the nozzle electrode. Provisions were made for operation of the apparatus in a darkened room in order to permit visual observation of afterglow phenomena.

Materials. Oxygen, extra dry grade, and helium, 99.99% purity, were obtained in cylinders from the Matheson Company and dried immediately before entrance into the reactor by passage over activated alumina.

The following polymer samples were supplied through the kindness of the manufacturers: polypropylene, pro-fax type 6420 (Hercules); polyethylene, hi-fax type 1625 (Hercules); polyester, Mylar (duPont); polytetrafluoroethylene, Teflon type T.F.E. (duPont); polytrifluorochloroethylene, Kel-F type KX 8202 (3M Corp.); and polyvinyl fluoride, Tedlar type 50-SG20 TR (duPont).

The printing ink, Excellobrite White 500 (Sun Chemical Corp.) was similarly obtained. The lacquer employed was Duragloss, Camelia (A. R. Winarick, Inc.); the India Ink used was Pelikan Waterproof Drawing Ink (Gunther Wagner Co.) and the pressure-sensitive resin was "Scotch" Brand 600 acetate tape (3M Corp.)

Weightings. To remove electrostatic charges, a sample of the desired film, 1.0 mil thickness by 3.0 inches in diameter, was placed on the target, hooded and subjected to a 200 to 300 watt discharge at a pressure of about 1.0 Torr for a period of one second. The specimen was immediately weighed to 1/10 mg. on an analytical balance, replaced in the apparatus, exposed to the partially dissociated oxygen stream, reweighed and stored in air-tight containers. Finger cots and forceps were used in handling the specimens at all times.

Scratch Test. Exposed and control specimens of film were painted with commercial printing ink, lacquer and drawing ink, air-dried for at least 24 hours at room temperature, and manually scratched with a pointed stylus. Ratings were 1, 2 or 3 on a scale corresponding to unimproved, improved or greatly improved resistance to scratch removal relative to the control specimen.

Peel Strength Test. Exposed and control specimens of film were cut to 1/2 inch width and welded to pressure-sensitive tape of equal width. The weld was peeled apart at one end of the laminate. From the peeled end, the polymer was secured to a fixed point and the pressure-sensitive tape was attached to a balance pan, the weld itself being perpendicular to the force to be applied. The minimum force, in grams per inch, necessary to peel apart the remainder of the weld¹¹ was obtained by a successive increase of weights on the balance pan.

Surface Wetting Test. Exposed and control film specimens were secured to a horizontal table. A drop of water of 0.05 ml. volume was placed upon the film and the table slowly raised toward the vertical by a gear arrangement until the drop began to move across the surface. The angle which the film surface then made

with the horizontal is a measure of its surface wetting by water¹² and has been related to the adhesive properties of the film.¹³

Conditions. Unless otherwise noted, the conditions employed were as follows: 6 inch discharge electrode gap, 5/16 inch nozzle orifice diameter, 1 mil by 3 inch diameter sample, downstream pressure 3 Torr, upstream pressure 6 Torr, oxygen flow 5×10^{-3} mol/sec, axial distance 12 inches from discharge nozzle, radial distance from stream axis to sample 0.75 inches, maximum film temperature 80°C, and exposure time 900 seconds. The discharged gas contained 3 to 4% oxygen atoms at these conditions, as determined by light titration techniques.¹⁴

RESULTS

Reactor Parameters. A direct proportionality between weight loss and exposure time is shown in Figure 1 for polypropylene samples exposed under the conditions described earlier. The weight loss was also proportional to electric discharge power as shown in Figure 2. The intensity of the visually-observed afterglow¹⁴ was in qualitative agreement with the observed variation of weight loss. This was also true for the variation in afterglow downstream. Figure 3 shows that the effect of the stream on sample weight loss decreased as one proceeded further downstream from the nozzle exit. As the sample was moved from the center of the exhaust stream outward, the weight loss decreased rapidly and then leveled off. The leveling off at the wall boundary is consistent with the observation that the glow downstream of the discharge exit filled the whole tube, of 1.5 inches in diameter. No significance should be placed on the fact that the sample weight loss within this region decayed and was not flat, because the large structure of the sample holder would have destroyed any local atom distribution across the stream.

In the absence of electrical discharge or when oxygen was replaced by helium, no significant weight changes in the sample were observed. No significant deviation in the transmission of infrared spectra of the treated and control samples, was resolvable on a Beckman IR5 Spectrophotometer.

The results for the weight change and the scratch, peel strength and surface wetting tests for polyethylene, polypropylene,

polyvinyl fluoride, polyethylene terephthalate, polytetrafluoroethylene, and polytrifluorochloroethylene films exposed to the oxygen plasmastream are shown in Table I.

A rather good correlation is observed between the weight loss for polymers, upon exposure, with the scratch test, which is a measure of the strength of the substrate bond with inks and lacquers. Correlation with the other two properties, however, is not so clear. In the peel strength test, it is interesting to note that polypropylene has a greater strength than polyethylene before treatment, and is not essentially affected, while for polyethylene, a large change -- about three -- is effected. However, the opposite result is experienced when comparing polyethylene and polypropylene for the surface wetting test, *i.e.*, polypropylene is more affected. The surface wetting is most effective for the polyester and then, surprisingly, there is a large effect for the polytrifluorochloroethylene. In general, one might conclude from this table that the less stable hydrocarbon polymers of ethylene and propylene are relatively reactive to the oxygen stream, while the perfluorocarbon and perfluorochlorocarbon polymers are virtually inert, except for surface wetting. An intermediate order of reactivity is shown by the moderately stable and polar polyvinyl fluoride and polyethylene terephthalate (polyester).

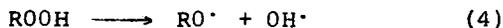
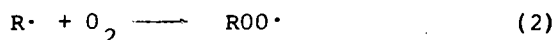
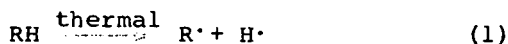
It is interesting to speculate on the effectiveness of the oxygen atoms in the stream for reacting with the surface. If we assume the oxygen atom reacts with a CH_2 group, we can then calculate the effectiveness of the stream by computing the number of oxygen atoms striking a CH_2 group on the surface. If we assume a surface cross-section for the CH_2 group in polyethylene of $25 \times 10^{16} \text{ cm}^2$, from the number of oxygen atoms which strike the surface under the experimental conditions, 6×10^{19} per $\text{cm}^2 \text{ sec}$, and from the observed weight loss, assuming the CH_2 group is removed from the surface, 2×10^{15} CH_2 groups per $\text{cm}^2 \text{ sec}$, will be removed. This means that about one in 10^4 oxygen atom collisions with the surface is effective. These numbers indicate that several monolayers of CH_2 surface are removed per second, which is difficult to rationalize with the observation in Table I that surface properties change considerably from one to 900 seconds.

DISCUSSION

Corona Discharge and Thermal Oxidations. Polyethylene film placed directly in a corona discharge of oxygen at one atmosphere has been shown to experience a loss in weight which is directly proportional to the time of exposure, and to gain weight when placed just below the discharge.¹⁵ Cooper and Prober related the formation of oxygenated surface products to reactions of the ozone (formed in the discharge) with double bonds of unsaturated polyethylene molecules. They ascribed the loss in weight of the polymer placed directly in the discharge to other reactions involving either electron or atom attack on the polymers, their data being inconclusive for a choice of mechanisms.

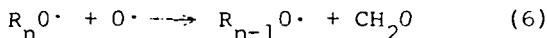
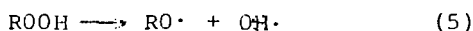
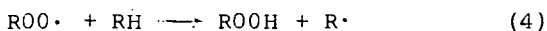
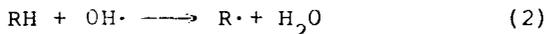
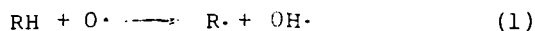
The present plasma work establishes that atom attack of the polymer is indeed a possible mechanism for surface reaction in the corona discharge although it does not rule out the possibility of other mechanisms.

Turning from corona discharge to thermally-induced oxidation of polyethylene and related compounds, the following simplified sequence of initial reactions has been discussed by Luongo¹⁶ and Grassie¹⁷



Plasmajet Oxidations. The data presented in this paper can be accounted for by the assumption of reaction of oxygen atoms with polymer to form oxygenated macromolecules which ultimately, through chain scission reactions, form products of lower molecular weight and higher vapor pressure. These volatilize and continuously expose fresh polymer surface. At steady-state conditions, an appreciable concentration of oxygenated macromolecular species must remain on this "fresh" polypropylene surface. The relatively polar oxygenated sites introduced on the polymer are responsible for the change in the surface properties of the treated samples shown by the data for the scratch, peel strength and wetting tests in Table I.

A possible series of reactions for the surface oxidation of polymer in the oxygen plasmajet is given below:



The collision of an oxygen atom with polymer initiates reaction as shown in steps (1) and (2). These free radical steps are unlike thermal initiation, in which energy must be supplied to the polymer.^{17,18} Steps (3) through (5), identical with the thermal sequence, show reactions of the undissociated oxygen (from the gas phase) with the surface polymer radicals. Degradation of polymer molecules by oxygen atoms is shown in step 6 to lead smaller radicals. These smaller radicals may sublime from the surface accounting for the weight loss. The surface recombination of polymer radicals is shown in step (7). Oxidation reactions may continue in the gas phase. Where chain termination steps such as (7) control the rate at which the polymer is degraded, the overall rate with respect to polymer consumption at a given free radical concentration can be expected to be constant with time in agreement with the data of Fig. 1.

COMMERCIAL CONSIDERATIONS

In corona discharge processes, the exact geometry and electrode separation as well as the composition and shape of the material treated can be expected to be of critical importance. Corona discharges concentrate at physical defects (pinholes, voids, and conductive occlusions) in polymers and rapidly enlarge them by electrical breakdown.⁷ In the nonequilibrium plasmajet process, the isolation of the discharge from the material treated

will make these factors relatively unimportant. The technique described in the paper has been experimentally used to treat small cubes, cylinders, partly-metallized films, and even textiles of polypropylene. There was no observed alteration of the physical integrity of the objects.

Cost estimations show the proposed plasmajet process to be competitive with corona discharge processes for polymer surface activation.

SUMMARY

A nonequilibrium plasmajet process for activation of polymer surfaces has been developed. A stream of oxygen is partially dissociated by a glow discharge, expanded to high velocity through an orifice into a region of lower pressure and impinged on the desired surface. Parameters measured before and after treatment of a variety of polymers include weight, surface bonding characteristics, and wettability. The weight loss of the polymer increases with exposure time, discharge power, and proximity to the atom source. In general, there is a correlation between the weight loss and the surface properties.

ACKNOWLEDGMENT

This research was sponsored by the Pfaunder Permutit Corporation. The authors gratefully acknowledge the contributions to this research of Mrs. H. F. Calcote, A. Fontijn, L. E. Rosner, S. C. Kurzius, and many other persons of the AeroChem Research Laboratories, Inc.

REFERENCES

1. Staff Article; Chem. & Eng. News 40, 30 (1962).
2. Horton, P.V.; U.S. 2,658,134 (1954).
3. Wolinski, L. E.; U.S. 2,715,075-6 (1955).
4. Kreidl, W. H. and Hartman, F.; *Plastics Tech.* 1, 31 (1955).
5. Kritchevar, M. F.; U.S. 2,648,097 (1957).
6. Traver, G. W.; B. P. 771,234 (1953).
7. Oliphant, Murray, Jr.; *Insulation* 9, 33 (1963).
8. Patent Applications on the process have been filed.
9. Rosner, L.E. and Calcote, H.F., AeroChem TM-10 October 1958; ASTIA AD 207 590.
10. Fontijn, A., Rosner D.E., Kurzius, S.C., *Can. J. Chem.* (submitted).
11. Wechsberg, L. E., and Webber, J.B.; *Soc. Plastics Eng. Tech. Papers* 5, 846 (1959).
12. McLaughlin, T.F.; *Soc. Plastics Eng. Tech. Papers* 6, 37 (1960).
13. Allan, A. J. G.; *J. Polymer Science* 38, 297 (1959).
14. Kaufman, F.; *Proc. Roy. Soc. A* 247, 123 (1958).
15. Cooper, Glenn D. & Prober, Maurice; *J. Polymer Science* 44, 397 (1960).
16. Luongo, J. P.; *J. Polymer Science* 42, 139 (1960).
17. Grassie, N.; Chemistry of High Polymer Degradation Processes, Butterworths Publications, Ltd., London, England (1956).

TABLE I

EFFECTS OF NONEQUILIBRIUM OXYGEN STREAM
ON POLYMER SURFACE PROPERTIES

TEST	Scratch, Numerical Rating ^a	Peel Strength, grams/inch	Surface Wetting, degrees tilt	Weight Loss, mg/sample ^b
TIME, sec	1 900	0 1 900	0 1 900	900
Polyethylene	2.7 3.0	360 420 1000	35 38 51	3.8
Polypropylene	3.0 3.0	1400 1350 1300	16 52 42	3.7
Polyvinylfluoride	2.0 2.5	100 120 200	23 38 23	3.4
Polyester	1.2 2.1	200 290 520	41 13 12	1.1
Polytetrafluoro- ethylene	1.0 1.5	66 50 54	25 33 39	0
Polytrifluoro- chloroethylene	1.5 1.5	210 220 200	20 36 53	0

a. Ratings 1 - 3 correspond to no change to great change.

b. 7.06 in² of surface area per sample were used.

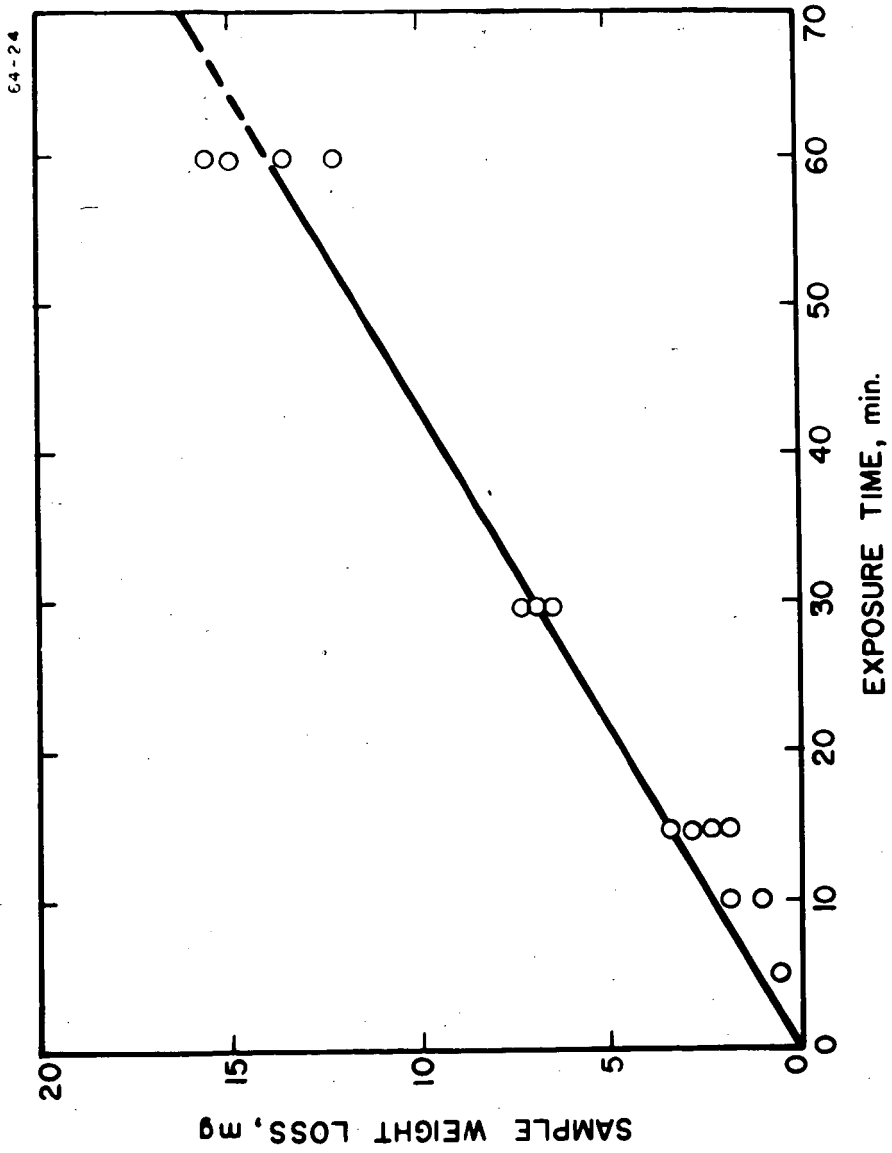


FIG. 1 THE INFLUENCE OF EXPOSURE TIME ON THE WEIGHT LOSS OF POLYPROPYLENE

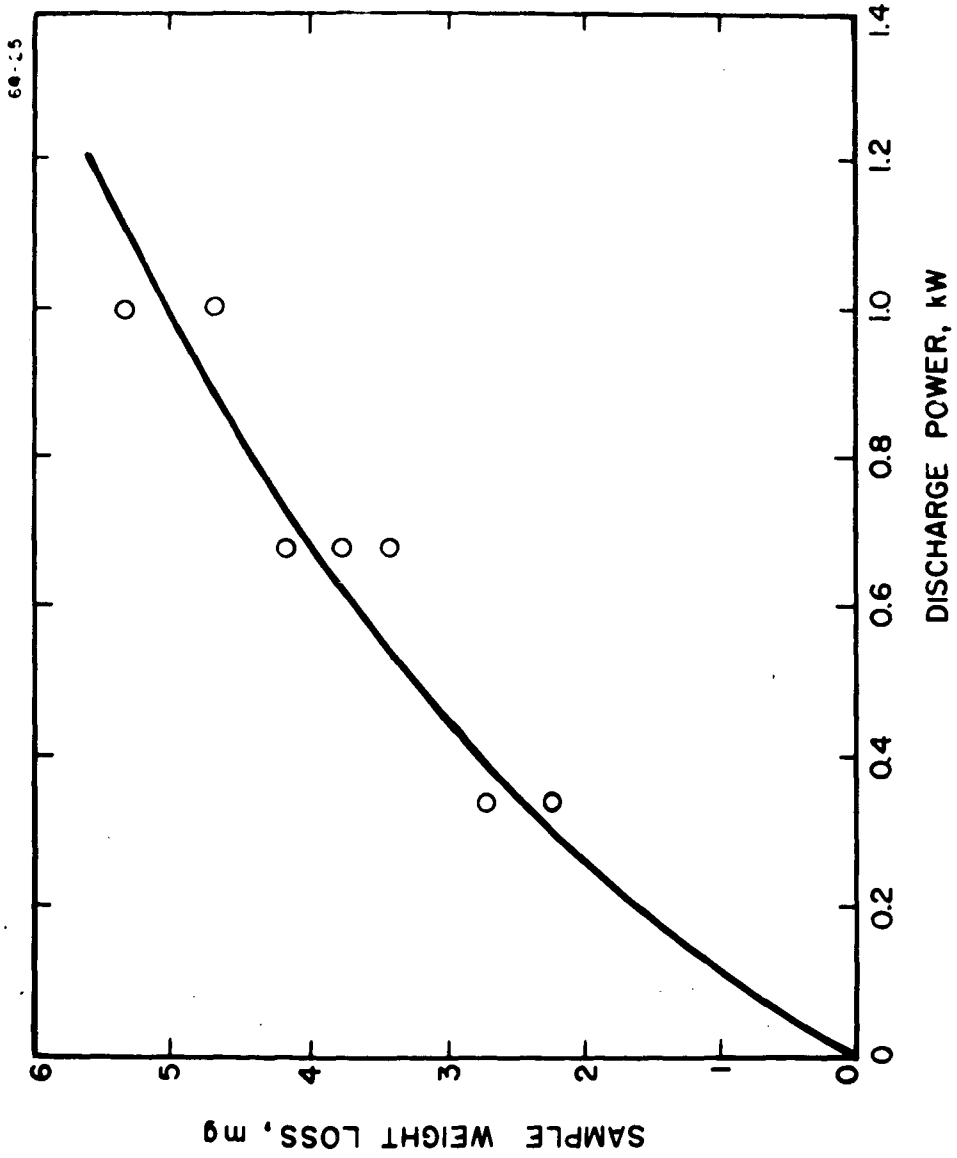


FIG. 2 THE INFLUENCE OF DISCHARGE ELECTRIC POWER ON THE WEIGHT LOSS OF POLYPROPYLENE

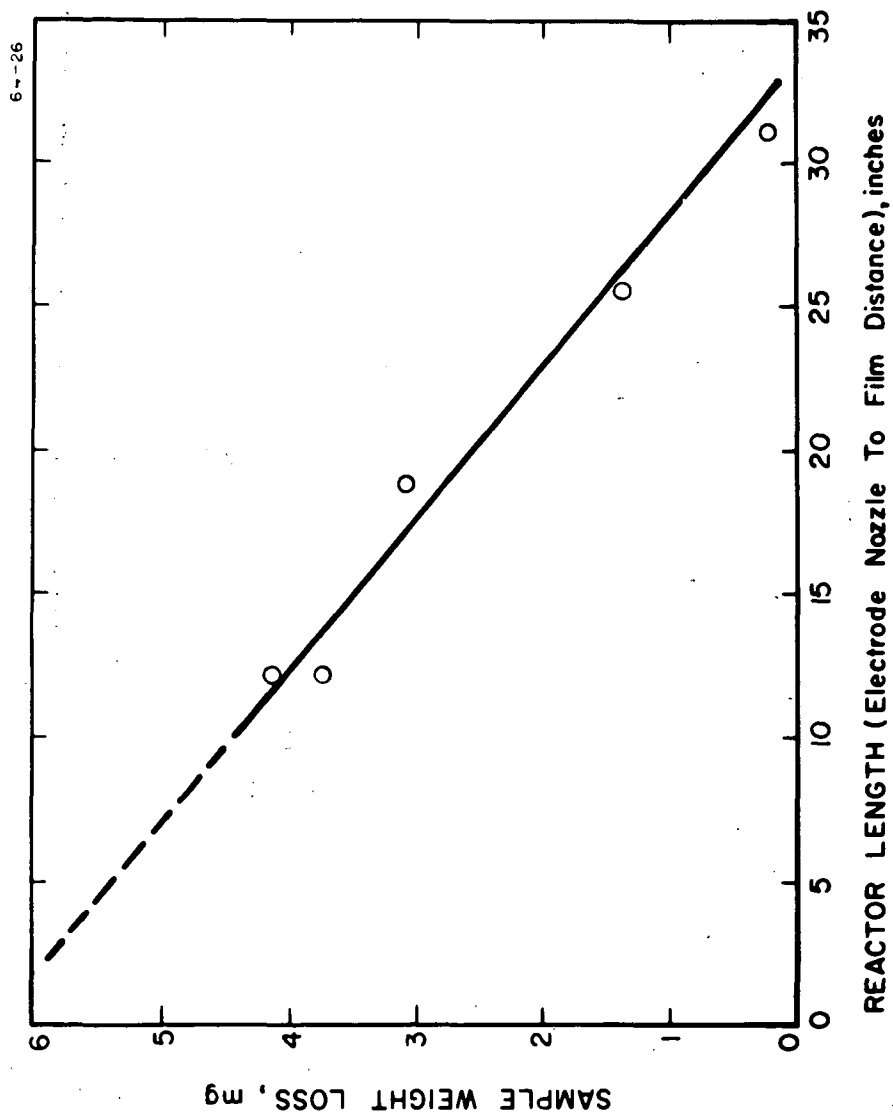


FIG. 3 THE INFLUENCE OF REACTOR LENGTH ON THE WEIGHT LOSS OF POLYPROPYLENE

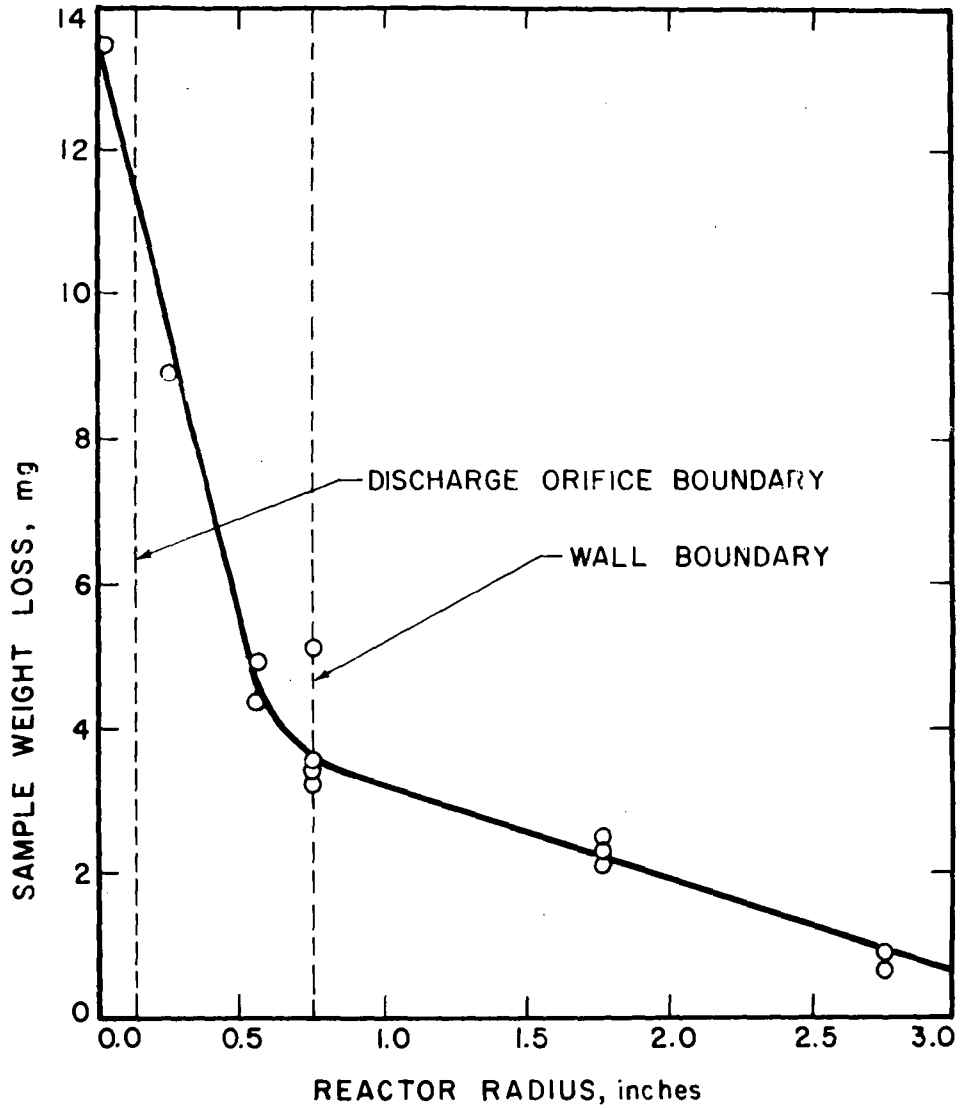


FIG. 4 THE INFLUENCE OF RADIAL DISTANCE ON THE WEIGHT LOSS OF POLYPROPYLENE

Interaction of Materials and Plasmas:
Spectroscopic Studies of Chemical Phenomena

L. Isaacson, T. Wentink Jr., G.J. Economou

Avco Corporation
Research and Advanced Development Division
Wilmington, Massachusetts

I. Introduction

Webster defines ablation as a removal or a carrying away. Thus, the ablation process, as applied to materials, denotes the removal or carrying away of material. To study this process, arc jets or plasma jets have been employed as sources to "ablate" samples. Reported here are the results from using various configurations of commercially available plastics. Surface characteristics (e.g., surface temperature, emissivities, and absence or presence of char formation and removal) and plasma interaction (e.g., the formation of gaseous degradation products) have been studied. To accomplish this, emission spectroscopic and spectrographic techniques were employed over the wavelength range 0.2-9.0 μ . Results of measurements on Delrin*, $(-\text{CH}_2-\text{O}-)_x$, Zelux, $(-\text{C}_6\text{H}_4-)_x$, $\text{C}(\text{CH}_3)_2-\text{C}_6\text{H}_4-\text{O}-(\text{C}=\text{O})-\text{O}-)_x$, and to some extent Teflon, $(-\text{CF}_2-\text{CF}_2-)_x$, will be cited as illustrative examples.

When heat is applied (in this case from the arc jet), the surface temperature of the materials rises until at some point the ablation process, and not the heating process, becomes the dominant mechanism controlling the chemistry. However, this ablation process can occur in several ways. First, a pseudosublimation may take place at the surface; namely, degradation of the polymer to gaseous products with no resulting surface changes; second, degradation of the polymer which leads to a change to the liquid state with subsequent flowing away of the liquid phase; and third, degradation of the polymer yielding some type of a char which either forms and blows off, or adheres to the model surface. Combinations of the above may also take place. Examples of the various types of ablators are graphite, quartz and Zelux respectively. A good discussion of ablation is given in reference 1.

II. Plasma Jet Characteristics

For the polymeric materials used, the heat inputs (enthalpies) and heat fluxes from the various plasma jets are more than enough to cause ablation to be

*Delrin is the DuPont trade name for Polyoxymethylene, the Celanese Corp. produces this material under the tradename Celcon. Lexan is a commercially available polymer resin which in the final, fabricated form is known as the plastic Zelux.

¹M.C. Adams, ARS J., 29, 625 (1959).

the dominant decomposition mechanism. One type of plasma jet employed is of the same type as that described by Watson, Ferguson, and Nicholls.² Another type is similar except that a plenum chamber (for adding gas downstream and thus being able to produce simulated air) was used. The electrodes are of the noneroding type (a copper anode and a thoriated tungsten cathode).

Although the plasma jets are not in complete thermal equilibrium, the approach to equilibrium is much closer here than in glow discharges at the same pressure.

With nitrogen as the propellant gas, the arc power was of the order of 25 kw while the enthalpy (H/RT) was 220 (7392 Btu/lb).

III. Experimental Techniques

It is possible, with infrared techniques, to follow the surface behavior of plastic materials when they are subjected to the plasma jets by determining surface temperatures as a function of time, and surface temperature and emissivity as a function of wavelength. Dramatic changes in surface temperature will also give an indication of char formation and propagation. To carry out these measurements, a CaF₂ or NaCl prism was used in a Littrow configuration which was coupled with a Au-doped Ge detector chopped at 690 cps. The spectra or other traces were displayed on a Tektronix Type 502 oscilloscope by sweeping the scope at the desired rate. For time histories, the wavelength is kept fixed. For spectral scans, the Littrow mount is driven by a cam which oscillates the mount and scans the desired $\Delta\lambda$ every 0.2 second. For wavelength calibration, a helipot is attached to the Littrow arm and a periodic wave is displayed on one beam of a dual-beam oscilloscope; the signal output is displayed on the other. A Barnes black-body is used to give absolute temperature calibration.

For all visible and ultraviolet results, the spectra were recorded photographically on a Hilger E498 (all quartz) or E528 (quartz and glass employing quartz optics) using Kodak 103-F plates. The F plates were used because the widest wavelength coverage (0.23 to 0.70 μ) could be obtained without serious loss of sensitivity.

The IR gaseous spectra (0.8 to 1.5 μ) were taken with a single pass monochromator employing an SiO₂ prism and PbS detector and were recorded on a dual-beam oscilloscope (signal output on one beam and drum number readings on the other).

IV. Surface Characteristics

Figure 1 is the room temperature absorption spectrum of Delrin, while figure 2 is the emission spectrum (2 to 7 μ) for a Delrin sample ablating in a nitrogen plasma jet. Note the strong absorption and emission in the 3.3 μ region and beyond 7 μ while there is weaker absorption and emission in the 4.0 to 6.5 μ regions. Thus, from figure 2, we have determined the surface temperature of Delrin at $\lambda = 3.3\mu$ to be $725 \pm 10^\circ\text{K}$. The approach used to deduce the surface

²M.D. Watson, H.I.S. Ferguson, R.W. Nicholls, Can J. Phys., 14, 1405 (1963).

temperature was to compare the absolute radiant emittance obtained with that from a calibrated blackbody in a spectral region where the assumption of the emissivity, ϵ , near unity is valid. This assumption in turn, is based on transmission measurements of absorption spectra of thin films to determine the wavelengths where the absorptivity is so large that the emissivity also must be near one; i. e., Kirchoff's Law is invoked. This assumption of near unit emissivity is most uncertain in the case of charred materials where often the reflectivity can be high in the infrared.

With a heavy char former such as Zelux, the surface temperature varies quite widely with time, so in order to watch this behavior a constant wavelength is picked and the behavior is scanned as a function of time. Figure 3 gives the IR emission from ablating Delrin and figure 4 gives the IR emission from ablating Zelux; both taken at $\lambda = 3.4\mu$. The big difference between the heavy char former (Zelux) and the non-char former (Delrin) is readily apparent when the two figures are compared. The spikes in figure 4 show the super-heating and blowing off of the char layer.

Figure 3 will also illustrate another point. Note that in the beginning (up to 1/2 second) the voltage rises very rapidly and then changes slope. We have called this point the "breakpoint" and ascribe it as the point where the rate of ablation has become large enough to control the surface temperature. For a number of materials, the breakpoint temperature obtained from these plasma jet measurements has been correlated with those obtained from thermogravimetric analysis (TGA) decomposition experiments. One such experiment for Delrin in air is illustrated in figure 5. For Delrin, we measure the breakpoint temperature as $593 \pm 10^\circ\text{K}$, and from TGA, the temperature for 100 percent decomposition is 605°K . Because of char formation, the heavy char formers do not usually yield a well defined breakpoint (note figure 4).

V. Gaseous Products

The sample configurations used to date to obtain gaseous spectra are pipes and cones. The pipes are 4-1/2 inches long and 2 inches in diameter. The hole through which the gas flows is initially 1 inch in diameter. Because of the nature of the jet, the flow through the pipe is laminar. The cones employed have 1-inch base diameters and an included angle of 20 degrees. When the plasma interacts with the cone, a shock wave is set up and the region between the shock envelope and the surface consists of high temperature gas highly contaminated with ablation products, and as an emission source has considerable intensity.

Figures 6, 7, and 8 are spectra of a Zelux pipe in a Helium jet, a Zelux pipe in a nitrogen jet, and a Zelux cone in a nitrogen jet, respectively. Table I is a compilation of the species identified as present and illustrates the effect of a change in the plasma gas and in the sample configuration. The helium plasma jet produces a hotter jet (higher gas temperature) than the nitrogen jet while the effect of a higher temperature due to shock wave effects can be seen by comparing figures 7 and 8.

A close examination of figure 8 shows that three of the dominant radiating species in the visible are CN, CH, C₂. Kokline³ firing preheated Zelux models at 16,000 ft/sec in a ballistic range also finds the three predominant visible radiators as CN, CH and C₂. Thus, although two widely different experimental media have been used, under the proper conditions there is correlation in the results obtained. In this way, one sees that plasma jet results can point the way to, and act as, a starting point for more sophisticated experiments. One such experimental medium is the shock tube. In noting the various species that are formed during degradation of a plastic in a plasma jet, mixtures of gases which, when shocked, will yield the appropriate species, can then be studied by simultaneously monitoring the important wavelengths. With a drum camera, it would be possible to monitor variations in the behavior of some species in the visible region. One advantage of the plasma jet is the large test time one has when compared with ballistic ranges and shock tubes.

Infrared measurements in the 0.8 to 2.0 micron region showed strong gas radiation characteristic of the CN red system when a Zelux model ablated in a nitrogen arc. A similar scan of the nitrogen jet without any model produces the first positive system of nitrogen, but at a much lower intensity level.

Figure 9 is the spectrum obtained when a Teflon model ablates in an Argon plasma jet. The principal diatomic, UV radiator is CF along with some continuum radiation. The CF spectrum that is produced is quite pure and avoids many of the impurities (e.g., CF₂, S) encountered by other investigators. The relatively short test times needed to obtain decent intensity compared with other methods (e.g., flames) is well illustrated. Thus, by picking the proper material and arc gas, one can obtain and study, relatively easily, high temperature diatomic species.

VI. Acknowledgment

The work reported in this paper was supported by contracts with the Air Force Ballistic Systems Division (AFBSD) of the Air Force Systems Command.

The authors acknowledge with appreciation the advice and help of many individuals at RAD during the course of this work and to Dr. T. Marshall for reading and commenting on this manuscript.

³A. Dmitrieff-Kokline, Spectrographic Studies of the Radiation Emitted by Hypersonic Projectiles, Canadian Armament Research and Development Establishment, TN-1564, May, 1963.

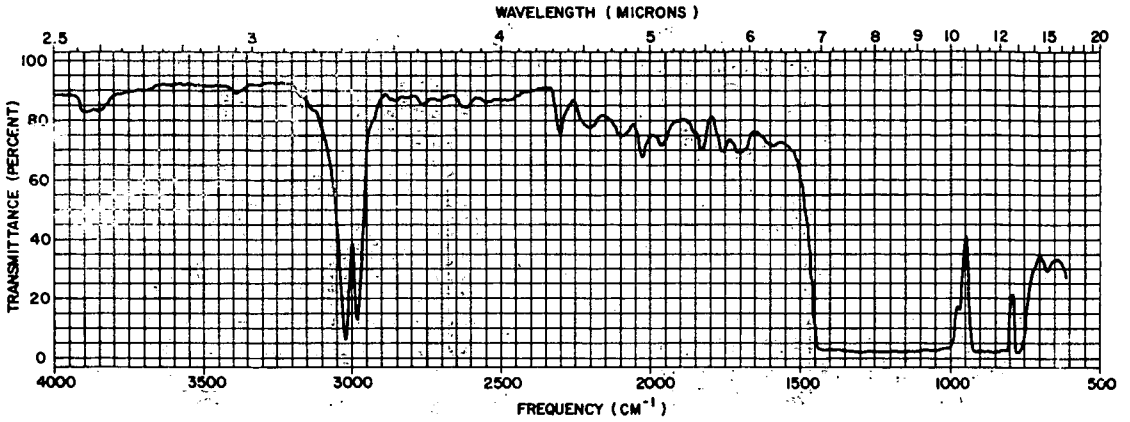
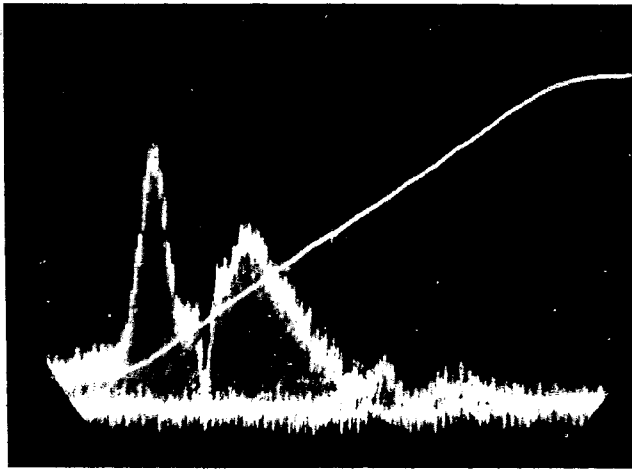
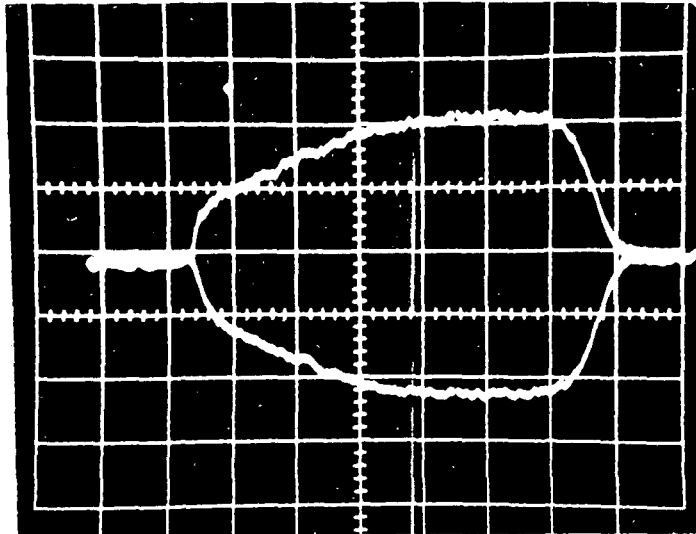


Figure 1 ROOM-TEMPERATURE INFRARED ABSORPTION SPECTRUM OF DELRIN (0.003-inch Film)

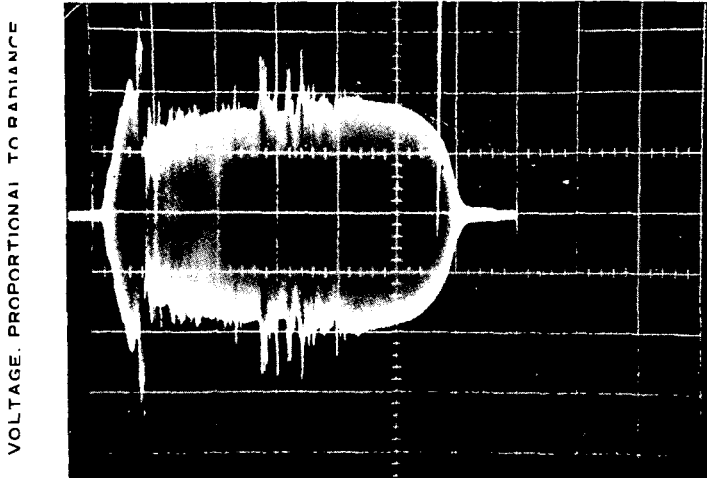


3.0 3.4 4.3 4.9 6.2 7.5 μ
 CO₂ H₂O null

Figure 2 DELRIN INFRARED EMISSION SPECTRUM (0.5 V/cm)



($\lambda = 3.4$ MICRONS)



64-1245

Figure 4 INFRARED EMISSION HISTORY OF ABLATING ZELUX
($\lambda = 3.4$ MICRONS, 5 SEC/CM SWEEP)

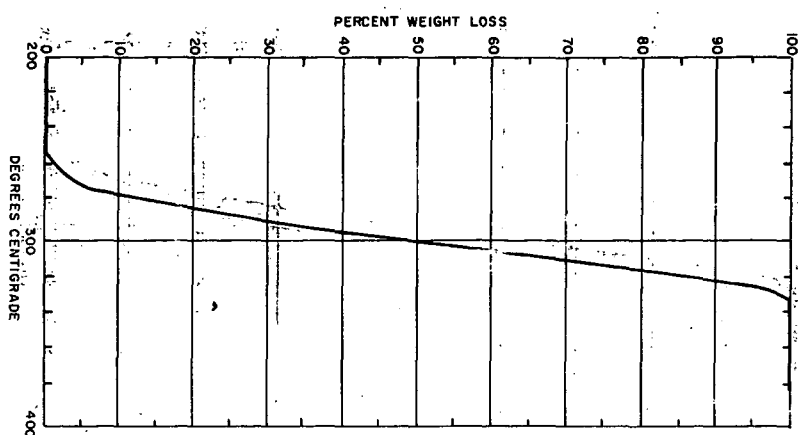
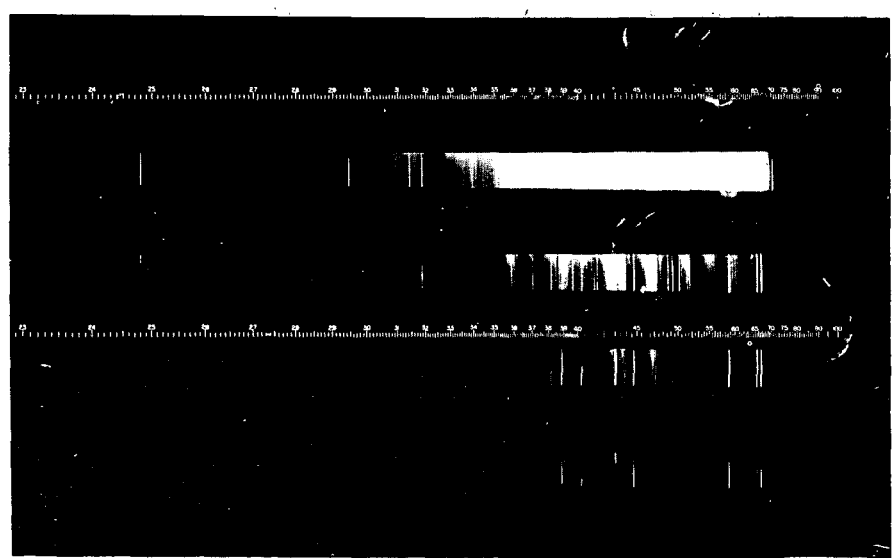


Figure 5 THERMOGRAVIMETRIC ANALYSIS, DELRIN IN AIR

ZELUX PIPE/HELIUM
2300 A

- a NO ARC SPECTRUM
- b Sw, 10 SECONDS
- c Sw, 1 SECOND
- d Sw, 1/5 SECOND
- e Sw, 1/25 SECOND



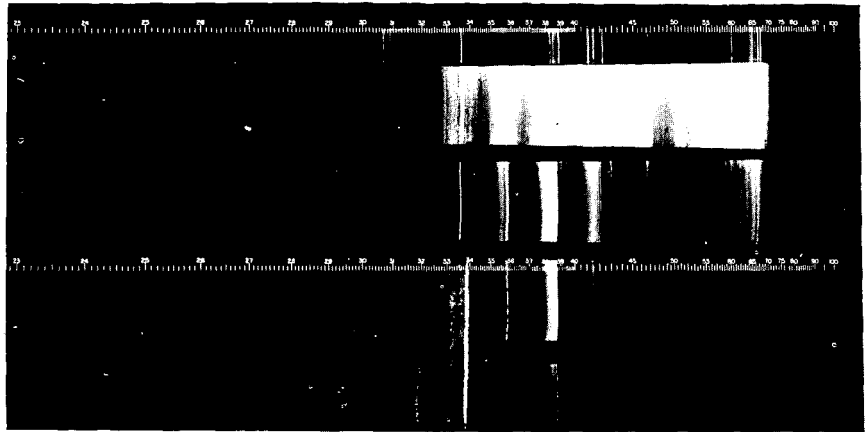
Sw = 60-micron slit
EXPOSURE TIMES AS GIVEN ; a PLUME ONLY ;
b THROUGH e WITH MODEL IN STREAM

63-7171

Figure 6 ZELUX PIPE -- HELIUM

ZELUX PIPE / NITROGEN
2300A

- a Sw, 10 SECONDS
- b Sw, 10 SECONDS
- c Sw, 1 SECOND
- d Sw, 1/5 SECOND
- e Sw, 1/25 SECOND

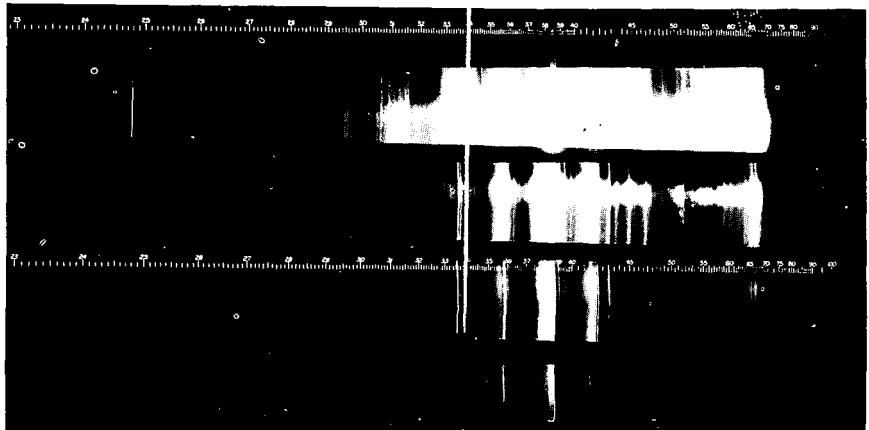


Sw = 60-MICRON SLIT
EXPOSURE TIMES AS GIVE; a PLUME ONLY;
b THROUGH e WITH MODEL IN STREAM

Figure 7 ZELUX PIPE -- NITROGEN

ZELUX CONE / NITROGEN
2300A

- a Sw, 1 SECOND
- b Sw, 10 SECONDS
- c Sw, 1 SECOND
- d Sw, 1/5 SECOND
- e Sw, 1/25 SECOND

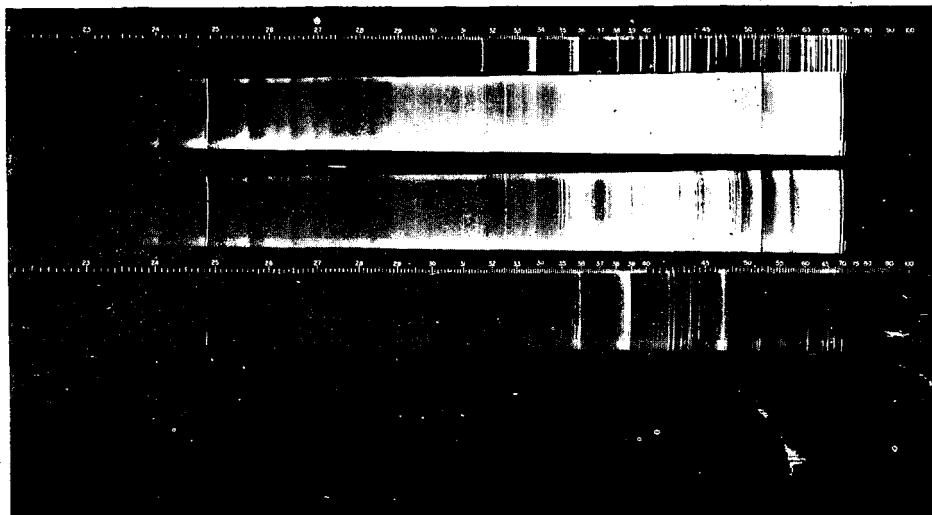


Sw = 60-MICRON SLIT
EXPOSURE TIMES AS GIVE; a PLUME ONLY;
b THROUGH e WITH MODEL IN STREAM

Figure 8 ZELUX CONE -- NITROGEN

TEFLON CONE / ARGON
2200 A

- a. Sw, 10 SECONDS
b. Sw, 20 SECONDS
c. Sw, 10 SECONDS
d. Sw, 1 SECOND
e. Sw, 1/5 SECOND



Sw = 60 micron slit
EXPOSURE TIMES AS GIVEN; a PLUME ONLY;
b THROUGH e WITH MODEL IN STREAM

Figure 9 TEFLON CONE -- ARGON

TABLE I

SPECIES IDENTIFIED IN SPECTRA OF ZELUX-CONTAMINATED GASES

ZE Pipe/He (Figure 2)	ZE Pipe/N ₂ (Figure 3)	ZE Cone/N ₂ (Figure 4)
C (s) ^a	C (m)	C (s)
H (s)	H (w)	H (m)
-	CN (s)	CN (s)
CH (m)	CH (m)	CH (m)
C ₂ ^b (m)	C ₂ (m)	C ₂ (m)
-	NH (m-w)	NH (s)

a: s = strong, m = medium, w = weak mean relative intensities from visual estimates of spectral plates.

b: Besides the C₂ Swan systems that are identified, the following C₂ systems (with bandhead values) also are identified as present when ZE pipe is in a helium plasma jet: Fox-Hersberg (heads at 2855, 2987, 3129, and 3283 Å), Deslandres-D'Azambula (heads at 3400, 3588, 3607, 3850, 4040, 4060, and 4100 Å).

Edwin S. Campbell

Department of Chemistry
New York University
New York 53, N.Y.

1. Introduction.

A new solution of the one-dimensional time-independent hydrodynamic equations for an ozone flame which avoids some approximations made in earlier calculations yields some qualitatively different results.

The mathematical model is summarized in Section 2, the physical model and numerical parameters in Section 3, the numerical methods and the character of the eigenvalue problem in Section 4. The solution curves are analyzed in Section 5 in terms of the physical and chemical processes within the flame as a part of a study of how these processes depend upon fuel properties. The main conclusions are summarized in Section 6.

2. Mathematical Model.

This study uses the one-dimensional time-independent hydrodynamic equations in the forms suggested by Hirschfelder and Curtiss¹

$$\text{Continuity of species } i: dG_i / dZ = m_i R_i / M \quad (1a)$$

$$\text{Diffusion of species } i: dx_i / dZ = (K / n) \sum_{j \neq i} D_{ij}^{-1} \left\{ (x_i G_j) / m_j - (x_j G_i) / m_i \right\} \quad (1b)$$

$$\text{Energy balance: } dT / dZ =$$

$$(M / \lambda) \sum_j \left\{ (H_j G_j) / m_j - \lim_{Z \rightarrow \infty} (H_j G_j) / m_j \right\} \quad (1c)$$

$$P = n R T \quad (1d)$$

where

$$G_i = \text{the fractional mass-flow rate of species } i = m_i n_i v_i / M \quad (1e)$$

m_j : the mass of species j in g./gmol.

n_j : the concentration of species j in molecules/cc.

v_j : the average velocity of particles of type j with respect to a fixed axis system.

M : the total mass-flow rate with respect to a fixed axis system = $\sum_j n_j m_j v_j$.

D_{ij} : the binary diffusion coefficient for the pair i, j in $\text{cm}^2 \cdot \text{sec}^{-1}$.

$x_j = n_j / n$, the mol-fraction of species j

n : the total concentration in molecules/cc. = $\sum_j n_j$

H_j : the enthalpy of species j in cal./gmol

λ : the thermal conductivity of the gas mixture in $\text{cal} \cdot \text{cm}^{-1} \cdot \text{sec}^{-1} \cdot \text{deg}^{-1}$

P : the pressure in atm.

R : the ideal gas constant in $\text{cc} \cdot \text{atm} \cdot \text{deg}^{-1} \cdot \text{gmol}^{-1}$

T : the absolute temperature.

The approximations required to derive these equations have been discussed elsewhere². However, for the ozone flame, special justification is required for the omission of terms in kinetic-energy of gas flow in the equation of energy balance (cf. Section 4).

The Hirschfelder-Curtiss model assumes that the hot boundary is defined by an asymptotic approach to chemical, thermal, and diffusion equilibrium

$$\lim_{Z \rightarrow \infty} dT / dZ = \lim_{Z \rightarrow \infty} dx_i / dZ = \lim_{Z \rightarrow \infty} dG_i / dZ. \quad (2)$$

The cold boundary is defined by a non-zero value of the temperature gradient, $(dT / dZ)_{Z \text{ cold}} > 0$ (3)

$Z \text{ cold}$: cold boundary, and the continuity of the fractional mass-flow rates.

The mol-fractions may be subject to a discontinuity and are mathematically unspecified. For one class of idealized systems, it has been shown that: (a) the discontinuity exists; (b) its magnitude depends upon $(dT / dZ)_{Z \text{ cold}}$. The latter quantity can be varied over a range of values which will leave the discontinuity experimentally insignificant and which will not affect the flame solution as much as 0.01%.³

It has been shown that M can be viewed as an eigenvalue to be adjusted in fitting the cold-boundary conditions on the fractional mass-flow rates for one of the major constituents of the fuel.⁴

3. Physical Model and Numerical Parameters.

A critical review of experimental studies of oxygen and ozone-oxygen reaction kinetics⁵ supported Hirschfelder and Curtiss' choice of the three following reactions to describe the ozone flame:



Let: f_i^f (f_i^r): specific rate with respect to mol-fractions for the i -th forward (reverse) reaction at a total pressure of 1 atm. (5)

The specific rates have been assigned a functional form recommended for use in flame studies⁷

$$f_i^p(T) = a_i^p T^{b_i} \exp(-\epsilon_i^p / T), \quad p = f, r \quad (6)$$

a_i^p , b_i^p , ϵ_i^p : constants.

If the reactions occur at a rate which allows approximate equilibration among the states of the reacting species, then the forward and reverse rates must approximately satisfy the thermodynamic equation

$$K_i^x = f_i^f / f_i^r \quad (7)$$

K_i^x : the equilibrium constant with respect to mol-fractions for the i -th reaction.

The equations given in the review for the equilibrium constants were changed for mol-fractions.^{5a} The parameters are recorded in Table 1.

Table 1

Parameters In Mol-Fraction Equilibrium Constants At $P = 1$ atm.

Reaction	a_i^x	b_i^x	ϵ_i^x
1	(+6) + 1.2799 <u>33367</u>	(-1) + 2.5	(+4) + 1.2920 <u>85</u>
2	(+2) + 6.0937 <u>32368</u>	(-1) - 7.5	(+4) - 4.6783 <u>15</u>
4	(-4) + 4.7609 <u>76251</u>	(+0) - 1.0	(+4) - 5.9704 <u>00</u>

Legend: The parameters are for the equation

$$K_i^x = a_i^x T^{b_i^x} \exp(-\epsilon_i^x / T).$$

The reaction numbers refer to Eq. (4).

$$(\pm Z) y.yy \text{ is } (y.yy) \times 10^{\pm Z}.$$

The equations for reactions (1, $M = O_3$) and (2) were taken from the review ^{5b} and changed for mol-fractions. The thermodynamically consistent reverse rates were obtained from the data of Table 1. The results are shown in Table 2.

Table 2

Parameters In Eq. (6) For Mol-Fraction Specific Rates When $P = 1$ atm.

i	p	a_i^p	b_i^p	ϵ_i^p
1, $M=O_3$	f	(+12) 1.98	- 2.0	(+4) + 1.243
	r	(+6) 1.546 <u>9555</u>	- 2.25	(+2) - 4.908 <u>5</u>
2*	f	(+8) 8.08	- 2.0	(+3) + 2.133
	r	(+6) 1.325 <u>9520</u>	- 1.25	(+4) + 4.891 <u>615</u>
4, $M=O_2$	f	(+12) 4.6	- 4.0	0
	r	(+15) 9.661 <u>8839</u>	- 3.0	(+4) + 5.970 <u>400</u>

Legend: An entry ($\pm Z$) y.yy denotes the number $(y.yy) \times 10^{\pm Z}$. A line beneath digits of a_i^p or ϵ_i^p for $i = 1, 2$ indicates that according to the review, the digits are uncertain. They are retained to maintain thermodynamic consistency to eight significant figures.

* Within the accuracy of existing data, $a_{1,M} \equiv f_{1,M}^p / f_{1,O_3}^p$ is constant.

$a_{1,O_2} = 0.33$ ^{5c}. a_0 was arbitrarily assigned the value $a_0^3 = 1.5$.

+ The specific rates for reaction 2 are for the consumption of O_3 (i.e., one-half of the rates for the production of O_2).

** The specific rates for reaction 4 are for the production of O_2 , i.e., one half of the values for the consumption of O . $a_{4,O} \equiv f_{4,O}^p / f_{4,O_2}^p$ was assumed to be constant. The following values were arbitrarily assumed:

$a_{4,O_3} = 2$, $a_{4,O} = 1.33$

Several investigators have published data on reaction (4) since the preparation of the review. Unfortunately, there is only order of magnitude agreement for specific rates as shown in Table 3.

Table 3

M	10 ⁻¹⁴ k _{4,M} ^f cc. ² -mol ⁻² -sec. ⁻¹ at 3500°		
	[8]	Reference [9]	[10]
A	—	0.52	0.45
X _e	1.3	—	—
O ₂	4.6	1.6	4.8
O	14.	13.	9.9

Legend: The data are taken from reference [8]. They are for

$$d [O_2] / dt = k_{4,M}^f [M] [O]^2.$$

The most reliable determinations of recombination rates have been made by inserting dissociation rates measured in a shock tube into the thermodynamic equation between forward and reverse rates. The applicability of the equilibrium relation has been checked in shock tube studies of the coupling between dissociation and recombination ¹¹. Under the conditions of the experiment, the vibrational relaxation in dissociating O₂ - A mixtures was sufficiently rapid that the coupling was completely negligible up to 5000°.

Since it seemed difficult to select one significantly more reliable value, the equation suggested by reference [8] was arbitrarily adopted. It should be recognized that the temperature dependence for recombination was selected arbitrarily by the authors on the basis of other people's results. Their equation for recombination was changed for use with mol-fractions and the thermodynamically consistent dissociation rate was obtained using the parameters of Table 1. The results are recorded in Table 2.

While reactions (2) and (4) are important for determination of the asymptotic equilibrium values as Z → ∞, because of the large activation energies, they would not be expected to affect the first few digits in calculations at any other point in the flame. Comparisons with rates used in previous theoretical studies are made in Sections (5.1, 5.6).

The transport coefficients suggested in the review ⁵ have been adopted. They will be tabulated for reference.

Table 4

Parameters For Binary Diffusion Coefficients At P = 1 atm.

β γ	$d_{\beta\gamma} \times 10^5 \text{ cm.}^2 \text{ - sec.}^{-1} \text{ - deg.}^{-3/2}$	$d_{\beta\gamma}^0 \times 10^{-2} \text{ deg.}$
O ₂ O ₃	<u>4.59</u>	<u>1.808</u>
O ₂ O	<u>7.36</u>	<u>1.471</u>
O O ₃	<u>5.81</u>	<u>1.808</u>

Legend: The parameters are taken from the review [5d] for use in the empirical equation

$$D_{\beta\gamma}(T) = d_{\beta\gamma} T^{3/2} / (1 + d_{\beta\gamma}^0 T^{-1}).$$

A line beneath a digit indicates that in the review that digit was considered to be uncertain.

Table 5

Parameters For The Thermal Conductivity of The Pure Gases

	$a(\text{cal.}\cdot\text{cm.}^{-1}\cdot\text{sec.}^{-1}\cdot\text{deg.}^{-1})\text{deg.}^{-1/2}$	$b^{\circ}\text{K}$	$c^{\circ}\text{K}$
O_2	6.726×10^{-6}	265.9	10
O_3	5.83×10^{-6}	<u>467</u>	<u>10</u>
O^*	3×10^{-6}	400	0

Legend: The parameters are taken from the review ^{5e} for use in the empirical equation

$$\lambda = a T^{1/2} / \{1 + bT^{-1} \exp[-cT^{-1} \ln 10]\}.$$

A line underneath a digit indicates that in the review that digit was considered to be uncertain.

* As a result of an error, parameters for O atom were used which predict a lower thermal conductivity for O than for O_2 . At 1097° , where x_{O} has its maximum, the thermal conductivity for O is about a factor of 3 smaller than recent theoretical estimates. However, the maximum in x_{O} is less than three per cent and the estimated error in λ_{mix} is only 2.6%.

The thermal conductivity of the gaseous mixture was estimated from the thermal conductivity of the pure components by the simple linear combination rule ^{5f}:

$$\lambda_{\text{mix}} = \sum_i \lambda_i x_i. \quad (8)$$

The enthalpies were assumed to be linear functions of temperature given by the review ^{5g}. The values used for the heat capacities were averages taken over the range $[300^{\circ}\text{K}, 1300^{\circ}\text{K}]$, rounded to the nearest one-quarter in C_{α}/R . The parameters are summarized for reference in Table 6.

Table 6

Parameters For The Enthalpy Equations

α	$H_{\alpha}(1300^{\circ})$ cal./gmol	C_{α}/R
0	(+4) 6.563 <u>6</u>	2.5
O_2	(+4) 1.004 <u>5</u> <u>2</u>	4.0
O_3	(+4) 4.93 <u>59</u>	6.25

Legend: The parameters are for $H_{\alpha}(T) = H_{\alpha}(1300^{\circ}) + C_{\alpha}(T-1300^{\circ})$.

($\pm Z$) y.yy denotes the number $(y.yy) \times 10^{\pm Z}$. The review ^{5g} considered the underlined digits to be uncertain.

The total mass-flow rate, M, is an eigenvalue. The value required for solution of the flame equations can be compared with one calculated from the experimental burning velocity $v(Z_c)$,

$$M = \rho(Z_c) v(Z_c) \quad (9)$$

$\rho(Z_c)$: gas density at the burner in g./cm^3 .

$v(Z_c)$: mass average velocity at the burner in cm./sec.

Z_c : the (arbitrary) distance coordinate for the burner.

Streng and Grosse measured the burning velocity of a set of ozone-oxygen mixtures ¹². The data in this paper are for their mixture with the parameters

$$\begin{aligned}
 P &= 1 \text{ atm.} \\
 T(Z_c) &= 300^{\circ}\text{K} \\
 x_{O_3}(Z_c) &= 0.23 \\
 x_{O_2}(Z_c) &= 0.72 \\
 v(Z_c) &= 52.2 \text{ cm./sec.}
 \end{aligned} \tag{10}$$

The Hirschfelder-Curtiss model for the flame holder has been shown for one idealized flame to require an experimentally negligible discontinuity in the mol-fractions at Z_c (vide Section 2). Thus, for the mathematical model the mol-fractions of Eq. (10) represent $\lim_{Z \rightarrow Z_c^-} X_\alpha(Z) \neq \lim_{Z \rightarrow Z_c^+} X_\alpha(Z)$. The remaining boundary values were calculated using the boundary conditions for the Hirschfelder-Curtiss model (cf. Section 2). The entire set of values is summarized for reference * :

$$M = 0.07736 \text{ g.-cm.}^{-2}\text{-sec.}^{-1}$$

	$Z = Z_c$	$\lim_{Z \rightarrow +\infty}$	
G_0	0.0	(-7) 1.904 4986	
G_{O_2}	(-1) 6.315 7895	(-1) 9.999 9981	
G_{O_3}	(-1) 3.684 2105	(-9) 1.101 6955	
X_0	—	(-7) 3.808 9965	(11)
X_{O_2}	—	(-1) 9.999 9962	
X_{O_3}	—	(-10) 7.344 6352	
T^*	(+2) 3.00	(+3) 1.344 2328	

4. Methods of Numerical Integration; Character of the Eigenvalue Problem.

Previously published techniques¹³ were used to construct a Taylor Series of the thirtieth order about the hot boundary temperature, T_{\max} (which is a singular point of the differential equation system), as a local solution over an interval

$$\begin{aligned}
 & [T_1, T_{\max}] \\
 T_{\max} &= \lim_{Z \rightarrow \infty} T(Z) \quad **
 \end{aligned} \tag{12}$$

- * ($\pm Z$) y.yy denotes the number (y.yy) $\times 10^{\pm Z}$.
- + This value corresponds to $(dT/dZ)_{Z_c} = 0$. The actual value of $T(Z_c)$ must be such that $(dT/dZ)_{Z_c}$ has a positive value. The exact value is of no importance³.
- ** In order to scale the magnitudes of successive power series coefficients, it is essential to use a reduced temperature. $t = (T - T_{\max})/T_{\max}$ has been found to be a suitable choice⁴.

The power series coefficients were checked by a test which has been used repeatedly to detect any errors of inconsistency ^{13a}.

Mathematical instability of the equation system ⁴ prevents continuation of the solution from T_1 by a straightforward application of conventional methods of numerical integration. Alteration of the last of eight digits in single precision computer calculations was sufficient to cause the solution to diverge either positively or negatively along a priori ridiculous curves (e.g., dG_{O_3}/dT goes to zero in the high temperature region).

Furthermore, the first stage of a previously published method of successive approximation could be constructed over only a part of the remaining temperature range of interest ⁴. Therefore, the results discussed in this paper were obtained by further development of previous work ¹⁴. A computer program was developed in which the machine made the necessary logical choices to correct its integration and to follow the desired solution ¹⁵. The validity of the procedure was tested with: (a) the check discussed at the end of this Section; (b) comparison of the solution with that obtained by the first stage of the successive approximation technique. Over a temperature range common to both, the difference between the function values for the two solutions was at most a few per cent *.

All previous calculations on ozone which took diffusion into account were based either on the kinetic steady-state ^{18,19} or on improved algebraic approximation related to the kinetic steady-state ²⁰ which gave solutions approximately following the kinetic steady-state. It has been shown that ⁴: (a) the kinetic steady-state incurs a solution with a satisfactory approximation to the boundary condition $G_0 = 0$; (b) with this approximation any three component system requires only a single eigenvalue, M .

Since the present calculation neither assumes nor predicts any reasonable approximation to the kinetic steady-state, it is surprising that the solution for this mixture could be constructed with M as the sole eigenvalue. The basis for the last statement consists of the following facts: (1) Starting values at T_1 off the hot boundary which give negative or positive divergence agreed with the sum of the series constructed at T_{max} to within one unit in the eighth digit; (2) Solutions which approximately satisfy the cold boundary conditions $G_0 = 0$, $x_0 \approx 0$ were obtained (in the sense that (a) x_0 and $|G_0|$ decreased to less than 0.01 of their maximum values; (b) Inspection of the bounding curves showed that the ratios would have been lowered if the bounds were brought closer); (3) M could be adjusted to fit $G_{O_3}(Z_c)$.

Conversely, for richer ozone flames (i.e., higher T_{max}) calculations already performed show that: (1) the series solution including EE terms in some cases predicts starting values which differ by a factor; (2) it seems impossible to fit the cold boundary value on $G_{O_3}(Z_c)$ and G_0 using only a single eigenvalue and the equations present a two eigenvalue problem.

- In previous studies, similar numerical techniques were applied to a hypothetical flame (with the difference that all decisions were made manually). A similar comparison supported the validity of the solution for the idealized system ^{14b, 17}.

Contrary to previous belief 18, 19, 20, 21, it seems that a single eigenvalue approximation is adequate only for (a) sufficiently lean flames, or, (b) an incorrect approximation omitting the kinetic energy term in the equation of energy balance for richer flames.

5. Discussion of Results.

5.1. Free Radical Curves; Applicability of the Kinetic Steady-State Approximation; Comparison With Other Calculations.

Consider an intermediate, α , whose net rate is given as a sum of rates for forward and reverse reactions

$$R_{\alpha} = \sum_i (R_{\alpha,i}^f - R_{\alpha,i}^r) . \quad (13)$$

Since the kinetic steady-state approximation

$$R_{\alpha} = 0 \quad (14)$$

has been frequently used to determine x_{α} , a convenient measure of the adequacy of the approximation is given by a relative deviation, r_{α} , defined as 3a

$$r_{\alpha} = R / R_{\alpha,i}^f \quad (15)$$

Graph (1) shows that r_0 is of the order of unity for most of the flame so that the kinetic steady-state is not a useful approximation for calculations which are at all sensitive to the profile $x_0(T)$. von Karman and Penner ¹⁸

conjectured that the approximation would be useful in calculating burning velocities. Since there is evidence that flame speeds are comparatively insensitive, their suggestion seems to be useful for rough approximations. Thus, previous calculations on an idealized system showed that M varied by only a factor of about 0.75 with changes in kinetic and diffusion parameters which removed any approximation to the kinetic steady-state (cf. Section 5.6). The assumption that a similar result holds for the ozone flame suggests that, for a fixed set of parameters, the use of the steady-state approximation might give a result of the right order of magnitude even if it grossly distorts profiles.

The existence of a single internal maximum in an intermediate mol-fraction has been attributed to the kinetic steady-state approximation *+. Since

*When von Kármán and Penner ¹⁸ interpreted the existence of a maximum in terms of the kinetic steady-state approximation, they contrasted their suggestion with Hirschfelder and Curtiss' ²² interpretation. However, the contrast was based on an incomplete paraphrase which omitted the words in italics: "The reason for this is that the free radicals, in this case oxygen atoms, are essentially in equilibrium with fuel molecules in the region of the hot boundary. This is the significance of setting $K_1=0$." In Hirschfelder and Curtiss' notation, K_1 is the net rate of O atom production, so that $K_1=0$ is just the kinetic steady-state approximation.

+See Westenberg and Fristrom ¹⁶, p. 598 for comments on experimental studies which have shown maxima in radical concentrations and for references to the literature.

Graph (2) for $x_0(\gamma)$ shows such a maximum in the absence of the kinetic steady-state, this interpretation must be abandoned. However, another one which predicts a single internal maximum for a wide class of intermediates ³ does apply. Furthermore, if

$$t = (T - T_{\max}) / T_{\max} \quad (16)$$

$$\mathcal{J} = [M C_{O_3} / \lambda(T_{\max})] Z, \text{ where } \mathcal{J}=0 \text{ is}$$

an arbitrary origin,

then Graphs (2) of $x_0(\gamma)$, (3) of $x_0(\mathcal{J})$, and (4) of dt/dZ show that the previous conjecture ³ for such intermediates applies to the O atom in the ozone flame: despite the steeper τ gradient on the hot side of the maximum, the larger \mathcal{J} gradient lies on the cold side (due to the rapid increase in dt/dZ in the region of rapid chemical reaction).

These results on the significance of the deviations from the kinetic steady-state differ qualitatively from the assumptions of earlier studies ^{23,19} and the conclusions of a third ²⁰. The extremely large deviations reported here would have been somewhat lower in the region about the hot boundary if the older specific rate for O atom recombination had been used. In the earlier study the recombination rate was determined from Eq.(7) using the dissociation rate calculated with the pre-exponential factor for the simple bimolecular collision theory. Subsequent experiments have shown that dissociation reactions have abnormally large pre-exponential factors*. Thus the specific recombination rate used was too low by a factor of the order of 100 at 1250° and of the order of 1000 at 400°. To obtain a lower bound on the effect of this difference, $R'_0 = R_0 + 2 R_4^f$ can be computed using the data of this study.

At a temperature 120° off the hot boundary, use of R'_0 rather than R_0 would give a relative deviation of -0.15 instead of -0.80.

However, this decrease does not alter the qualitative difference which can not be due to the difference between the specific rates and transport coefficients adopted in this study and those assumed in previous investigations. This conclusion was deduced from

$$\text{PS}_1 : \text{a local solution at the hot boundary} \\ \text{in the form of a twentieth order power} \\ \text{series constructed with the earlier set} \quad (17) \\ \text{of parameters.}$$

PS_1 predicted the same qualitative result found in this study. It is not x_0 , but x_{O_3} which approximately obeys the steady-state over a wide temperature interval about the hot boundary:

$$\begin{aligned} T \geq 1217 (\tau \geq 0.88) : r_{O_3} &\leq 0.01 \\ T \geq 1167 (\tau \geq 0.83) : r_{O_3} &\leq 0.033. \end{aligned} \quad (18)$$

* Br_2 can be taken as a typical example ²⁴.

† The sign of the temperature coefficient was also wrong since the estimate was made before experiments established the negative temperature coefficient for recombination rates.

Although the net production rates of O and of O₃ are related by the equation

$$R_{O_3} = R_{O_2} - 2(R_1 + R_4) \quad (19)$$

and $R_{O_2} \gg 100R_{O_3}$ through a temperature range of over 100°, two of these studies equated R_{O_2} to zero and left R_{O_3} be non-zero. von Karman and Penner made this approximation when they were attempting to simplify the ozone equations in their study of flame speeds. They argued that R_1 would be negligible compared with other reactions except in a temperature range about the hot boundary which they felt would be unimportant for the calculation of flame speeds. Sandri made the same approximation in his calculations [19]. According to the results of this study, omission of R_1 alters R_{O_3} by orders of magnitude over this region. While it is true that previous studies of an idealized system would support the contention that any change which left R_{O_2} comparatively small could be expected to be without significant effect, it does not necessarily follow that this could be expected for a drastic alteration in R_{O_3} unless the temperature range itself were a negligible fraction of the whole. Unfortunately, this approximation also gives an erroneous estimate of the size of the temperature region. In any case, it should not be made in any study of flame structure and processes.

In the third study, a Taylor series approximation using second derivatives was used to predict values at $T = T_{max} - 2^\circ$. Tangent integration with 2 degree intervals starting from these values gave solution curves which oscillated violently. After a change to much larger values for G_{O_3} and x_{O_3} gave solution curves which were smooth and more reasonable. The oscillations in the earlier solution were attributed to the "much too small" values of G_{O_3} and x_{O_3} given by the Taylor series. This explanation does not appear to be correct since: (a) Inspection of PB₁ showed that use of second derivatives gave starting values certain to about one decimal, which were not off in magnitude; (b) This study has shown that the ozone differential equations in the neighborhood of the solution determined by the hot boundary conditions are so mathematically unstable that the curves are sensitive to the last of eight digits carried in usual computers. Therefore, they require special methods of solution (see Section 4). The introduction of the larger values of G_{O_3} and x_{O_3} avoided the unstable region in which G_{O_2} and x_{O_2} are increasing and x_{O_3} approximately follows a kinetic steady-state. Thus these larger values were responsible for the report that x_{O_3} has a maximum within two degrees of the hot boundary. For the remainder of the flame, x_{O_3} was calculated not from the kinetic steady-state approximation but from the equation

$$d [x_{O_3}/x_{O_3}^{ss}]/dT = 0 \rightarrow d x_{O_3}/dT = [x_{O_3}/x_{O_3}^{ss}] d x_{O_3}^{ss}/dT \quad (20)$$

$x_{O_3}^{ss}$: the value of x_{O_3} given by the kinetic steady-state approximation.

The present study shows that this would not be useful approximation for a solution determined by the hot boundary conditions. In the neighborhood of the hot boundary, a kinetic steady-state is a better approximation by two orders of magnitude for x_{O_3} than for x_{O_2} . Thus for such a solution, Eq. (20) replaces the larger

$d [x_0/x_0^{ss}] / dT$ by zero rather than the smaller $d [x_{O_3}/x_{O_3}^{ss}] / dT$.

The previous studies agree within about 13% on predicted flame speeds (cf. Section 5.6). Although it may be that the assumptions and approximations as discussed above did not greatly affect the calculated flame speed, this could only be proven by repeating the present calculations for the older parameters (cf. Section 5.6).

The following considerations suggested that it would be worth-while to determine how a change in the specific rate for free-radical recombination would affect the calculated M . Table 7 shows that radical recombination provides one of the most important terms in R_0 , the net rate of O atom production, until R_0 becomes positive. As this occurs, R_0 , and therefore G_{O_3} , begin a much more rapid rise to provide the major change in G_{O_3} . Therefore, it seemed possible that a change in recombination rate might significantly affect the temperature at which R_0 becomes positive. The resulting shift in the temperature at which G_{O_3} begins its rapid rise would change M . This suggested that if there is any flame in which recombination rates have a marked effect upon burning velocities, ozone might be one.

The tests were performed using somewhat different free-radical diffusion coefficients (cf. Section 5.5). Two different calculations were made with the specific rates of Section 3:

M	$G_{O_3}(Z_c)$	$P \equiv M G_{O_3}(Z_c)$	
0.07736	0.7097	0.05490	(21)
0.149	0.3977	0.05918	

According to Section 5.6 the product P can be approximated roughly as a linear function of $G_{O_3}(Z_c)$. A straight line through the data of Eq. (21) gave

$$P = 0.05958 \quad M = 0.1617. \quad (22)$$

A third calculation with doubled rates for atom recombination and dissociation and the same value of M gave:

$$M = 0.149 \quad G_{O_3}(Z_c) = 0.3986 \quad P = 0.05939. \quad (23)$$

The assumption that $dP/dG_{O_3}(Z_c)$ would be about the same for the data of Eqs. (21,23) gave

$$P = 0.05981 \quad M = 0.1623. \quad (24)$$

Thus a two fold increase in the recombination rate gave only a 0.4% increase in M . Therefore, the sensitivity to free-radical recombination and

Table 7

Rates of Reactions

T	τ	R_1^f	R_1^f	R_2^f	$2R_4^f$	R_0	R_{O_3}
(+3)+1.231	0.8214	(-3)+1.207	(-3)+1.287	(-5)+8.929	(-4)+8.644	(-3)-1.034	(-6)-8.592
(+3)+1.205	0.8567	(-3)+1.534	(-3)+1.678	(-4)+1.643	(-3)+1.409	(-3)-1.718	(-5)-1.979
(+3)+1.168	0.8508	(-3)+2.040	(-3)+2.329	(-4)+3.569	(-3)+2.550	(-3)-3.196	(-5)-6.799
(+3)+1.159	0.8222	(-3)+2.196	(-3)+2.502	(-4)+4.304	(-3)+2.899	(-3)-3.636	(-4)-1.247
(+3)+1.151	0.8148	(-3)+2.407	(-3)+2.655	(-4)+5.195	(-3)+3.224	(-3)-3.992	(-4)-2.714
(+3)+1.135	0.7999	(-3)+3.702	(-3)+2.975	(-4)+9.647	(-3)+3.941	(-3)-4.173	(-3)-1.692
(+3)+1.126	0.9251	(-3)+5.550	(-3)+3.136	(-3)+1.587	(-3)+4.324	(-3)-3.488	(-3)-4.011
(+3)+1.120	0.7651	(-3)+9.208	(-3)+3.293	(-3)+2.871	(-3)+4.705	(-3)-3.1661	(-3)-8.765
(+3)+1.104	0.7703	(-2)+2.611	(-3)+3.555	(-3)+2.871	(-3)+4.705	(-3)-1.661	(-3)-3.208
(+3)+1.089	0.7554	(-2)+5.843	(-3)+3.590	(-3)+9.519	(-3)+5.350	(-3)+7.688	(-2)-3.208
(+3)+1.066	0.7332	(-1)+1.159	(-3)+3.674	(-2)+2.400	(-3)+5.637	(-2)+2.511	(-2)-7.874
(+3)+1.035	0.7335	(-1)+1.533	(-3)+3.674	(-2)+5.383	(-3)+5.428	(-2)+5.300	(-1)-1.661
(+3)+1.001	0.5144	(-1)+1.653	(-3)+3.571	(-3)+6.624	(-3)+4.676	(-2)+7.156	(-1)-2.535
(+2)+9.596	0.6319	(-1)+1.679	(-3)+3.190	(-1)+1.204	(-3)+3.793	(-2)+6.701	(-1)-2.933
(+2)+9.030	0.5775	(-1)+1.164	(-3)+2.841	(-1)+1.118	(-3)+2.639	(-2)+4.176	(-1)-2.855
(+2)+8.927	0.5976	(-1)+1.035	(-3)+2.306	(-1)+1.066	(-3)+1.843	(-4)+3.423	(-1)-2.253
(+2)+8.411	0.5182	(-2)+6.236	(-3)+2.509	(-3)+6.956	(-3)+1.698	(-3)-6.187	(-1)-2.128
(+2)+7.668	0.4490	(-2)+2.301	(-3)+1.953	(-2)+6.115	(-3)+1.112	(-2)-3.020	(-1)-1.500
(+2)+7.609	0.3997	(-3)+7.617	(-3)+1.246	(-2)+4.044	(-4)+5.964	(-2)-4.027	(-2)-8.263
(+2)+6.449	0.3303	(-3)+1.905	(-3)+1.016	(-2)+2.472	(-4)+3.412	(-2)-3.441	(-2)-4.680
(+2)+5.417	0.2315	(-4)+7.204	(-3)+8.763	(-3)+8.763	(-4)+1.910	(-2)-2.403	(-2)-2.561
					(-5)+6.696	(-3)-9.470	(-3)-8.124

Legend: The reactions are defined by Eq. (4). R_0 and R_{O_3} are the net rates of production of O and of O_3 respectively. $R_0 = R_1 - R_2 - 2R_4$, $R_{O_3} = -R_1 - R_2$. The number (\pm) $\pm Y.YY$ denotes ($\pm Y.YY$) $\times 10^{12}$.

dissociation rates appears to be of the same order for the ozone system and for a previously studied free-radical system^{26a}. In the latter flame a 300 fold decrease in the free-radical specific rates increased M by a factor of about 1.3. Inspection of the calculations suggests that the difference in the direction of the shift can be attributed to the fact that an increase in free-radical rates* in ozone disturbs the kinetic steady-state approximation for O_3 in the region about the hot boundary.

5.2 Energy Transfer; Constant Specific Enthalpy Approximation.

For consideration of the relative contribution which various physical processes make to energy transfer, the terms in the energy balance equation (1c) will be regrouped. Since the equation assumes an asymptotic approach to thermal and diffusion equilibrium as $Z \rightarrow +\infty$, the energy conservation can be conveniently expressed in the form

$$M \sum_i H_i G_i / m_i - \lambda dT/dZ = M \lim_{Z \rightarrow \infty} \sum_i H_i G_i / m_i = M \lim_{Z \rightarrow \infty} (H/m) \quad (25)$$

$$H = \sum_i H_i x_i = \text{enthalpy/mol}$$

$$m = \sum_i m_i x_i = \text{mean molecular weight.}$$

The first term in Eq. (25) can be written as the sum of a term due to diffusion and a convection term due to the mass average gas velocity:

$$M (H/m) + n \sum_i H_i x_i V_i - \lambda dT/dZ = M \lim_{Z \rightarrow \infty} (H/m) \quad (26)$$

V_i : the diffusion velocity of species i .

In order to show the relative importance of the three processes in dimensionless units, the following ratios have been graphed:

$$\begin{aligned} R_{DIFF} &\equiv \frac{\text{Diffusion Term}}{\text{Conduction Term}} = \frac{n \sum_i H_i x_i V_i}{\lambda dT/dZ} \\ R_{CONV} &= \frac{\text{Convection Term}}{\text{Conduction Term}} = \frac{M [H/m]}{\lambda dT/dZ} \end{aligned} \quad (27)$$

* In this system, Reaction (1) is the idealized analogue of a free-radical dissociation-recombination reaction.

Since dT/dZ approaches zero as $Z \rightarrow Z_{\text{cold}}$ and has a limiting value of zero as $Z \rightarrow \infty$, it is apparent that $RGMV$ must increase as $Z \rightarrow Z_{\text{cold}}$ and must approach infinity as $Z \rightarrow +\infty$. In contrast with the idealized flame previously studied, for which convection was the least important process, Graph 5 shows that convection is the most important process throughout the entire flame and is over a factor of 10 more important throughout the hottest region until G_3 has attained between 0.4 and 0.5 of its limiting cold boundary value. Hirschfelder²⁵ has shown that when the approximations of Eqs. (1b, 1c) are used, the enthalpy per gram is constant \leftrightarrow all Lewis numbers are unity. Thus the processes of diffusion and thermal conduction are of equal importance $\leftrightarrow RDIFF = 1 \leftrightarrow$ the specific enthalpy is constant \leftrightarrow all Lewis numbers are unity. Thermal conduction will be the more important process $\leftrightarrow RDIFF < 1 \leftrightarrow H \lim_{Z \rightarrow \infty} H$.

Graph 6 of $RDIFF$ shows the quantitative effect of non-unit Lewis numbers upon the relative importance of the two processes. The ratio has the same qualitative variation found in an idealized system for "light" free-radicals (those whose binary diffusion coefficients are larger than the coefficients for major component pairs)³: diffusion is the more important process in the hotter region ($\tau > 0.75$) and thermal conduction is the more important for ($\tau < 0.75$).

The suggestion has been made that the constant specific enthalpy approximation might be used to determine one of the mol-fractions. This approximation has been applied specifically to the ozone flame by von Kármán and Penner²⁶. Let

α' : be the species such that $H_{\alpha'} x_{\alpha'}$ is the largest term in

$$H/m = m^{-1} \sum H_{\alpha} x_{\alpha} . \quad (28)$$

Then, at this point the ratio

$$RH = \frac{(H/m) - \lim_{Z \rightarrow \infty} (H/m)}{\lim_{Z \rightarrow \infty} (H/m)} \quad (29)$$

Shows the relative error in $x_{\alpha'}$, that would be made if this approximation were used. For this ozone flame, Graph 7 shows the variation in the error which is never greater than eight per cent. However, if this approximation were used in any theoretical calculation, the effect on the integral curves might be greater than the effect at one arbitrary point.

5.3 Heat Release by Radical Recombination.

To test the suggestion²⁷ that, since radicals are highly energetic species they might serve as an important means of energy transport by diffusing toward the cold boundary and recombining, the relative contribution free-radical recombination makes to the total volume rate of heat release due to chemical reaction

$$HREL = \frac{R_4 (H_0 - 2H_0)}{R_1 (H_0 - H_0 - H_0) + R_2 (H_0 + H_0 - 2H_0) + 2R_4 (H_0 - 2H_0)} , \quad (30)$$

is given by Graph 8.

Contrary to this suggestion, the contribution of the main combustion reaction in the colder region is more important by an order of magnitude. This contrasts strikingly with the fact that the fraction contributed by radical recombination $\geq 1/2$ for sufficiently hot T ($\tau \geq 0.77$).

For the ozone flame, HREL is qualitatively different than a previously studied idealized flame³. In the latter flame Reaction (1) is the analogue of the recombination-dissociation reaction. It contributes much less than a few percent of the total volume rate of heat release. Whereas in the ozone system, dissociation is completely negligible and the contribution is always positive, in the idealized system the contribution is both positive and negative. This is qualitatively the same as the contribution of the $\text{Br} - \text{Br}_2$ reaction in the $\text{H}_2 - \text{Br}_2$ system.

5.4. Spatial Separation of Processes.

There are both experimental and theoretical reasons for examining the spatial separation of processes in the ozone flame. Theoretically, study of the relative importance of processes in the neighborhood of the hot boundary might suggest useful alternative models. Experimentally, studies of the methane-oxygen system have shown that the adiabatic model (which is used in theoretical studies) is rather good for that system: the calculated and corrected experimental flame temperatures differ by only 10° ²⁸.

What is of particular interest here is that the methane-oxygen flame has a rather marked separation into three spatial regions^{28a}: (1) a low temperature region, commonly expected in flames, in which there is comparatively little chemical reaction but a marked temperature rise due to energy transport; (2) an intermediate temperature region dominated by one sequence of reactions; (3) a higher temperature region extending to the maximum flame temperature dominated by a different sequence of reactions. The Table 7 of reaction rates and the Graph 9 of τ (τ) [cf. Eq. 16] shows the separation of the ozone flame into the first two regions. The separation into two different kinetic regions will now be demonstrated. When the temperature is still 200° ($T = 1143^\circ$) below its limiting hot boundary value, the fuel mol-fraction has decreased to 10^{-3} of its maximum value which occurs at the cold boundary. Conversely, x_{O} is still 0.67 of its maximum value. Both are, of course, orders of magnitude greater than those for complete thermodynamic equilibrium.

Inspection of the graphs (10,11,2) for the mol-fractions and fractional mass-flow rates shows the greater importance of changes for O atom in this region.

In terms of reaction kinetics, $-R_{\text{O}} > -R_{\text{O}_3} > 0$ and $R_{\text{O}}/R_{\text{O}_3}$ increases rapidly with increasing T until it reaches a value of over 100 [cf. Table 7]. Thus, in this region the net rate of free-radical production is more important. Table 7 of reaction rates shows the importance of recombination to the net production. For example, at $T = 1143^\circ$, recombination contributes 0.84 of the total (negative) net rate of production. This recalls Fristrom's²⁹ observation that recombination reactions must be important in the high temperature region of the methane-oxygen flame. The Section 5.3 on heat release has already shown that O recombination is the dominant source of heat release by chemical reactions in this region.

Just as R_{O} dominates R_{O_3} in kinetics, G_{O} dominates G_{O_3} by two orders of magnitude so that free-radical mass-flow makes a more important contribution to energy conservation than fuel mass-flow does.

As Section 5.5 shows, there is an approach to diffusion equilibrium prior to thermal equilibrium. Conversely, there is no approach to chemical equilibrium prior to thermal equilibrium. Both x_0 and x_{O_3} increase rapidly with respect to thermal equilibrium values, although not so rapidly as in a previous study²⁰. Thus at a temperature one degree below the hot boundary temperature, x_0 and x_{O_3} are 77 and 79 times greater, respectively, than their equilibrium values.

5.5 The Role of Diffusion.

To provide a basis for estimating the significance of diffusion throughout the flame, two different sets of graphs are given: (1) the ratios (v_i/v) of the average speed for a particle of type i to the mass average speed (Graph 12); (2) the ratios of V_i/M of the actual diffusion velocity to the total mass flow rate, M (Graph 13). Although Section 5.4 shows that there is no approach to chemical equilibrium before thermal equilibrium, there is a prior approach to diffusion equilibrium ($v_i/v \approx 1$). Conversely, at certain lower temperatures, diffusion contributes more than the average mass flow to the motion of both O_3 and of O . Thus v_1/v attains values of 2.75 and -2.5 for O_3 and O respectively.

von Karman and Penner's approximate equation for the burning velocity predicts that it will vary as the inverse square root of the ozone-oxygen molecule binary diffusion coefficient^{18b}. By accident, there has also been a test of the significance of the oxygen atom binary diffusion coefficients. A key-punch error in one run, and a duplication error in a second altered their temperature dependence so that they were decreased twenty-five percent and more in the x_0 diffusion equation in the region of most rapid chemical reaction. This gave an estimated M of 0.1617 [cf. Eq. (22)] compared with $M = 0.1812$ [cf. Eq. (34)] for the diffusion coefficients of Section 3.

5.6 Comparison with Experiment and Other Calculations.

The sole experimental data on the ozone flame are burning velocities determined for several mixtures. Strick and Crooke¹² report a burning velocity of 52.2 cm./sec. for the ozone-oxygen mixture considered here. This corresponds to an experimental value for the total mass-flow rate of

$$M_{\text{exp}} = 0.07730. \quad (31)$$

The M assumed in the calculations reported here

$$M_{\text{use}} = 0.177 \text{ g.-cm.}^2/\text{sec.} \quad (32)$$

gave

$$C_{O_3}(Z_{\text{cold}}) = 0.3759.$$

* His α_1 , defined by his Eq. (41) is inversely proportional to D_{O_2, O_3} .

Previous studies by the author have shown that for a three component flame, the product of $M G_{\text{fuel}}(Z_c)$ varies slowly with $G_{\text{fuel}}(Z_c)$ and can be roughly approximated as a linear function. Therefore, a theoretical value corresponding to the experimental G_{O_3} at the cold boundary was estimated by passing a straight line through two different calculated values:

$$M G_{O_3}(Z_c) = 0.06653 - 0.03086 (G_{O_3} - 0.3769). \quad (33)$$

This gave

$$M_{\text{the}} = 0.1812. \quad (34)$$

Since Professor Grosse feels that this discrepancy greatly exceeds the likely experimental error³⁰, it is necessary to consider possible sources of the disagreement. Results of previous calculations on an idealization of a free-radical flame can be used to suggest probable sources of error^{26,3}. For an appropriate choice of dimensionless variables, it was found that M could be combined with other parameters to form a dimensionless constant, μ^* , which varied rather slowly with certain parameters:

$$\mu^* = \frac{(m^*)^2 \lambda (T_{\text{max}})}{M^2 C^*} \quad (35)$$

m^*, C^* : The molecular weight and constant pressure heat capacity for a species, β , where M is adjusted to make $G_{\beta}(Z)$ satisfy its cold boundary condition.

k^* : any multiplicative factor in the specific rate for one of the most important reactions in the net rate of production of β .

Thus for 13 and 15-fold variations in the two binary diffusion coefficients involving free-radicals and a 300 fold variation in the ratio of the specific rates for the main combustion reaction to those for the free-radical reaction, μ^* varied only by a factor of 1.8. This suggests that the large ratio $M_{\text{the}}/M_{\text{exp}}$ should be attributed to either too high a value for one or more of the following quantities: (a) $\lambda(T_{\text{max}})$, and, therefore, $\lambda(T)$; (b) the specific rates of reactions which contribute most to dG_{O_3}/dT in the region of most rapid chemical reaction. For the ozone flame, the two most important reactions in the temperature domain responsible for most of the rise in G_{O_3} are: (1) R_1^1 at the higher temperatures within this region; (2) R_2^1 at the

lower. (Note that because of the failure of the kinetic steady-state, R_1^1 and R_2^1 are not directly related). Although further experimental work would be required to choose between the alternatives, it seems less likely that the thermal conductivity is off by over a factor of two. It is worth noting that the activation energy for both R_1^1 and R_2^1 are subject to considerable uncertainty. For example, the ratio of the (1) specific rate assumed here to the one proposed by Benson and Asworthy³¹ is

$$2.9 \exp[-350/T]. \quad (36)$$

At $T = 1000^\circ$, a temperature in the range where R_1^1 makes a large contribution, this ratio is approximately two. Correction of Benson and Asworthy's parameters for (2)

to take account of their use of an older equilibrium constant gave a higher activation energy than the one used in this report ^{5f}. Apparently this was due to their use of graphical instead of least squares data analysis ^{5g}. Conversely, flow system studies gave a lower value which would predict a somewhat lower specific rate at flame temperatures.

Previous theoretical studies predicted burning velocities for a mixture of similar composition

$$x_{O_3} (Z_{cold}) = 0.25 \quad (37)$$

for which Lewis and von Elbe reported a burning velocity of 55 cm.-sec.⁻¹ ³². The results, depending upon the value assumed for the reduced diffusion coefficient range from 47 or 51 ²⁰ to 42 or 46 ¹⁸. There is much better agreement between their calculations and experiment than between the results presented here and experiment.

As shown in Section 5.1, it is not certain that the calculated speeds are correct for the parameters assumed. If they are correct, inspection of Eq. (35) shows that the discrepancy between them and the present results is not related in a simple fashion to the difference in parameters since: (1) The values for the thermal conductivity of the gas mixture used in the two studies are within several percent of each other; (2) According to preceding discussion in this section, the two reactions which are responsible for most of the change in G_{O_3} (which determines M) are R_1^f and R_2^f . Whereas a decrease in either would decrease the theoretical M, the ratios of specific rates in the present study to those used in the earlier work are:

Reaction	\bar{f}	\bar{f}	
T = 1230°	9.9	0.045	(38)
872°	13.1	0.07	
397°	15.8	0.36	

5.7 Test of the Significance of the Kinetic Energy Term in the Equation of Energy Balance.

Previously, heuristic argument has been given to support the contention that kinetic energy of over all gas flow can be an important term in the energy balance equation even when viscosity makes no significant contribution. The argument suggested that the former term would be most important where there was the greatest cancellation in the usual terms of the equation of energy balance, i.e., in the neighborhood of the hot boundary ⁴. Therefore, as a check upon the importance of kinetic energy, a thirtieth order power series was constructed including those terms. The series sums are:

$$(T - T_{max}) = -0.1125 T_{max}$$

	without K.E.	with K.E.	% Error
G_{O_3}	1.9409×10^{-4}	1.9959×10^{-4}	2.8
x_{O_3}	1.1540×10^{-4}	1.1835×10^{-4}	2.5
G_0	1.0607×10^{-2}	1.0936×10^{-2}	3.0
x_0	1.9129×10^{-2}	1.9990×10^{-2}	2.8

(39)

Although these values suggest that the kinetic energy term does not make an important contribution to this flame, calculations on richer ozone flames with higher maximum temperatures (to be included in a later paper) show that it changes the eigenvalue character of the problem.

5.6 Significance of Theoretical Flame Calculations.

As Sandri³³ observed, it is simpler to measure burning velocities than to make theoretical calculations. He argued that the calculations should be used as a means of studying chemical kinetics by comparing theoretical and experimental velocities for appropriate models. The discussion of Sections 5.1, 5.6 illustrates the facts that flame speeds are not particularly sensitive to many parts of a kinetic scheme and that such a comparison could be useful only if the transport coefficients and all but one specific rate which contributed markedly to the rate of consumption of a major fuel component were reasonably well known. However, theoretical calculations could be very useful when the greater detail given by experimental studies of temperature and composition profiles are known. For major components, these have been determined for the methane-oxygen system³⁴. Work on determining free-radical profiles is in progress³⁵. Theoretical calculations would obviate the use of approximations in the diffusion equations made in analyzing current experimental studies and the uncertainty from double differentiation of experimental data³⁶.

Alternatively, they can be used to develop a general understanding of the relation between fuel properties and the comparative importance of various processes. For the particular case of ozone, it seems unlikely that uncertainties in the parameters will qualitatively alter any of the results presented here. This conclusion is founded on a comparison of: (a) the various calculations discussed here; (b) unreported calculations using different specific rates for reactions (1) and (2) which were 6 fold larger for (1) and 45 fold larger for (2) at the hot boundary; (c) unreported calculations for various assumed values of K ; (d) unreported calculations on richer ozone mixtures.

6. Summary of Major Conclusions.

The major conclusions will be summarized according to sections for convenient reference.

Section 4. A single eigen value approximation appears to be adequate for the 20 mole percent ozone flame. Two eigenvalues must be used for sufficiently rich ozone mixtures burning at higher temperatures.

Section 5.1.

(a) It seems that the kinetic rate k_1 may give burning velocities accurate within a factor of about 2 and generally better. Since x_0 does not follow a semblance of the approximation in this (and a fortiori in higher temperature ozone flames), the approximation should be used in calculating any property at all sensitive to x_0 (1).

(b) It is not x_0 but x_0 ^{not} which approximately satisfies a kinetic steady-state condition in a temperature interval of over 175° about the hot boundary.

(c) The existence of a single internal maximum should not be interpreted in

terms of the kinetic steady-state approximation. An alternative approximation applies.

(d) Radical recombination in this ozone flame plays an important role but only for temperatures within about 300° of the hot boundary.

(e) von Karman and Penner underestimated the temperature range over which $R_1^r : M+O_2+O \rightarrow M+O_3$ would be important. It exceeds $R_1^r : M+O_3 \rightarrow O_2+O+M$ over a temperature range of about 200° . The effect of this upon the flame velocity is uncertain.

Sections 5.1 and 5.6. The qualitative differences between the results reported here and those of earlier studies is due to the removing of certain earlier approximations.

Section 5.2.

(a) Convection is the dominant process at all temperatures. Diffusion is more important than conduction at higher temperatures, less at lower.

(b) The specific enthalpy varies over a range of $\pm 8\%$.

Section 5.3. The rate of heat release per unit volume due to radical recombination is over half the total rate for a temperature interval of over 200° about the hot boundary. Contrary to a previous suggestion, it becomes negligible in the cooler part of the flame. Radicals which diffuse there from the hotter regions are effective primarily in $R_2^r : O+O_3 \rightarrow 2 O_2$.

Section 5.4. The spatial separation of kinetic processes is reminiscent of the separation found experimentally in the methane-oxygen flame. There is no approach to chemical before thermal equilibrium.

Section 5.5. There is an approach to diffusion equilibrium before thermal (and chemical) equilibrium. The magnitude of the diffusion velocity exceeds the mass average speed for $T < \text{ca. } 1020^\circ$ for O and from about $T = 910^\circ$ to $T = 1130^\circ$ for O_3 .

Section 5.6. The theoretical M is too large by over a factor of 2. The most likely major sources of the error are too high values at flame temperatures of the rate of $R_1^r : O_3+M \rightarrow O_2+O+M$, or of $R_2^r : O_3+O \rightarrow 2 O_2$, or both.

Section 5.7. The kinetic energy of overall gas flow does not appear to be very important for this ozone flame. Conversely, it can not be ignored for sufficiently rich ozone flames where it changes the character of the eigenvalue problem.

REFERENCES

1. Hirschfelder, J. O., Curtiss, C. F., and Bird, R. B.: Molecular Theory of Gases and Liquids, John Wiley and Sons, New York (1954), Chapter II.
2. Klein, G.: Phil. Trans. Roy. Soc. (London) A249, 389-457 (1959).
3. Campbell, E. S., Heinen, F. J., and Schalit, L. M.: Submitted for publication. (a)[Sect. 4, Eq. 29].
4. Campbell, E. S., Heinen, F. J., and Schalit, L. M.: Submitted for publication.
5. Campbell, E. S. and Nudelman, C.: Reaction Kinetics, Thermodynamics, and Transport Properties in the Ozone-oxygen System. AFOSR TN-60-502. (1960); (a) Table IX, p. 14; (b) Table XIII, p. 76; (c) pp. 57,77; (d) p. 90; (e) pp. 90, 91; (f) pp.90-94; (g) Tables III, V, pp. 7,8.
6. Hirschfelder, J. O., Curtiss, C. F., and Campbell, D. E.: J. Phys. Chem. 57, 403-14 (1953).
7. Campbell, E. S. and Fristrom, R. M.: Chem. Rev. 58, 173-234 (1958); cf. p. 182-4.
8. Rink, J. P., Knight, H. T., Duff, E. E.: J. Chem. Phys. 34, 1942-7 (1961).
9. Camac, M., Vaughan, A.: Avco Everett Research Laboratory Research Report 84, AFBMD-TR-60-22; J. Chem. Phys. 34, 460-470 (1961).
10. Byron, S. R.; J. Chem. Phys. 30, 1380-1392 (1959).
11. Wray, K. L.: J. Chem. Phys. 37, 154-63 (1962).
12. Streng, A. G. and Grosse, A. V.: Sixth Symposium (International) on Combustion, Reinhold Publishing Corp., New York (1957), pp. 265-72, cf. p. 269.
13. Campbell, E. S., Buehler, R., Hirschfelder, J. O., and Hughes, D.: J. Assoc. Compt. Mach. 8, 374-83 (1961); (a) p. 383.
14. Schalit, L. M.: Ph.D. Thesis "Deviation from the Kinetic Steady-State Approximation in a Free-radical Flame", New York University, October, 1961; (a) cf. p. 158; (b) pp. 150-158, 160.
15. Campbell, E. S.: To be submitted for publication.
16. Westenberg, A. A. and Fristrom, R. M.: J. Phys. Chem. 64, 591-601 (1961) cf. p. 598.
17. Heinen, F. J.: Ph.D. Thesis, New York University, August 1962.
18. von Kármán, T. and Penner, S. S.: Selected Combustion Problems I (Agents), Butterworths Scientific Publications (1954), pp. 5-41; (a) cf. p. 40; (b) Eq. (107).
19. Sandri, R.: Can. J. Chem., 34, 324-30 (1960).

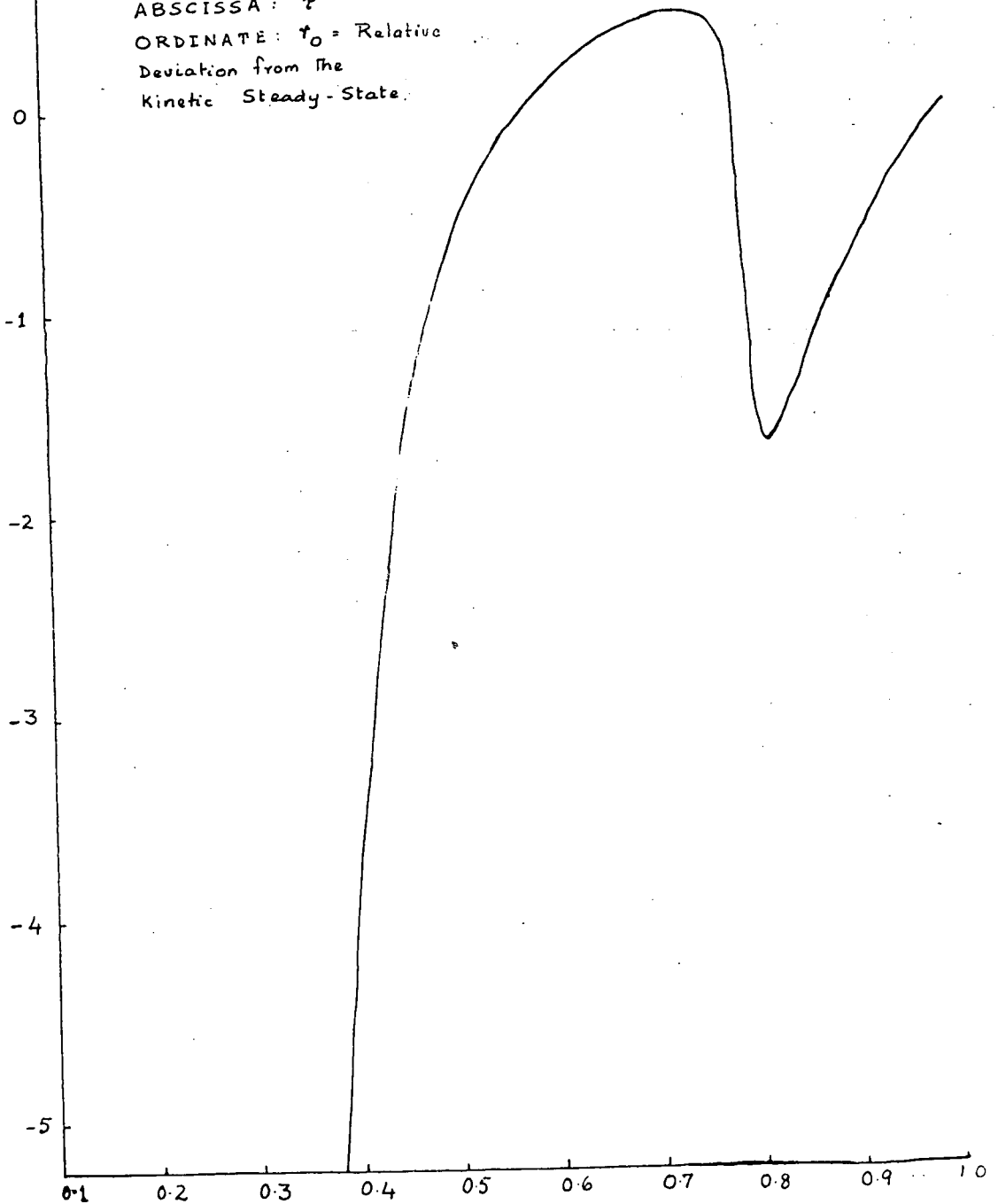
20. Hirschfelder, J. O., Curtiss, C. F., Campbell, D. E.: *J. Phys. Chem.*, 57, 403-14 (1953).
21. Ninth Symposium on Combustion, Academic Press, New York (1963), p. 80, (comment by J. F. Wehner).
22. Hirschfelder, J. O., Curtiss, C. F. and Campbell, D. E.: University of Wisconsin, CM-724, Nov. 24, 1952, cf. p. 35.
23. von Kármán, T., Millán, G., Penner, S.S.: Sixth Symposium (International) on Combustion, Reinhold Publishing Corp., New York (1957), pp. 1-11, cf. pp. 5,7.
24. Palmer, H. B. and Hornig, D. F.: *J. Chem. Phys.* 28, 98-105 (1957).
25. Hirschfelder, J. O.: *Phys. Fluids*, 3, 109 (1960).
26. Campbell, E. S., Heinen, F. J., and Schalit, L.M.: Ninth Symposium on Combustion, Academic Press, New York (1963), pp. 72-80, (a) cf. pp. 75-77.
27. Bartholomé, E.: *Z. Elektrochem.* 54, 169-73 (1950).
28. Fristrom, R. M., Grunfelder, C., and Favin, S.: *J. Phys. Chem.*, 65, 580-90 (1961), (a) cf. p. 590.
29. Westerberg, A. A. and Fristrom, R. M.: *J. Phys. Chem.* 64, 591-601 (1961), cf. p. 597.
30. Private communication.
31. Benson, S. W. and Axworthy, A. E.: *J. Chem. Phys.* 26, 1718-26 (1957).
32. Lewis, B. and von Elbe, G.: *J. Chem. Phys.* 2, 283-90 (1934).
33. Šandri, R.: *Canadian J. Chem.* 34, 313-23 (1956).
34. Fristrom, R.M., Grunfelder, G., and Favin, S.: *J. Phys. Chem.* 65, 580-90 (1961).
35. Private communication from R.M. Fristrom and J. F. Wehner.
36. Westerberg, A. A. and Fristrom, R.M.: *J. Phys. Chem.* 64, 1393-98 (1960).

100

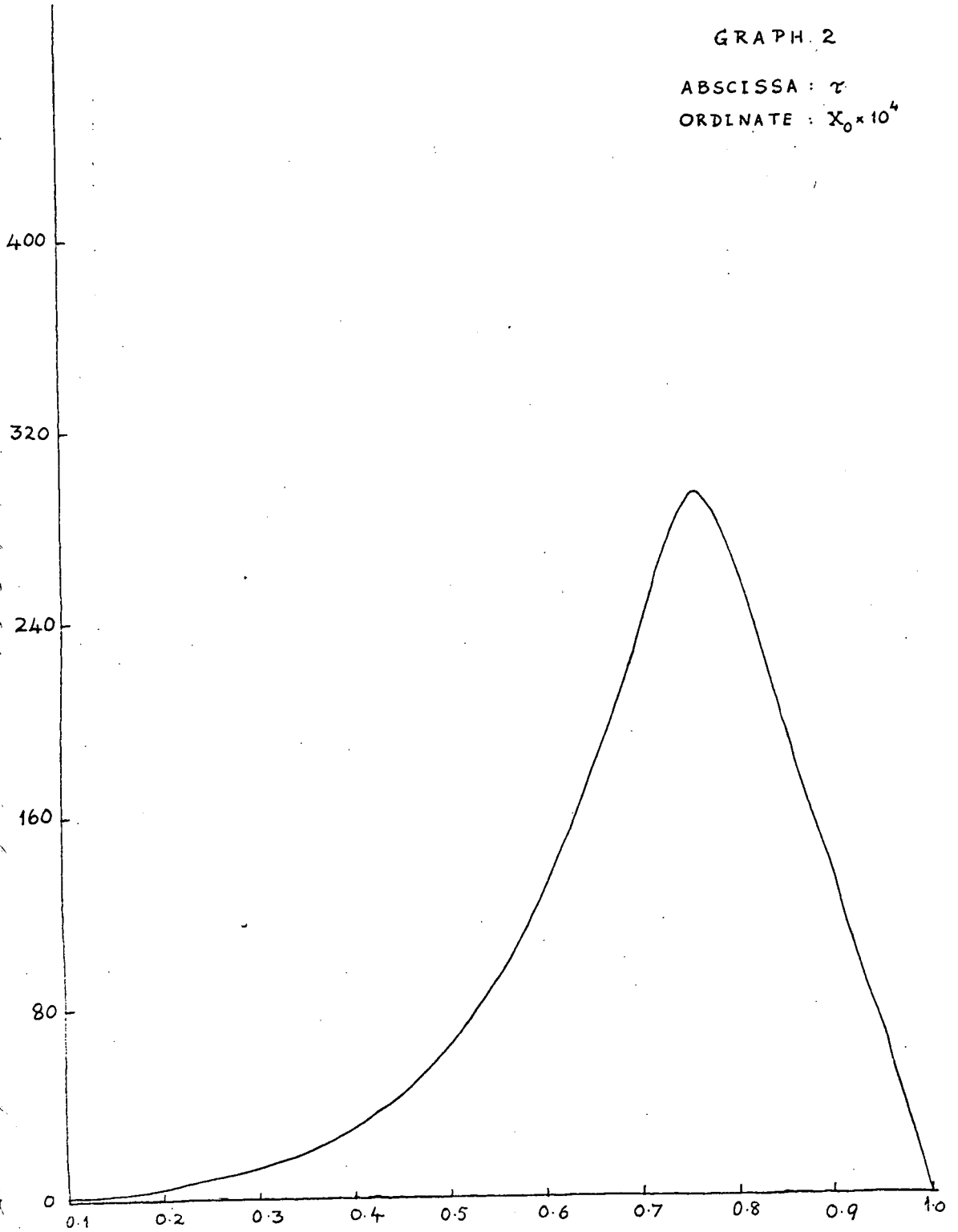
1

GRAPH 1

ABSCISSA: τ
ORDINATE: f_0 = Relative
Deviation from the
Kinetic Steady-State.



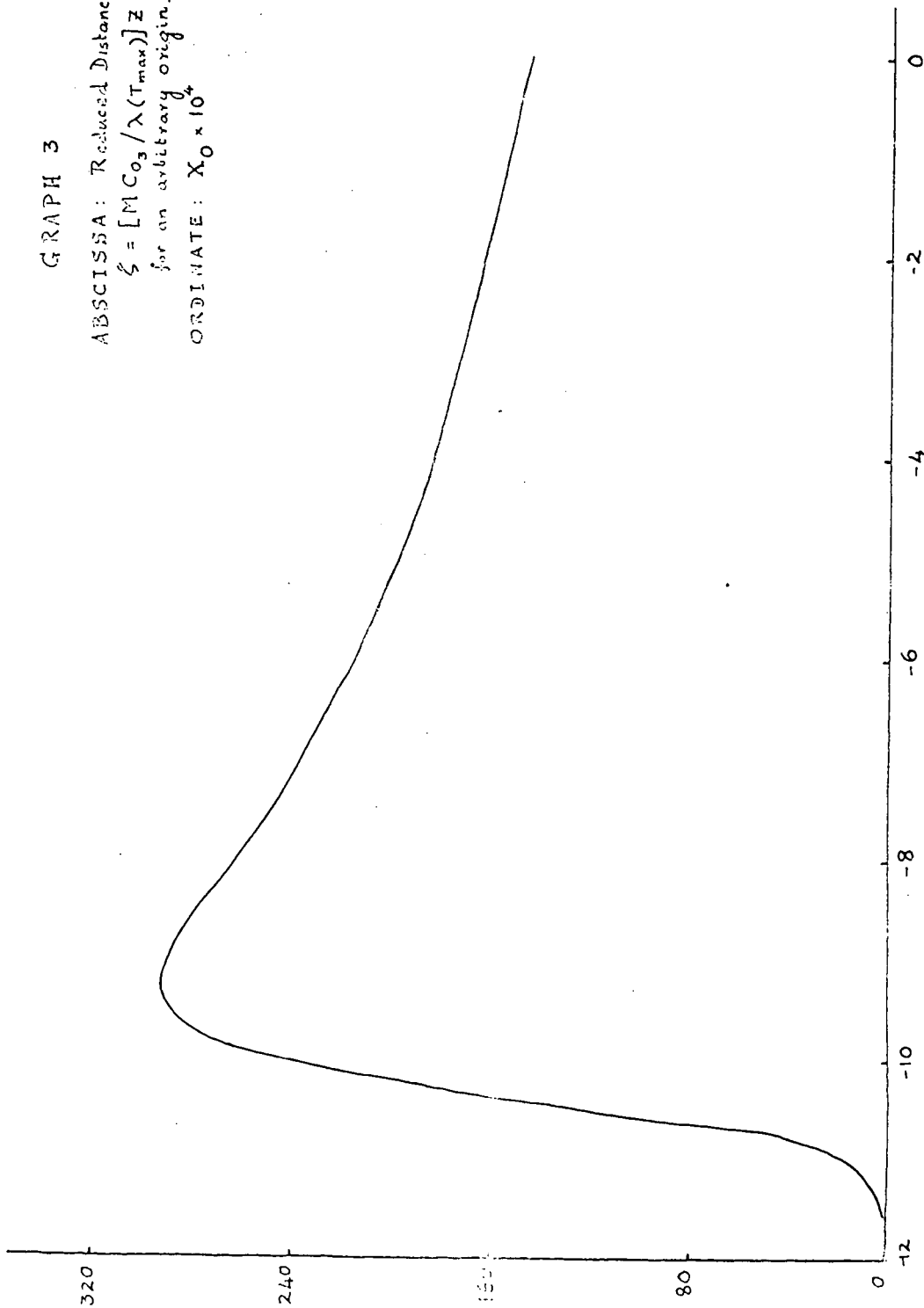
GRAPH 2

ABSCISSA : τ ORDINATE : $X_0 \times 10^4$ 

GRAPH 3

ABSCISSA: Reduced Distance,
 $\xi = [M C_{O_3} / \lambda (T_{max})] Z$
for an arbitrary origin.

ORDINATE: $X_0 \times 10^4$

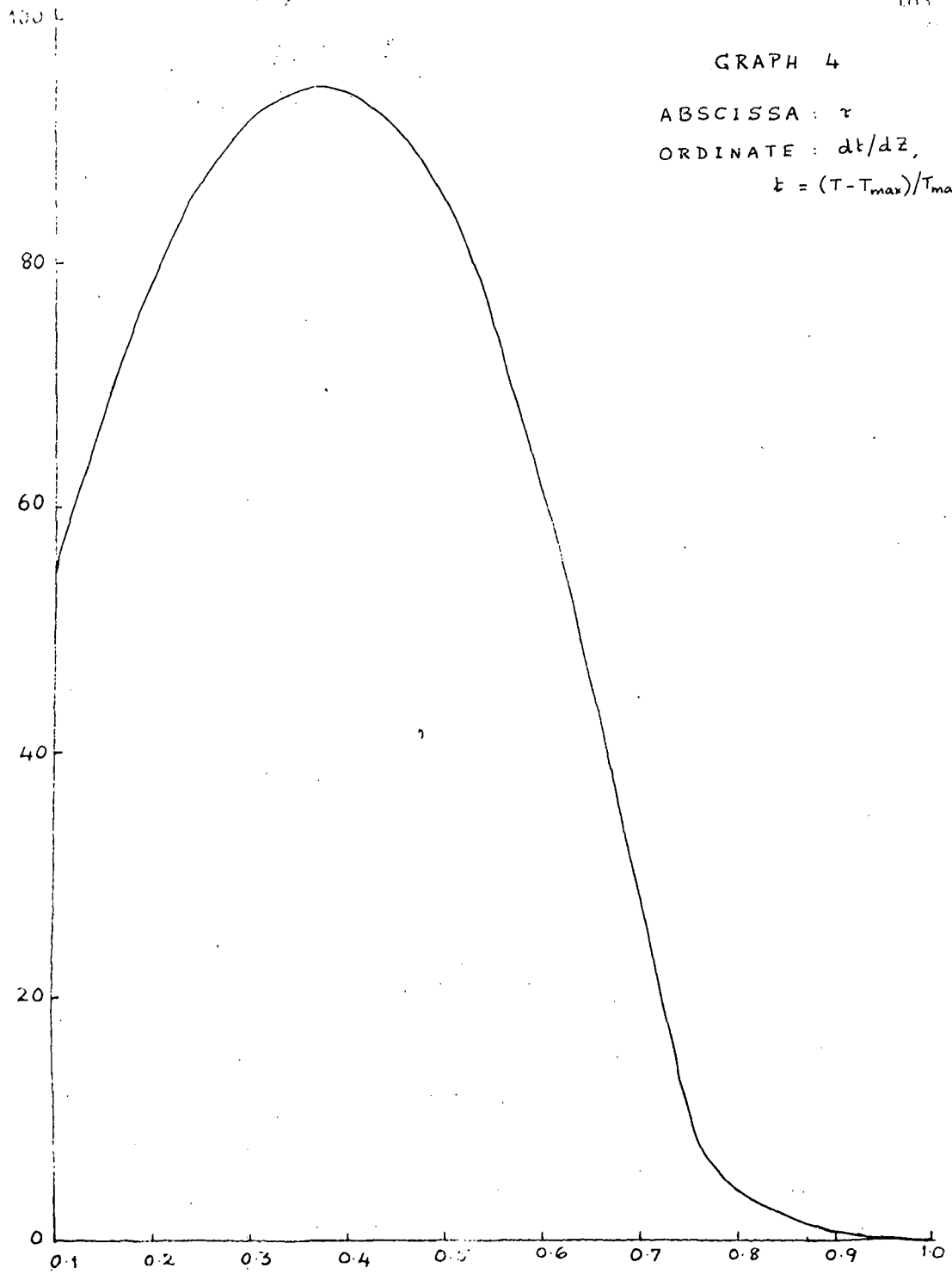


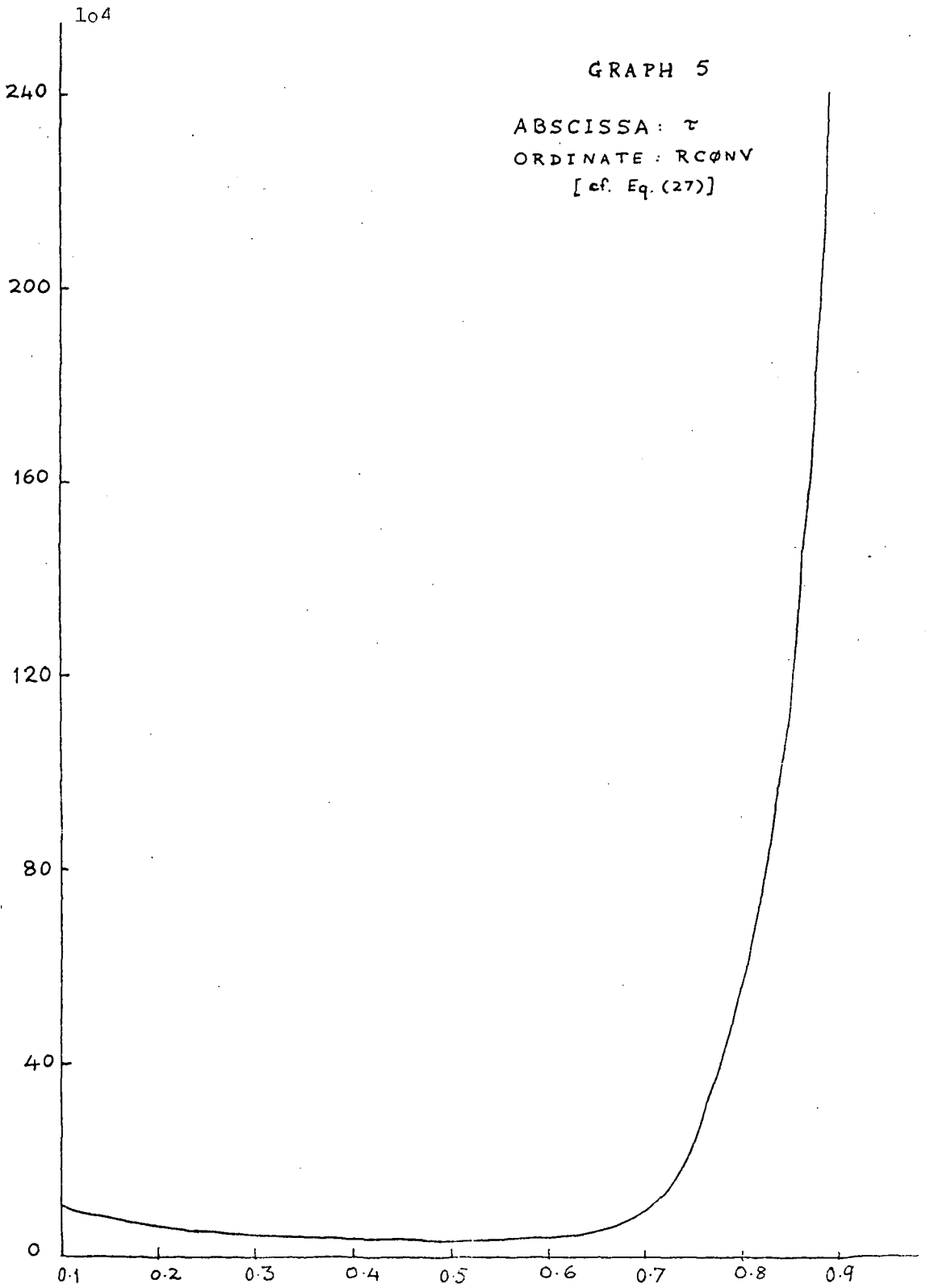
GRAPH 4

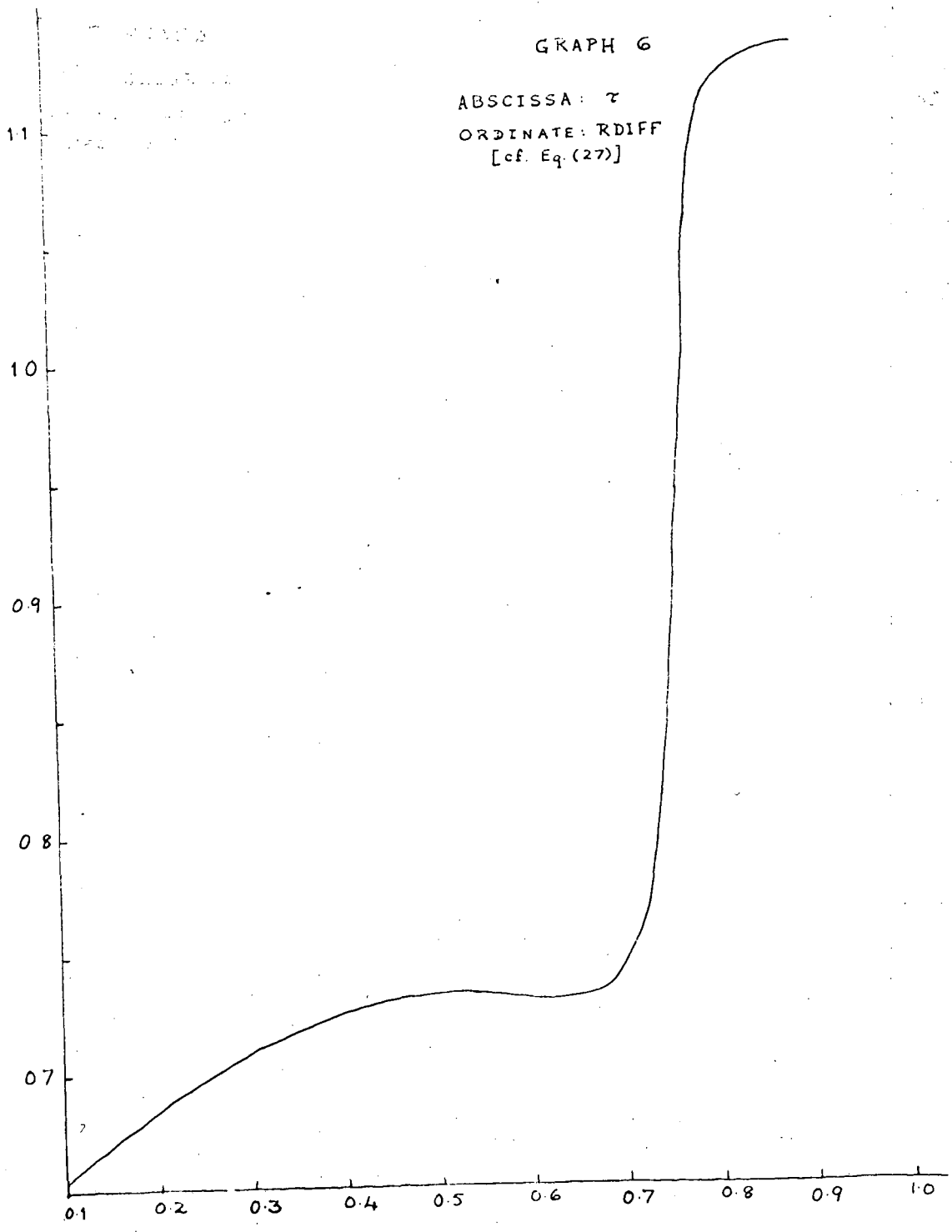
ABSCISSA : τ

ORDINATE : dt/dz ,

$$t = (T - T_{max}) / T_{max}$$







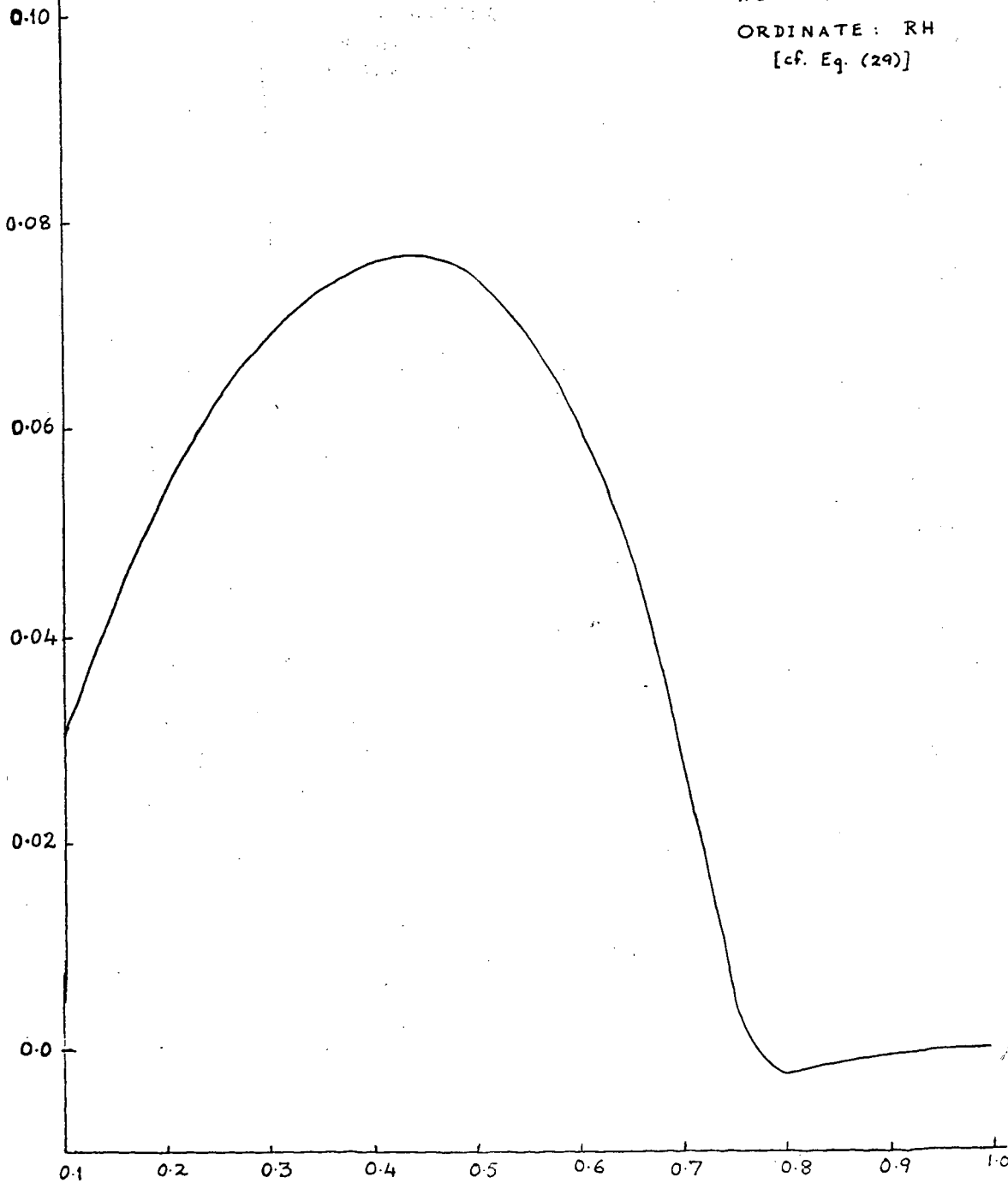
106

GRAPH 7

ABSCISSA: τ

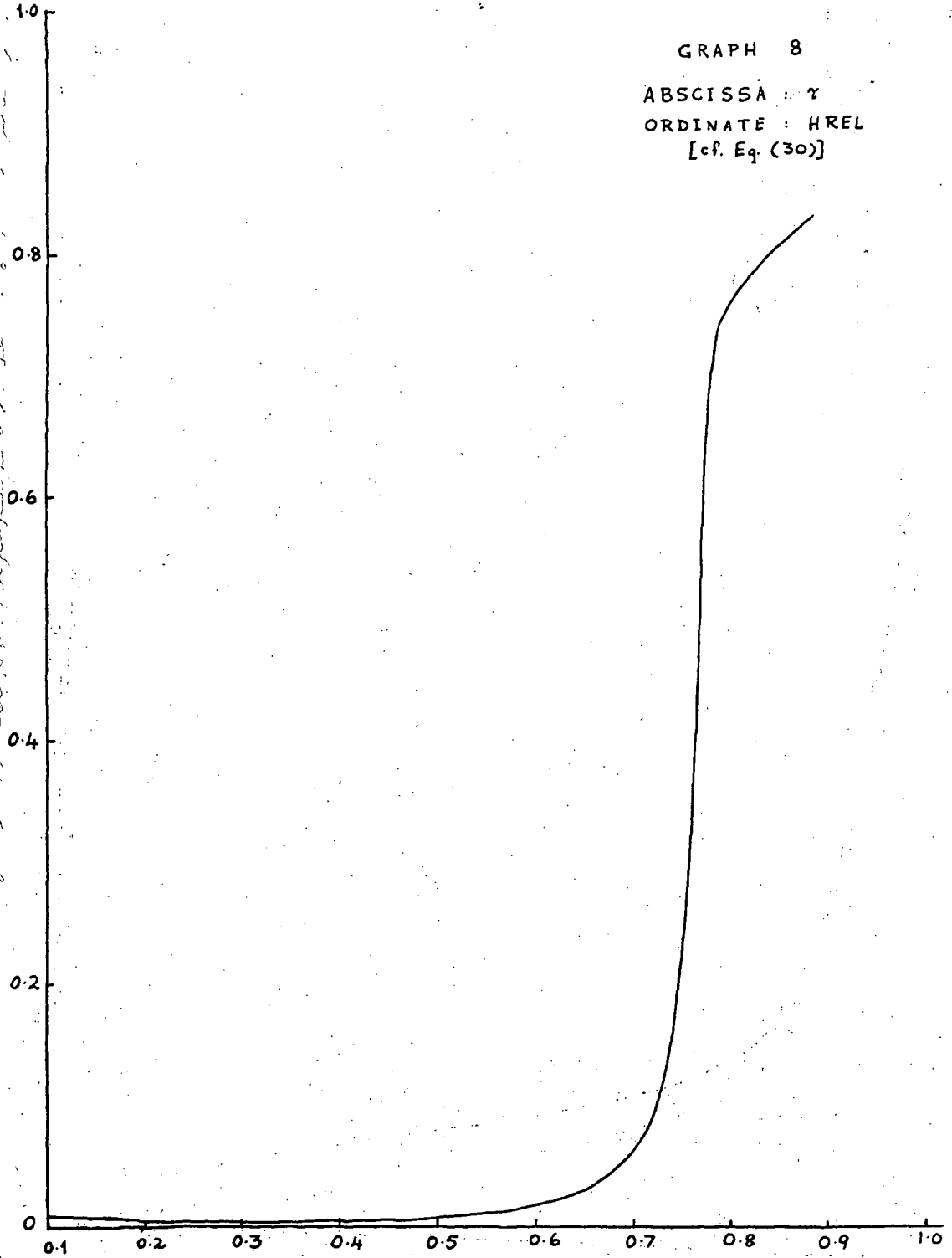
ORDINATE: RH

[cf. Eq. (29)]



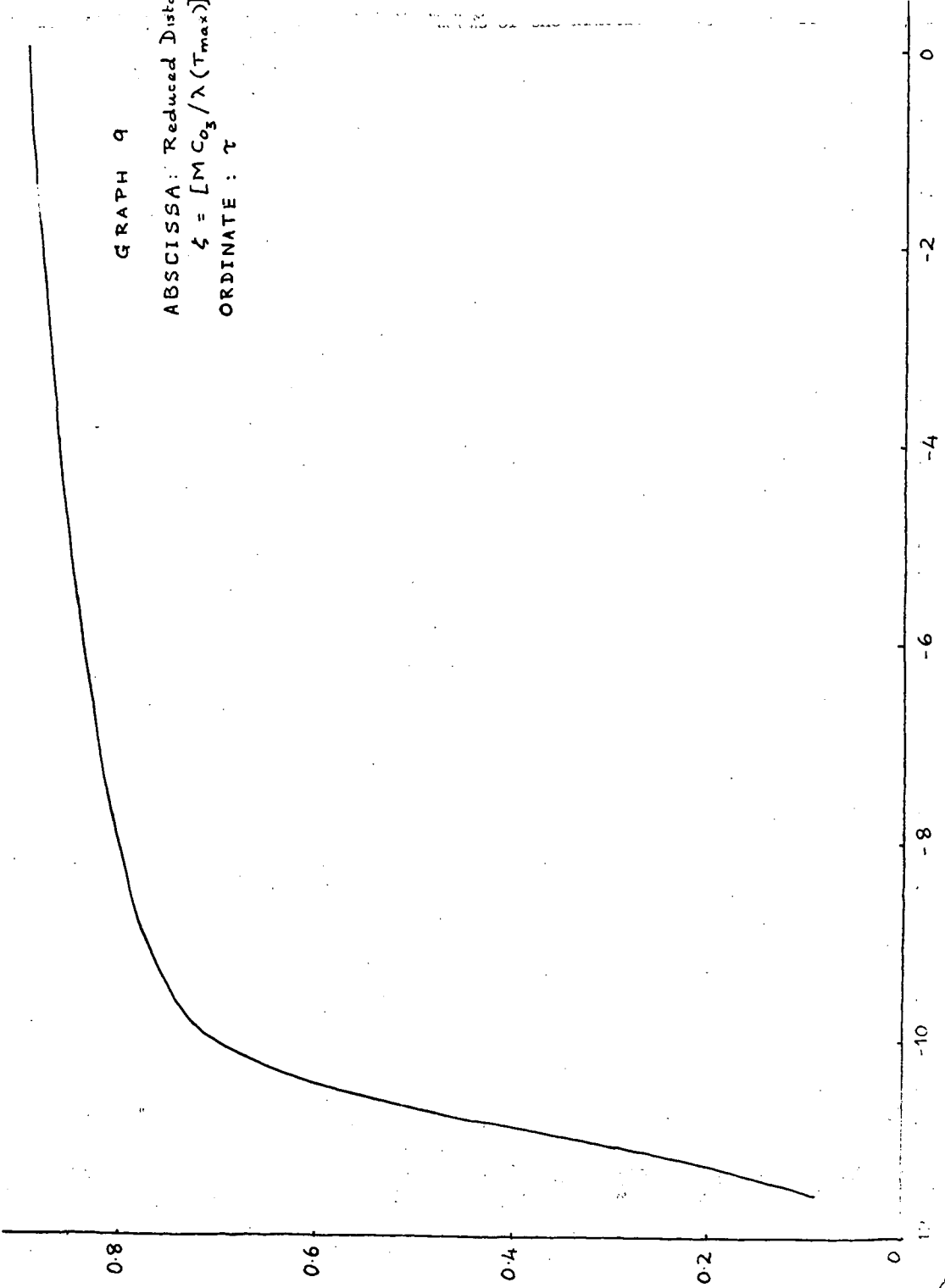
GRAPH 8

ABSCISSA : γ
ORDINATE : HREL
[cf. Eq. (30)]



GRAPH 9

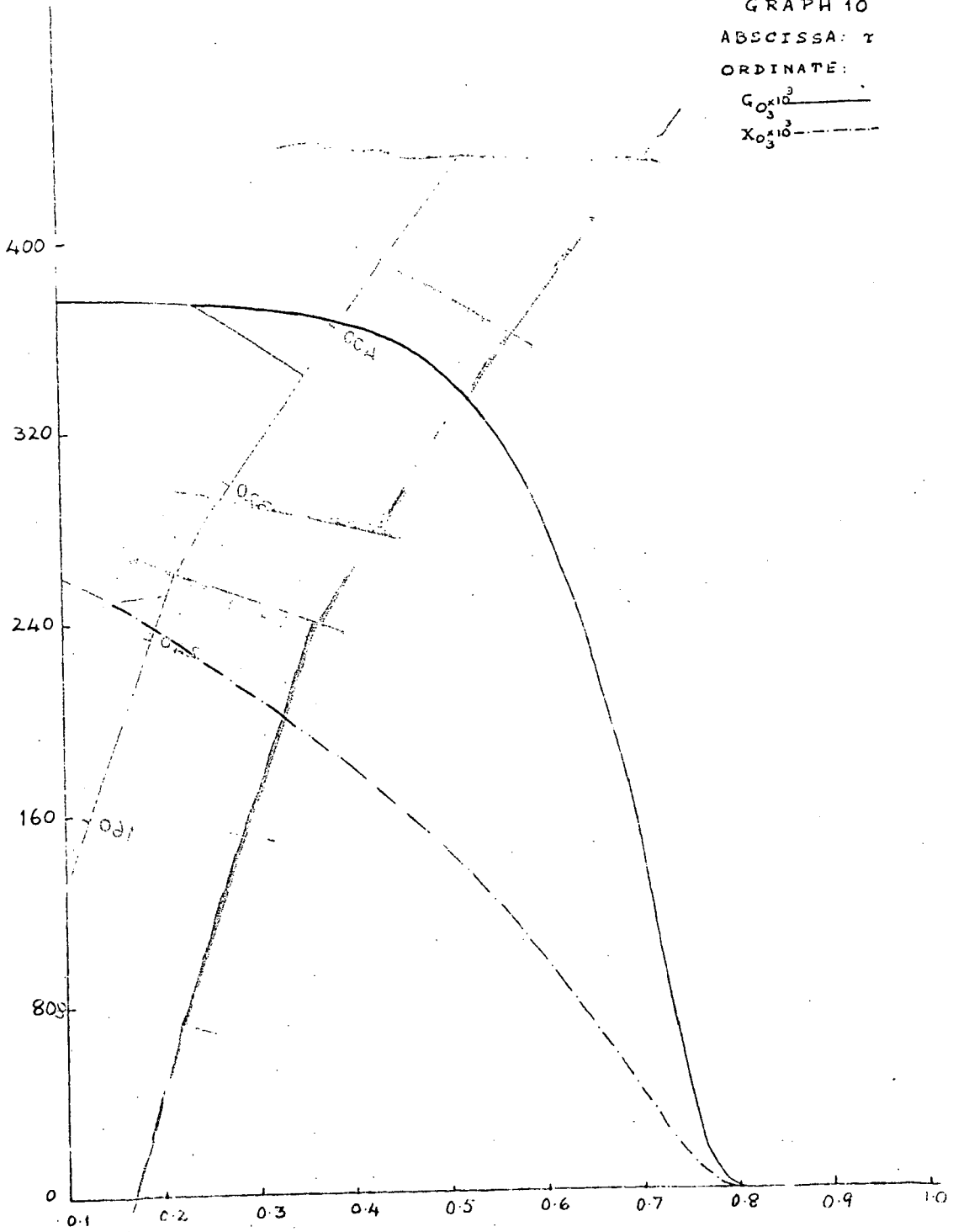
ABSCISSA: Reduced Distance,
 $\xi = [M C_{O_3} / \lambda (T_{max})] Z$
ORDINATE: τ



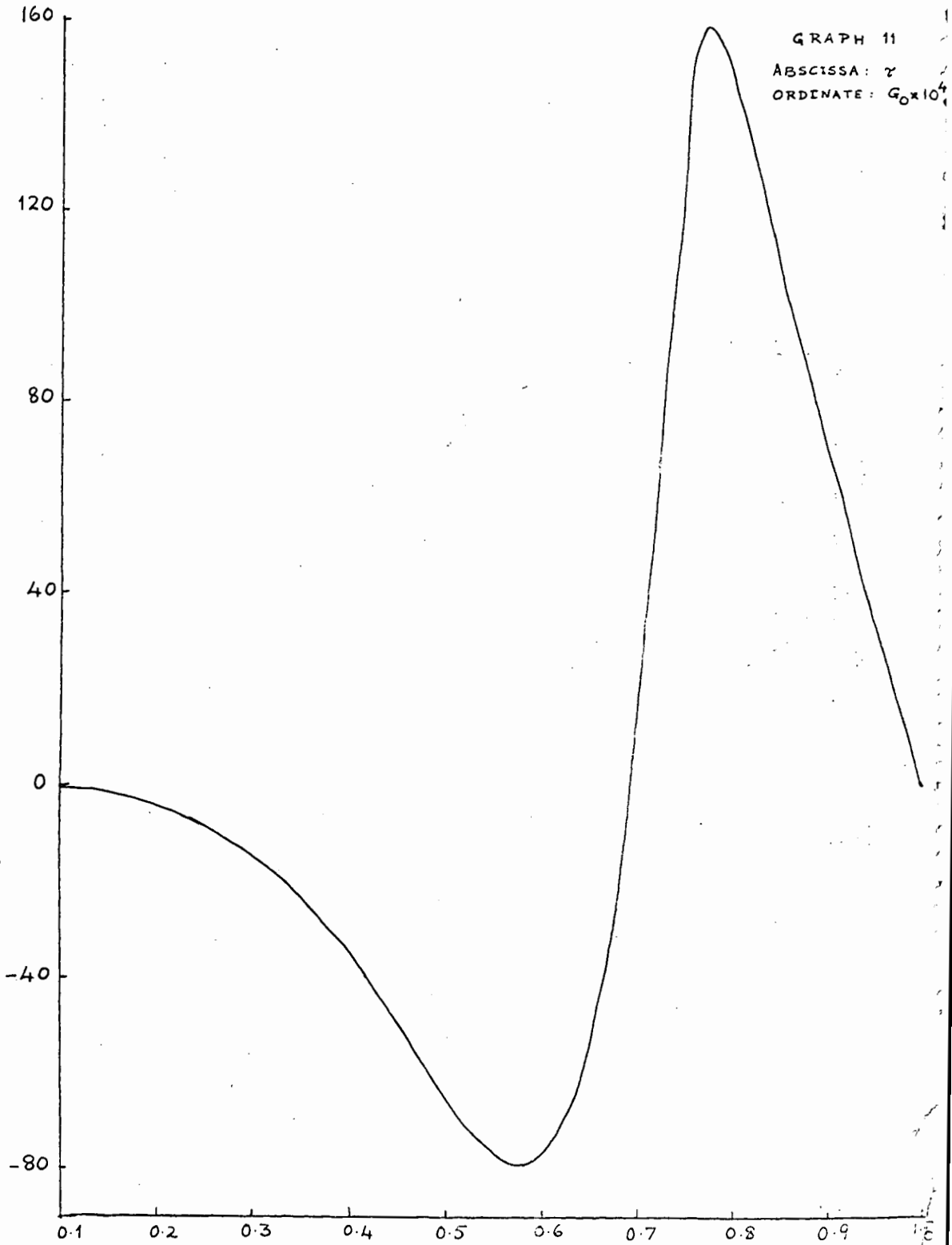
100

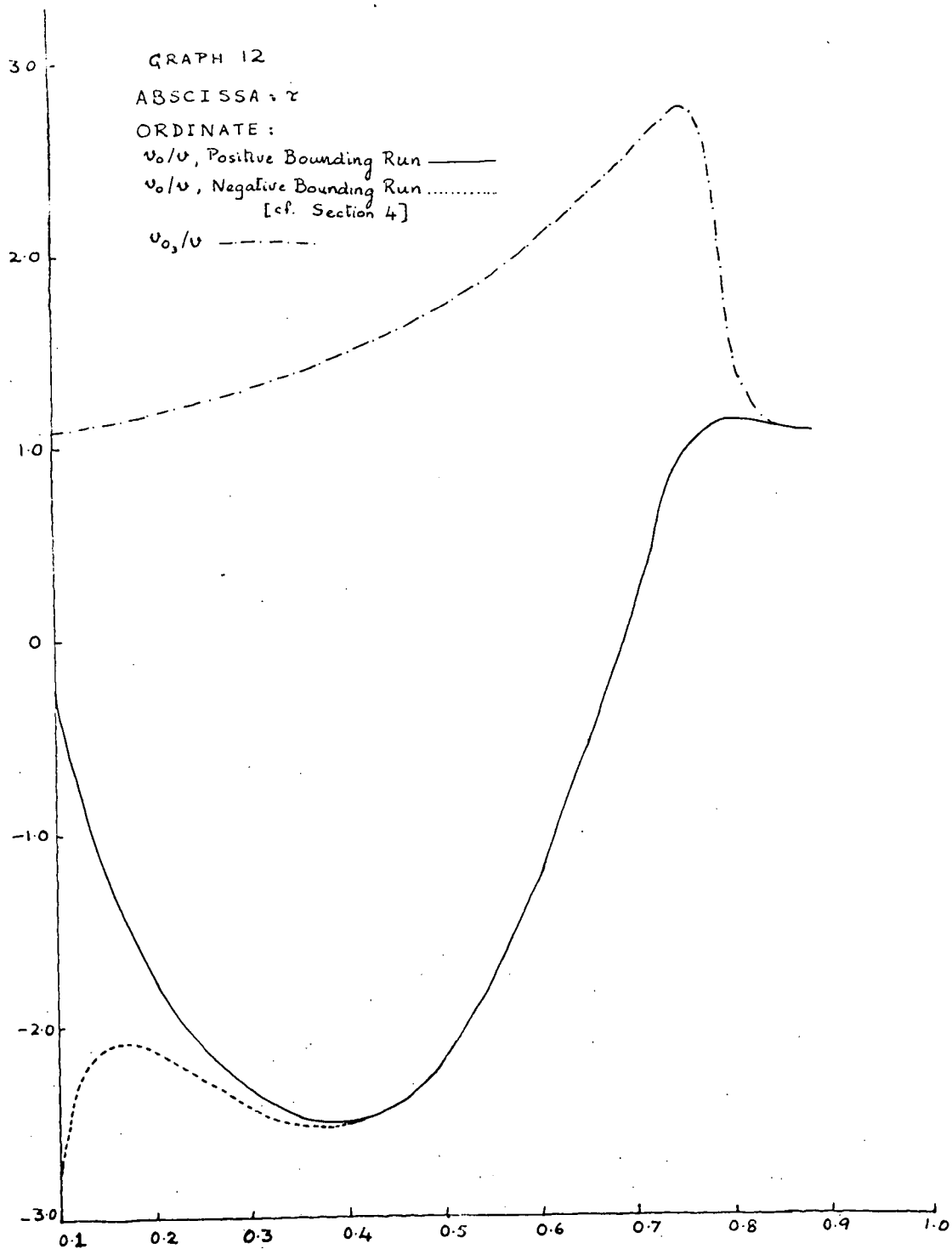
GRAPH 10
ABSCISSA: τ
ORDINATE:

$G_{O_3} \times 10^3$ ———
 $X_{O_3} \times 10^3$ - - -

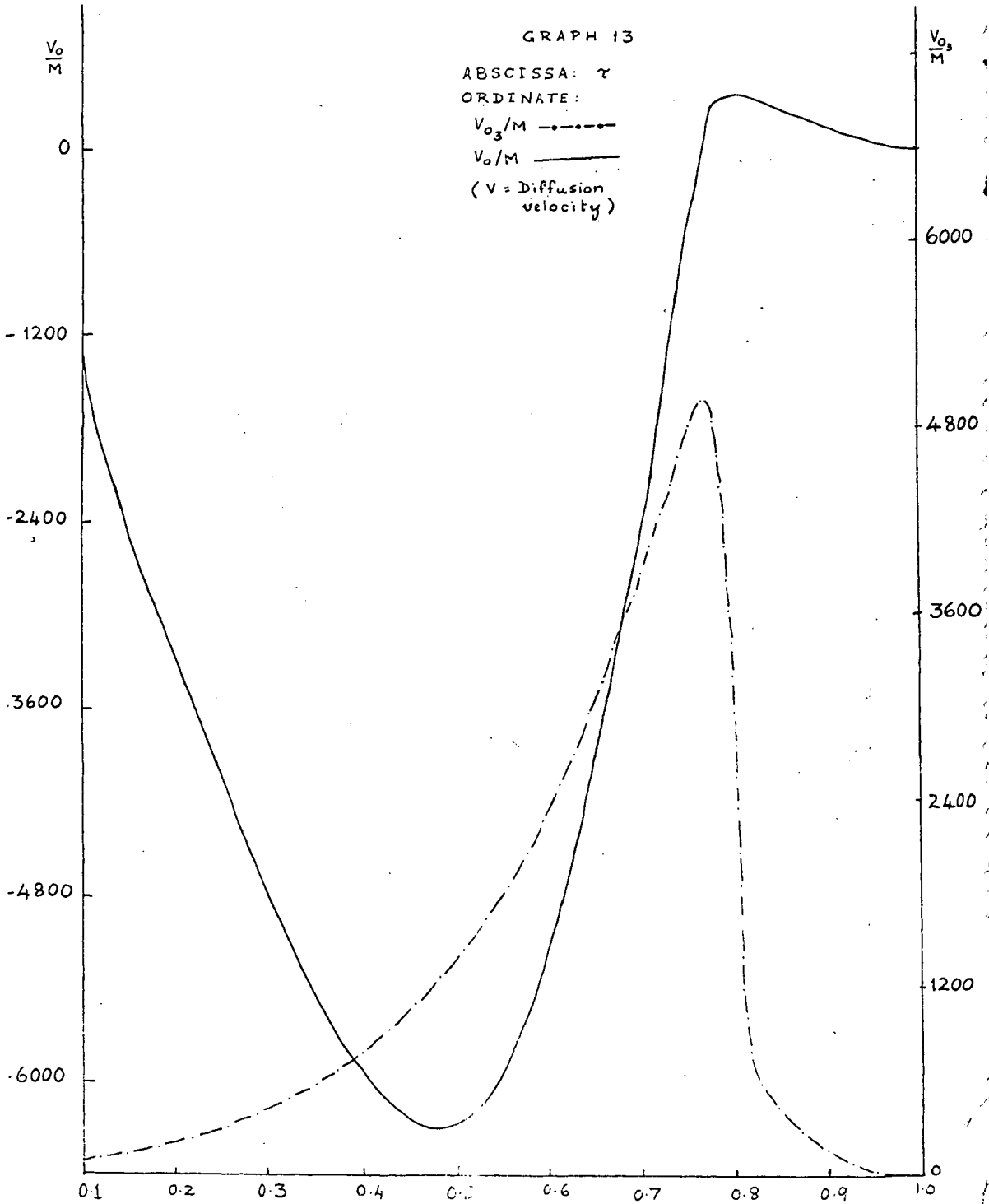


110





GRAPH 13

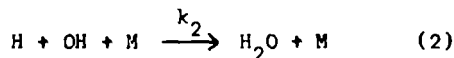
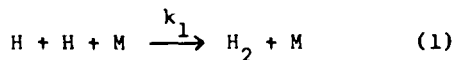


Kinetic Studies of Hydroxyl Radicals in Shock Waves. IV
Recombination Rates in Rich Hydrogen-Oxygen Mixtures

Garry L. Schott and Paul F. Bird

University of California, Los Alamos Scientific Laboratory
Los Alamos, New Mexico

Previous work^{1,2,3} in rich hydrogen-oxygen-diluent flames has shown that in the final stage of the combustion reaction, several reversible reaction steps are maintained substantially in equilibrium, while net progress is achieved by the removal of excess species through three-body recombination reactions. The reversible reactions couple the recombination paths, so that each recombination reaction has the same degree of nonequilibrium (ratio of equilibrium constant to the quotient of the activities of products and reactants), and a single measurement serves to determine the chemical composition. Kinetics studies in such flames^{3,4} have shown that the important recombination reactions are:



and have provided values of the rate coefficients k_1 and k_2 under flame conditions.

Observations on this reaction system in shocked gas mixtures have been reported in earlier papers of the present series,^{5,6,7} and have indicated establishment of equilibrium conditions in the reversible reaction steps promptly at the end of the induction period. This paper reports measurements of the kinetics of the slow disappearance of OH following its maximum concentration in shocked $\text{H}_2\text{-O}_2\text{-Ar}$ mixtures.

EXPERIMENTAL METHODS

Basic shock wave techniques and the ultraviolet line absorption method of determining OH concentration have been discussed in Part I⁵. However, many modifications of apparatus and procedures have been incorporated in the present work, and it is appropriate to present the methods used in this investigation.

The dimensions of the circular shock tube were: internal diameter, 10 cm throughout; driver chamber length, 192 cm; test chamber length, 373 cm. Its construction was of brass, and the interior surface of the test chamber was plated with nickel to decrease its porosity. Single and multiple layer brass shim stock diaphragms were used. Evacuation of the test chamber was accomplished through a side port located 13 cm from the diaphragm position. Final evacuation was done with an NRC B-2 oil diffusion-ejection booster pump backed by a Kinney KC 5 mechanical pump. Vacuum measurements in the test chamber were made with a CVC Philips gauge connected to a side port midway along its length.

Shock velocity measurement was made by a series of five deposited platinum resistor gauges. These gauges were 1 mm by 6 mm and had resistances between 30 and 200 Ω . They were flush mounted with the shorter dimension disposed axially

at intervals of 60.00, 50.00, 30.00, and 29.94 cm, beginning 198 cm from the diaphragm. The gauge outputs were amplified, shaped by 2D21 thyratrons, echoed after 6.25 μ sec, mixed with 10 μ sec timing marks, and presented on an oscilloscope raster⁸ operating at 100 μ sec/line. A modified Tektronix 545 instrument was used.

The quartz windows for the light beam used in measuring OH concentrations were located 1.3 cm downstream from the fourth velocity gauge, some 34 cm from the end of the shock tube. This setup allowed several hundred microseconds for observation of the moving gas behind the incident shock wave before the arrival of the reflected wave from the end plate or the hydrogen driver gas from upstream.

The optical train from the flash discharge lamp to the photomultiplier detector was mounted independently of the shock tube. The flash lamp was operated in the way described in Part I⁵. The lamp itself differed, however, in that the H₂O vapor pressure was regulated at 0.9 mm Hg by $\text{NaC}_2\text{H}_3\text{O}_2 \cdot 3\text{H}_2\text{O} + \text{NaC}_2\text{H}_3\text{O}_2$ at 0°C.²

At this working pressure the luminosity was much freer of spurious fluctuations in intensity than at higher pressures, and its intensity was only slightly diminished. A 2.5 cm focal length spherical lens immediately in front of the lamp focused the luminous region inside the toroidal anode crudely at the monochromator entrance slit 70 cm away, providing condensation of the beam in the (vertical) direction along the 2 mm by 10 mm collimating slits on either side of the shock tube windows. The luminous region itself was substantially as wide as the slits. At the monochromator entrance slit a crude $f = 1.0$ cm cylindrical lens was used with its axis parallel to the slit to condense the beam onto the entrance slit and provide for filling the width of the grating. The 1P28 photomultiplier detector was placed immediately outside the exit slit of the monochromator.

The anode resistor used was 22 K Ω , and 4 ft of RG-71 cable delivered the signal to the input terminal of a type L preamplifier in a Tektronix type 545 oscilloscope. Thus the electronic response time was about 2 μ sec, which approximately matches the time inhomogeneity in the gas sample within the 2 mm width of the beam. Faster response can be achieved, but for recombination rate measurements over periods like 10^{-4} seconds it is unnecessary, and reduction in statistical noise is achieved by relaxing the time resolution.

The oscilloscope photographs contained, in addition to the light transmission record, a base line of zero photoelectric signal, and in displaced positions, a trace bearing timing marks and a trace of the unabsorbed photoelectric signal from a separate flashing of the lamp. This monitor trace was synchronized with the lamp firing in the same way as in the experimental trace. It was needed because the lamp signal, while reproducible in shape, was not quite constant over the time of the experiment.

The JACO model 8200 monochromator was operated in an air thermostat at $36 \pm 1^\circ\text{C}$. The first order spectrum was used with the entrance slit width 0.050 mm and the exit slit width 0.570 mm. The instrument was calibrated with a low pressure mercury discharge spectrum and set to transmit (ideally uniformly) between $3088.7 \leq \lambda_{\text{air}} \leq 3097.3\text{\AA}$, with transmission decreasing linearly to zero at $3087.9\text{\AA} \geq \lambda_{\text{air}}$ and $3098.1\text{\AA} \leq \lambda_{\text{air}}$. Precision of the calibration and thermal stability are estimated at $\pm 0.3\text{\AA}$. Photographic spectra made with film held against the exit slit confirmed the isolation of the lines⁹ between R₂20 ($\lambda_{\text{air}} = 3089.0\text{\AA}$) and Q₂8 ($\lambda_{\text{air}} = 3096.8\text{\AA}$).

Experimental gas mixtures were prepared manometrically from commercial cylinder gases in a thoroughly evacuated glass-lined (domestic hot water) tank and heated from beneath to be mixed by diffusion and convection for at least 24 hours before use. Mass spectrographic analysis of each batch confirmed the absence of unintended components beyond traces of N₂ and CO₂.

DATA REDUCTION

The raw data obtained in each experiment consist primarily of the recorded initial conditions, the shock velocity data contained in the photograph from the raster oscilloscope, and the OH concentration data contained in the oscilloscope photograph of the photoelectric signal. Prior to any chemical kinetics analysis these data are reduced to the apparent OH concentration as a function of time under particular conditions of temperature, pressure, and concentrations of other species. These preliminary data reduction procedures are discussed first.

Shock Velocity

Evaluation of the shock wave velocity from the gauge positions and shock arrival times was done by adjusting each time for small differences in circuitry response (corrections of a few tenths of a microsecond), fitting the five x, t data points to the quadratic expression $t = a + bx + cx^2$, and evaluating $(dt/dx)^{-1}$ at the observation window position. Except in shots at 15 and 20 cm Hg initial pressure, c was invariably positive, and the average attenuation of the shock velocity was about 1% per meter (0.1% per tube diameter). The heavier diaphragms used for the higher pressure shots apparently opened more slowly and sometimes caused the shock velocity to reach its maximum further downstream¹⁰. From least squares treatment, the indicated uncertainty in b , which is most of the uncertainty in dt/dx , was usually a few tenths of a percent. In a few cases it was as great as 1%, indicating irregular behavior of the shocks and/or the detection system.

Hugoniot Calculations

Solution of the Rankine-Hugoniot equations was carried out by means of a computer code¹¹ to obtain the temperature, density, and composition behind each shock wave as functions of the initial conditions, the shock velocity, and the progress of chemical reaction. The computations for equilibrium conditions were obtained straightforwardly by the general method of Brinkley¹² which is incorporated in the shock equations code. The restricted equilibrium computations for selected extents of recombination less than the final equilibrium extent were made by arbitrarily constraining¹³ the number of moles per original mole of material in the system. The species Ar, H₂, O₂, H₂O, OH, H, and O were considered in the computations. Ideal gas thermodynamic functions for H₂, O₂, H₂O, OH, and O were obtained from the JANAF tables¹⁴ and formulated for interpolation in the polynomial form used previously in this¹¹ and other¹⁵ laboratories. Ar and H were treated as calorically perfect and the coefficients were evaluated accordingly.

Determination of [OH]

The calibration curve relating absorbance and OH concentration used in the earlier work was an empirical one based on observations of equilibrium gases in shock waves. For the present work, a much more refined method has been developed. It is a semi-empirical method based in part on absorbance measurements in equilibrium shocked gas, but it makes use of the fundamental molecular properties of OH to extend the calibration to regimes of OH concentration, temperature, and pressure where equilibrium observations could not be made.

The calibration program consists of three parts: (1) experimental determination of the spectral intensity distribution of our OH line source, (2) formulation of the absorption spectrum of OH on the basis of theory and integrated absorption coefficients derived from independent experiments, and (3) numerical synthesis of the response of thermal absorber to the lamp spectrum in order to account, within existing uncertainty in the absorption spectrum parameters, for the experimentally determined absorbance of equilibrium mixtures. The details of these steps are being reported separately; the methods used and their application to the old, higher

pressure lamp spectrum are described elsewhere¹⁶. The principal features of the calibration are summarized as follows. The line shapes and relative intensities in the lamp spectrum were determined from high dispersion photographic spectrograms made by repeated flashes. The source spectrum and the absorber spectrum were each described in the computations by superposition of lines having combined Doppler and Lorentz broadening¹⁷. The line strengths given by Dieke and Crosswhite⁹ as modified by Learner¹⁸ were used. The values of the transition probability coefficient, F , and the pressure broadening parameter, a , (as defined in the literature¹⁹) found to describe suitably the measured equilibrium absorbances were $F = 3.50 \times 10^{-4}$ and $a = 335 P(\text{atm})/T(^{\circ}\text{K})$. These values are in reasonable agreement with those reported elsewhere^{19,20}. Perhaps the present calibration is not significantly more accurate than the old empirical one in the regime where the latter was determined, but the extension to other regimes is superior, and the whole calibration is on a much firmer basis.

The computer program generates the absorbance ($-\log_{10}$ of the fractional transmission) of the incident spectrum for a specified absorber temperature, pressure, and optical density (product of OH concentration and path length). Points covering the ranges of these parameters involved in the experiments were assembled and a numerical interpolation scheme was used to derive the OH concentration for a series of absorbance values during each experiment. For this purpose an average temperature and pressure for each experiment was obtained as the mean of the values computed for partial equilibrium conditions with zero recombination and complete equilibrium conditions. The absorbance for each optical density in the table was first interpolated to the appropriate temperature and then the appropriate pressure. Finally the several measured absorbances were interpolated to optical densities and hence OH concentrations. A quadratic interpolation formula was used in each step, with two of the three values of the independent variable bracketing the desired value.

Rate Equation

The rate equation for the disappearance of OH in a reacting mixture of H_2 , O_2 , H_2O , OH, H, and O is developed for conditions of variable density shock wave flow in a manner which incorporates the recombination mechanism, reactions (1) and (2), and anticipates the insertion of partial equilibrium relationships among the several species. Let us define the mole number of each species, n_i , by the relationship

$$\rho n_i = [I] \quad (3)$$

where ρ is the density in grams per liter and $[I]$ is the concentration of species I in moles per liter. We then identify the partial derivative with respect to time ($\partial[I]/\partial t$) = $\rho dn_i/dt$ as the net volumetric rate of chemical production of species I²¹.

Now it has been shown that^{1,2,22} in the system being considered, equating the total volumetric rate of production of all species to the combined chemical recombination rate from all paths, R_{recomb} , leads to

$$\rho d(n_{\text{H}} + n_{\text{OH}} + 2n_{\text{O}} + 2n_{\text{O}_2})/dt = -2 R_{\text{recomb}} \quad (4)$$

To formulate n_{H} , n_{O} , and n_{O_2} , and their derivatives in terms of the measured $[\text{OH}]$, we proceed as follows. Let

$$[\text{OH}] = \alpha [\text{H}]. \quad (5)$$

Then

$$n_{\text{OH}} = \alpha n_{\text{H}} \quad (6)$$

and

$$\rho \frac{dn_H}{dt} = (\rho/\alpha) \frac{dn_{OH}}{dt} - (\rho n_{OH}/\alpha^2) \frac{d\alpha}{dt}. \quad (7)$$

Similarly let

$$[O] + [O_2] = \beta [OH]^2, \quad (8)$$

so that

$$n_O + n_{O_2} = \beta \rho n_{OH}^2 \quad (9)$$

and

$$\rho \frac{d(n_O + n_{O_2})}{dt} = 2\beta \rho^2 n_{OH} \frac{dn_{OH}}{dt} + \rho^2 n_{OH}^2 \frac{d\beta}{dt} + \beta \rho n_{OH}^2 \frac{d\rho}{dt}. \quad (10)$$

The scale of time, t , experienced by an element of shocked gas is converted to the scale τ at an observation point stationary with respect to the unshocked gas by

$$dt = (\rho/\rho_0) d\tau \quad (11)$$

where ρ_0 is the density of the unshocked gas.

The variables ρ , α , and β are considered as functions of the independent variable $[OH]$. Then from the definition, equation (3), it follows that

$$\rho \frac{dn_{OH}}{dt} = \frac{d[OH]}{dt} (1 - \frac{d \ln \rho}{d \ln [OH]}) \quad (12)$$

Finally, for conditions in which the recombination mechanism consists of reactions (1) and (2) and all dissociation rates are negligible, we express the total recombination rate, R_{recomb} , in terms of concentrations and conventional rate coefficients by

$$R_{recomb} = k_1 [M_1][H]^2 + k_2 [M_2][H][OH] \quad (13)$$

where $[M_1]$ and $[M_2]$ are the total gas concentrations acting as third bodies in recombination reactions (1) and (2).

Then substitution of equations (5) - (13) into equation (4) and rearrangement of terms leads to

$$\begin{aligned} \rho \frac{d(1/[OH])}{d\tau} = & 2(\rho/\rho_0) k_1 [M_1] \left(1 + \frac{\alpha k_2 [M_2]}{k_1 [M_1]}\right) \\ & \left\{ (1 + \alpha + 4\alpha\beta[OH])(1 - \frac{d \ln \rho}{d \ln [OH]}) - \frac{d \ln \alpha}{d \ln [OH]} \right. \\ & \left. + 2\alpha\beta[OH] \left(\frac{d \ln \beta}{d \ln [OH]} + \frac{d \ln \rho}{d \ln [OH]}\right) \right\}^{-1}. \end{aligned} \quad (14)$$

For convenience we now refer to the factor 2 and the complicated expression in braces on the right hand side of equation (14) as A , and for lack of information to the contrary, identify the third body concentrations $[M_1]$ and $[M_2]$ with the total gas concentration, $[M]$. Thus the rate coefficients are referred to the experimental gas mixture, and we re-write the rate equation as

$$\rho \frac{d(1/[OH])}{d\tau} = A (\rho/\rho_0) [M] (k_1 + \alpha k_2) \quad (15)$$

Equation (15) has been cast in this form in anticipation of finding the disappearance of OH to be effectively second order in OH and of determining the slope of an approximately linear plot of $1/[OH]$ versus τ from each experiment.

RESULTS

Experiments have been done with three different gas mixtures, whose compositions are given below:

Mixture Designation	%H ₂	%O ₂	%Ar
R-1	4.03	1.00	94.97
R-2	2.02	0.50	97.48
R-3	8.07	1.00	90.93

The results of thirty-one experiments in the temperature range $1400^\circ \leq T \leq 2000^\circ\text{K}$ are assembled in Table I. In these experiments, the plots from which $d(1/[\text{OH}])/d\tau$ was determined were approximately straight over the entire interval plotted, which in most cases was from about 50 μsec to about 500 μsec after passage of the shock front. During this period $[\text{OH}]$ fell from the values given in column 3 to those given in column 4. Column 5 contains the slopes derived from the plots. Columns 6 and 7 contain the values of $[\text{OH}]$ and temperature computed from the initial data and shock velocity for each experiment on the basis of equilibrium with respect to all reactions except dissociation-recombination reactions and no change in the total mole number $n = \sum n_i$, from the value n_0 in the unshocked gas mixture. Implicit in these computations are the relationships:

$$\alpha = [\text{OH}]/[\text{H}] = K_{18}[\text{H}_2\text{O}]/[\text{H}_2] \quad (16)$$

and

$$\beta = ([\text{O}] + [\text{O}_2])/[\text{OH}]^2 = K_{19}/[\text{H}_2\text{O}] + K_{20}/[\text{H}_2] \quad (17)$$

where K_{18} , K_{19} , and K_{20} are the equilibrium constants for the reactions



and



Complete conversion of the initial O₂ to H₂O with no production of OH, H, or O corresponds to final values of n/n_0 of 0.990 in mixtures R-1 and R-3 and 0.995 in mixture R-2, and computations show that $[\text{OH}]$ varies approximately linearly with n/n_0 .

To interpret $d(1/[\text{OH}])/d\tau$ by equation (15) for conditions prevailing early in the recombination reaction, computations were made of partial equilibrium conditions with $n/n_0 = 1.000$ and $n/n_0 = 0.999$. The values of $[\text{M}]$, α , (ρ/ρ_0) , and β $[\text{OH}]$ were taken as the means of these two computations, and the logarithmic derivatives which appear in the factor A were approximated from the finite differences between these two computations. $[\text{M}]$ and α so evaluated are listed in columns 8 and 9 of Table I. (ρ/ρ_0) was invariably between 3.2 and 3.6. The factor A varied systematically from 1.7 to 1.0 as α varied from 0.01 to 0.1.

The derived values of $k_1 + \alpha k_2$ given in the last column of Table I were obtained from the measured slopes in column 5 by multiplication by the factor $\alpha\rho/\rho[\text{M}]A$. The following values of k_1 and k_2/k_1 have been derived by linear least squares fitting of the entire set of values of $k_1 + \alpha k_2$ in Table I and the indicated subsets thereof.

Group of Experiments				k_1	k_2/k_1
T range (°K)	[M] range mole/liter $\times 10^3$	Mixtures	No.	liter ² mole ⁻² sec ⁻¹ $\times 10^{-8}$	
1400-2000	8-36	All	31	6.6	7.1
1400-1700	8-36	All	17	6.1	11.4
1700-2000	9-30	All	14	5.9	8.5
1400-1700	8-10	R-1,R-3	6	5.6	17.8
1400-1700	17-19	R-1,R-3	7	6.1	9.5
1700-2000	9-10	R-1,R-3	6	6.6	7.7
1700-2000	17-19	R-1,R-3	4	4.9	14.0

We conclude that k_1 in an atmosphere consisting primarily of argon is $6 \pm 1 \times 10^8$ liter²mole⁻²sec⁻¹ between 1400° and 2000°K, and that $k_2/k_1 = 10 \pm 5$ under these same conditions. No variation of either k_1 or k_2/k_1 with temperature can be established. When the points are plotted, a small trend toward lower apparent rate coefficients at higher values of [M] or [OH] is shown between the groups of points in mixtures R-1 and R-3 with [M] = 9×10^{-3} mole/liter and [M] = 18×10^{-3} mole/liter. However, this trend is not consistently borne out by the few experiments at still higher densities or the rather scattered data from mixture R-2. Such a trend may or may not be due to a small systematic error in the OH absorption spectrum calibration.

To be sure, significant departure of α from the assumed partial equilibrium value of $K_{18} [H_2O]/[H_2]$ would lead to serious error in the rate coefficients deduced. However, the available data²³ on the rates of the bimolecular reaction paths by which this equilibrium is approached indicate that α does not depart from its ideal value by more than one percent under the conditions of the present experiments. Departure of [O] and [O₂] from their assumed equilibrium relationship to [OH] would be less serious in the rich mixtures studied here.

The composition of the gas acting as the third body in the present work differs greatly from that which has been used in any of the other studies in this system, and the rate coefficients determined cannot be compared in detail. The values found here are generally lower than those reported^{3,4} in mixtures composed primarily of H₂, N₂, and H₂O. Within our own experiments, the only component of [M] to vary appreciably and systematically as α was varied is [H₂], which was about eight times as large (after formation of H₂O, H, and OH) in the experiments with mixture R-3 as in those with mixture R-2. If H₂ were markedly more efficient than Ar in catalyzing reactions (1) and (2), the apparent rate coefficients at lower α would be increased, producing higher k_1 values and lower k_2/k_1 values. Other workers^{3,4} have not found evidence for marked efficiency of H₂ as third body.

GASDYNAMIC INSTABILITY

Nine additional experiments were attempted at temperatures between 1100° and 1300°K. These yielded apparent rate coefficients which scattered between 50% and 200% of those found above 1400°K. In several of these experiments, particularly those at higher densities, there were undulations of the OH absorption record and other indications of spin-like instability in the flow behind the shock wave. Investigation of this behavior is outside the scope of the present paper. However it may well be that such instabilities are in fact present in the higher temperature experiments, but their scale is evidently fine enough not to disrupt the kinetics dramatically.

Table I
Summary of Experimental Results

Concentrations are in moles/liter, times in seconds, temperatures in °K, and velocities in km/sec.

Mix	Shock Velocity (obs'd.)	[OH] × 10 ⁶ (obs'd.)	initial	final	$\frac{d(1/[OH])}{dt}$ × 10 ⁻⁹	[OH] × 10 ⁶ (calc'd.)	T (calc'd.)	[M] × 10 ³ (calc'd.)	$\alpha \times 10^2$ (calc'd.)	(k ₁ + ak ₂) × 10 ⁻⁸
R-1	1.226	5.2	2.5	2.5	.80	6.64	1546	8.84	4.49	10.5
R-1	1.232	5.1	2.2	2.2	.68	6.87	1560	8.87	4.65	9.3
R-1	1.251	7.2	2.4	2.4	.75	7.56	1599	8.92	5.13	11.3
R-1	1.396	14.2	4.5	4.5	.42	13.78	1921	9.31	9.71	12.1
R-1	1.408	13.0	3.5	3.5	.37	14.35	1949	9.34	10.15	11.4
R-1	1.417	16.9	4.1	4.1	.37	14.81	1972	9.36	10.50	11.8
R-1	1.200	6.9	1.8	1.8	1.47	11.57	1494	17.52	3.89	8.4
R-1	1.223	11.0	1.2	1.2	1.39	13.12	1541	17.67	4.43	9.0
R-1	1.275	14.0	1.4	1.4	1.05	16.97	1651	17.99	5.79	9.0
R-1	1.293	17.1	2.2	2.2	1.09	18.40	1689	18.09	6.31	10.2
R-1	1.385	26.7	2.9	2.9	.88	26.54	1896	18.58	9.33	12.3
R-1	1.388	28.2	2.9	2.9	.74	26.80	1903	18.59	9.42	10.4
R-1	1.196	13.4	0.6	0.6	3.23	22.58	1485	34.99	3.80	9.0
R-2	1.209	3.4	2.1	2.1	.65	3.27	1543	8.79	4.42	7.0
R-2	1.345	6.6	2.8	2.8	.55	6.04	1844	9.15	8.52	12.4
R-2	1.362	6.4	3.5	3.5	.28	6.44	1885	9.19	9.14	6.8
R-2	1.381	13.6	2.5	2.5	.64	13.80	1931	18.46	9.86	8.6
R-2	1.184	5.9	0.5	0.5	3.53	8.21	1490	25.21	3.81	11.1
R-3	1.247	1.8	0.6	0.6	2.31	2.20	1525	8.97	1.26	6.2
R-3	1.253	2.1	0.7	0.7	2.76	2.28	1537	8.99	1.31	7.6
R-3	1.279	2.4	0.7	0.7	2.35	2.69	1589	9.07	1.53	7.3
R-3	1.408	3.9	1.1	1.1	1.56	5.32	1863	9.43	2.97	8.2
R-3	1.409	4.6	1.4	1.4	1.37	5.35	1866	9.44	2.99	7.3
R-3	1.417	4.9	1.3	1.3	1.63	5.55	1884	9.46	3.10	8.9
R-3	1.185	2.2	0.3	0.3	7.84	2.85	1405	17.53	.835	7.8
R-3	1.212	2.7	0.4	0.4	5.64	3.47	1457	17.72	1.01	6.4
R-3	1.217	2.7	0.4	0.4	4.91	3.59	1466	17.75	1.04	5.7
R-3	1.396	6.9	1.1	1.1	2.66	10.09	1838	18.81	2.82	6.7
R-3	1.399	7.2	1.0	1.0	2.74	10.21	1843	18.82	2.85	7.0
R-3	1.348	8.7	0.4	0.4	4.63	12.79	1733	29.92	2.23	6.0
R-3	1.229	4.7	0.4	0.4	11.1	7.76	1488	35.65	1.12	6.8

ACKNOWLEDGMENTS

The authors acknowledge gratefully the participation of Mr. John G. Williamson and Mr. James L. Young in the performance of the experiments and Mr. Michael P. Eastman in the measurement of the photographic records.

REFERENCES

1. Bulewicz, James, and Sugden, Proc. Roy. Soc. (London) A235, 89 (1956).
2. W. E. Kaskan, Combust. Flame 2, 229 (1958).
3. Dixon-Lewis, Sutton, and Williams, Discussions Faraday Soc. 33, 205 (1962).
4. E. M. Bulewicz and T. M. Sugden, Trans. Faraday Soc. 54, 1855 (1958).
5. Bauer, Schott, and Duff, J. Chem. Phys. 28, 1089 (1958).
6. G. L. Schott and J. L. Kinsey, J. Chem. Phys. 29, 1177 (1958).
7. G. L. Schott, J. Chem. Phys. 32, 710 (1960).
8. H. T. Knight and R. E. Duff, Rev. Sci. Instr. 26, 257 (1955).
9. G. H. Dieke and H. M. Crosswhite, J. Quant. Spectr. Radiative Transfer 2, 97 (1962).
10. D. R. White, "Influence of Diaphragm Opening Time on Shock-Tube Flows", General Electric Research Laboratory Report No. 58 RL 1999, June, 1958.
11. Bird, Duff, and Schott, Los Alamos Scientific Laboratory Report LA 2980, 1964.
12. S. R. Brinkley, Jr., J. Chem. Phys. 15, 107 (1947).
13. G. L. Schott, J. Chem. Phys., accepted for publication, 1964.
14. JANAF Interim Thermochemical Tables, The Dow Chemical Company, Midland, Michigan, December, 1960, and Supplements through December, 1962.
15. Eschenroeder, Boyer, and Hall, Phys. Fluids 5, 615 (1962).
16. P. F. Bird, "Absorbance of the OH Radical in a Specific Wavelength Interval near 3090Å", Thesis, University of New Mexico, Department of Physics, 1961.
17. S. S. Penner, "Quantitative Molecular Spectroscopy and Gas Emissivities", Addison-Wesley, Reading, Massachusetts, 1959, Sections 3-5 and 4-4.
18. R. C. M. Learner, Proc. Roy. Soc. (London) A269, 311 (1962).
19. T. Carrington, J. Chem. Phys. 31, 1243 (1959).
20. W. E. Kaskan, J. Chem. Phys. 31, 944 (1959).
21. S. S. Penner, "Chemistry Problems in Jet Propulsion", Pergamon Press, New York, 1957, Section 72.
22. W. E. Kaskan and G. L. Schott, Combust. Flame 6, 73 (1962).
23. F. Kaufman and F. P. Del Greco, Ninth Symposium (International) on Combustion, Academic Press, New York, 1963, page 659.

RATE AND MECHANISM OF THE HOMOGENEOUS D/H SUBSTITUTION
REACTION BETWEEN C_2H_2 and D_2 , as STUDIED IN A SHOCK TUBE

Kenji Kuratani and S. H. Bauer

Department of Chemistry, Cornell University
Ithaca, New York

INTRODUCTION

One of the most intriguing facts which came to our attention during the course of our shock tube studies is the occurrence of unsuspected reactions which take place at high temperatures, but under conditions which heretofore had been assumed to be insufficiently severe for appreciable reactions to occur. One example, discussed in detail in this paper, is the reaction between acetylene and hydrogen at temperatures up to 1700°K. When one mixes acetylene and hydrogen at these temperatures no change in the concentration of the acetylene can be detected for as long as one millisecond. During this interval, each acetylene molecule is subjected to an enormous number of collisions with argon (the ambient gas), acetylene and hydrogen molecules. That the acetylene and hydrogen are actually involved in an extensive association reaction, but that the acetylene is rapidly replenished by the reverse processes, becomes evident when deuterium is used in place of hydrogen. The mechanism derived from our studies have given us an insight to possible structures of the transition states of acetylene and of ethylene. The following special features of shocks of operation are thereby demonstrated:

- (a) the samples are heated very rapidly and homogeneously, and
- (b) it is possible to follow in time a sequence of steps for a selected reaction.

EXPERIMENTAL

The Shock Tube

The studies described below were conducted in a stainless steel shock tube, 6" in diameter, for which the driver section was 8 feet long and the driven section 22 feet long. Observations were made by recording the infrared emission at selected wave lengths for incident shocks. The windows were located 18 feet downstream from the diaphragm. Shock speeds were measured with platinum strip thermal detectors and displayed on a raster; the pressure profile was monitored at the window position with a rapid-response Kistler piezo-electric gauge. Mylar diaphragms in a variety of thicknesses were used and in all cases were ruptured by exceeding their yield pressures. The experimental section of the shock tube was pumped down with a diffusion pump to pressures of the order of 1×10^{-4} mm mercury; the leak rate was less than 1 micron per minute. Shocks were run between 2 to 3 minutes after filling the tube with pre-mixed gas samples.

The Optics

Infrared transmitting windows of calcium fluoride were mounted flush with the inner walls of the shock tube. These are 2" in length and 10mm in width. The monochromator is a modified Perkin-Elmer instrument in which a 83 x 83mm B and L grating, 150 lines per mm, blazed at 6μ for the 1st order, had been inserted. A gold-doped germanium detector, liquid nitrogen cooled, was mounted at the focus on a Cassegrain mirror system, which served to reduce the image of the exit slit by a factor of 6. External mirrors focused

a Nernst glower at the center of the shock tube. The image was then transferred by off-axis paraboloids and flat mirrors to the entrance slit of the monochromator. The glower was used for alignment of the optics and wave length calibration of the monochromator. In the parallel ray portion of the external optics a 150 cps sector and various test cells can be inserted. When used in this configuration the detector output was registered by a tuned amplifier and pen recorder. To limit the transit time for the shocked gas various masks were inserted in front of the mirrors. For a signal/noise ratio of 15 to 1, the spectral resolution of this system as calibrated with HBr lines was found to be:

$$\begin{aligned} \text{At } 3195 \text{ cm}^{-1}, \text{ with slits } 0.4 \sim 0.8 \text{ mm} &: & 11.4 \text{ cm}^{-1}/\text{mm slit} \\ 2555 \text{ cm}^{-1}, \text{ with slits } 0.5 \sim 0.7 \text{ mm} &: & 7.3 \text{ cm}^{-1}/\text{mm slit} \end{aligned}$$

The design features of this system have been described¹ as constructed performance proved superior to that anticipated in the design.

The Samples

Various mixtures of acetylene, deuterium and argon were mixed in glass-lined tanks of 200 liter capacity and allowed to remain at room temperature several days before use. The deuterium was the best available commercial grade and was used without purification. The acetylene was washed thoroughly with concentrated sulphuric acid to remove the acetone. The shock tube was cleaned after each run. Since the reflected shock temperatures were considerably higher than those needed for the incident shock exchange experiments the acetylene was extensively pyrolyzed by the reflected shocks. Much carbon soot had to be removed from the tube walls and the windows after each run.

Selection of the Analytical Frequencies for Acetylene

To select the optimum analytical frequencies at which the unsubstituted and deuterated acetylenes emit at these elevated temperatures and to determine the extent of their mutual interference theoretical intensity envelopes were computed for the various bands, based on the reported rotational constants for the ground and first excited vibrational states of acetylene^{2a, b, c, d}. These are illustrated in Figure 1. For estimating the concentration of acetylene present we selected the frequency 3195 cm^{-1} , at which the contribution by C_2H_2 exceeds by a factor of 5 that due to C_2HD . At 2555 cm^{-1} the relative contribution due to C_2HD is largest.

Quantitative calibrations were obtained at these selected frequencies. Note that at $t = 0$ (immediately after passage of the shock) all the acetylene is present as C_2H_2 ; whereas at a sufficiently long time, when the sample had attained equilibrium under shock conditions, its composition may be computed from the known equilibrium constants for the isotope exchange reaction. Thus, at $t = 0$,

$$I_0 = g [\epsilon (\text{C}_2\text{H}_2)_0 \cdot c_0 (\text{C}_2\text{H}_2)] \chi_{3195}$$

in which g represents the geometric factor of the optical and detecting system, c_0 is the initial concentration of the C_2H_2 (in moles/l) and ϵ represents the emissivity of the gas at the shock temperature. Furthermore, at equilibrium ($t \rightarrow \infty$),

$$I_\infty = g [\epsilon (\text{C}_2\text{H}_2)_\infty \cdot c_\infty (\text{C}_2\text{H}_2) + \epsilon (\text{C}_2\text{HD}) \cdot c_\infty (\text{C}_2\text{HD})] \chi_{3195}$$

Note that at 3195 cm^{-1} the contribution to the emission by the fully deuterated acetylene is negligible. In the above equations it was assumed that the concentrations are sufficiently low so that no correction for self absorption need be made, for self absorption. One can then

obtain the ratio I_∞/I_0 , and since the ratios of the concentrations of the species may be computed, the ratio $\epsilon(C_2HD)/\epsilon(C_2H_2)$ may be evaluated.

$$\frac{I_\infty}{I_0} = \frac{c_\infty(C_2H_2)}{c_0(C_2H_2)} + \frac{\epsilon(C_2HD)}{\epsilon(C_2H_2)} \frac{c_\infty(C_2HD)}{c_0(C_2H_2)}$$

Typical data are given in Table I.

The ratio of emissivity coefficients at 2555 cm^{-1} were obtained by a similar procedure. In this case however one cannot measure I_0 since at $t = 0$ no C_2HD is present and the emissivity increases relatively slowly from $I = 0$ at $t = 0$. In part, this is due to the finite time for vibrational relaxation of this mode, and the resolving time of our detector-amplifier system. Instead we must use I'_0 , which is the emission intensity measured under the identical experimental conditions for a mixture of $C_2H_2 + H_2$.

$$I_\infty(C_2H_2 + D_2) = g[\epsilon(C_2H_2) \cdot c_\infty(C_2H_2) + \epsilon(C_2HD) \cdot c_\infty(C_2HD)]\chi_{2555}$$

$$I'_0(C_2H_2 + H_2) = g[\epsilon(C_2H_2) \cdot c_0(C_2H_2)]\chi_{2555}$$

$$\frac{I_\infty(C_2H_2 + D_2)}{I'_0(C_2H_2 + H_2)} = \frac{c_\infty(C_2H_2)}{c_0(C_2H_2)} + \frac{\epsilon(C_2HD)}{\epsilon(C_2H_2)} \frac{c_\infty(C_2HD)}{c_0(C_2H_2)}$$

The results are included in Table I. Hence, the emission intensity recorded at each of the frequencies is related to the corresponding concentrations by:

$$I(3195) \propto [c(C_2H_2) + 0.48 c(C_2HD)]$$

$$I(2555) \propto [c(C_2H_2) + 3.10 c(C_2HD)]$$

Calculation of Shock Parameters

The gas temperature behind the incident shock (T_2) and the gas density ratio across the shock front (ρ_2/ρ_1) were computed from the measured shock velocities and the known enthalpies of the gaseous mixtures. The initial temperature was assumed to be 298°K . No correction was made for the very small enthalpy change due to the isotopic substitution. It was observed that the shock speed attenuated slightly during its passage down the tube; the measured values were extrapolated to provide the shock velocity at the plane of observation.

THE KINETIC DATA

Kinetics of the decrease in C_2H_2 (as measured by the emission intensity at 3195 cm^{-1})

When a mixture of acetylene, hydrogen and argon is shock heated to a temperature in the range 1300°K to 1700°K the emission intensity rises sharply to a level which depends on the concentration of C_2H_2 , due to the compression by the shock and the vibrational excitation of acetylene to the 1st level. This emission remains constant over the period

of observation. Further, when deuterium and argon are shock heated under the same conditions no appreciable emission is observed. However, a mixture of acetylene, deuterium and argon produces a sharp rise in emission which slowly decreases with time. We propose that this decrease is due to the conversion of some of the acetylene to deuterioacetylene. To a first approximation (to be corrected later), the emitted intensity is proportional to the product of a geometrical factor, the sensitivity of the recording system, and the instantaneous concentration of the acetylene. Let ρ_2^0 represent the gas density immediately after passage of the shock. Then one may write

$$\frac{\rho_2^0}{I_0} \frac{dI}{dt} = \frac{d \cdot \rho(C_2H_2)}{dt} + \frac{\epsilon(C_2HD)}{\epsilon(C_2H_2)} \frac{d \cdot \rho(C_2HD)}{dt}$$

only

for the rate of change in emission with time. Note that in the analysis given below the initial reaction rates were considered, as derived from the initial slopes of the emission intensities as recorded by the oscilloscope. The time scale observed on the oscilloscope trace must be multiplied by the density ratio across the shock front (ρ_2/ρ_1) to convert the "laboratory" reaction rate to particle time. The initial reaction rate constant is then defined by the equation:

$$R_0 \equiv \frac{\rho_2^0}{I_0} \frac{\Delta I}{\Delta t} = k (C_2H_2)_0^n (D_2)_0^m (Ar)_0^l$$

To establish the reaction order for this ^{exchange} with respect to D_2 , values of R_0 were plotted against $1/T$ for a series of shocks in which the initial C_2H_2 and Ar were almost constant but $(D_2)_0$ differed by a factor of two, see Figure 2. The difference in rates over the temperature range covered is equal to $m \log 2$, so that $m = 1$ is experimentally determined.

To establish the order of the reaction with respect to the acetylene, the observed values of $R_0/\rho_2^0(D_2)$ were plotted against the reciprocal of the absolute temperature; see Figure 3. In this graph three reference temperatures were selected, centered at regions for which there were significant numbers of points. Effective rate constants at different temperatures were reduced to the nearest reference temperature by reading rates parallel to the average slope. Then the logarithms of these reduced values of $R_0/\rho_2^0(D)$ were individually plotted (for T_1, T_2, T_3) against ^{the} logarithm of the density of acetylene; see Figure 4. The slopes vary somewhat with temperature; they are respectively,

$$\begin{aligned} n &= 0.29 \pm 0.01 & \text{at} & \quad 1350^\circ\text{K} \\ &= 0.20 \pm 0.03 & \text{at} & \quad 1455^\circ\text{K} \\ &= 0.23 \pm 0.03 & \text{at} & \quad 1612^\circ\text{K} \end{aligned}$$

We have adopted the average $n = 0.24$.

The overall order for the exchange reaction as measured by the rate of disappearance of the C_2H_2 was then obtained from a series of experiments corrected to a single temperature, in which the total pressure was changed by a factor of 5, while maintaining the composition of the mixture constant. In these experiments the concentration of each component may be expressed in terms of a single variable which could be the density of the acetylene. The slope of a logarithmic plot of the initial rates against the logarithm of the initial acetylene

density thus gives the total order. The result of six runs in which the acetylene density varied from 0.53×10^{-3} to 2.51×10^{-3} gave at $T = 1455^\circ\text{K}$ a value for $(n + m + l) = 1.20 \pm 0.05$. Since it was established above that $m = 1.0$ and $n = 0.24$ it follows that $l = 0$; that is, the argon concentration does not affect the initial rate of disappearance of the acetylene. The rate constant k_H as evaluated on the basis of the equation

$$R_o = k_H (C_2H_2)_0^{0.24} (D_2)_0^{1.0} (Ar)_0^0$$

was plotted against the reciprocal of the absolute temperature: see Figure 5. The deduced activation energy is $E_H = 33.8 \pm 0.4$ kcal/mole, and the corresponding $\log A = 7.9$, for the rate of disappearance of acetylene due to reaction with deuterium, in the temperature range 1200° to 1700°K .

Kinetics of Production of C_2HD (as measured by emission at 2555 cm^{-1})

The procedure for measuring the growth in concentration of C_2HD during shock and deduction of the corresponding rate law was essentially the same as that described above for the disappearance of C_2H_2 . In this case there was a small additional complexity. The acetylene originally present in the shocked gas produced a large emission at zero time. This showed up as a step function with a finite rise time, due to the combined effect of the vibrational relaxation of the C_2H_2 , the resolving time of the recording system, and the particle passage time as the shock sped by the calcium fluoride windows. Below 1600°K this emitted intensity showed a rapid initial rise covering a period of about 20 microseconds, followed ^{by} an almost linear slower increase due to the production of C_2HD by the exchange reaction. Above this temperature the inflection point could not be easily detected; hence the data cited below were restricted to runs made below 1600°K . Again it was established that the order of the reaction was unity with respect to the initial deuterium concentration. As tested previously, $R_o/\rho_2^0(D_2)$ values were plotted against the reciprocal temperature and the points were corrected to the reference temperature of 1470°K . The reduced $R_o/\rho_2^0(D_2)$ were then replotted against the density of acetylene. The slope of this curve gave for the order of the reaction with respect to acetylene $n = 0.24 \pm 0.04$, checking the value deduced for the rate of disappearance of C_2H_2 . Another plot provided a value for the total order, which proved to be 1.24 ± 0.07 . Thus we have demonstrated that the rate of appearance of C_2HD and the rate of disappearance of C_2H_2 , under the conditions of our experiment follow the same functional dependence on the initial concentrations of reactants. A plot of the reduced rate constant against the reciprocal of the temperature is shown in Figure 6. The activation energy is $E = 29.3 \pm 1.1$ kcal/mole and the corresponding $\log A = 7.5$. The limits of error quoted for E_H and E_D are based on the internal consistency of each set of runs; we consider these activation energies to be equal within their absolute limits of error.

Corrected Values for the Rate Constants

In the preceding paragraphs it was demonstrated that the functional dependencies of the rate of depletion of C_2H_2 and the rate of formation of C_2HD on the initial concentrations of the reactants and on the temperature are equal. It is now possible to correct the apparent rates, deduced directly from the changes of the emission intensities at 3195 cm^{-1} and 2555 cm^{-1} , to obtain absolute rates, by noting the relative contributions of each species to the intensities recorded at these frequencies:

$$-k_H (C_2H_2)^{0.24} (D_2) = -\frac{dC_{2H_2}}{dt} + \left[\frac{\epsilon(C_{2HD})}{\epsilon(C_{2H_2})} \right] \frac{dC_{2HD}}{dt} = -\frac{dC_{2H_2}}{dt} + 0.48 \frac{dC_{2HD}}{dt}$$

3195

$$+k_D (C_2H_4)^{0.24} (D_2) = -\frac{dC_{2H_2}}{dt} + \left[\frac{\epsilon(C_{2HD})}{\epsilon(C_{2H_2})} \right] \frac{dC_{2HD}}{dt} = -\frac{dC_{2H_2}}{dt} + 3.10 \frac{dC_{2HD}}{dt}$$

2555

On rearranging terms:

$$-\frac{dC_{2H_2}}{dt} = k_{C_2H_2} (C_2H_2)^{0.24} (D_2) = \frac{3.10 k_H + 0.48 k_D}{3.10 - 0.48} (C_2H_2)^{0.24} (D_2)$$

$$+\frac{dC_{2HD}}{dt} = k_{C_2HD} (C_2H_4)^{0.24} (D_2) = \frac{k_H + k_D}{3.10 - 0.48} (C_2H_2)^{0.24} (D_2)$$

Specifically, at 1470°K,

$$k_{C_2H_2} = 1.17 \times 10^3 \text{ (liter/mole)}^{0.24} \text{ sec}^{-1}$$

$$k_{C_2HD} = 0.82 \times 10^3 \text{ (liter/mole)}^{0.24} \text{ sec}^{-1}$$

We thus find that the rate of increase of C_2HD is almost equal to 2/3 of the rate of decrease in the C_2H_2 . Since the acetylene is removed only by the isotopic exchange reaction (as demonstrated by the fact that C_2H_2 plus H_2 does not show a decrease in the emission at 3195 cm^{-1}), it follows that the remaining 1/3 of the C_2H_2 leads to the production of C_2D_2 . The rate of production of C_2D_2 is then roughly 1/2 of that of C_2HD .

To substantiate this conclusion we cite rough analytical data obtained in a single-pulse experiment based on a sample composition and temperature pulse comparable to that used for the infrared runs. Mass spectrometric analysis of a shocked mixture of $C_2H_2 + D_2$ showed:

- The amount of H_2 generated was definitely less but comparable to that of HD.
- The decrease in the amount of C_2H_2 was larger than the amount of C_2HD generated.
- No methane or ethylene was produced.

A few preliminary IR runs at 2350 cm^{-1} showed that emission due to C_2D_2 did rise following shock heating of a mixture of acetylene and deuterium. However, this experiment was not completed and no quantitative data on the rate of production of C_2D_2 were obtained by the infrared technique.

The weighted average of the energies of activation obtained from the $\ln k$ vs $1/T$ plots (using internal consistency as the basis for weighting E_H and E_D) is 32.7 ± 1 kcal/mole. This leads to:

$$k_{C_2H_2} = 8.5 \times 10^7 \exp(-32700/RT), \quad (\text{liter/mole})^{0.24} \text{sec}^{-1}$$

$$k_{C_2HD} = 6.0 \times 10^7 \exp(-32700/RT), \quad (\text{liter/mole})^{0.24} \text{sec}^{-1}$$

Typical sets of data are summarized in Table II. These are but examples of the large number of shocks run. The values given are for the 3195 cm^{-1} band.

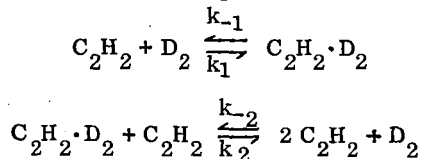
DISCUSSION OF MECHANISM

A thorough search of the literature has yet to be completed. To date we found only one report on a gas phase study of the $(C_2H_2 + D_2)$ reaction. Coats and Anderson³ heated equimolar mixtures of the two gases in 25 ml bulbs for 2 - 10 minutes to temperatures $500^\circ - 900^\circ\text{C}$, at a total initial pressure of 300 mm Hg. The reaction bulbs were allowed to cool to room temperature and their contents were analyzed. In view of the diversity of products produced (ranging from methane to benzene, toluene and carbon deposits) heterogeneous steps evidently played prominent roles in these conversions. Their product distribution suggested that free radical reactions as well as molecular processes had occurred. There are, of course, numerous reports on the rates and mechanisms of D/H substitution in hydrocarbons as catalyzed by a variety of surfaces,^{and} as induced by radiations which generate atoms. In the latter, the primary attack is an atomic displacement or an abstraction.

The pyrolysis^{of} acetylene in shock tubes has been investigated⁴. In this laboratory shock tube studies of the homogeneous substitution reactions between $(NH_3 + D_2)$ ⁵, $(H_2S + D_2)$ ⁵, and $(HCl + D_2)$ ⁶ have been completed. For these systems the rate laws are significant different in that they show an overall second order dependence, in contrast to the overall 1.24 order dependence deduced for $(C_2H_2 + D_2)$. The observation that the activation energy is low ($\sim 33 \text{ kcal/mole}$) and that the rate depends on the first power of the deuterium concentration argues against all the chain reactions we have been able to devise. Indeed, the observed rates are much too high to be consistent with the known or estimated homogeneous rates of dissociation of D_2 ⁷ and of $C_2H_2 \rightarrow C_2H + H$. Finally, the fact that the rate of production of C_2D_2 is about half of that of C_2HD suggests that these species are derived from the same transition state, which we designate $C_2H_2D_2^*$. The following mechanism is consistent with all the observations.

We postulate the occurrence of two types of unstable intermediates:

- $C_2H_2 \cdot D_2$, which is a molecular complex between acetylene and deuterium, and which is particularly sensitive to dissociation by collision with another acetylene; and
- $C_2H_2D_2^*$, which is an electromcally excited ethylene, with V_g symmetry, approximately 3 e.v. above the ground state $[E_A + \Delta H_{\text{hydrog}}(C_2H_2) \approx 3 \text{ e.v.}]$. Species in this state have a much greater probability for dissociation than for interval conversion to stable ethylene. The formal rate expression is based on the sequence:



REFERENCES

1. A Survey of Methods for Chemical Analysis of Transient Species of Microsecond Resolution, S. H. Bauer, N. C. Rol, and J. H. Kiefer, Physical Chemistry in Aerodynamics and Space Flight, Ed. A. L. Meyerson and A. C. Harrison, Pergamon Press, NY., 1961 (p. 118).
2. a) M. T. Christensen, et al, Proc. Roy. Soc., A238, 15 (1957)
b) H. C. Allen, et al, J. Amer. Chem. Soc., 78, 3034 (1956)
c) J. Overend and H. W. Thompson, Proc. Roy. Soc., A234, 3061 (1956); A232, 291 (1955)
3. F. H. Coats and R. C. Anderson, AFOSR TN-56-491 (AD 110-305) University of Texas, Oct. 1956 under AF18(600)-430, Chem. 50-1.
4. a) C. F. Aten and E. F. Greene, Dis. Farad. Soc., 22 162 (1956)
b) S. S. Penner et al, AGAR Dograph No. 61
Fundamental Data Obtained from Shock Tube Experiments
Ed. A. Ferri, Pergamon Press, NY., p.219, p. 183 (1961)
c) J. N. Bradley, Shock Waves in Chemistry and Physics, John Wiley and Sons, Inc., New York, 1962, p.128, 267, 321, 325
5. Assa Lifshitz, Chava Lifshitz and S. H. Bauer, unpublished
6. C. Sadowski, S. K. Addecott and S. H. Bauer, unpublished
7. J. P. Rink, J. Chem. Phys., 36 1398 (1962)

TABLE I. Experimental Determination of the Ratios of ϵ 's

	at 3195 cm^{-1}			at 2555 cm^{-1}	
	(α)	(β)		(γ)	(δ)
$\frac{I_{\infty}}{I_0}$	0.225	0.315	$I_{\infty}(\text{C}_2\text{H}_2 + \text{D}_2)$	25.4	27.0
$\frac{c_{\infty}(\text{C}_2\text{H}_2)}{c_0(\text{C}_2\text{H}_2)}$	0.053	0.111	$I_0(\text{C}_2\text{H}_2 + \text{H}_2)$	14.0	15.0
$\frac{c_{\infty}(\text{C}_2\text{HD})}{c_0(\text{C}_2\text{H}_2)}$	0.352	0.440		0.25	0.25
$\frac{\epsilon(\text{C}_2\text{HD})}{\epsilon(\text{C}_2\text{H}_2)}$	0.49	0.465		0.50	0.50
Ave.	< 0.48 >			< 3.12 >	

(α) Average of 4 runs with $\frac{c_0(\text{C}_2\text{H}_2)}{c_0(\text{D}_2)} = 3.333$, at 1600 - 1700°K

(β) Average of 4 runs with $\frac{c_0(\text{C}_2\text{H}_2)}{c_0(\text{D}_2)} = 2.00$, at 1550 - 1650°K

(γ) At about 1670°K

(δ) At about 1720°K

TABLE II: Typical Data for the 3195 cm⁻¹ Band

Run No.	465	397	404	410	405	458	451	430	424
C ₂ H ₂ /D ₂ /Ar	10/10/80	10/10/80	10/10/80	5/10/85	5/10/85	3/10/87	3/10/87	10/5/85	10/5/85
p ₁ (total)	26	82	41.5	80	80	61	61	81	43
ρ ₂ ⁰ (C ₂ H ₂)	0.59 x 10 ⁻³	1.91 x 10 ⁻³	0.99 x 10 ⁻³	0.78 x 10 ⁻³	0.87 x 10 ⁻³	0.34 x 10 ⁻³	0.378 x 10 ⁻³	1.80 x 10 ⁻³	1.01 x 10 ⁻³
ρ ₂ ⁰ (D ₂)	0.59 x 10 ⁻³	1.91 x 10 ⁻³	0.99 x 10 ⁻³	1.57 x 10 ⁻³	1.74 x 10 ⁻³	1.14 x 10 ⁻³	1.26 x 10 ⁻³	0.90 x 10 ⁻³	0.51 x 10 ⁻³
T ₂ °K	1390	1545	1665	1245	1680	1200	1700	1410	1695
ρ ₂ ⁰ /ρ ₁	4.19	4.34	4.44	3.65	4.01	3.47	3.83	4.12	4.35
R ₀	0.0422	0.545	0.489	0.0306	0.970	0.0111	0.753	0.0900	0.329
R ₀ ⁰ /ρ ₂ ⁰ (D ₂)	0.715 x 10 ²	2.85 x 10 ²	4.96 x 10 ²	0.195 x 10 ²	5.59 x 10 ²	0.097 ₅ x 10 ²	5.98 x 10 ²	1.00 x 10 ²	6.45 x 10 ²
k _H	0.426 x 10 ³	1.28 x 10 ³	2.61 x 10 ³	0.109 x 10 ³	3.04 x 10 ³	0.065 ₅ x 10 ³	3.94 x 10 ³	0.455 x 10 ³	3.38 x 10 ³

p₁⁰, in mm Hgρ₂⁰, the corresponding gas density (moles/l) immediately after passage of the shock

$$R_0 = \frac{\rho_2^0}{I_0} \left(\frac{\Delta I}{\Delta t} \right)_0 \left(\frac{\rho_1}{\rho_2} \right), \text{ in mole liter}^{-1} \text{ sec}^{-1}$$

$$k_H = R_0 / \rho_2^0 (D_2)^{0.24} \rho_2^0 (C_2H_2)^{0.24}, \text{ in (1/mole)}^{0.24} \text{ sec}^{-1}$$

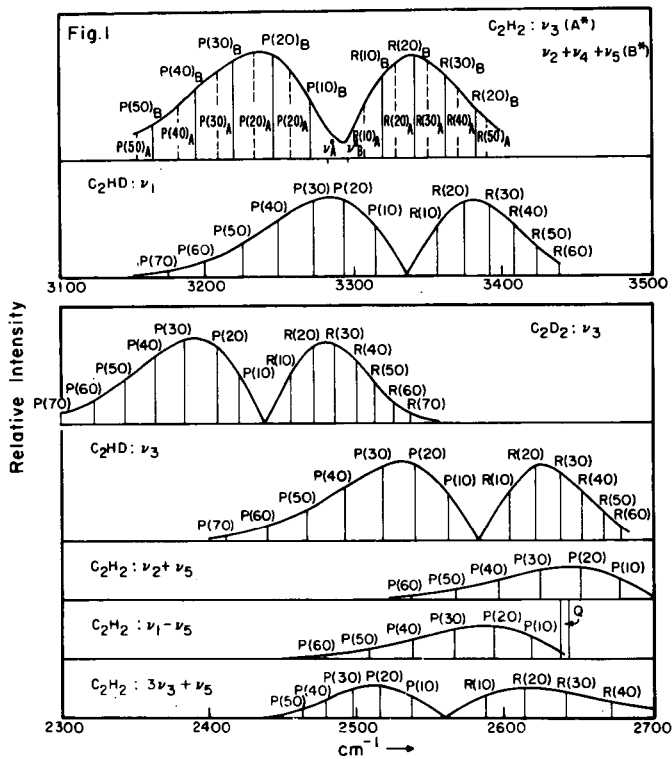


Fig. 1 Theoretical envelopes showing relative emission intensities of acetylene, mono- and dideuteroacetylene at 1700 °K.

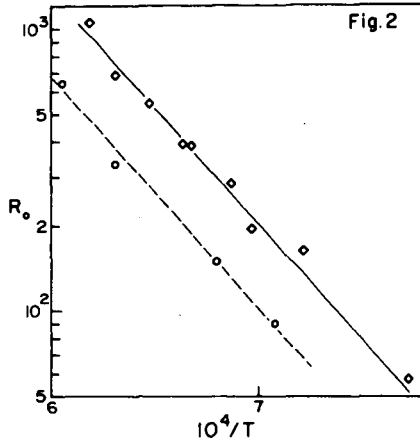


Fig. 2 Logarithmic plot of R_0 vs $10^4/T$, for runs with constant $(C_2H_2)_0$, and $(Ar)_0$, but $(D_2)_0$ differs by a factor of two:

Solid Line: $C_2H_2/D_2/Ar = 10/10/80$

Dashed Line: $C_2H_2/D_2/Ar = 10/5/85$

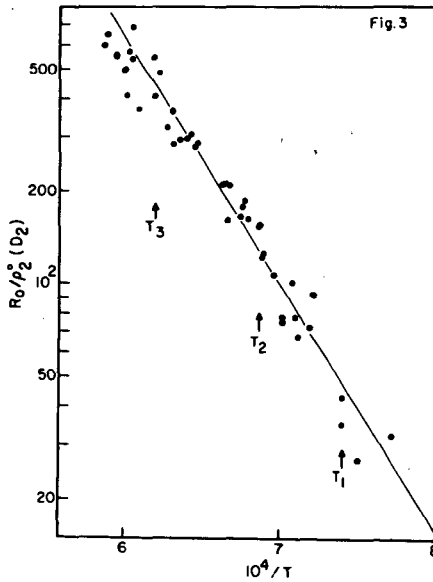


Fig. 3 Logarithmic plot of $R_0/\rho_2^0(D_2)$ vs $10^4/T$, for all runs:

$C_2H_2/D_2/Ar = 10/10/80; 5/10/85; 3/10/87; 10/5/85$

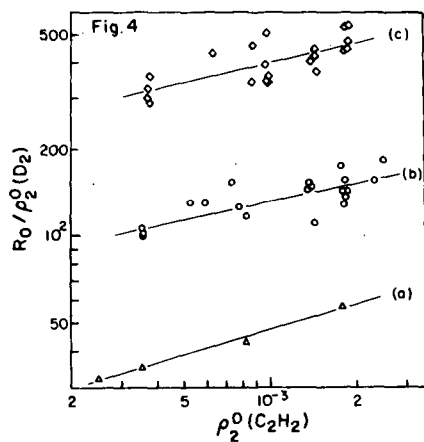


Fig. 4 Logarithmic plots of the reduced values of $R_0 / \rho_2^0(D_2)$ vs $\rho_2^0(C_2H_2)_0$, corresponding to the temperatures

(a) 1350°K (b) 1455°K (c) 1612°K

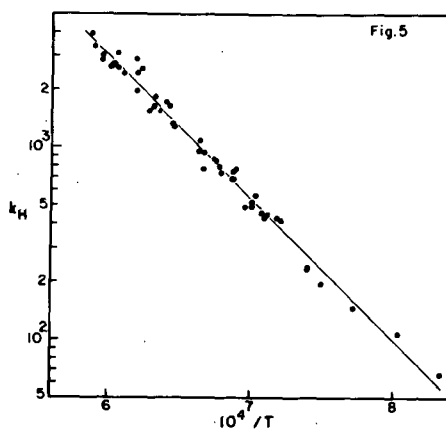


Fig. 5 Plot of the rate constant for the disappearance of C_2H_2 , due to reaction with D_2 , as measured from the decline in emission intensity at 3195 cm^{-1} , vs the reciprocal temperature.

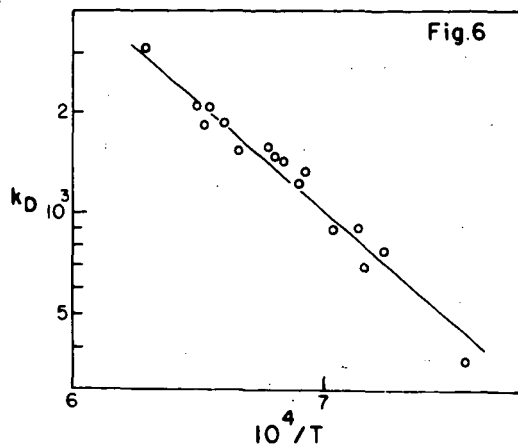


Fig. 6 Plot of the rate constant for the production of C_2HD , as measured from the rise in emission intensity at 2555 cm^{-1} , vs the reciprocal temperature.

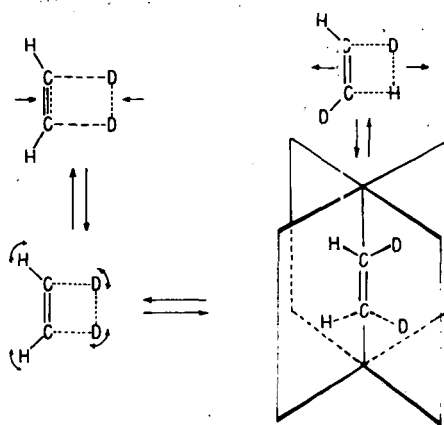


FIG. 7

Fig. 7 Proposed sequence of configuration for the H/D exchange.

The Kinetics of Decomposition of Acetylene in the 1500°K Region

Howard B. Palmer and Frank L. Dormish

Department of Fuel Technology, The Pennsylvania State University
University Park, Pa.

Introduction

The thermal decomposition of acetylene is one of the most-studied phenomena in the chemistry of gases. Despite the apparent simplicity of the C_2H_2 molecule, its thermal behavior is exceedingly complex. Within the past ten years, it has been studied in static systems (1, 2, 3), in flow systems (4-8), in shock tubes (9-12), and in flames (13). The temperature range covered in these studies has spanned the region from about 625°K to 2500°K, but with a gap in the 1000°K region that has been studied only very recently (6, 14). Explorations have been made of the product distributions, of the effects of vessel surfaces, of changing surface-to-volume ratios, of adding free radical capturers such as NO, and of adding organic compounds that might participate in the mechanism. The rate of formation and the characteristics of the carbons and polymers formed in the decomposition have been studied extensively.

There is substantial agreement on some aspects of the decomposition. It appears to be settled that at low temperatures, a homogeneous reaction which is second order in $[C_2H_2]$ dominates the behavior. The reaction is a chain and leads to the formation of high molecular weight compounds, with some side products such as H_2 , C_2H_4 , CH_4 , and C_4H_4 . The activation energy is approximately 50 kcal and the frequency factor of the uninhibited reaction is very large. Silcocks (3) gives

$$k = 3.72 \times 10^{16} \exp(-50.2 \text{ kcal/RT}) \text{ cc/mole sec.}$$

A heterogeneous reaction is also observed at low temperatures.

Silcocks reports that it is first-order in $[C_2H_2]$, with an activation energy of 42.7 kcal. He gives values of the rate constant at five temperatures.

The situation at high temperatures contains more conflict. It has been difficult to determine the order of the reaction and the activation energy, either with flow systems (8) or in shock tubes. However, if one presumes the reaction order to be integral, the best choice at high temperatures appears to be second-order in acetylene. The rate constants at the highest temperatures (9, 12) disagree by a factor of about 10, but agreement is considerably better at temperatures below 1900°K.

Both Aten and Greene (9) and Minkoff and Tipper (15) agree that the rate constants at high and low temperature can be used to define the rate over the whole range; i.e., they agree that the mechanism remains the same, at least up to and including the rate-determining step. However, Aten and Greene prefer their own high temperature data, while Minkoff and Tipper prefer those of Kistiakowsky and Bradley (12). These choices yield markedly different results, respectively:

$$\text{(data of ref. 9) } k = 10^{12.89} \exp(-39 \text{ kcal/RT}) \text{ cc/mole sec}$$

$$\text{(data of ref. 12) } k = 10^{15.15} \exp(-45.8 \text{ kcal/RT}) \text{ cc/mole sec}$$

Quite aside from questions raised by such a discrepancy, we think it unjustifiable to assume that one is measuring the rate of the same reaction sequence at 2000°K and at 700°K. The low temperature homogeneous reaction is a chain of length (3) on the order of 100 or more. There is no evidence that the reaction at high temperature is a chain. Indeed the only direct experimental evidence (12) of which we are aware indicates that it is essentially a simple sequence of consecutive reactions.

It is clearly important to discover what happens between the lower limit of the shock tube studies, ca. 1400°K, and the upper limit of the studies in vessels, ca. 800°K. This intermediate region is appropriate for studies using flow systems. Anderson and his colleagues (4, 5) have done exactly this, but have concentrated most of their attention upon product distributions and the implications of these regarding the mechanism. Very recently, however, Munson and Anderson (6) have published work from which it is possible to extract rate constant data and we shall discuss these later. Towell and Martin (8) used a flow reactor to study the decomposition over temperatures from about 1200°K to 1450°K. They had difficulty in defining the order of reaction, but their data compare reasonably well with shock tube data if one assumes second order behavior.

The present experiments represent an effort to study the decomposition very carefully at three temperatures, the highest of which overlaps

the shock tube studies. Particular attention has been given to determining the order of reaction and the absolute magnitudes of rate constants at these three temperatures. The work is basically an extension of that performed by Kinney and Slysh (7).

Experimental Procedure

The apparatus was only slightly modified from the arrangement used by Kinney and Slysh (7) and will therefore be described only briefly. It was a flow system operating at ambient pressure. The pyrolysis tube was 5 mm i.d. refractory porcelain, sealed to Pyrex at the ends, and mounted in a furnace capable of attaining 1500°C. C_2H_2 was metered with a capillary flowmeter before being mixed with the helium carrier. Input rates were varied so as to produce mixture compositions ranging from 0.20 to 1.30 mole per cent C_2H_2 .

Temperature profiles within the pyrolysis tube were measured with a Pt-Pt:Rh thermocouple for each of three temperature settings and at several flow rates. They were found to be essentially independent of flow velocity, from which it is inferred that the gas temperature was indeed being measured. This conclusion is supported by estimates of the radial temperature distribution in the tube based upon approximate values for the thermal diffusivity of the gas. The estimates show that the temperature at the center of the tube (2.5 mm from the wall) should not differ from the wall temperature by more than a few degrees. Because the furnace was short, the temperature profiles did not possess a plateau region. A typical profile is shown in Fig. 1, together with what we call the "staircase" approximation to it, by means of which it was possible to correct the experimental data to the temperature of an imaginary 5-cm-long hot zone having a constant temperature near the actual temperature peak. It was also convenient to discuss the effect of flow velocity upon the per cent decomposition in terms of the fictitious residence time ("contact time") of the gas in the imaginary hot zone.

Calculations of the extent of decomposition in the hot zone were carried out for each run by an iterative procedure in which an equation for the rate constant was assumed in order to compute the relative contributions from decomposition at each of the temperature levels on the staircase. Most of the decomposition occurred on the top level, which meant that it was quite easy to correct for the other contributions, using rough values for the rate constants in the first trial. From the results of the runs at three different temperature settings, a better expression for the temperature-dependent rate constant was derived and used in the second calculation of corrections. This single iteration was found to yield satisfactory values for rate constants at each of the three hot zone temperature levels (1333°K, 1433°K, and 1528°K). Details of these calculations are presented in reference 16.

The helium used was Matheson "research grade" gas, purity approximately 99.99%. It was passed through a bed of Cu at 400°C for O₂ removal and then through a tower containing Ascarite and Anhydrons to remove CO₂ and H₂O. The C₂H₂, a purified grade of 99.5% minimum purity, was bubbled through concentrated H₂SO₄ to remove acetone before introduction into the helium stream. The mixture of C₂H₂ and He was routed through a dry ice-cooled, glass wool-packed trap before entering a coil of tubing 4 feet in length that served to ensure homogeneity of the mixture that entered the pyrolysis tube.

Beyond the water-cooled exit of the furnace were three traps in series. The first was cooled by dry ice and served principally as a pre-cooler to ensure good trapping efficiency in the subsequent liquid N₂-cooled traps. These traps captured acetylene, diacetylene, vinylacetylene, methyl acetylene, and allene. Hydrogen and methane were not trapped, but were converted to H₂O and CO₂ over CuO filings at 700°C. Vitreous carbon that formed on the tube wall during the run was determined by burning it off with oxygen at 1255°C, running the effluent gas through a CuO trap, and capturing the CO₂ in Ascarite. A very small amount of reddish polymer, deposited just beyond the furnace exit, was the only product ignored. Analyses were performed using vapor chromatography and (for CO₂ and H₂O) by weighing Ascarite and Anhydrons absorption towers.

Results and Discussion

The decomposition has been studied at three temperatures: 1333°K, 1433°K, and 1528°K. These represent the effective hot zone temperatures to which the decomposition data were corrected. Because the emphasis in the present paper is upon the kinetics of decomposition, details of product analyses are not presented here. They were in broad agreement with the results of other investigations (6, 7). A note of special interest is that the more prominent C₄ product at 1333°K was vinylacetylene, but at 1528°K it was diacetylene.

In Table I are summarized the experimental data on the extent of decomposition of C₂H₂ at various nominal contact times. These formed the basis for calculations of rate constants. The order of reaction has been determined at the three hot zone temperatures by examining the extent of decomposition as a function of the initial concentration at fixed flow rate--i.e. at fixed effective contact time in the hot zone. The results appear in Fig. 2, and represent mixed first- and second-order behavior. This may be seen as follows: consider a reaction with rate given by

$$\frac{-dc}{dt} = k_u c + k_b c^2 \quad (1)$$

Integration yields

$$\left(\frac{c}{c^0}\right) = k_u t + \int_0^t k_b c dt \quad (2)$$

$$= (k_u + k_b \bar{c}) t \quad (3)$$

where \bar{C} is a mean concentration over the time interval, and will approximately equal $(C_0 + C)/2$ when the extent of decomposition is small. When this is the case, Eq. 3 yields

$$\left(1 - \frac{C}{C_0}\right) = (k_u + k_b \bar{C})t \quad (4)$$

Thus for mixed first and second order, a study at fixed time (i.e. fixed flow rate) and small extent of decomposition should show an approximately linear dependence of the extent of decomposition upon the input concentration, with a finite intercept at $C_0 = 0$ if there is in fact a first-order contribution. This is the case in Fig. 2.

One can calculate first-order rate constants from the intercepts in Fig. 1. The result for 1528°K is not as reliable as the other two because of the smaller number of points, the long extrapolation to $C_0 = 0$, and the larger extent of decomposition. The calculations involve a correction to yield the extent of decomposition in the effective hot zone. This is in principle a multiply iterative procedure, but we found that the correction was sufficiently small that a rough treatment of the data could provide crude rate constants from which corrections could be formed to yield good rate constants in a single iteration, as discussed earlier.

The k_u values obtained are 0.221 sec⁻¹ at 1333°K; 0.482 sec⁻¹ at 1433°K; and 0.745 sec⁻¹ at 1528°K. On an Arrhenius plot, these define a line given by

$$k_u = 4.2 \times 10^3 \exp(-26 \text{ kcal/RT}) \text{sec}^{-1}$$

The uncertainties in the numerical values of this expression are surely considerable (but difficult to estimate). Nevertheless it is clear that both the frequency factor and the activation energy rule out a homogeneous unimolecular reaction. If we assume that the reaction is heterogeneous, the rate constant k_{het} will be $k_{\text{het}} = k_u (V/S)$, where (V/S) is the volume-to-surface ratio. In our reactor, this ratio was 1.25×10^{-4} liter/cm², where the units have been chosen so as to permit easy comparison with the low-temperature results of Silcocks (3). The comparison is shown in Fig. 3. k_{het} is now given by

$$k_{\text{het}} = 5.25 \times 10^{-1} \exp(-26 \text{ kcal/RT}) \text{ liter cm}^{-2} \text{sec}^{-1}$$

An extension of this line goes through the middle of Silcocks' data. It is tempting to conclude that the heterogeneous reactions are the same, but caution is required because a modest alteration of the parameters in the expression for k_{het} could cause the extension to miss Silcocks' points altogether. There is much more to be explored on the matter of a heterogeneous decomposition. We have noted with interest that the yields of H₂, C₄H₄, and C₄H₆ all move toward zero at $C_0 = 0$, and carbon plus CH₄ become virtually the only products. Clearly the mechanism of the surface decomposition must be grossly different from the gaseous process.

172

Fig. 2 shows that the gaseous decomposition conforms nicely to second-order kinetics, and it is possible to obtain k_b from the slopes. We have preferred to use data on the per cent decomposition as a function of the effective contact time in the hot zone, averaging the rate constants obtained from a number of runs (6 to 8) at the same temperature but at various flow rates and input concentrations. The results have been corrected, in each case, for the first-order contribution. The procedure (16) is tedious and will not be outlined here.

The results for k_b , in units of cc/mole sec, are: $(1.40 \pm 0.10) \times 10^3$ at 1333°K ; $(3.42 \pm 0.23) \times 10^3$ at 1433°K ; and $(2.49 \pm 0.36) \times 10^3$ at 1528°K . The uncertainties attached to each result are the average absolute deviations of the experimental points.

Figure 4 is an Arrhenius plot of all available data for k_b , ranging from about 650°K to 2500°K . The solid curve will be discussed later. Our data and those of Skinner and Sokolski (11) agree very well, in the sense that their higher-temperature points fall on the best line through our results. However, their values below about 1500°K (not included in the figure) show a change in slope that requires comment at a later point in this discussion. The data of Towell and Martin (8), obtained in reactors very similar to ours, parallel our data well. Agreement would be even better if their results could be readily corrected for the contribution from the heterogeneous decomposition. The results of Aten and Green (9) are in reasonable agreement with ours and with Skinner's but show a smaller slope. The best high temperature line, which we have selected by eye, defines k_b as

$$k_b = 3.2 \times 10^{14} \exp(-50 \text{ kcal/RT}) \text{ cc/mole sec.}$$

The frequency factor seems close to normal, in contrast to that cited earlier for the low-temperature reaction. This does not prove that one is observing an elementary reaction at high temperatures, but suggests that the hot reaction is not a chain. An extrapolation of the best high temperature line falls below the low temperature k_b values by a factor of 10^2 or more.

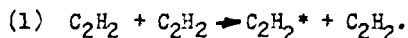
Thus the question remains: what happens between 800°K and 1400°K ? The work of Munson and Anderson (6) contributes much toward an answer. They used a flow reactor of diameter 2.2 cm and, at high concentrations of C_2H_2 (20-21 mole per cent at $p_{\text{tot}} = 1 \text{ atm}$), covered temperatures from 773°K to 1123°K . They did not obtain rate constants, but they do report the time-dependence of the C_2H_2 concentration at six temperatures. These results are of precision sufficient to permit examination of the reaction order by the usual methods of kinetics. Our analysis shows that the reaction is second-order in $[\text{C}_2\text{H}_2]$ at 873°K , 923°K , and 973°K , but that the order is not well defined at the higher temperatures. The second-order rate constants at the three lower temperatures are in remarkably good agreement with an extrapolation of low-temperature data.

If one approximates the kinetics at the three higher temperatures (1023°K , 1073°K , and 1123°K) by a first-order expression, the rate constants

so obtained show a temperature coefficient corresponding to an activation energy in the vicinity of 30 kcal. It thus seems quite clear that the kinetics of the decomposition undergo a transition at about 1000°K, and that one cannot make a direct comparison of second-order rate constants at low and high temperatures.

In view of the known complexity of the decomposition, it is not really surprising to find complications in the kinetics; but the behavior does seem extraordinary. An acceptable mechanism must: (a) give second-order kinetics at low temperature, with a rate constant similar to that cited from the results of Silcocks; (b) there must be some sort of transition region at intermediate temperatures; and (c) at high temperatures the reaction must be second-order but now with k_D similar to that cited previously from our data and the shock tube data.

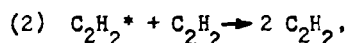
Behavior of this sort can occur in the mechanism presented below. This is offered as a stimulus to further work. It makes no attempt to account in detail for all products, and there is no direct evidence for the steps involved in it. Our comments follow each reaction postulated.



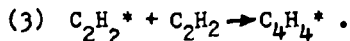
This represents unimolecular excitation of acetylene to its lowest-lying triplet state. C_2H_2 is shown as the collision partner for the excitation on the presumption that in a mixture of C_2H_2 and a monatomic gas, e.g. He, C_2H_2 will be many times more effective than He because it can possess vibrational energy. The actual change of multiplicity probably occurs most rapidly when the amount of energy to be transferred is not very large (17). Thus a detailed mechanism for reaction 1 would include vibrational excitation. However, because establishment of vibrational equilibrium is probably rapid relative to the rate of reaction 1, one can think of at least one of the C_2H_2 molecules as being highly excited vibrationally without introducing a necessity for modifying the simple equation above.

Minkoff (2) has suggested that the first step is double excitation, $2 C_2H_2 \rightarrow 2 C_2H_2^*$. This has the virtue of being spin-allowed, but the energy requirement will be very much greater (roughly double) than for step 1 above; this should weigh more heavily against the double excitation than does the forbiddenness factor (perhaps 10^{-4}) entering into the rate constant of reaction 1.

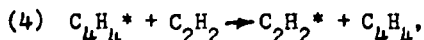
Reaction 1 will probably have an energy barrier somewhat higher than the singlet-triplet excitation energy, which has been estimated (9) to lie between 42 and 67 kcal above the ground state, using data discussed by Laidler (17).



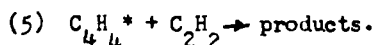
deactivation of triplet acetylene. By microscopic reversibility, C_2H_2 must be much more effective than He in the deactivation. There will presumably be a small activation energy in the rate constant, and a forbiddenness effect in the pre-exponential factor.



This is an addition reaction to yield a triplet dimer. The reaction will be in competition with step 2, and will be fast. The rate constant for a reaction that may be comparable, viz, the addition of NO_2 to C_2H_2 , has been reported (18) to equal $10^{12.1} \exp(-15 \text{ kcal/RT})$ cc/mole sec.



a chain-transfer reaction that is not simply an exchange of multiplicities because formation of vinylacetylene from C_4H_4^* requires H atom migration. There should be an appreciable but small activation energy. We suspect that in a reaction of this type the collision efficiency ("steric" factor) may be very low.



This alternative to reaction 4 is thought of as a radical addition reaction leading to stable products such as benzene. It is oversimplified for the sake of allowing a tractable expression for the overall kinetics. That is, it might also be thought of as a deactivation; or it might not end the chain at all, but rather continue it by a subsequent transfer reaction analogous to step 4; or the product might in turn add to C_2H_2 . However, observations by Robertson *et al.* (19) of the yield of benzene in C_2H_2 pyrolysis do support the suggestion that a large fraction of the reaction events in step 5 do not lead to a continuation of the chain. It further appears from that work that reaction 5 has a large temperature coefficient. We shall assume that its activation energy is much larger than that for step 4, and that its collision factor is also much larger; in this way it becomes possible for its rate to be less than that of step 4 at low temperature but to exceed it at higher temperatures.

The postulated reaction scheme is terminated at this point. It is of course recognized in doing so that other reactions must occur. The scheme is a simplified version of that discussed by Minkoff and Tipper (15), but with the difference in the singlet-triplet excitation step noted previously.

A steady-state treatment of the scheme yields

$$-d[\text{C}_2\text{H}_2]/dt = [\text{C}_2\text{H}_2]^2 k_3(k_1/k_2) \left\{ \left[3 - k_4/(k_4 + k_5) \right] / \left[1 + (k_3/k_2)k_5/(k_4 + k_5) \right] \right\} \quad (4)$$

At low temperatures, we expect $k_4 \gg k_5$. Then

$$-d[\text{C}_2\text{H}_2]/dt = 2[\text{C}_2\text{H}_2]^2 k_3(k_1/k_2) \left[1/(1 + k_3k_5/k_2k_4) \right] . \quad (5)$$

We expect k_3 to be considerably greater than k_2 ; but with $k_4 \gg k_5$, the result is

$$-d[\text{C}_2\text{H}_2]/dt = 2[\text{C}_2\text{H}_2]^2 k_3(k_1/k_2) \quad (6)$$

At higher temperatures, k_5 will compete with k_4 and the chain length

will be reduced. In the limit that $k_5 \gg k_4$, continuing to assume $k_3 \gg k_2$, the steady-state treatment yields

$$-d[C_2H_2]/dt = 3k_1[C_2H_2]^2 \quad (7)$$

This rate will be substantially less than that given by the previous result, if extended to high temperature. The consequence is that at the temperature where k_2 begins to compete effectively with k_4 , an Arrhenius plot of the apparent second-order rate constant should begin to show a decreasing slope. Once the condition, $k_5 \gg k_4$, is reached, the slope will rise again to that characteristic of k_1 . This seems to conform rather well to the plot in Fig. 4. The transition region for k_4 versus k_5 appears to begin at about 900°K and extends to about 1400°K.

The high-temperature results cited earlier now yield

$$k_1 = 1.1 \times 10^{14} \exp(-50 \text{ kcal/RT}) \text{ cc/mole sec}$$

and, using this k_1 , the low-temperature results of Silcocks yield

$$(k_3/k_2) = 1.60 \times 10^2 .$$

If we require that $(k_4/k_5) = 10(k_3/k_2)$ at 700°K and $(k_4/k_5) = 0.2$ (i.e. $\ll 1$) at 1400°K, the temperature dependence of (k_4/k_5) is found to be

$$(k_4/k_5) = 4.2 \times 10^4 \exp(-25.1 \text{ kcal/RT}) .$$

Employing these three parameters, k_1 , (k_3/k_2) , and (k_4/k_5) , Equation 4 may be used for a computation of the second-order rate constant over the whole temperature range. The result is shown by the solid curve in Fig. 4. The fit seems quite successful, particularly when it is realized that the C_2H_2 disappearance rates reported by Munson and Anderson may have been appreciably enhanced by heterogeneous decomposition on carbon particles formed in their reactant stream. It is not possible to make a correction for this effect; the point is that the k_0 values computed from their results are probably too large.

Some comment on the parameters is in order. k_1 has a surprisingly large pre-exponential factor, in view of the violation of spin conservation in reaction 1. However, in a recent study of SO_2 decomposition, Gaydon *et al.* (20) have found that unimolecular excitation of SO_2 to its lowest triplet state appears to be aided by energy transfer from internal degrees of freedom. This has the effect of raising the pre-exponential factor so as to largely compensate for the forbiddenness of the reaction. The apparent energy of activation is lowered in such a case. In $C_2H_2-C_2H_2$ collisions, there are many possibilities for energy transfer from internal modes and it is possible to rationalize k_1 on this basis. If the interpretation is correct, then the true activation energy of step 1 probably lies between 55 and 60 kcal, and a simple Arrhenius expression for k_1 is not very realistic. However, refinement of k_1 does not yet seem justifiable.

The (approximate) temperature independence of (k_3/k_2) is about what one would expect on the basis of the earlier discussion of these reactions. The magnitude of the ratio, i.e. 160, is also reasonable.

As for (k_3/k_4) , the large ratio of pre-exponential factors is not unexpected, but no particular significance can be attached to the 25 kcal difference in activation energies except to say that it seems consistent with the experimental results of Robertson *et al.* (19). Beyond this, our ignorance of the details of the postulated steps 4 and 5 is almost total.

A final remark should be made on the report by Skinner and Sokoloski (11) that the rate constant for formation of vinylacetylene below about 1500°K lies above the low-temperature extension of their results for conversion to all products at temperatures above 1500°K (points shown in Fig. 4). If the result is real, it presents a severe complication. We would suggest tentatively that their low yields of vinylacetylene may have led to analytical errors, as indicated to some extent by their difficulty in obtaining a mass balance on reactants plus products.

Conclusions

It is possible to reconcile most low- and high-temperature data in the literature on acetylene pyrolysis by a chain mechanism in which the main chain-ending reaction has a stronger temperature dependence than does one of the chain-carrying reactions. This leads to long chains at low temperatures and essentially non-chain behavior at high temperatures. It seems very probable that the first step in the mechanism is excitation of C_2H_2 to its lowest-lying triplet state, and that one of the chain steps is a spin-exchange reaction.

In systems possessing high surface-to-volume ratios, e.g. in heavily sooting systems, a first-order heterogeneous decomposition reaction, the products of which appear to be principally carbon and CH_4 , is expected to dominate the kinetics.

Acknowledgment

We are indebted to the U. S. Atomic Energy Commission for partial support of this work under Contract AT(30-1)-1710.

References

1. G. J. Minkoff, D. M. Newitt, and P. Rutledge, *J. Appl. Chem.* 1957, 406.
2. G. J. Minkoff, *Can. J. Chem.* 36, 131 (1958).
3. C. G. Silcocks, *Proc. Roy. Soc.* A242, 411 (1957).
4. F. C. Stehling, J. D. Frazee, and R. C. Anderson, Sixth Symposium (International) on Combustion, New York, Reinhold (1957), p. 247.
5. F. C. Stehling, J. D. Frazee, and R. C. Anderson, Eighth Symposium (International) on Combustion, Baltimore, Williams and Wilkins (1960), p. 775.
6. M. S. B. Munson and R. C. Anderson, *Carbon* 1, 51 (1963).
7. C. R. Kinney and R. S. Slysh, Proceedings of the Fourth Carbon Conference, Oxford, Pergamon Press (1960), p. 301.
8. G. D. Towell and J. J. Martin, *A.I.Ch.E. Jour.* 7, 693 (1961).
9. C. F. Aten and E. F. Greene, *Combustion and Flow* 5, 55 (1961).
10. W. J. Hooker, Seventh Symposium (International) on Combustion, London, Butterworths (1959), p. 949.
11. G. B. Skinner and E. M. Sokoloski, *J. Phys. Chem.* 64, 1952 (1960).
12. J. N. Bradley and G. B. Kistlakowsky, *J. Chem. Phys.* 35, 264 (1961).
13. J. D. Chase and F. J. Weinberg, *Proc. Roy. Soc.* A275, 411 (1963).
14. C. F. Cullis, Dept. of Chemical Engineering and Chemical Technology, Imperial College, London; private communication of work in press.
15. G. J. Minkoff and C. F. H. Tipper, Chemistry of Combustion Reactions, London, Butterworths (1962).
16. F. L. Dormish, M. S. Thesis, Dept. of Fuel Technology, The Pennsylvania State University, University Park, Pa., 1962.
17. K. J. Laidler, The Chemical Kinetics of Excited States, Oxford, 1955.
18. J. H. Thomas, *Trans. Faraday Soc.* 48, 1142 (1952).
19. W. W. Robertson, E. M. Magee, J. Fain, and F. A. Matson, Fifth Symposium (International) on Combustion, New York, Reinhold (1955), p. 628.
20. A. G. Gaydon, G. H. Kimbell, and H. B. Palmer, *Proc. Roy. Soc.* A276, 461 (1963).

Table I.

Summary of experimental data on the decomposition rate

1333° K [†]			1433° K [†]			1528° K [†]		
c.t.* (sec)	C ₀ (mole %)	% Dec.	c.t.* (sec)	C ₀ (mole %)	% Dec.	c.t.* (sec)	C ₀ (mole %)	% Dec.
0.100	0.58	3.9	0.100	0.50	8.2	0.046	0.50	9.1
0.150	0.57	5.6	0.150	0.22	11.2	0.094	0.50	18.2
0.150	0.81	6.3	0.150	0.27	11.4	0.150	0.50	31.2
0.150	0.96	6.5	0.150	0.52	12.8	0.150	0.69	37.7
0.150	1.02	7.2	0.150	0.97	14.3	0.150	0.78	39.7
0.150	1.28	7.5	0.150	1.25	16.5	0.180	0.50	37.0
0.200	0.52	7.5	0.150	1.30	16.8	0.190	0.50	37.8
			0.200	0.53	18.1			

† Hot zone temperature.

* Nominal contact time = (hot zone volume)/(vol. flow rate at hot zone temperature).

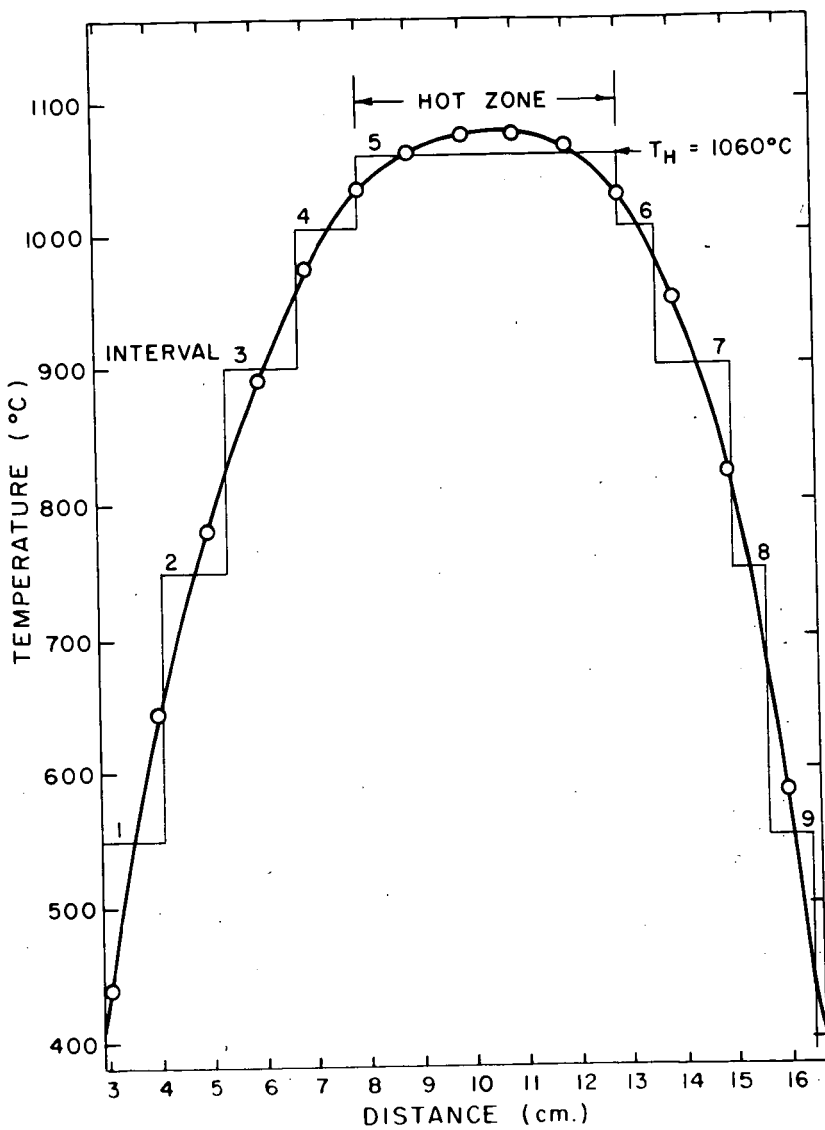


Fig. 1. Temperature profile for the furnace having the hot zone at 1060°C (1333°K). The "staircase" approximation to the profile is illustrated.

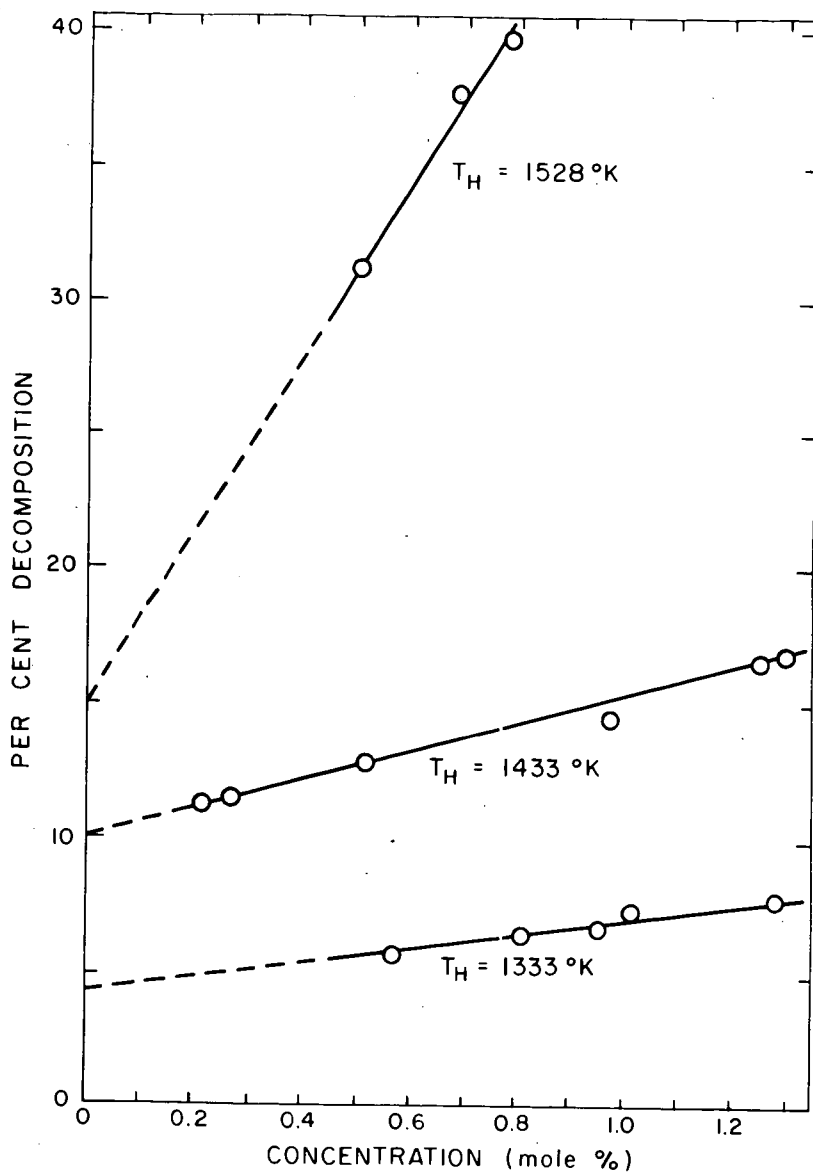


Fig. 2. Effect of change in initial concentration upon extent of decomposition at fixed contact time (0.150 sec).

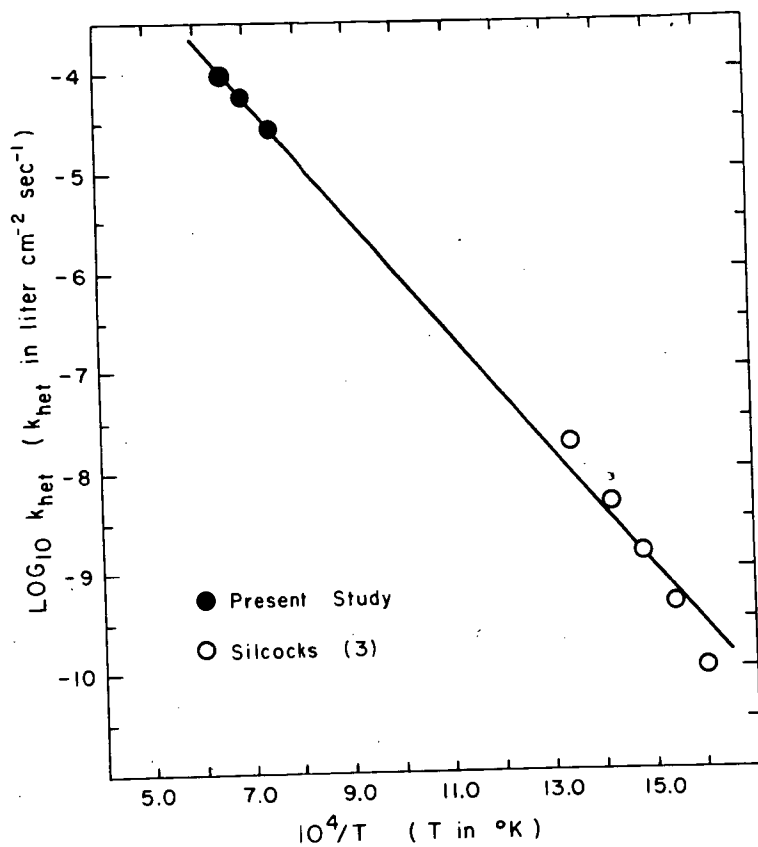


Fig. 3. Arrhenius plot of heterogeneous rate constants for C_2H_2 decomposition from the present work and from Silcocks (3).

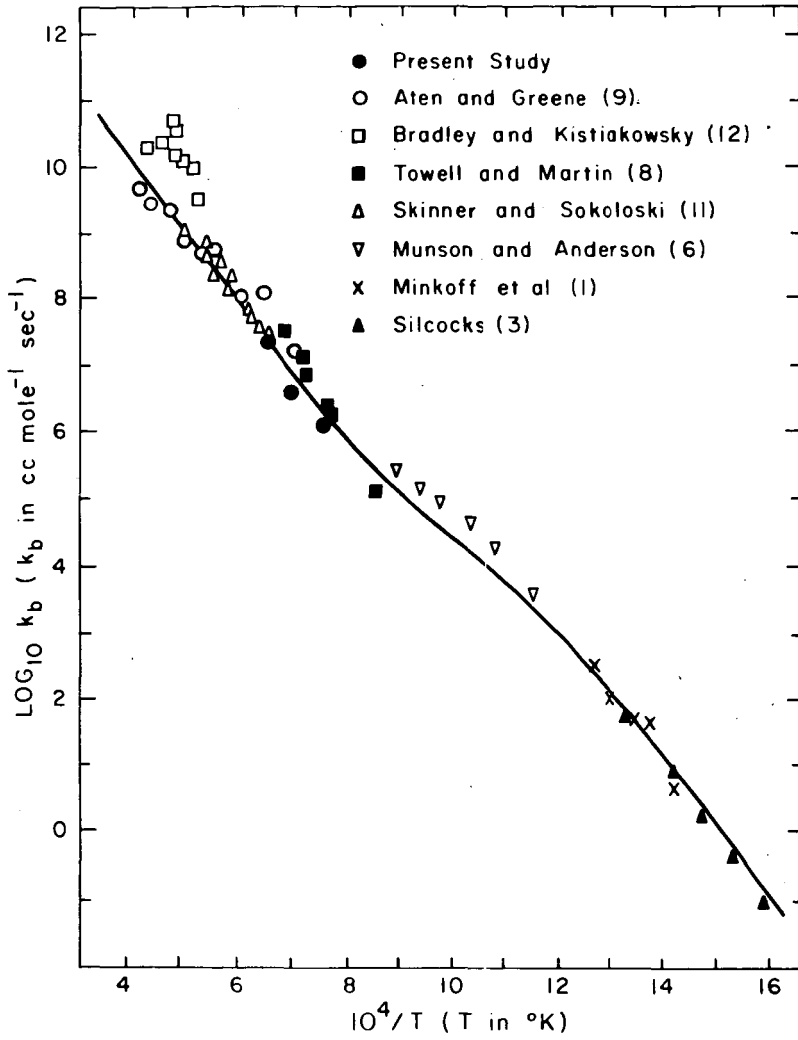


Fig. 4. Arrhenius plot of second-order rate constants for acetylene decomposition from the present work and from the literature.

Shock Tube Study of the Acetylene - Oxygen Reaction

R. F. Stubbeman* and W. C. Gardiner, Jr.

Department of Chemistry, The University of Texas, Austin, Texas

A number of investigations of the high temperature combustion of acetylene have been reported in recent years. The techniques employed have included probe studies of low pressure flames, spectroscopic studies of atomic flames, and various observations on detonation and shock waves in acetylene - oxygen mixtures. We report here a shock tube study of visible continuum emission, ultraviolet emission and OH absorption in incident shock waves through acetylene - oxygen mixtures.

EXPERIMENTAL

The shock tube was constructed of 2" x 4" aluminum tubing. Observations were made through quartz and lucite windows mounted flush with the tube walls. Velocity measurements were made with a series of flush resistance gauges spaced on either side of the observation station. Continuum emission was observed through the lucite window using an interference filter of about 80 Å bandwidth centered at 4320 Å for wavelength selection and a 1P28 photomultiplier tube for detection. The photomultiplier current pulses were amplified and then converted to logarithmic scale with a high frequency operational amplifier for oscilloscope recording. Ultraviolet emission was observed using a Beckman DU monochromator for wavelength selection and a 1P28 for detection. Absorption studies were made using a light source consisting of a microwave discharge in about 10 mm of argon containing a trace of bismuth vapor. The bismuth resonance line at 3067 Å was isolated with the DU monochromator and used for monitoring OH concentration. Sensitivity of the absorption system was calibrated by observations of OH concentration at chemical equilibrium in shocks through H₂-O₂ mixtures. The arrangement of the equipment was such that either OH absorption or ultraviolet emission could be observed simultaneously with the continuum emission, and that the origin of the effects observed in the two measuring systems was identical with maximum error of 3 microseconds. The shock tube was readily evacuated to the 10⁻⁵ mm range and had an outgassing and leak rate of about 2 microns per hour.

Experimental mixtures were prepared in a conventional mercury-pumped vacuum system. The acetylene concentration was about one percent and oxygen concentrations varied from .34 to 7.3 percent, the remainder being argon diluent. Conventional precautions in purification and mixing were observed. Initial pressure in all experiments was 5 mm. No-reaction temperatures computed from shock velocities covered the range 1500 - 2200 °K.

*Present address: Esso Research and Engineering Company, Linden, N. J.

RESULTS

Both the visible and the ultraviolet radiation appeared as a pulse, following an induction period. The ultraviolet emission, which was observed at 2196 Å, was far weaker than the visible emission, but both had essentially the same pulse shape and appeared simultaneously. Hydroxyl radical concentration rose to values above the detectability threshold, about 10^{-8} moles/liter in these experiments, just the emission pulses were returning to baseline.

Induction times defined by appearance of OH could be plotted as $\log(O_2)_{xt}$ versus $1/T$ as in the hydrogen - oxygen study of Schott and Kinsey or in earlier studies of the acetylene - oxygen reaction by Kistiakowsky and coworkers. The resulting plot showed that the OH induction times were about 2-3 times longer than induction times previously measured for this reaction using observations of onset of density change due to heat release in reaction, vacuum ultraviolet emission or ionization to define the end of the induction periods.

Time constants for the exponential rise in intensity of the continuum emission were obtained from the linear portions of the logarithmically recorded pulses. These, when plotted in the above form, showed no temperature dependence, in contrast to the strong temperature dependence (activation energy about 20 kcal/mole) found by Kistiakowsky and Richards for the time constants of the vacuum ultraviolet exponential rise.

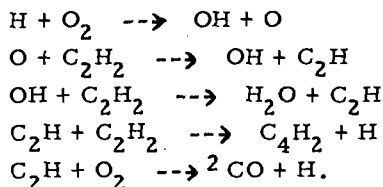
The lack of temperature dependence for the exponential rise constants led to a very strong temperature dependence of the ratio of continuum emission induction time to decadic time constant, which is a measure of the number of decades of concentration through which the emitting species rises as chain branching reactions proceed. At 1800 °K these values scattered around 30, but at 2100 °K they were down to less than 10.

Peak intensity of the continuum pulses was also strongly dependent on temperature. Between about 1600 °K and 2100 °K this was found to increase by about a factor of 10. Emission was strongest in mixtures near stoichiometric.

A search was made for structure in the ultraviolet emission intensity in the region 2000 - 2200 Å. This was done in a series of shocks of nearly constant strength in a lean mixture. The intensity distribution appeared to be uniform.

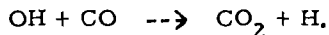
DISCUSSION

Previous shock tube studies on this reaction indicated that the main reaction sequence of the induction period could be understood in terms of the following branching chain sequence:

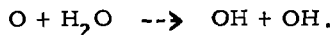


This mechanism was proposed in order to account for the similarity of $\text{H}_2 - \text{O}_2$ and $\text{C}_2\text{H}_2 - \text{O}_2$ induction period behavior and for the appearance of diacetylene in mass spectrometric studies of shocked $\text{C}_2\text{H}_2 - \text{O}_2$ mixtures. Several features of the high temperature reaction are not accounted for, as for example ionization or the appearance of formaldehyde; this provisional mechanism would have these features considered as side reactions not contributing to the main chain. Any side product whose concentration depends on the concentration of main chain species, however, is a satisfactory diagnostic for the progress of the chain reactions. It was proposed by Hand, for example, that the vacuum ultraviolet radiation observed by Kistiakowsky and Richards was due to excited CO produced by reaction of O with CH produced by oxidation of C_2H . The CO emission, therefore, would be an indirect measure of the chain carrier concentrations at any given time. Likewise, the continuum emission observed in this work comes from electronically excited CO_2 , which is produced from reaction of O with CO, and is, therefore, also an indirect measure of chain reaction progress.

Consideration of this reaction sequence shows that OH concentration should become observable when the chain has progressed to the point of giving macroscopic evidence of reaction, i. e. final products or heat evolution. In this work, however, it was found that the OH concentration rises only much later, after most of the final products have been formed. It follows, therefore, that OH is rapidly suppressed against its high rate of production in the chain by other reactions. When the acetylene concentration begins to decrease, this could be



The decay of continuum and ultraviolet radiation appeared to be simultaneous under all conditions, indicating that they probably have a common source. Since one of the reaction partners producing the emitter of the continuum radiation is a stable product, O is the most likely candidate for this role. Its destruction can only be by a final product. A probable pathway is



The lack of temperature dependence found for the exponential growth constant is probably complex in origin. It is likely to be due to a counterbalance of the increasing rate of chain center multiplication, as temperature increases, by increased rate of destruction of those particular species leading to the continuum emission, namely O and CO.

Failure to find the CO 4th positive system in the 2000 - 2200 Å region is probably due to instrumental limitations.

This work was supported by the U.S. Army Research Office - Durham.

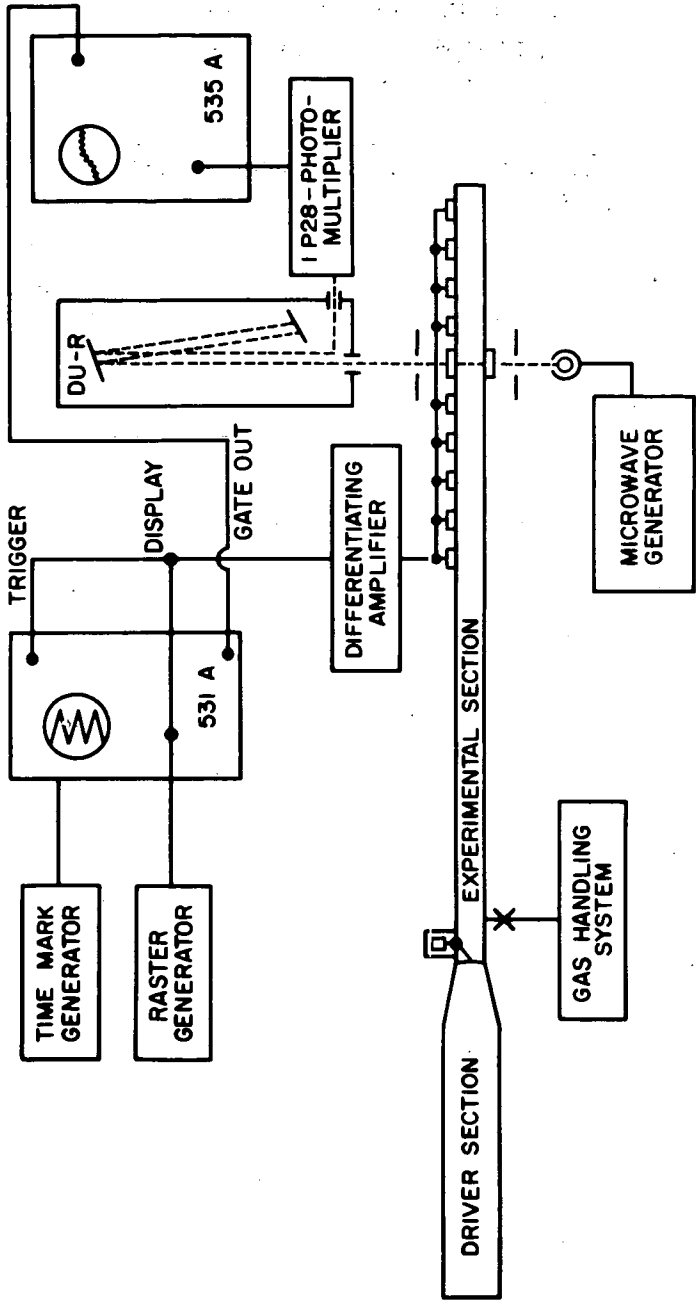


Fig. 1. Block Diagram of Apparatus.

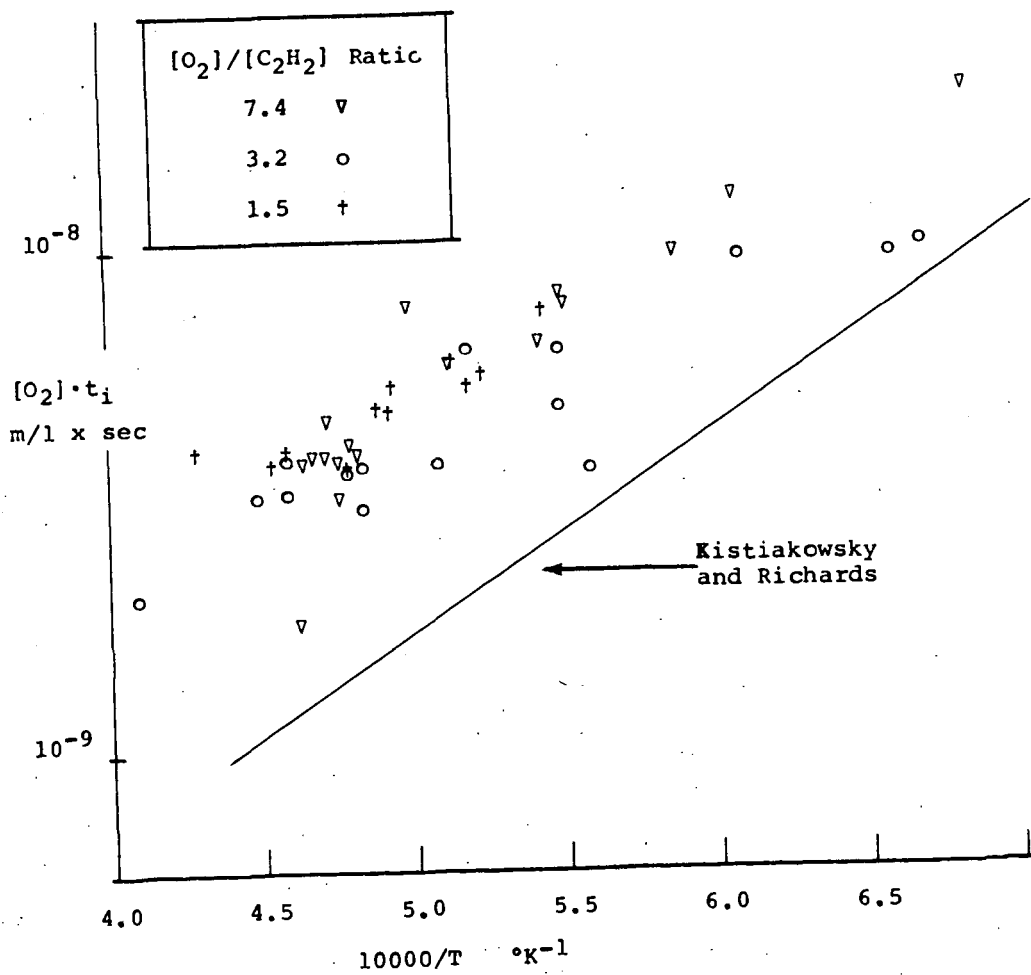


Fig. 2. Induction Times for OH appearance.

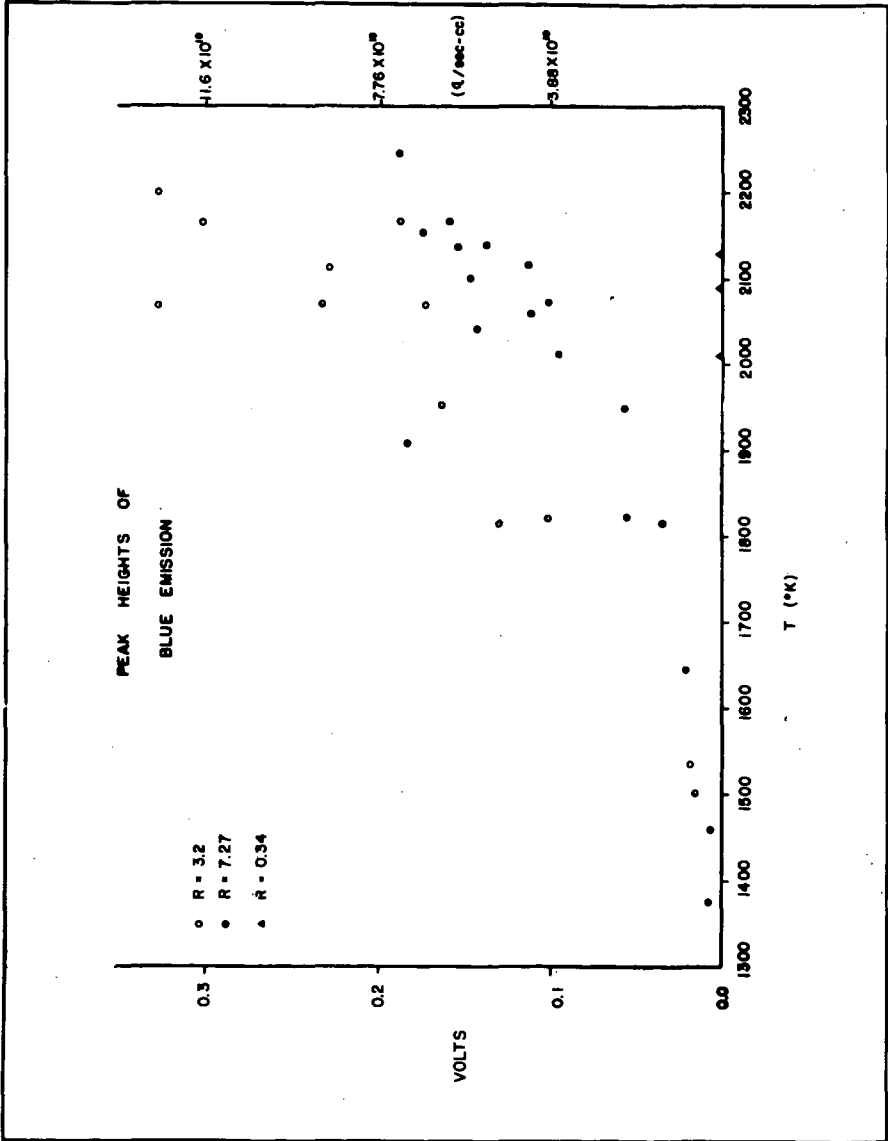


Fig. 3. Peak Intensity of Continuum Emission.

Chemi-ionization Reactions in High Temperature Hydrocarbon Oxidation

Joe V. Michael and Graham P. Glass

Chemistry Department, Harvard University, Cambridge, Mass.

Introduction

The mechanism of chemi-ionization in hydrocarbon oxidation reactions has attracted much interest in recent years. Ionization in hydrocarbon flames has been studied by means of Langmuir probes,² mass spectrometric sampling,³ and microwave attenuation measurements.^{4,5} By using these techniques the concentration of ions in the flames of lower hydrocarbons has been measured and has been shown to be too great to be accounted for by thermal excitation. Most investigators agree that the ions are formed by chemical reactions but the nature of these reactions as yet is not absolutely clear. The high heats of formation of most organic ions places severe energetic restrictions on the reaction which produces ions, and much effort has been spent considering reactions exothermic enough to do this. The reaction, $\text{CH} + \text{O} = \text{CHO}^+ + \text{e}^-$, has been suggested as a probable ion forming reaction, but no conclusive evidence for it has been found. To be sure CHO^+ (mass 29) has been observed by many investigators in flames, but it has always appeared in concentrations much below that of the more abundant ions (e. g. H_3O^+). Calcote⁶ has pointed out that CHO^+ would be expected to undergo rapid proton transfer reactions with water, a product of these oxidations, thus explaining its presence in such low concentrations.

Calcote² has detected the C_3H_3^+ ion in a mass spectrometric investigation of low pressure acetylene-oxygen flames. This ion was observed in the flame profile ahead of H_2O^+ in quite large concentrations and its abundance was independent of the stoichiometry of the flame. It is difficult to account for these observations on the basis of charge transfer reactions from CHO^+ .

The work described in this paper was performed using shock tubes, and the reactions which occur during the oxidations of both methane and acetylene were studied by means of a Langmuir probe and also by means of a time-of-flight mass spectrometer which was adapted to detect the chemi-ions formed during the reactions.

Experimental

The apparatus in which the Langmuir probe measurements were made was substantially the same as that described by Hand and Kistiakowsky. Shock waves were generated in a three inch I. D. steel tube and shock wave velocities were measured by gold film resistance gauges the outputs of which were displayed on a raster sweep oscilloscope. Radiation from the heated gas behind the shock wave passed through a lithium fluoride window and was detected by means of an RCA 1P28 photomultiplier. An interference filter was used to isolate the $A^2\Delta \rightarrow X^2\Pi$ system of CH. The probe consisted of a 12 mil diameter tungsten wire placed in the shock tube in a plane defined by the optical slits. All but the last one-quarter inch of the wire was insulated with Armstrong A2 cement, the tip of the probe being near the shock tube axis. The major modification to the apparatus was the introduction of a removable piston which could be placed seven millimeters behind the cross sectional plane which contained the probe. This allowed the reactions in the stationary gas behind the reflected shock to be studied, thus removing the complicating effect of the aerodynamic interaction of the moving gas with the probe.

The second technique combines a shock tube and a Bendix time-of-flight mass spectrometer in a redesigned apparatus which is a significant improvement over the one described by Bradley and Kistiakowsky. Complete mass spectra of the reacting gases can be obtained every 20 or 50 μ sec. Data is recorded by means of Polaroid 10000 ASA speed film. Normally a total of twenty-one spectra are displayed on three Tektronix 531-A oscilloscopes so that the amount of observable reaction time is a little over a millisecond with 20 KC operation. The mass range can be adjusted at will before the start of an experiment.

Sampling is through a small pinhole (.004 in. diameter) in the tip of a small conical nozzle (1 mm. by 1 mm. pointed away from the mass spectrometer) at the end of the shock tube. It is felt that this small nozzle reduces problems caused by boundary layer build up on the reflection plate onto which the nozzle is mounted.

The shock tube is one inch in diameter and 2.75 meters long. Shock velocities are measured with four thin film resistance gauges (either Pt or Au) spaced ten centimeters apart. The signals from these gauges are displayed on a raster oscilloscope. Shock temperatures are calculated using ideal shock relations in both incident and reflected shocks.

All experiments with the time-of-flight mass spectrometer reported here were carried out with five percent reactants in ninety-five percent krypton. The experiments with the Langmuir probe apparatus were carried out with one percent reactants in ninety-nine percent argon.

Ions and stable products were observed using the time-of-flight mass spectrometer in the oxidations of both acetylene and methane. Both types of species arose concurrently after an induction period characteristic of a branching chain reaction. In both systems the total ionization was observed using the Langmuir probe technique. The ionization rises exponentially with time and the measured time constants provide a convenient method for determining the rates of the branching chain reactions. Ionization is not, however, a major part of the reaction since, for example, in the oxidation of acetylene, the maximum concentration which the ions achieved was about 10^7 ions/cc. This was 10^{-6} of the initial acetylene concentration.

The individual ions produced were identified with the time-of-flight mass spectrometer. The largest mass peaks in the acetylene-oxygen system were 39 and 19. 39, 31, 19, and 37 were observed in the methane-oxygen system. By using deuterated acetylene and methane the following assignments were made for the different species:

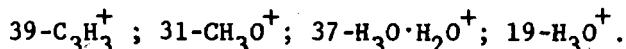


Figure 1 shows the time history of the ionization in two typical experiments with acetylene-oxygen. It is seen that $C_3H_3^+$ is the first ion observed followed later by H_3O^+ . In these experiments the reactant mixtures were: (A) $3 O_2 + 2 C_2H_2 + 95 Kr$, and (B) $3.75 O_2 + 1.25 C_2H_2 + 95 Kr$. Ionization was not observed in mixtures where acetylene was in excess over oxygen.

$C_3H_3^+$ was also the first ion observed in the oxidation of methane. CH_3O^+ arose at nearly the same time as did $C_3H_3^+$ but its concentration was much lower. H_3O^+ and $H_3O \cdot H_2O^+$ arose concurrently at still later times.

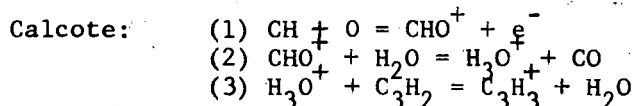
In the acetylene-oxygen system the time constant measured for the growth of ionization, using the Langmuir probe technique, was found to be identical to that measured for the simultaneous growth of chemi-luminescent radiation from the $CH(A^2\Delta \rightarrow X^2\Pi)$ system.

In earlier experiments with the time-of-flight mass spectrometer, the stable products observed in the oxidation of acetylene were CO , H_2O , CO_2 , and C_2H_2 . These results were confirmed in the present study. CO , CO_2 , H_2O , and C_2H_2 were observed as stable products in the methane-oxygen system. CO_2 was a major product in $3 O_2 + 2 CH_4 + 95 Kr$, and it was absent in $1.4 O_2 + 3.6 CH_4 + 95 Kr$. C_2H_2 was found to be a major product in the latter mixture but was formed in quite small quantities in the former.

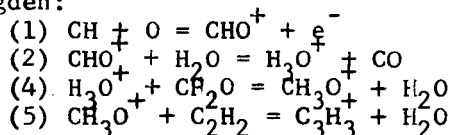
Discussion

$C_3H_3^+$ has been observed by several investigators in hydrocarbon

oxidation systems. As has been stated previously, Calcote² detected this ion ahead of H_3O^+ in a dilute low pressure flame of acetylene and oxygen. Green and Sugden³ have also observed this ion in flames at somewhat higher pressures. The following reaction schemes have been suggested by these workers for the formation of $C_3H_3^+$.



Green and Sugden:



In both of these mechanisms, $C_3H_3^+$ is formed by charge transfer reactions from CHO^+ . However, the time history in the stationary gas behind a reflected shock wave is much better defined than in a flame where diffusion and cold boundary layer effects could invalidate measurements, and it is felt that $C_3H_3^+$, and CHO^+ , is the first ion formed since it is the first ion observed in these experiments.

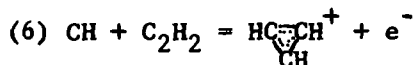
Two structures appear to be feasible for the $C_3H_3^+$ ion:



The cyclopropenyl ion (B) is believed to be the more probable structure, since it has great stability due to delocalization of its π electron system. Tri-substituted aliphatic and aromatic analogs of the cyclopropenyl ion have been synthesized and halogen salts are completely dissociated in polar solvents.¹⁰ Furthermore, a plausible mechanism for it can be suggested which is energetically possible, whereas such a mechanism for the formation of (A) is difficult to justify on an energetic basis.

If (B) is the correct species it should be extremely stable and should undergo little or no charge transfer. The ion probably is removed from the system by chemical reaction, perhaps with oxygen resulting in the production of other ions. Indeed in experiments where oxygen is in excess the rate of fall off for $C_3H_3^+$ is faster and the total yield of H_3O^+ is greater than in experiments where oxygen is present in stoichiometric quantities (see Figure 1).

The following mechanism is proposed for the formation of $C_3H_3^+$:



The heat of formation has been determined by Wiberg et al.¹¹ for C_3H_3^+ to be 271 kcal/mole. This value is higher than that estimated by a simple molecular orbital calculation coupled with thermodynamic considerations, and the value measured by Wiberg et al may refer to structure (A). However if the Wiberg value does apply to (B) then reaction (6) is nearly thermoneutral if the CH radical is in its $A^2\Delta$ or $B^2\Sigma$ state. If the calculated value is correct then the CH radical could even be in its ground state and reaction (6) would be close to thermoneutrality. Both CH ($A^2\Delta$) and CH ground state are known to be present in the oxidation of acetylene.^{12,13} Since there is some evidence for the existence of acetylene in the oxidation of methane, reaction (6) could also explain the observation of C_3H_3^+ in this system.

The above mechanism has received some support from the observation of chemi-ionization in the reaction of iodoform and acetylene. The chemi-ionization had an "activation energy of formation" much below that usually found (55 kcal/mole), and the ionization was believed to be produced from the reaction of acetylene with the breakdown products of iodoform (CH and CHI).

This mechanism is also consistent with the observation that the time constants for the rise of ion concentration and $\text{CH}(A^2\Delta \rightarrow X^2\Pi)$ radiation were identical in the early stages of the acetylene-oxygen reaction. However the mechanism, $\text{CH}(A^2\Delta) + \text{O} = \text{CHO}^+ + e^-$, which has previously been proposed for the formation of ions in these systems is not consistent with this observation. Both CH ($A^2\Delta$) and O would be expected to be intermediates in the branching chain reaction, and therefore the concentrations of both would be expected to rise exponentially in the early stages of reaction. Thus the inverse time constant for the growth of ionization would be equal to the sum of the inverse time constants for the rise of CH and O concentrations.

The authors wish to thank Professor G. B. Kistiakowsky for his many helpful suggestions. We also wish to thank Dr. Hiromi Niki and Dr. J. L. Michael for help in the experiments with the time-of-flight mass spectrometer. The work with the Langmuir probe technique was supported by the Office of Naval Research and that with the time-of-flight mass spectrometer by the National Science Foundation.

Bibliography

1. Van Tiggelen, A.; Experimental Investigation of Ionization Processes in Flames, University of Louvain ARL Report 68, May, 1961.
2. Calcote, H. F.; Ninth Symposium (International) on Combustion, p. 622, Academic Press (1963).
3. Green, J. A. and Sugden, T. M.; Ninth Symposium (International) on Combustion, p. 602, Academic Press (1963).
4. Sugden, T. M.; Fifth Symposium (International) on Combustion, p. 406, Reinhold (1955).
5. Schneider, J. and Hoffman, F. W.; Phys. Rev. 116, 244 (1959).
6. Calcote, H. F.; Eighth Symposium (International) on Combustion, p. 184, Williams and Wilkins Co. (1962).
7. Hand, C. W. and Kistiakowsky, G. B.; J. Chem. Phys. 37, 1239 (1962).
8. Bradley, J. N. and Kistiakowsky, G. B.; J. Chem. Phys. 35, 256 (1961).
9. Dove, J. E. and Moulton, D. M.; To be published.
10. Breslow, R., Höver, H., and Hai Won Chang; J. Am. Chem. Soc. 84, 3168 (1962).
11. Wiberg, K. B., Bartley, W. J., and Lossing, F. P.; J. Am. Chem. Soc. 84, 3980 (1962).
12. Gaydon, A. G.; The Spectroscopy of Flames, p. 113, Chapman Hall, Ltd., (1957).
13. Gaydon, A. G., Spokes, G. N., and Van Suchtelen, J.; Proc. Roy. Soc. A256, 323 (1960).

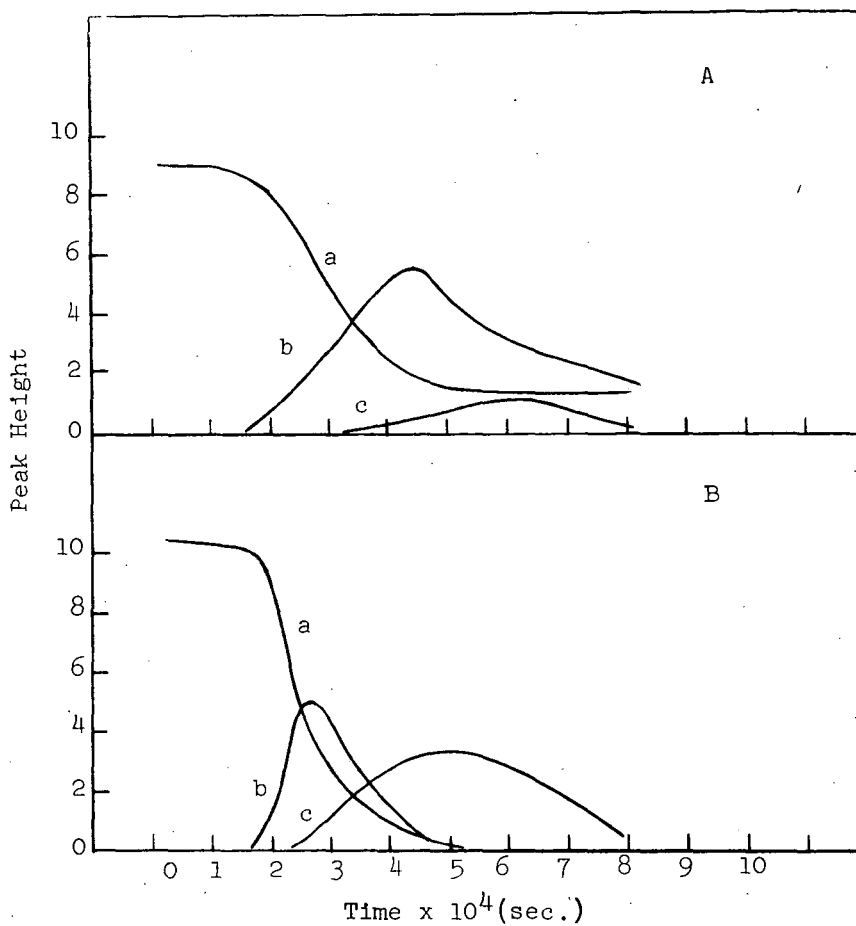


Figure 1. Height of ion peaks versus time in two experiments.

Experiment A:

$2 \text{C}_2\text{H}_2 + 30 \text{O}_2 + \text{Kr}$ at 1600°K ;
 curve a is acetylene, b is $m = 39$
 (C_3H_3^+), c is $m = 19$ (H_3O^+).

Experiment B:

$1.25 \text{C}_2\text{H}_2 + 3.75 \text{O}_2 + 95 \text{Kr}$ at 1700°K ;
a, b, and c refer to the same species
 as in A.

SHOCK TUBE EVALUATION OF HYDRAULIC FLUIDS

Gordon B. Skinner

Monsanto Research Corporation, Dayton 7, Ohio

INTRODUCTION

While the shock tube has been used extensively in the study of gas-phase reactions, relatively few studies have been made of gas-liquid reactions. The main reason for this has been the difficulty in interpreting the data obtained when two phases are initially present, because the additional steps of drop break-up, evaporation and mixing need to be considered, as well as chemical kinetics.

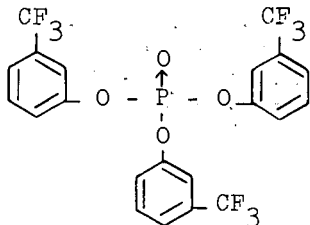
A study of the combustion process when n-hexadecane is injected as a fine spray into shock-heated air was made by Mullaney (Ref. 1). By high-speed photography he was able to observe injection of the spray, evaporation of the droplets, and spontaneous ignition. In most of his experiments combustion started before evaporation was complete. Shock tubes have also been used by Morrell and co-workers (Ref. 2,3) and by Hanson, Domich and Adams (Ref. 4) to study the break-up of liquid jets by rapidly moving gas streams. These investigators used inert liquids to study atomization of the liquids without the complications introduced by combustion, and were able to obtain equations relating atomization time to physical properties of the liquid and gas.

The original intent of this work was to develop a method of rating the ignition characteristics of fire-resistant hydraulic fluids that could be related to the single-cylinder engine test (Ref. 5) currently used, yet require much less fluid for an evaluation. The results shed some light on the parameters governing liquid-gas reactions.

EXPERIMENTAL

The shock tube used for these experiments has been described in detail elsewhere (Ref. 6). Briefly, it is 3 inches in diameter, with 12-foot low-pressure and 20-foot high-pressure sections. Shock speeds are measured by timing the passage of a shock wave between stations 55 and 7 inches from the closed end of the low-pressure section. Gas temperatures and flow velocities are calculated from the shock speeds. A piezoelectric pressure transducer is mounted in the top of the tube, 3 inches from the closed end, while a fused quartz window (covered except for a 2 mm vertical slit) is in the side of the tube, also 3 inches from the end. Light emitted by combustion in the tube is detected by a photo-multiplier tube 8 inches away from the tube, which also was covered except for a 2-mm vertical slit. Because of the slits, light emitted only from gas 3 inches from the end of the tube was detected.

Of a number of exploratory hydraulic fluids tested one, of formula



had the high ignition temperature of 1365°K., which from the extrapolation of Figure 2 would indicate an engine test rating of about 80.

DISCUSSION

There is, and probably will be for some time, a question as to the relative importance in the ignition process of the physical factors of drop break-up, evaporation, convective and diffusive mixing on the one hand, and chemical reactivity on the other.

Morrell and Povinelli (Ref. 3) have developed an equation for the time for break-up of liquid cylinders by shock waves, which should also apply approximately to drops. The break-up times of the 0.01 ml drops of "standard" liquids used in the above experiments have been calculated, as follows:

<u>Liquid</u>	<u>Calculated Break-up Time, milliseconds</u>
MS-2110-H	0.24
Fluid AV	0.31
Xylene	0.81
MIL-H-19457	0.25

These drop break-up times do not correlate with the ignition data, since the break-up times of the most and least flammable liquids are the same, while the calculated break-up times for Fluid AV and xylene, which have similar ignition temperatures, are different. Moreover, the boiling points of these latter two compounds differ considerably, being 325° and 140°C, respectively. It seems, therefore, that under these conditions the physical properties of the fluids are less important than chemical reactivity in controlling the ignition delays.

The author wishes to acknowledge the suggestion, made by Gordon H. Ringrose, that the shock tube could be used to test the reactivity of hydraulic fluids; and the assistance of Edward S. Blake and Ralph E. DeBrunner who furnished the experimental hydraulic fluids.

REFERENCES

1. G. J. Mullaney, Ind. Eng. Chem. 50, 53 (1963).
2. G. Morrell, Eighth Symposium (International) on Combustion, Williams and Wilkins Co., Baltimore, Md., 1963, p. 1059.
3. G. Morrell and F. P. Povinelli, NASA Lewis TP 3-63, Paper presented at Fifth Liquid Propulsion Symposium of the Chemical Propulsion Information Agency, Tampa, Florida, Nov. 12-14, 1963.
4. A. R. Hanson, E. G. Domich and H. S. Adams, Phys. Fluids 6, 1070 (1963).
5. C. L. Brown, NAVENGRXSTA Report 95 648 C, Fluid Structural Factors Versus Fire Resistance, November 1962.
6. G. B. Skinner and R. A. Ruehrwein, J. Phys. Chem 63, 1736 (1959).

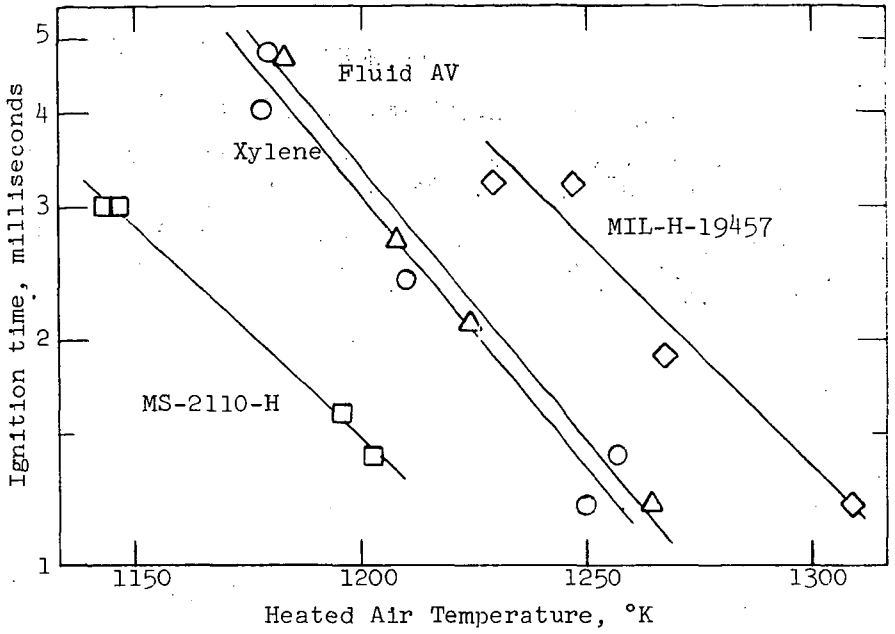


Figure 1. Shock tube ignition of hydraulic fluids

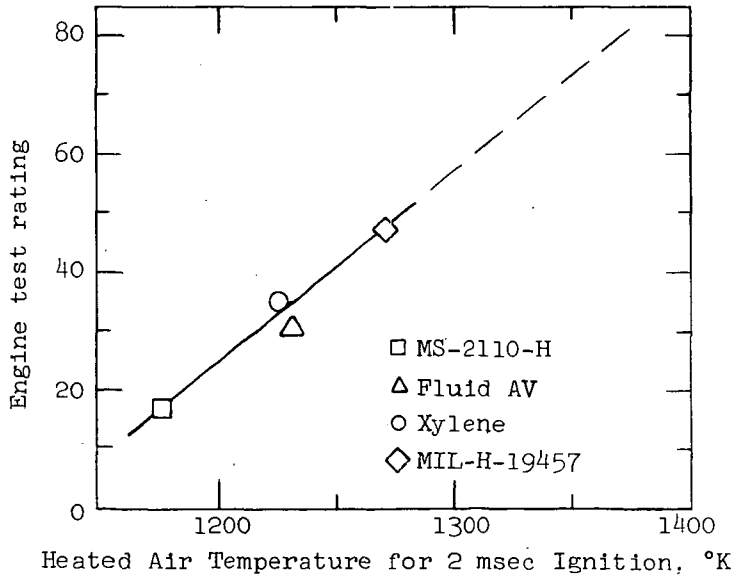


Figure 2. Calibration curve - shock tube versus engine test rating

On the Stability and Combustion Intensity of Pulverized
Anthracite Flames

J. W. Beer

Pennsylvania State University
Department of Fuel Technology
College of Mineral Industries
University Park, Pennsylvania

ABSTRACT

Recent experiments on pulverized anthracite flames carried out by the International Flame Research Foundation at IJmuiden (Holland) are discussed. It is shown that ignition is considerably aided by the entrainment of hot combustion products into the fuel rich primary jet. This indicates that it is advantageous if the mixing between the primary jet and the rest of the combustion air is preceded by the mixing of the primary jet with the hot combustion products.

Experimental evidence to prove this point is presented. Flame stability improves also with finer grinding. Flame speeds in this case increase partly due to the increased radiation from the flame front owing to the burning of the fine particles and also due to the higher absorption of such a dust cloud. It is shown from the comparison of the values of "mixedness" and "reactedness" along the flames that the combustion of the solid residue follows mixing more closely in flames with finer ground pulverized anthracite. The rates of combustion of the anthracite calculated from measurements on jet flames are of the same order of magnitude as those determined in a laboratory "plug flow" type flame.

Reaction Rates of Single Coal Particles: Influence
of Swelling, Shape, and Other Factors

By Robert H. Essenhigh
Department of Fuel Technology, College of Mineral Industries
The Pennsylvania State University, University Park, Pa.

and G. C. Yorke
Department of Fuel Technology and Chemical Engineering
University of Sheffield, England

1. INTRODUCTION

Coal particles burning in oxygen-vitiated and enriched atmospheres, at about 1000°C, have been shown by Previous work (1,2,3) to burn in the expected two-stage process of: volatiles combustion; followed by burn-out of the solid carbon residue remaining. The same work also showed that the solid residues burned according to the Nusselt-predicted (4) "square-law", by which the burn-out time (t_b) was directly proportional to the square of the initial particle diameter (d_0). However, although the agreement between prediction of the residue behavior and experiment was generally found to be adequate to good (1,2) there were several questionable points in the theoretical assumptions made in the modified (5,6) Nusselt theory used. These assumptions centered principally on the suggested behavior of the particles on swelling, and the ultimate effect this could have on the combustion behavior, particularly if the particles formed hollow cenospheres (7,8). Several questions were set up by this, as follows: (1) How much did the particles swell? (2) Was this swelling reasonably isotropic? (3) How did swelling change with coal rank? (4) Did the particles form cenospheres? (5) Did cenosphere formation, if any, affect the mechanism of burn-out, and if so how would this affect the theoretical analysis? (6) What influence did particles shape have on the final shape after swelling, and therefore on the combustion behavior?

To answer these questions as far as possible, a number of particles from each of the 10 coals used in the previous investigations (1,2,3) were photographed during combustion, and it was found that reasonably satisfactory answers to all six questions were obtained with, in addition, further information on swelling properties of coal particles.

The purpose of this paper is now to describe the photographic experiments carried out, the results obtained, and the answers that were provided, by these, to the questions given above.

2. EXPERIMENTAL

Whilst the coal particles were burning, in the combustion unit described in the previous papers (1,2,6), they were photographed using a continuously running camera adapted to take intermittent exposures.

2.1 Combustion Unit - The method of burning the particles was exactly the same as that described in the first two publications of this work (1,2). The particles, in the size range 0.5 to 2 m.m., were cemented to fine silica

threads with a high temperature cement and then suspended, cantilever fashion, between two heating coils made of electrical resistance wire wound in flat spirals. These coils were about 1.5 m.m. across, and mounted with their planes horizontal about 1.5 m.m. apart. The coils were heated electrically, to about 1000°C.

2.2 Pyrolysis Unit - For a few experiments, carried out on one coal alone, the combustion unit described above was enclosed in a brass box, with observation windows, that could be flushed out with CO₂. This made it possible to observe the behavior, and measure the swelling of particles just pyrolysing without burning..

2.3 Optical Unit - To illuminate the particles, a 36-watt car headlamp bulb was placed at the focal point of a 10-cm. f.l. lens to produce a parallel beam of light. The particle combustion, or pyrolysis, unit, was placed in this parallel beam, about 20-cm. from the first lens, and about the same distance from a similar lens which then created a real image of the burning particle at about a one-to-one magnification. This image, therefore, could exist also as a real object, well clear of any heat source, that could be magnified to any required degree by a suitable short-focus objective close to this real object. The second image from this could then be projected onto a screen, or into a suitable camera.

2.4 Camera - The one used was a Cossor 35 m.m. Oscilloscope camera, with an adaptation to provide intermittent exposures on continuously moving film. A glass screen was lightly ground with abrasive and placed at the end of the camera tube, in the same relative position as that normally occupied by the Oscilloscope screen. The particle image provided by the optical unit was projected onto this screen, at a net magnification of about 5, and this image was then photographed (from the reverse side) by the Oscilloscope camera. This final stage diminished the image, but the overall magnification was still about 2. By trial and error it was found that the glass screen could not be too lightly, or too heavily ground: in the first instance the contrast between image and surroundings was too faint; and in the second, too little light was reaching the film.

2.5 Exposure Unit - Since the 35 m.m. recording strip was moving continuously, it would have blurred any time exposure that was of adequate duration to affect the emulsion used, even at the low speed of traverse involved. (The emulsion was on opaque recording paper, not on transparent film strip.) A rotating glass plate was therefore placed in the parallel light beam, between the particle and the second lens. As the plate rotated, it moved the image formed at the camera and, by adjusting the rate of rotation, the speed of motion of the image and recording paper could be matched (on the same principle as that used by the Fastax camera). This produced a clear image and, by incorporating a simple shutter, a series of single exposures could be taken. Finally, the rotation was synchronized with the camera by using gears and spindles of Meccano (a type of Erector set) to take a drive off the camera motor. Timing of the frames was then obtained by timing a given number of revolutions of the rotating plate.

2.6 Coal Preparation and Data - Information on grinding and sieving the coals is given in detail in the previous papers (1,2,6). They were crushed and ground by hand in a pestle and mortar, and then sieved mechanically using the complete sequence of British Standard sieves from 3/16" to 52 mesh (4760 to 295 microns). In these photographic studies, the particle sizes mostly used were about 2 m.m.

Table 1
Coal Analyses and Data

Coal	<u>(1A) Ultimate Analysis (d.m.f.)</u>						C_F	C_V	(C_V/C_F)
	C	H	O	N	S	V			
(1) Stanllyd (Blaunhirwaun)	93.00	3.35	1.59	1.33	0.73	9.9	90.1	2.9	0.03
(2) Five ft. (Deep Duffryn)	91.80	4.08	2.32	1.42	0.38	14.9	85.1	6.7	0.08
(3) Two ft. Nine -unknown-	91.20	4.35	2.54	1.65	0.26	28.8	71.2	20.0	0.28
(4) Red Vein (Cilely)	89.70	4.66	3.55	1.67	0.42	23.3	76.7	13.0	0.17
(5) Garw (Cwm Tillery)	88.90	4.99	4.50	1.33	0.28	30.6	69.4	19.5	0.28
(6) Silkstone (Elsecar)	86.90	5.79	5.50	1.51	0.30	41.5	58.5	18.4	0.49
(7) Winter (Grimethrope)	84.00	5.47	8.29	1.85	0.39	39.3	60.7	23.3	0.38
(8) Cowpen (Northumberland)	82.70	5.40	9.60	1.80	0.50	40.2	59.8	22.9	0.38
(9) High Hazel (Thorne)	81.90	5.57	10.52	1.58	0.43	40.7	59.3	22.6	0.38
(10) Lorraine (Faulquemont)	79.25	5.13	14.16	0.95	0.51	40.2	59.8	19.5	0.32

(1B) Proximate Analysis and Other Data

Coal	V.M.	H ₂ O	Ash	CO ₂	B. S. Sw. No.		M	
					g/cc.		M	m
(1) Stanllyd	7.9	1.3	2.9	0.73	n.c.	1.38	0.871	3.06
(2) Five ft.	12.6	0.9	3.9	0.26	1	1.40	0.993	3.20
(3) Two ft. Nine	28.9	0.8	22.2	13.3	1	1.36	1.150	3.15
(4) Red Vein	20.5	1.0	1.6	0.04	6 ^{1/2}	1.34	1.794	3.01
(5) Garw	27.7	1.0	3.7	0.05	4	1.31	0.934	3.04
(6) Silkstone	39.6	1.3	1.7	0.35	4 ^{1/2}	1.28	0.690	3.00
(7) Winter	36.0	2.6	1.7	0.77	3	1.25	0.848	3.06
(8) Cowpen	34.6	7.3	4.1	0.95	1	1.27	1.000	3.17
(9) High Hazel	36.7	5.1	1.0	0.0	1	1.27	0.941	3.04
(10) Lorraine	35.0	5.0	5.9	0.52	n.c.	1.36	0.919	3.01

The coal analyses are given in Table 1, which also gives for the full particle size range, the size coefficients (M and m) in the empirical relation between weight (w_0) and initial diameter (d_0):

$$w_0 = M \cdot d_0^m \quad (1)$$

where M and m are empirical constants determined experimentally. The method for determining M and m has already been described (2) but, briefly, required the weighing of groups of particles from a number of sieve cuts to determine w_0 (the mean weight per particle) at a given mean sieve aperture as diameter, d_0 . The best values of M and m were then determined by the method of least squares.

3. THEORY

The "square-law" relation referred to in the Introduction was first derived by Nusselt (4) for heat and mass transfer to and from a sphere. This theory, and necessary modifications for application to swelling coal particles, has been adequately covered in the previous papers and publications (1-3,5,6); the purpose of this section is to indicate how the theory may be modified further if needle-like coal particles are treated as cylinders instead of spheres.

For both systems the approximation of single diffusion of oxygen through stationary nitrogen is used. The Stephan flow (9) is also neglected since the previous studies (1,2) showed this to be a valid approximation for oxygen in air and vitiated air atmospheres (though not for enriched atmospheres (3)).

The starting point for both theories (sphere and cylinder) is Fick's Law for diffusion:

$$\dot{g} = -D(dN/dr) \quad (2)$$

where \dot{g} is the number of molecules diffusing across unit area in unit time; D is the diffusion coefficient; and dN/dr is the oxygen concentration gradient at any distance r from the center of the sphere.

The next step is to write the continuity equation which is slightly different for each system. For the sphere we have:

$$a^2 \cdot \dot{g}_s = r^2 \cdot \dot{g} \quad (3a)$$

whilst for the cylinder

$$a \cdot \dot{g}_s = r \cdot \dot{g} \quad (3b)$$

This makes the difference in the solutions for \dot{g}_s since, on substitution for \dot{g} and integrating, we have:

$$\text{sphere:} \quad -\dot{g}_s = D(N_0 - N_s) / a \quad (4a)$$

$$\text{cylinder:} \quad -\dot{g}_s = D(N_0 - N_s) / a \cdot \ln(r_0/a) \quad (4b)$$

where the subscripts to N are for the main stream values and the solid surface values respectively; a is the particle radius; and r_0 in eqn. (4b) is the distance at which the main stream value of N is reached. In eqn. (4a) this is taken as infinity, and the term in r vanishes. In eqn. (4b) the equation becomes meaningless, if r is taken as infinity. All we can do then is to consider the equation for the mass transfer coefficient k . This is:

$$g_s = -k(N_0 - N_s) \quad (5)$$

But the mass transfer coefficient is related to the Nusselt number for mass transfer by the definitive group;

$$Nu = k(2a) / D \quad (6)$$

For the sphere, it can be shown from eqn. (4a) that in quiescent conditions, Nu takes the value 2. Experimentally, it has also been shown by data (10) quoted by Gruber and Erk (11) that Nu also tends to a constant value, of 0.43, for the cylinder in quiescent ambient conditions. If we assume that this holds generally, we then get the alternative equation for the cylinder:

$$-g_s = 0.215D(N_0 - N_s) / a \quad (4c)$$

which, clearly, differs from eqn. (4a) only by the factor 0.215. From either equation, we have that the specific reaction rate is inversely proportional to the radius. Integrating, as in the previous analyses for the sphere, we get for the variation of diameter with time:

$$d^2 = d_0^2 - t / K \quad (7)$$

where K is the burning constant, given by (2,3)

for the sphere
$$K_s = \sigma / 3 \rho_0 D_0 p_0 (T/T_0)^{0.75} \quad (8a)$$

and for the cylinder
$$K_L = K_s / 0.215 = 4.65K_s \quad (8b)$$

so a cylinder of radius a should still burn according to a square law, but take up 4 or 5 times longer to burn out than a sphere.

3. RESULTS

3.1 General Behavior - In these photographic studies, between 30 and 40 particles were burned (compared with over a 1000 in the previous total-burnin time studies). The particles were mostly cubic in nominal appearance, this being the same principal basis of selection as in the previous studies, but a few were needle shaped particles selected to study the influence of shape.

The burning particles all exhibited the characteristic behavior of volatiles generation and combustion, with swelling during the volatiles combus phase; this was followed by residue burn-out. Diameters were measured from the photographic records and plotting the square of the diameter against frame number (as Time), to test eqn. (7). The Figures 1 and 2 show the type of plots obtained. Figure 1 is for the Stanlyd anthracite, and Figure 2 for the Cowpen coal. In the latter, the effect of swelling is clearly illustrated by the sudden rise and fall of the curve at the start of combustion. Swelling in air is therefore a two-stage process; first there is a large expansion, followed by a contraction. In CO_2 there was only expansion, no contraction.

the end of the contraction, the line is seen to flatten out: this is the residue combustion. The curve of Fig. 2 is typical of all the bituminous coals, whatever their swelling number.

Swelling and Swelling Factor - f - The identification of the peak in Fig. 2 during the period of volatiles generation was more or less self-evident, but further, positive identification was provided by simultaneously recording the heat output from the particle with a photocell. This technique had been used in the previous studies (1,2) to determine the total burning time, and it had been found during those that the period of volatiles evolution during combustion correlated with a characteristic trace in the record of the photocell output. This trace was a random high frequency oscillation due to the flickering flame from the volatiles combustion. Identification of this characteristic trace, and comparison with the photographs, showed that the particles started to swell a little in advance of the start of the volatiles combustion; the volatiles continued to burn right through the main expansion and contraction period; and the start of the residue combustion correlated well with the start of the final linear portion of the plot of Fig. 2.

With this positive identification, measurements were then made of some regular shaped particles to check the degree of isotropism in the swelling. The particles selected for this were quite long, rectangular or needle-shaped particles, the selection being based on the assumption that if they broke non-isotropically, they would be the most likely to swell non-isotropically. At the event, they swelled quite uniformly, all dimensions changing in approximately the same proportion, as with substantially all the other particles studied.

Swelling determinations were then carried out on selected particles of all the coals to determine their average swelling factors. The swelling factor, f , was defined as the ratio (d_s/d_0) , d_0 being the initial, cold diameter, and d_s being the diameter at the start of the residue combustion. The values of this ratio, f , are summarized in Table 2 for the ten coals. As can be seen, the scatter is quite wide for any given coal, but the average values are very close to 1.5 for all the bituminous coals used, irrespective of the swelling numbers. This result was quite unexpected, and it raises in question the meaning of such quantities as B.S. swelling number. The difference between swelling factor and number is obviously dependent on the different experimental conditions in the methods of measurement. In contrast to the swelling-factor measurements on single, unconstricted particles, as described above, Swelling Number tests are made on groups of particles under some degree of constriction, and are, therefore, partly able, and partly forced to swell to each other. Initially, at low volatile content in the bituminous range, there is little loss, and therefore little increase in porosity. However, as the volatile content (and loss) increases, there is more and more space between adjoining particles for others to swell into, thus producing the characteristic inverted 'U' curve of the swelling or caking index against coal rank.

3 Residue Burn-Out - Study of the residue burn-out was the most crucial part examined. The particular point of interest here was in the change of diameter as the particle burned out. Sinnatt and others (7,8) had shown many years ago that coal particles carbonizing in neutral or reducing atmospheres will form hollow shells, generally known as cenospheres, the optimum temperature of formation being between 600 and 700°C. If such a change occurred to a single particle before the residue combustion, then the theory of the swelling analysis, or any other similar analysis, would be quite inapplicable.

since these depend on the assumption of reaction at the exposed nominal or superficial surface, alone; also the integral of the burning rate depends on the further assumption of uniform particle density, right down to zero radius.

This was in essence the basis of Ornings criticism (12) of one of the previous papers (2). Explicitly he mentioned the need to integrate to some finite radius as the lower limit, and not to zero radius. However, the experimental results do not support the expectations based on the cenosphere formation, but they do support the results based on the original assumption of uniform density right down to zero radius. The curves of the type of Fig. 2 show quite clearly that the results obey eqn. (10). This means that the rate of burning (dm/dt) is proportional to the radius or diameter, down to quite small radii. Few particles could be followed right down to zero radius because of the difficulty of measuring less than one millimetre on the recording strips, but most could be followed to between 70 and 90% loss of mass, so the agreement found over the measured range justified extrapolation to burn-out.

The slope of the burn-out section of the curves is given by eqn. (7) as $1/K$. As a check on the magnitudes to be expected, these were calculated for many of the particles, and the values found ranged from 1000 to 2000 sq.cm./sec in good general agreement with the values previously reported (2). This is further substantiation of the conclusion that the particles are of uniform density right to the center. Because of the variation in the behavior of single particles, the scatter was about the same as that found for the total burning-time measurements made previously, but because of the much smaller number of measurements made, these additional values have less meaning and precision compared with the previously determined values.

4. DISCUSSION

4.1 General - With the data available, there is little more that can usefully be added to comments already made on the foregoing results. To our mind these establish that the particles usually swell isotropically, with a swelling factor that is remarkably constant over a wide range of coal rank (10 to 40% V. This alone is thought to be a point of considerable interest and importance. There was greater scatter in the swelling factor, f , between particles of the same coal than there was between the average values for different coals. This suggests that useful attention could well be directed towards pure maceral behavior as this might conceivably be responsible for the variations found. The particles evidently do not form cenospheres under these conditions though it is always possible that the peak swelling was a condition of true cenosphere formation, with destruction of the cenospheres as the temperature rose above the optimum for their formation. In this connection, it is not always realized that true cenosphere formation does not generally take place in oxidizing atmospheres above 1000°C. This again is thought to be a point worth further investigation. The only point not yet considered is the influence of shape factor.

4.2 Determination of Shape - To discuss the influence of shape, it is first necessary to determine what shapes the particles have. With the information on mass and diameter given in Table 2, considerable information can be obtained as to the most probable shapes of the particles. The mass/diameter data is correlated by eqn. (1). If we divide through by the coal densities, (Table 1), the data are converted to a volume/diameter correlation. Let us now consider a number of regular shapes as follows: (1) cube of side

(2) sphere of diameter d_0 ; (3) cylinder of diameter d_0 and length d_0^{1+y} ; (4) rectangular block of length d_0^{1+x} : (i) with square cross section of side d_0 ; (ii) with rectangular cross section of sides d_0 and d_0^{1+y} ; (5) spheroids, in both forms: (i) oblate and (ii) prolate, with minor axes of length d_0 and major of length d_0^{1+x} . These all have volumes that can be related to the dimensions with a multiplying factor, F, as in the Table following:

Table 3

Particle Shape Factor, F

3. (A)		Regular Shapes				
		Volume	Factor (F)			
1.	Cube	d^3	1			
2.	Sphere	$(\pi/6) d^3$	0.524			
3.	Cylinder	$(\pi/4) d^{3+x}$	0.7855			
4.	Rectangular block					
	(i) regular	d^{3+x}	1			
	(ii) irregular	d^{3+x+y}	1			
5.	Spheroid					
	(i) oblate	$(\pi/6) d^{3+2x}$	0.524			
	(ii) prolate	$(\pi/6) d^{3+x}$	0.524			
3. (B)		Coal Data	F	K(calc)	K(expt)	K(calc)/K(expt)
		(x + y)				
1.	Stanllyd	0.06	0.63	2680	2125	1.26
2.	Five ft.	0.20	0.708	1725	1290	1.34
3.	Two ft. Nine	0.15	0.845	1365	1470	0.93
4.	Red Vein	0.01	0.592	1500	1475	1.02
5.	Garw	0.04	0.713	1335	1610	0.95
6.	Silkstone	0.00	0.54	1080	1119	0.97
7.	Winter	0.06	0.674	1095	1125	0.97
8.	Cowpen	0.17	0.787	1055	1060	1.00
9.	High Hazel	0.04	0.735	1075	1450	0.74
10.	Lorraine	0.01	0.675	1165	992	1.07

From this it can be seen that the cube and rectangular blocks have F factors of unity; the sphere and spheroids, values of 0.524; and the cylinder is intermediate, at 0.7855. For the data quoted, the particles chosen were those that, by eye, looked closest to cubes, so we expected to find F factors close to unity. In fact, as Table 3 shows, the values indicated that the shapes approximated more closely to something between the spheroid and the cylinder than to a cube or rectangular block. Table 3 also gives the experimental and calculated values of K obtained previously (2); there seems to be no correlation between the (x+y) exponent difference, or the F factors. We therefore conclude that treating the particles as spheres was an adequate approximation to reality, the more so as the particles definitely derived a more rounded shape as they swelled, in spite of the general retention of their original shape. The final difference between the calculated and experimental values of K is most probably due to random scatter. Any closer practical identification with shape will require more precise experiments than those reported here.

4.3 Influence of Shape - Although determination of shape did not provide any further practical interpretation of the available data, the factor of shape can, nevertheless, be usefully considered and discussed in general. Shape may be partly a function of the inherent physical properties of a given coal that control the shape on breakage, but Perry (13) has shown that it is also dependent on the type of grinder used. Perry reported that a disc mill produced lamellar shapes whilst those from a hammer mill were polyhedral, tending to cubical. With decreasing particle size, the lamellar shapes tended to vanish, and even the disc mill produced substantially polyhedral shapes at very small sizes. In our experiments, the particles were crushed by hand, in a pestle and mortar and, as described above, their shapes seemed to approximate most closely to spheroids and cylinders.

In influencing combustion behavior, we might expect that, broadly speaking, the smaller the radius of curvature of any part of the particle surface, the faster that area would be likely to react, since the boundary layer above that part should be a little thinner. It is difficult to say for certain, however, from a study of the photographs, that this does or does not occur; irregularities in the shapes of the particles are maintained for quite an appreciable length of time - as long as 10 or 20 seconds - but most of the particles appeared to have been reduced to good approximations to spheres by the time they were half burned. The photographs in some instances were misleading as the ash would occasionally remain as a fairly coherent, though fragile, tracery, in the center of which the glowing, shrinking sphere could be clearly seen by eye, though the photographs showed only the barely changing outline of the ash. This was generally the case with the high-ash Two Ft. Nine coal, but occasionally happened with the others.

What we would suggest, from both the visual and photographic studies of the particles, is that reaction is in fact fastest at exposed projections, and sharply curving surfaces. This means that shapes like cubes, prolate spheroids, and polyhedral shapes in general will be reduced approximately to spheres by the time they are half burned. Short cylinders and short rectangular blocks of near uniform cross-section would therefore burn down first to something approaching prolate spheroids, and thence again would reduce to spheres. This means that excess material might burn off fairly rapidly, and the overall behavior would then approximate to spheres of diameter equal to the cube side, the shorter side of the rectangular block, or the minor diameter of the prolate spheroids. Since these are the dimensions most likely to determine whether or not a given particle would remain on, or pass through, a given sieve mesh, it may well substantiate and justify the successful use of the sieve mesh dimension in specifying the particle diameter to be used in the combustion calculations.

Other shapes such as needles, long cylinders, long regular blocks, or prolate spheroids with a big ratio of major to minor axis would be expected to burn at rates rather closer to those expected of regular cylinders. The square law relation of eqn. (7) should still obtain, but the burning rates and overall burning times should be rather longer. This expectation was never tested quantitatively but it could quite possibly account for some of the scatter in burning times found at any particular given diameter.

Finally, there are shapes like oblate spheroids, flat rectangular plates and lamellae. The behavior of these has yet to be investigated either theoretically or experimentally, but our expectation is that they would very likely burn in from the edges rather fast, giving burning times many times in excess of expectation on the basis of either the total mass involved, or on

sieve diameter. It is also likely to be sharply dependent on the orientation of the plane or flatter surface to the horizontal or vertical as this could strongly influence the natural convection currents and therefore the boundary layer thickness. This, however, is an area of investigation still open to study.

5. CONCLUSIONS

The conclusions that may be drawn from this study are in answer to the questions set out in the Introduction.

(1) Particles swell or not according to coal rank. Particles from anthracites (under 5% V.M.) swell negligibly or not at all. Particles from bituminous coals, on the other hand, (greater than 10% V.M.) swell in air by a net factor of about 1.5, this factor being substantially independent of coal rank.

(2) The swelling process is in two stages: first an expansion to 2 or 3 times the original diameter, followed by a contraction down to the final diameter of 1.5 times the original diameter. In CO_2 , the swelling finishes at the end of the first stage; there is no contraction which presumably, therefore, is conditioned by the presence of oxygen.

(3) In swelling, the process was reasonably isotropic, and apparently uniform throughout, with no cenosphere formation.

(4) In burn-out, the particles evidently burned uniformly at the exposed surface only. There was no evidence of internal burning (as is only to be expected with boundary-layer diffusion control of the reaction). The diameters therefore diminished with time quite regularly according to the equation:

$$d^2 = d_0^2 - t/K$$

with values of the burning constant K in agreement with those obtained previously from studies of the "integrated" or total burning times.

(5) Finally, shape appeared to have no detectable effect on the burning rates, other than maybe to increase the scatter in the burning times. Detection of any such effect will almost certainly require more accurate studies, using more precisely specified materials, both with regard to composition as well as shape.

6. REFERENCES

1. Essenhigh, R.H. and Thring, M.W. Conference on "Science in the Use of Coal" (Sheffield, 1958) Paper 29, p. D21 Institute of Fuel (London) 1958
2. Essenhigh, R.H. J. Engrg. for Power 85 (1963) 183
3. Beeston, G. and Essenhigh, R.H. J. Phys. Chem. 67 (1963) 1349
4. Nusselt, W. V.D.I. 68 (1924) 12⁴
5. Essenhigh, R.H. J. Inst. Fuel 34 (1961) 239
6. Essenhigh, R.H. Ph.D. Thesis (University of Sheffield: U.K.) 1959
7. Sinatt, F.S. and Slater, L. Fuel 1 (1922) 2
8. Newall, H.E. and Sinatt, F.S. Fuel 3 (1924) 424
9. Stephan, A. Ann. der Physik 17 (1882) 550; 41 (1890) 725
10. Eckert, E.R.G. and Soehngen, E. Trans. A.S.M.E. 74 (1952) 343
11. Grober, H. and Erk, S. "Fundamentals of Heat Transfer" (3rd Ed.) (Trans.) McGraw Hill, 1961
12. Orning, A.A. J. Engrg. for Power 85 (1963) 189
13. Perry, M.G. Univ. Sheffield Fuel Soc. J. 8 (1957) 28

7. ACKNOWLEDGMENT

The work described in this paper completes publication of research on single coal particles carried out as part of a general program of research on Pulverized Coal Combustion sponsored by the Electricity Supply Research Council of Great Britain. The work was carried out in the Department of Fuel Technology and Chemical Engineering, University of Sheffield, England, during the tenure by one author (R.H.E.) of the Research Fellowship granted under the terms of the sponsorship. The authors are indebted to the ESRC both for the financial support of the research appointment, and for permission to publish this paper.

Table 2

Values of Swelling Factor, f (d_s/d_o)

	<u>c%</u>	<u>V.M. %</u>	<u>Values of f</u>	<u>Mean (f)</u>
1. Stanllyd	93.0	9.9	1.1, 1.1	1
2. Five ft.	91.8	14.9	1.5, 1.25, 1.9	1.55
3. Two ft. Nine	91.2	28.8	1.1, 1.25, 2.2	1.48
4. Red Vein	89.7	23.3	1.75, 1.6, 1.7	1.72
			1.7, 1.9, 1.7	
5. Garw	88.9	30.6	1.8, 1.6, 1.4	1.64
			1.9, 1.5	
6. Silkstone	86.9	41.5	1.8, 1.4	1.6
7. Winter	84.0	39.3	1.3, 1.1, 1.6	1.58
			1.9, 2.0	
8. Cowpen	82.7	40.2	1.6, 1.5, 1.9	1.67
9. High Hazel	81.9	40.7	1.4, 1.5, 1.4	1.56
			1.8, 1.6, 1.7	
10. Lorraine	79.3	40.2	1.3, 1.5, 1.5	1.54
			1.8, 1.6	

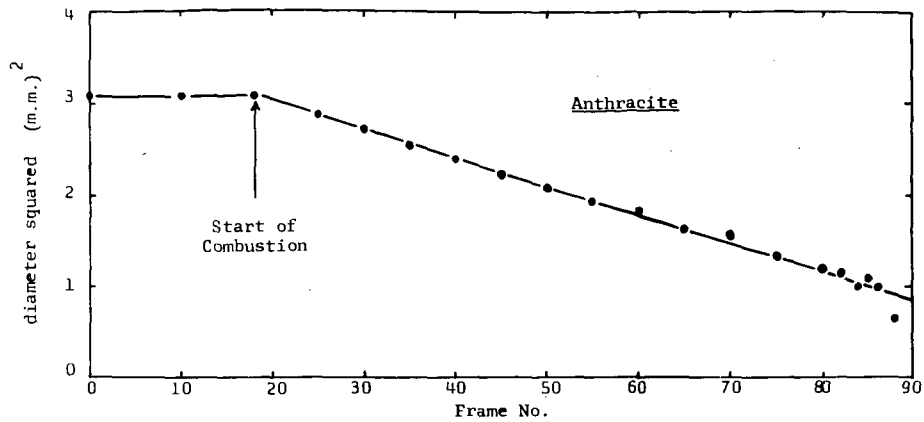


Figure 1 - Variation of diameter squared with time of burning anthracite particle (Stanlyd)

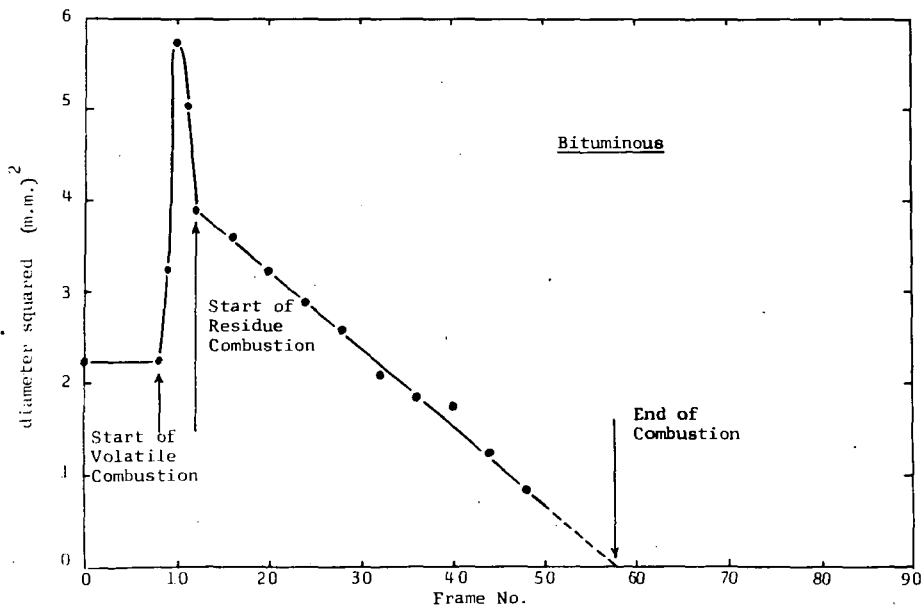


Figure 2 - Variation of diameter-squared with time of burning bituminous coal particle (Cowpen)

Predicted Burning Rates of Single Carbon Particles

Robert H. Essenhigh, Robert Froberg
and Jack B. Howard

Department of Fuel Technology
The Pennsylvania State University
University Park, Pennsylvania

1. INTRODUCTION

In spite of the immense amount of research on combustion of carbon in the last 30 years, the classic experiments of Tu, Davis, and Hottel (1) on 1" spheres are still of the best, and perhaps still the most widely quoted, of all experimental work on the subject, carried out at atmospheric pressure, and in this range of particle size and temperatures. The theory, of course, has advanced in several particulars since then (see Reviews (2-5)) and it has long been known that the original Tu *et al.* theoretical analysis was inadequate. In the original analysis, only desorption and boundary layer diffusion were considered as possible rate-controlling steps in the reaction: chemisorption and internal reaction were neglected. This neglect was simply that, at that time of writing, these two latter concepts had not been formulated, or not generally accepted; also, as a bias against considering adsorption, this was always assumed to be so fast as to be effectively instantaneous. According to Brunauer (6), the concept of activated adsorption was first formulated in the early 1930's - about the time of writing of the Tu *et al.* paper, or soon after - but, even a decade later, it still had not been generally accepted, with the consequence that many true chemisorption processes even then were being incorrectly interpreted in terms of solution, diffusion, migration (mobile adsorption), or reaction at the solid surface itself (6). Analysis of the internal reaction processes came even later, and has only been developed in the last decade or so.

Thirty years of research, therefore, has largely inverted the relation between theoretical to experimental work: that is to say, theory now leads experiment in consolidated development. Even so, the theoretical position is still confused: confidence in many of the theoretical concepts is still low as there are now almost too many theoretical possibilities available to explain any given set of new experimental data. Further definitive experiments are required to clarify quite a number of theoretical ambiguities, inconsistencies, and contradictions. One particular such point of major fundamental and practical concern at the present moment is the relative importance of the three principal "resistances" (1,7) in the carbon oxidation reaction. The three resistances are those of: boundary layer diffusion (S_0); adsorption (S_1); and desorption (S_2). For many years, only diffusion was ever considered as the rate control at temperatures in excess of 1000°K. Hottel and Stewart (8) had in fact shown conclusively, 25 years ago, that this was definitely not the case for small particles of pulverised-coal size, in flames, but little or no notice seems to have been taken of this paper till recently. Latest work, (9,10) however, has now confirmed the essential correctness of Hottel and Stewart's conclusion, but this now brings in question the basis of the previous belief, and also over what range of particle sizes and temperatures the new conclusion is valid.

In support of the original contention of diffusional control at high temperatures, the paper most frequently quoted would seem to have been that of Tu *et al.* Since, however, the original analysis was incomplete or inadequate, for the reasons given above, our thought was that the Tu *et al.* data might not be inconsistent with the new concepts, but simply had never been tested against them. It is true that their data apparently gave full support to the concept of diffusion control, but it has been shown elsewhere (2) (following Brunauer's (6) suggestion), that many combustion data can reasonably be reinterpreted in terms of an activated adsorption control, instead of the generally assumed diffusion control - if it can be accepted that the activation energy, though low, is finite, in the region of 2000 to 4000 cal., and therefore able to generate a small, but not negligible, resistance. Given this assumption, the Tu *et al.* data can then, apparently, be shown to give equally full support to the alternative hypothesis of adsorption control. This evident contradiction (i.e., equal support to both hypotheses), means of course, that the interpretation of the data, as analysed to date, is ambiguous; but it seemed to us, nevertheless, that the ambiguity was in the analysis, not in the data. Therefore, if the data were of the high quality that is generally claimed for them, it might be possible to remove the ambiguities by using the data to test the full equations now available in the literature (3-5), instead of the partial equations used hitherto (1) (see also (11,12)) which were generally based on unverified assumptions of very rapid, and therefore neglectable, adsorption.

The purpose of this paper, therefore, is to present this re-analysis. It shows that the data are indeed of excellent quality (thus eliminating the need for repeat of the experiments). It also shows that adsorption presents a small, but significant resistance, which increases in importance as the particle size drops, becoming dominant at something under 100 microns. There are, therefore, no essential inconsistencies with other and more recent data, so the tested equations can be used to some extent to predict combustion behaviour of very small particles.

2. THEORY

The literature and general theory of carbon combustion has been reviewed so often, and so extensively (2-5), in the last few years, that we do not intend, in this section, to do more than set out the essential equations in the best form for our immediate purpose of testing them by re-analysis of the Tu *et al.* (1) experimental data. The most exhaustive of the reviews is that by Walker *et al.* (4) who paid particular attention to mechanism details, internal reaction, CO_2 and other reactions, and influence of radiation. For our purposes here, however, the nomenclature of the other reviews is more convenient, and has therefore been followed.

2.1 General Model - The classic picture of heterogeneous reaction between a flowing fluid and the solid it surrounds (e.g., (13,14)) is that of a three stage process. (1) The reacting fluid diffuses through a boundary layer against the counter diffusion of inerts and/or reaction products - e.g., N_2 , CO_2 , CO . (2) At the solid surface the reacting fluid is chemisorbed, requiring activation energy of adsorption, E_1 . (3) After a finite residence time, which can be microseconds, the final reaction step is completed with the desorption of the adsorbed material which carries with it the underlying atom of the solid, so forming the reaction products: this requires activation energy, E_2 . The total process is then completed with counter-diffusional escape of these products into the main fluid stream. This general process can then be treated mathematically by setting up the simultaneous equations both for boundary layer and pore diffusion and for the appropriate adsorption isotherms. These are the subjects of the next two sections.

2.2 Diffusion - Potentially, this can operate in two ways: by boundary layer (external) diffusion; and by pore (internal) diffusion.

(i) Boundary layer diffusion: The existence of this process is well established, and the process well understood; and, as a result of excellent agreement between prediction and experiment (15-17), confidence in the absolute accuracy of the diffusion calculations for combustion rates is now high.

To treat diffusion mathematically, we define a velocity constant for mass transfer (transfer coefficient), k_o , by the equation:

$$R_s = k_o(p_o - p_s) \quad (1)$$

where p is the oxygen partial pressure, with subscripts o and s for values, respectively: in the main stream, and adjacent to, the solid surface. The velocity constant, k_o , is a function of particle size and general ambient conditions, including temperature and velocity in particular. Standard analysis of this system, following Nusselt (14), leads to an equation for k_o that may be written as the temperature function:

$$k_o = A_o (T/T_o)^{n-1} \quad (2)$$

where A_o is a velocity dependent coefficient, given below; and n is an index generally lying between 1.5 and 2, depending on the nature of the diffusing gases involved. For oxygen in nitrogen, which is the dominant system in air-combustion, experiment gives the best value for n as 1.75 (18,19). The coefficient A_o is given by:

$$A_o = (\rho_o M_c / M_o) (D_o / d) Nu = K.Nu \quad (3)$$

where ρ_o is the s.t.p. density of oxygen; M_c and M_o are the molecular weights of carbon and oxygen respectively; D_o is the s.t.p. diffusion coefficient of oxygen through nitrogen; d is the particle diameter; and Nu is the Nusselt number for mass transfer. In general, Nu is a function of the Reynolds and Prandtl numbers that can be written

$$Nu = 2 + c.Re^m.Pr^{1/2} \quad (4a)$$

where c is a numerical constant, ranging in value (according to both the heat and the mass transfer literature (20,21)) from 0.18 to 0.7, obtained by correlation of data. Grober and Erk (20), in their review of the mass transfer data, give only the one value of 0.6 (22). This is close to Khitrin's value of 0.7 (23), quoted by Golovina and Khaustovich (24). The Pr index, n , is given by nearly all as $1/3$, but in any case the Prandtl number in this instance is so close to unity that its cube root can be taken as 1 with less than 1% error. The Re index, m , is also given a range of values, from 0.5 to 0.8 (see (20,21)) in the heat transfer literature, but again, the purely mass transfer literature seems to agree on $1/2$. This is given by Ranz and Marshall (22) and by Khitrin, (23) and it is also the value used to correlate combustion data by Graham et al. (25) and by Day (26). Walker et al. (4) do quote lower coefficients than this for various combustion systems, but the systems are not isolated spheres. Taking the value of 0.6 for c , $1/2$ for m , unity for Pr , and expanding the Reynolds number into a coefficient and a velocity, we can rewrite eqn (4a) as:

$$Nu = 2 + c'.v_o^{1/2} \quad (4b)$$

where c' takes the value: 2.64 (at $c = 0.6$).

(ii) Pore diffusion: This potentially can play a part only in the event of pore or internal reaction. If it does so, however, it has been shown

elsewhere (27,5) that its effect is to generate modified velocity constants for the adsorption and desorption processes. This means that the equations to be developed in the next section (2.3) are potentially capable of accounting for pore reaction as they stand, with the sole modification of using apparent velocity constants in place of the true ones, with auxiliary equations to relate the true and effective constants. These modified and auxiliary equations are given in the literature (4,5,27), but we are not giving them here since, to anticipate our conclusion, we found no apparent or detectable influence of pore diffusion. This was not entirely unexpected since the burn-off on the whole was fairly low, and little development of internal surface would have had time to take place. An indicator to this result was also provided by the original conclusion of Tu *et al.* (1) that the low temperature reaction was zero order, with respect to the oxygen partial pressure, whereas this would have been a half order reaction had internal diffusion played a part.

We therefore saw no point in quoting the pore diffusion equations. We mention it here only to show that the point was considered and capable of being incorporated.

2.3 Adsorption Isotherm - (i) Basis of choice: To set up the equation for the reaction process itself requires first the selection of an appropriate isotherm. Our choice here has been made partly on the basis of the behaviour of the most likely isotherms and manipulation of the resulting equations, and partly on the basis of Occam's Razor (the Principle of Minimum Hypotheses).

The two isotherms considered were the Langmuir and the Temkin isotherms. Ideally, selection of an isotherm should be carried out by experiments to test and determine the most probable one, but this has not yet been done for this system. In general, however, the literature shows that most experimental data have been correlated on the basis of a Langmuir isotherm (28,29,30).

Information based on the variation of activation energies is also inconclusive. If a Temkin isotherm is involved, these energies must change with percentage coverage of the solid surface by the adsorbed layer. Data on these energies, however, are only plentiful for the desorption process; for the adsorption process they are very scarce. For desorption, the literature (3,4,21,30) gives values ranging from 20,000 to 80,000 cal.; but these seem principally to vary with the experimental system, and with the type of carbon used: the changes are never explicitly attributed to change of percentage coverage. For adsorption, it has already been mentioned in the Introduction that the value is expected to be low. This is the summary conclusion by Trapnell (31) in view of the speed and ease of chemisorption at normal and low ($\approx 70^\circ\text{C}$) temperatures. Trapnell also quotes values from Barrer (32) which start at 4000 cal. at low coverage, in agreement with Blyholder and Eyring's figure (30), and also in agreement with the re-estimates (2) of data in the literature. Barrer also shows that the value rises with coverage, the highest figure he found being 23,000 cal. At this degree of coverage, however, the activation energies are approaching those of desorption, and it will be shown below (Analysis sec. 3.3) that the effects of rising E_1 and falling E_2 with increasing coverage do in fact offset each other: the actual degree to which this occurs can only be determined by experiment, and this has never been done. This occurs in the middle range of the isotherm. At the extreme limits, at high and at low coverage, the two isotherms in any event tend toward each other, so the offsetting effect of changing E_1 and E_2 in the middle region of coverage will tend to restore a Temkin isotherm at least to a pseudo-Langmuir isotherm. Since the use of a Temkin isotherm renders the equations somewhat intractable, and in any event has never been conclusively established, we therefore decided to use the Langmuir isotherm (on the basis of Occam's Razor) since this involved fewer and simpler assumptions, though this use was still with the reservation that, if such an isotherm could be used successfully, it might still be only a pseudo-isotherm.

(ii) Langmuir isotherm: This isotherm depends on only two velocity constants: one for the adsorption process, k_1 ; and one for the desorption process, k_2 . Both are assumed to be invariant with respect both to oxygen concentration, and to percentage coverage of the solid surface by the adsorbed film. If the specific reaction rate is R_s (gm of carbon/sq. cm. sec.), the Langmuir isotherm then gives us (5)

$$1/R_s = (1/k_1 p_s) + (1/k_2) \quad (5)$$

where p is the oxygen concentration adjacent to the solid carbon surface. The velocity constants can be written in general as

$$k_1 = A_1 \cdot \exp(-E_1/RT) \quad (6a)$$

$$k_2 = A_2 \cdot \exp(-E_2/RT) \quad (6b)$$

where the E's are the activation energies as already defined; and A and A_2 are the pre-exponential constants or frequency factors. Like E and E_2 , A_2 can only be determined experimentally for the particular system under consideration; but A_1 can, in principle, be calculated from Kinetic Theory, which gives

$$A_1 = B_1 \sqrt{T/T_0} \quad (7a)$$

and

$$B_1 = M_c P \eta / \sqrt{2\pi MRT_0} \quad (7b)$$

where: P is the absolute total pressure (dynes/sq.cm.); M is the mean molecular weight of the ambient gas; R is the gas constant; and η is a steric, orientation, or entropy factor for the oxygen as it is adsorbed on the solid surface.

For reasons to be explained below (Analysis, sec. 3), it is convenient to incorporate the root-temperature term in an apparent or effective activation energy E_1' , whence we may write

$$k_1 = B_1 \cdot \exp(-E_1/RT) \sqrt{T/T_0} \quad (8a)$$

$$= B_1' \cdot \exp(-E_1'/RT) \quad (8b)$$

The objective of this is to reduce the temperature-dependent factor A_1 to a temperature-independent factor B_1 , and hence to B_1' , ($=B_1/b$, where $b = 3.9$), where the factors B are also independent of velocity.

2.4 Combined Kinetics - To take all the possible factors into account simultaneously, it is clear that we must set up the equation for the combined kinetics by elimination of the unknown partial pressure p_s by solving for this between eqns (1) and (5) and equating. This gives the quadratic:

$$R_s^2 - (k_o p_o + k_2 + k_o k_2 / k_1) R_s + (k_o p_o) k_2 = 0 \quad (9)$$

This is already cumbersome: it is clear that if the expressions for the velocity constants (k) are also inserted, the equation becomes totally unweildy. There are then so many coefficients that the expression could be fitted to anything at all, relevant or not. For this reason, we have tried, in our Analysis (sec. 3, below) to consider special cases that can be legitimately extracted, and to test the expression, unit by unit. For this reason we derive two of the special cases of importance, in this section, for use in the analysis below.

(i) k_2 large: For this special case, we divide the equation through by k_2 and, find that, when k_2 is large, the two terms (R^2/k_2) and $(k_0 p_0/k_2)$ both become vanishingly small.² This leaves only the familiar "resistance" equation:

$$1/R_2 = (1/k_0 p_0) + (1/k_1 p_0) \quad (10a)$$

$$= S_0 + S_1 \quad (10b)$$

where 'S' is the appropriate resistance.

The significant point of this equation is that the reaction rate is first order (proportional to p_0) whatever the relative values of k_0 and k_1 . This is important as this resistance equation applies only when k_2 is large, i.e., at high temperatures. This was the central error of the original Tu *et al.* (1) analysis since the authors started by assuming that the reaction was first order, over the whole temperature range; they then showed experimentally that the first order reaction was true only above 1100 or 1200°K, with a zero order reaction below this temperature (as later confirmed by others (33,34)); but yet they continued to analyse the full data in terms of their only-partially applicable equations. For these reasons, the activation energy was mis-identified, and the part played by adsorption in the high temperature region was not appreciated.

(ii) k_1 large: The original Tu *et al.* analysis therefore was based on the concept of full chemical control at low temperatures, and full diffusional control at high temperatures. This only follows if adsorption is so fast that k_1 is very large, and we then have another special case of great interest. For k_1 large, the term $(k_0 k_2/k_1)$ in eqn. (9) vanishes, and the resulting expression then factorises:

$$(R_s - k_2) (R_s - k_0 p_0) = 0 \quad (11)$$

What this implies is that: k_2 is controlling at low temperatures; $k_0 p_0$ is controlling at high temperatures; but, between the two, there is no transition region. Change from one region to the other is quite discontinuous. There is, of course, continuity in the reaction rate values; but there is complete discontinuity in the slopes of the two curves at the junction of the two regions. Experimentally, this has been shown explicitly for the carbon-hydrogen reaction (35), and implicitly for the carbon-oxygen reaction under such conditions that the reaction is possibly that by CO_2 , with the carbon, in a double film at the onset of diffusion (24).

(iii) k_0 large: For this condition, inserted for completeness, eqn. (9) reduces to the Langmuir isotherm of eqn. (5), though with p_0 substituted for p_s . We can then write in the resistance notation:

$$1/R_s = S_1 + S_2 \quad (5a)$$

3. ANALYSIS

In this analysis, now to be developed below, our essential objective was to extract experimental values, from the experimental data, in such a form that it would then be possible to check one dependent variable against one independent one, according to the developed equations, all other variables remaining constant in the particular process being checked. This seemed to us to be the only valid way of testing such involved and elaborate equations as those given above, though it is conceded that the methods of extracting the operating values may perhaps be regarded as somewhat questionable in one or two particulars. However, it is difficult to see what other approach could have been adopted.

The analysis starts with a re-presentation of the data.

3.1 Data Plot - Fig. 1 shows the plot of the original Tu, Davis, and Hottel data (1), but as an Arrhenius plot instead of the double-log plot that they used; also using carbon surface temperatures as being more relevant than furnace temperature.

On this plot, the almost-vertical dotted line on the right is the k_2 term, fitted to the data, with an activation energy (E_2) taken as 40,000 cal. This value was selected as it gave a better fit to the data than the 35,000 cal. quoted by the original authors; it was also closer to other values found for electrode carbon (see (3,4,21)).

The heavy lines are "back-plots" calculated according to eqn. (9) using values of the constant coefficients as determined by this analysis.

3.2 Empirical Correlation - If the calculated back-plots of Fig. 1 are carefully compared with the original curves drawn in the original Tu et al. paper, which latter were drawn empirically, the two sets will be seen to follow each other very closely. This agreement was quite fortuitous, but it so happened that the original curves were of considerable assistance in providing us with a starting point in the analysis. In the first place, the marked curvature of the lines in the original plot showed that the limiting approximation of eqn. (11) clearly did not apply. Therefore, if any approximation applied, it would be closer to a Langmuir isotherm; moreover, this expectation was strongly supported by the shape of the curves. These all have a common starting point at low temperatures, with "fine-structure" splitting at high temperatures due to both oxygen concentration, and velocity. What, therefore, we had to investigate was the possibility that the curves were modified Langmuir isotherms, obeying a two-term equation of the form:

$$1/R_s = 1/k_2' + 1/k_2 \quad (12)$$

where k_2 is identified from the start with the same k_2 desorption step as in the previous equations; but k_2' is inserted empirically. This is initially defined, also empirically, by:

$$k_2' = A_2' \cdot \exp(-E_1'/RT) \quad (13)$$

where E_1' is an effective activation energy that is identified below as the E_1' of eqn. (8b), and so is written as such here; and A_2' is an empirical velocity and concentration-dependent coefficient or frequency factor.

Our procedure now is: first, to show that this formulation has empirical value in correlating the data, to reduce these to specifications in terms of empirical equations, incorporating empirical definitive coefficients; and secondly, to show that the empirical definitive coefficients also have fundamental justification and meaning.

3.3 Data Fit - To correlate the data by means of eqn. (12), the method used is illustrated in Fig. 2. This illustrates the method for just three of the data sets: namely, for the three oxygen concentrations, 21.0%, 9.69%, and 2.98%, at the single approach velocity of 3.51 cm./sec. All the other data were treated similarly (plots not reproduced). On these data plots, two "fitting" lines were drawn, one equivalent to a slope of 2,000 cal., for E_1' , and the other equivalent to a slope of 40,000 cal., for E_2 . Parallel to these two lines, further lines were drawn which were expected to be the limiting asymptotes of the "Langmuir" curves when these were calculated and drawn in on top of the data. For the data of Fig. 2, this gave us, as can be seen, four such fitted lines, three for the slopes of E_1' , and one for the slope of E_2 .

As mentioned above, the k_1 line was retained as common to all the data (common A_2 and E_2), for all velocities and oxygen concentrations, but there were nine different values obtained of the empirical frequency factor A_2 , though at the common value of 2,000 cal. for E_1 . This splits the data into temperature-dependent, and temperature-independent groups or coefficients (i.e., $\exp(-E/RT)$ and A).

Once the k_2 and k_1 lines had been drawn in, the "Langmuir" curves were easily calculated and drawn in, as shown in Fig. 2. Because this was an empirical procedure, several tries were required for some of the lines to get a placing of the k_2 line that would give the best looking fit (by eye) of the Langmuir curves to the experimental data. In this fitting process, a value of 4,000 cal. was also tried for E_1 , but the fit given was very poor in comparison to the finally-adopted value of 2,000 cal. Two other values for E_2 were likewise tried: 35,000 cal. as proposed by Tu et al., and 58,000 cal. as proposed by Wicke (36). It was found by this that, within the limits of the experimental scatter, the fitted curves were somewhat insensitive to increase of E_2 above 40,000 cal. (the value finally selected), but the finally selected value seemed to be the best compromise between the slightly conflicting demands of all the data sets. It can also be seen, however, on both Fig. 1 and 2, that the final Langmuir curve has a long traverse at the lower temperatures, particularly for the 50.0 cm./sec. line at 21% oxygen, that has very little curvature and, within little error, a straight line could be drawn in, as an approximation, that would have an effective slope of close to 35,000 cal. This would appear to be the origin of Tu et al.'s figure of 35,000, and therefore substantiated our conclusion that our value should exceed theirs.

One final point can also be illustrated on Fig. 2. If we accept that the value of E_1 will rise, and E_2 will drop, with increasing surface coverage, (i.e., decreasing temperature), the effect is shown in Fig. 2 by the dotted curved lines. It is quite clear from this that, in plotting out the composite Langmuir curve, the two tendencies could very well offset each other, as described above, thus restoring what might be a Temkin isotherm to a pseudo-Langmuir isotherm. This helps to justify our procedure, at least from the empirical point of view.

3.4 Identification - The procedure outlined above demonstrates that the data can be described, to some degree of accuracy, by eqn. (12), with the k_2 and k_1 components described by eqns. (6b) and (13). Now, if the experiments had all been carried out at temperatures in excess of about 1100°K, and had been continued to higher temperatures still, the k_2 term would have been relatively unimportant, and the data could have been described empirically by the k_1 term alone. If, therefore, we now concentrate solely upon the k_1 term, what our fitting procedure has done is to correct the data for the k_2 component, and it now allows us to treat the data as if the k_2 term were very large - i.e., the low temperature resistance, S_2 , is very small. But, under these circumstances, the original eqn. (9) reduces to the familiar resistance approximation of eqn. (10), which can be written in the alternative form:

$$R_s \approx k_1 p_1 / (1 + k_1/k_0) \quad (\text{for } k_2 \text{ large}) \quad (14)$$

and this can now be compared with the empirically derived equation:

$$R_s = k_2' = A_2' \cdot \exp(-E_1'/RT) \quad (15)$$

this being the contraction of eqn. (12) when k_2 is very large. The A_2' coefficients are temperature independent, but still concentration and velocity dependent. If, therefore, the empirical coefficients A_2' have any fundamental justification, we must be able to set up an identity between eqns. (14) and (15). Testing this presumed identity is the subject of the rest of this section (3).

3.5. Concentration Properties of Empirical Coefficient A_2' - The identity between eqns. (14) and (15) may be simplified by writing:

$$A_2' = A_1' \cdot p_0 \quad (16a)$$

(and so $R_s = k_1' \cdot p_0$ (16b))

whence, if the identity holds, the new empirical coefficient A_1' should now be independent of temperature and oxygen concentration, and dependent only upon velocity. This can be substantiated, in the first instance, by testing the relation of eqn. (16) against the experimental data. This can only be done for the two lower velocities, at 3.51 and 7.52 cm./sec., but the results, shown in Fig. 3 support the identity. For completeness, eqn. (16) has been assumed to hold for the other three velocities, even though measurements were made only at one oxygen concentration, and straight lines for these three velocities have also been included. The slopes of these lines give the empirical coefficients A_1' , which should now be functions of velocity alone, with the temperature and concentration dependence eliminated.

3.5 Values and Properties of Empirical Coefficient A_1' - The variation of A_1' with velocity is shown graphically in Fig. 4; also shown, for reasons that will be developed, is its variation with $v_0^{1/2}$. This variation with the square root of the velocity follows from the identity between A_1' and k_1 , which now reduces to

$$R_s = A_1' \cdot p_0 \cdot \exp(-E_1'/RT) = B_1' \cdot p_0 \cdot \exp(-E_1'/RT) / (1 + k_1/k_0) \quad (17a)$$

or $A_1' = B_1' / (1 + k_1/k_0)$ (17b)

This formally incorporates the identification of E_1' in eqns. (8b) and (13) as being the same in both cases. It will be seen immediately from this that, if the adsorption rate is indeed very fast compared with the transport rate, k_0 , then the ratio k_1/k_0 would be large compared with unity, so we would get A_1' proportional to k_0 ; hence - from eqns. (2), (3), and (4) - to $v_0^{1/2}$. The significant curvature on the square-root plot of Fig. 4, substantiated by later plots, shows that k_1 is not very large compared with k_0 . However, before these additional plots can be examined, one further point concerning the temperature dependence of the identity must be investigated.

3.6 Temperature Dependence of Empirical Coefficient A_1' - By the method of derivation, the coefficients A_2' and A_1' are necessarily defined as being temperature independent. It is apparent, however, from the proposed identity of eqn. (17b) that the right hand side of the identity still contains temperature-dependent terms. The coefficient B_1' is defined as being temperature independent; the dependency is incorporated solely in the two velocity constants, k_0 and k_1 . Since the two constants appear in their ratio, k_1/k_0 , what we must establish, for the identity not to fail, is that this ratio has negligible temperature dependence. From eqns. (2) and (8b) we can write:

$$k_0/k_1 = (A_0/B_1') \cdot f \quad (18a)$$

where $f = (T/T_0)^{0.75} / \exp.(-E_1'/RT)$ (18b)

the quantity, f , being the temperature function ratio. Taking E_1' as 2,000 cal. this temperature function ratio has been calculated out for the temperature range 900 to 1700°K, and the result of the calculation is shown graphically in Fig. 5. It is clear from this that the ratio is very constant indeed. For the range from 1000°K, the value of the ratio can be taken as 7.1 ± 0.1. This represents less than 1.5% variation which, compared with the scatter of the original experimental points, is quite acceptable. This confirms that the coefficient A_1' has now been reduced to a function of velocity alone.

3.7 Velocity Dependence of Empirical Coefficient A_1' - By using the temperature function ratio, f , of eqn. (18b), we may now re-write eqn. (17b) in the form:

$$1/A_1' = (1/B_1') + (1/fA_0) \quad (19a)$$

$$\text{or} \quad = (1/B_1') + 1/f \cdot K(2 + c'\sqrt{v_0}) \quad (19b)$$

The only variable terms now left in this are; the independent variable of velocity, v_0 ; and the dependent variable, A_1' , obtained by reduction from the experimental data. Eqn. (19) is not a function that can be tested directly as it stands but, as a first approximation, we may assume that 2 is small compared with $c'\sqrt{v_0}$. The appropriate plot to test this is given in Fig. 6, which like the square-root plot of Fig. 4, also shows detectable curvature. In point of fact, apparently good-fit straight lines could have been run through both plots but, when this was tried, there was then an inconsistency amounting to an order of magnitude in the values of the ordinate intercepts of the two plots. By successive approximation between the two plots to remove the inconsistency, an ordinate intercept in Fig. 6 of value 100 was finally adopted for the quantity $1/B_1'$. This value was then used to test the following final arrangement of eqn. (19b):

$$1/[(1/A_1') - (1/B_1')] = 2fK + (fKc')\sqrt{v_0} \quad (19c)$$

This final equation was tested by the plot of Fig. 7. This shows that the function is satisfactorily obeyed with an intercept of value 0.6×10^{-3} , this being the value of the quantity $(2fK)$.

This functional agreement thus substantiated the identity of the empirical coefficient A_1' with the theoretical quantity $B_1/(1 + k_1/k_0)$, as in eqn. (17b).

3.8 Coefficient Values - What we have now established is that the proposed equations have the correct functional form, which therefore provides qualitative substantiation of the picture developed. However, the graphical plots do more than this: they also provide experimental values, by way of slopes and intercepts, of the various coefficients involved, and these experimental values can now be compared with the values predicted from theory. In general, these will be seen to show agreement between prediction and experiment that varies from adequate to excellent.

3.8.1 Diffusion and Velocity Coefficients - (i) Zero velocity: At zero velocity, we get the limiting value of 2 for the Nusselt number. Physically, this represents the situation where the particle is surrounded by a totally quiescent diffusion film exerting its maximum influence. To compare theory and experiment, the experimental coefficient relating to zero velocity is the ordinate intercept on Fig. 7. From this plot, this intercept has the value: 0.6×10^{-3} . By eqn. (19c), this value is predicted by the quantity $(2fK)$; i.e., $2f(\rho_c M_c/M_0)(D_0/d)$. Taking the following values for these quantities: ρ_c as 1.43×10^{-3} g/c.c.; M_c and M_0 as 12 and 32 respectively; D_0 as 0.181 sq. cm./sec.; and d as 2.54 cm.; we have $K = 3.83 \times 10^{-5}$. Since f , from Fig. 5, has the value 7.1, we also have

<u>predicted value:</u>	$2fK = 14.2 \times 3.83 \times 10^{-5}$	
	$= 0.545 \times 10^{-3}$	compared with
<u>experimental value:</u>	$= 0.60 \times 10^{-3}$	

This agreement is clearly acceptable. It is, however, no more than we now expect from diffusion calculations in view of the excellent agreement already obtained elsewhere (15-17) using such calculations. Confidence in the accuracy of diffusion calculations is now very high.

(ii) Finite velocity: In the following system, the agreement on coefficients is as good, though the order of agreement depends on whose equation is chosen from the literature for comparison of the coefficients; there are also two points that can be queried about the method of the theoretical calculation. To compare theory and experiment, we have in this instance the comparison of the values for the slope of Fig. 7. The experimental value, from the plot, is 0.725×10^{-3} . The predicted value is given, again from eqn. (19c), by its second term, as: fKc' . The value of fK is given above as 0.2125×10^{-3} ; and for c' is given (from Ranz and Marshall's data (22)) under eqn. (4b) as 2.64. Hence we have:

$$\begin{aligned} \text{predicted value:} \quad fKc' &= 0.2125 \times 10^{-3} \times 2.64 \\ &= \underline{0.7175 \times 10^{-3}} \quad \text{compared with} \\ \text{experimental value:} \quad &= \underline{0.725 \times 10^{-3}} \end{aligned}$$

This agreement is also excellent. The only reservations on the predicted value are concerned with: the use of the s.t.p. gas viscosity in evaluation of the c' coefficient (in eqn. 4b). Since the gas viscosity increases roughly in proportion to the square root of the temperature then, taking a mean temperature of 1500°K, the correction factor to be applied is division by the fourth root of 1500/273. This gives us about 1.5. However, we should also correct for the increased velocity past the sphere at its perpendicular diameter to the gas flow due to the constriction of the tube. This gives us a multiplying correction factor, for both corrections combined, of about 0.75. If, however, we then use Khitrins coefficient of 0.7 (23), instead of Ranz and Marshall's of 0.6 (22), the correction factor is about 0.9. This would still put the agreement between the predicted and experimental values within an acceptable 10%, but quite clearly, the possibilities of selecting values that will fit becomes so wide that better agreement finally becomes meaningless.

3.8.2 High Temperature Rate Coefficients - (i) Energy of Activation, E_1 : The choice of apparent energy of activation, E_1 , has been fully discussed above. This is not a quantity that can easily be predicted from first principles. A few have been (e.g.: adsorption of H_2 on carbon (37)), but no simple general method yet exists.

The apparent value is related to the true value by eqn. (8). The effect of dividing the Arrhenius exponential by $\sqrt{T/T_0}$ is to reduce the true value by about 1400 cal. By calculating the quantity $\exp(-E_1/RT) \times \sqrt{T/T_0}$, and making an Arrhenius plot, a value of 3,400 cal. was obtained for the true activation energy E_1 . This is clearly in line with the values given by Blyholder and Eyring (30), and by Barrer (32) for low area of coverage; it is also in line with the estimates made elsewhere (2). Another interesting figure can be extracted from the low temperature and pressure studies of Laine, Vastola, and Walker (38). They quote activation energies of 44,000 cal. for carbon gasification with oxygen, and 36,000 cal. for the simultaneous oxygen depletion. As with Gulbransen and Andrew (39) (whose respective figures were: 40,000 and 35,000 cal.), these represent respectively the values for the desorption process alone, and for the total reaction. If the latter figure is the value of $(E_2 - E_1)$, then we have a subtraction, values for E_1 of 8,000 and 5,000 cal.

from Laine *et al.* and Gulbransen and Andrew respectively. Both figures are in line with Barrer's values (32) at low to medium coverage, and the higher is close to Bannerjee and Sarjants value (40) of 8,300 cal.

(ii) Frequency factor: This is the quantity A_1 , or B_1 as the temperature-independent form of the coefficient, given theoretically by eqn. (7). It is related to the experimental quantity, B_1^e , through eqns. (7) and (8). The experimental value of B_1^e is 0.01, obtained as described in sec. 3.7 by successive approximation. By eqn. (3) we get, for B_1 , a value of 0.039. This, however, is substantially lower than the predicted value of B_1 when the orientation coefficient is unity. Taking P as 1.013×10^6 dynes/sq. cm.; M as 30; and R as 8.37 ergs/degree mole; we get a calculated value of 5.89 for B_1 . Since this is substantially above the experimental value of B_1^e , we may reasonably infer, following Laine *et al.* (38), that the difference is due to the orientation or steric factor, η . This can be calculated from the identity:

$$\begin{aligned}\eta &= B_1(\text{exptl.})/B_1(\text{predtd.}) \\ &= 0.039/5.88 \\ &= 1/150\end{aligned}$$

This is within a factor of 2 or 3 of the values for η given by Laine *et al.* (38), which ranged from 1/56 to 1/83. If the adduced explanation for the discrepancy between the two B_1 values is correct, the values of η are at least in order of magnitude agreement.

3.8.3 Low Temperature Rate Coefficients - Little need be said about the low temperature coefficients. The identification and interpretation of these has never been in dispute. The values of A_2 and E_2 adopted, as described above, of respectively: 1.05×10^4 g/sq.cm.sec., and 40,000 cal., are in line with other values given in original papers and reviews, to which reference may be made for comparison.

4. DISCUSSION

4.1 General - What these results clearly establish, to our mind, are: first, the general validity of the approach; second, substantiation of the high reliance that may be placed on the diffusion calculations; and, third, the degree of confidence to which the quoted equations may be used for calculating mass transfer in a flowing system. Given these, the most important final conclusion that may be drawn is the relative importance of the high-temperature resistance, S_1 , in comparison with the diffusional resistance, S_0 . This final point is now amplified in the sections following.

4.2 Resistance Ratios - (i) S_1/S_0 : To show the relative importance of S_1 to S_0 , which former has hitherto been generally neglected as too small, Fig. 8 shows a plot of their ratio as a function of velocity. The single line given is valid over the temperature range 1100 to 1700 K, to within about 1%; it is also independent of oxygen concentration. This shows that, over the velocity range of the experiments, the resistance ratio rises from 0.18 to 0.57. As percentages of the total reaction resistance, these figures show that S_1 rises from 15% to 36%, which clearly is not negligible. This confirms the conclusion drawn from eqn. (11) that continuity in the slopes of the curves can only mean that S_1 is significant.

At zero velocity, the ratio does become very small, dropping to about 20:1. This however, is true only for these very large spheres. Since S_0 is proportional to the sphere diameter, d , by eqns. (2), (3), and (4), we then have that the resistance ratio is inversely proportional to the diameter, d . Thus,

even in a quiescent system, reduction of d from one inch to 2.5 mm would raise the resistance ratio up to 2 to 1: i.e., the two would be comparable in value. At 250 microns, the ratio goes to 20 to 1 in favour of the chemical resistance; and at 25 microns, or pulverised coal particle size, the diffusional resistance, S_0 , becomes totally unimportant, in agreement with previous predictions and calculations (41,42) (also see below).

If, on the other hand, the high temperature frequency factor, A_1 ever attained its full theoretical value, the S_1 resistance would not become important till the particle size dropped below 100 microns. Above this, it would not matter. This may well have been the case for the carbons formed in situ from burning coal particles since no evidence of a chemical resistance was ever found (15-17) for particles ranging in size as low as 300 microns. This suggests that A_1 may depend as much on the inherent reactivity of the material as it does on any accommodation or orientation factor.

(ii) S_1/S_2 : This alternative plot is shown in Fig. 9. In this instance the two resistances are independent of velocity, but are very strongly influenced by temperature and oxygen concentration. Even so, the two resistances are equal, over the range 5 to 21% oxygen, at a temperature of around $1200 \pm 100^\circ\text{K}$; and there is substantial change from S_2 control to S_1 control (if S_0 is absent) in the temperature range $1200^\circ\text{K} \pm 200^\circ$. For the 1" spheres, inspection of Fig. 2 indicates a transition temperature of about $1000^\circ\text{K} \pm 200^\circ$ (cf. data in Review (3)), thus implying a surface oxygen concentration (p_s) of 1% or less. Since the oxygen concentrations can be read as surface values (i.e., of p_s), rather than main stream values, the progressive reduction of the diffusion layer, due to a rising velocity, or falling particle size, is seen to increase the surface oxygen concentration, and to raise the transition temperature.

4.3 Small Particle Behavior and Other Data - As mentioned above, the diffusion resistance, S_0 , becomes negligible as the particle size drops below 100 microns. Small particle behavior, as in pulverised coal flames (9), or soot particles in cracked hydrocarbon flames (10), can therefore be evaluated from eqn. (10) and Fig. 9. According to these, we should find that, even in the most favorable conditions for the resistance S_2 , the S_1 resistance should predominate above 1400°K . Data (9,10), however, show that high activation energies, of about 40,000 cal., can be adduced over the range 1300 to 1700 K. This, of course, is quite feasible if the S_1 value for particles formed from coal in situ can indeed drop by a factor of 10^2 , as discussed above. At 5% oxygen concentration, the S_2 resistance would not drop below 10% of the total resistance till the temperature exceeded 1900°K .

Such behavior would satisfactorily account for the results obtained, except that both reactions are claimed to be first order. A possible reason for this further discrepancy may be that there is even a fourth resistance or mechanism coming into play at the higher temperatures. Smith and Gudmundsen (43) measured burning rates of small spheres, 2 or 3 mm in diameter, at temperatures ranging from 1450 to 1750°K . At the lower temperatures in this range, the reaction rates obtained substantially agree with prediction from the equations developed in this paper, using the same experimental coefficients. The initial slopes of the curves with respect to temperature are also similar; but above 1650°K , where Tu et al. had very few data, the slopes of the Smith and Gudmundsen curves increase very rapidly indeed, with the activation energy evidently high. Golovina and Khaustovich (24) have shown the same effect, also using spheres of very similar diameter to those used by Tu (of 1.5 cm.) and in a 60 cm./sec. air flow. In agreement with Tu, the reaction rates rose fast up to 1000 or 1100°K , then levelling off at about 30×10^{-5} g./sq.cm.sec.

(cf. Fig. 3). Then, in agreement with Smith and Gudmundsen, they rose **fast** again over the temperature range 1400 to 1750°K, rising to about 70×10^{-5} g./sq.cm.sec.; but then they levelled off again, with calculated rates in agreement with a double film diffusion system, this being maintained up to the experimental temperature limit of 3000°K.

This phenomenon shown by Smith and Gudmundsen (43) and by Golovina and Khaustovich (24) in the temperature range 1500 to 1700°K may, therefore account for the Lee *et al.* (10) anomalies, but clearly this is a region now requiring examination, both theoretically and experimentally in much greater detail.

5. CONCLUSIONS

From this analysis, of the Tu, Davis, and Hottel data (1), on the burning rates of 1" carbon spheres, presented in this paper, we conclude that:

1. The three-resistance concept of: boundary-layer diffusion (S_0), activated adsorption (S_1), and desorption (S_2), which are deemed to take place physically in series, is essentially correct.
2. At low temperatures (below 1000°K) the desorption resistance (S_2) predominates, and the reaction order is zero. At high temperatures, (above 1000°K), the diffusion and adsorption resistances (S_0 and S_1) are both, simultaneously, important, and the reaction is first order.° For the 1" sphere at low velocities, S_1 is the lower of the two resistances, being 1/6 of S_0 at 3.5 cm./sec. gas velocity; but rising to 1/2 of S_0 at 50 cm./sec.
3. At higher velocities, or smaller particle sizes, the diffusion resistance, S_0 , becomes progressively less important. In general, it should be possible to neglect it with little error, at particle sizes less than 100 microns (pulverised coal size), even in quiescent ambient gas conditions.
4. The reciprocal of the three resistances are related to the velocity constants of the three processes, given generally by:

$$1/S_0 = k_0 p_0 = A_0 \cdot p_0 \cdot (T/T_0)^{0.75}$$

$$1/S_1 = k_1 p_0 = A_1 \cdot p_0 \cdot \exp(-E_1/RT) = B_1' \cdot p_0 \cdot \exp(-E_1'/RT)$$

$$1/S_2 = k_2 = A_2 \cdot \exp(-E_2/RT)$$

the coefficients A_0 , A_1 , and B_1' being given by eqns. (3) and (7). A_0 is velocity dependent, and temperature independent; A_1 is temperature dependent, and velocity independent; and B_1' and A_2 are both temperature and velocity independent.

5. The relation between specific reaction rate (R_s) and the velocity constants is given by the quadratic of eqn. (9). However, the data may be approximated by the modified Langmuir isotherm.

$$1/R_s = (1/k_1' \cdot p_0) + (1/k_2)$$

where

$$k_1' = A_1' \cdot \exp(E_1'/RT)$$

A_1' and E_1' are empirical quantities determined by experiment. A_1' , by definition, is independent of both temperature and oxygen concentration, but is velocity dependent.

6. The empirical activation energy, E_1' , is identified with the effective activation energy, obtained from first principles, after combining the $T^{1/2}$ term of A_1' with the E_1 term in S_1 (E_1 being the true activation energy). The value of the effective energy, E_1' , is found by best fit to experiment to have a value of 2000 cal./mole. By calculation from this, the true value, E_1 , is 3400 cal./mole, in adequate agreement with other values for this quantity in the literature.
7. The empirical frequency factor, A_1' , is identified with the theoretical group obtained from first principles:

$$A_1' = B_1' / (1 + k_1/k_0) \quad (17b)$$

From this, the following relation with velocity is obtained:

$$1 / [(1/A_1') - (1/B_1')] = 2fk + fk_0 \sqrt{v_0} \quad (19c)$$

Comparison with experiment confirmed the functional form of this equation; and excellent agreement was found between the predicted and experimental coefficients involved in the diffusion and velocity components of the calculation.

8. Agreement between the predicted and experimental values of the A_1 and B_1 frequency factors are in error by a factor of 150. This is attributed to an orientation or steric factor, ϕ , for which other values in the literature are in the range of 50 to 80. For this identification, agreement is therefore adequate.
9. A final point developing from this analysis is an ambiguity or inconsistency in higher temperature data, obtained by others, that just overlap in their bottom ranges with the top temperature range of those obtained by Tu et al. In the overlap, the data agree; but at higher temperatures, beyond the overlap, the data show a much more rapid rise in reaction rate than the equations and mechanism should permit. This phenomenon requires further study.

6. LIST OF SYMBOLS

- A - frequency factor
 A_0 - " " for diffusion = $K \cdot Nu$
 A_1 - " " for adsorption = $M_c P \eta / \sqrt{2\pi M R T}$
 A_2 - " " for desorption
 A_1' - first empirical factor = $B_1' / (1 + k_1/k_0)$
 A_2' - second empirical factor = $A_1' p_0$
 b - conversion factor (numerical) in $B_1 = b \cdot B_1'$: value 3.9
 B_1 - adsorption frequency factor (temp. indep.) = $A_1 \cdot \sqrt{T/T_0}$
 B_1' - effective adsorption frequency factor = B_1/b
 c - numerical constant in Nusselt/Reynolds No. equation
 c' - revised value of c for velocity equation = $c \sqrt{\rho_0 \mu}$
 d - particle diameter (this paper = 2.5 cm.)
 D_0 - diffusion coefficient at s.t.p. (for O_2 in N_2 = 0.181)
 E_1 - adsorption activation energy (true) = 3400 cal/mole
 E_1' - empirical and effective adsorption activation energies = 2000 cal./mole
 E_2 - desorption activation energy (true) = 40,000 cal./mole
 f - temperature function ratio: $(T/T_0)^{0.75} / \exp(-E_1'/RT)$: value = 7.1
 k - velocity constant
 k_0 - velocity constant for diffusion = $A_0 (T/T_0)^{0.75}$

- k_1 - velocity constant for adsorption = $A_1 \cdot \exp(-E_1/RT)$
 k_2 - " " for desorption = $A_2 \cdot \exp(-E_2/RT)$
 k_1' - first empirical velocity constant
 k_2' - second empirical velocity constant = $k_1' p_o$
 K - diffusional constant group = $(\rho_c M_c / M_o) (D_o / d)$
 m, n - general indices, for Re and Pr numbers
 M_c - molecular weight of carbon
 M_o - molecular weight of oxygen
 Nu - Nusselt number for mass transfer
 p_o - oxygen partial pressure, main stream value
 p_s - oxygen partial pressure, solid surface value
 P - total pressure (1 atmos.)
 Pr - Prandtl number
 Re - Reynolds number
 R_s - specific reaction rate - g/sq.cm.sec.
 S_o - diffusional resistance = $l/k_o p_o$
 S_1 - adsorption resistance = $l/k_1 p_o$
 S_2 - desorption resistance = l/k_2
 T - temperature (absolute)
 T_o - s.t.
 V_o - s.t.p. gas velocity
 ρ_o - s.t.p. density
 η - orientation or steric factor in adsorption
 μ - gas viscosity

7. REFERENCES

1. Tu, C.M.; Davis, H.; and Hottel, H.C. *Ind. Eng. Chem.* 26, (1934) 749.
2. Essenhigh, R.H. *Sheffield Univ. Fuel Soc. J.* 6 (1955) 15.
3. Essenhigh, R.H. and Perry, M.G. *Introductory Survey "Combustion and Gasification"*, Proc. Conf. "Science in the Use of Coal", Sheffield, 1958, p. D1: Institute of Fuel, London, 1958.
4. Walker, P.L., Rusinko, F. and Austin, L.G. *Advances in Catalysis*, Vol. II, pp. 134-221, Academic Press Inc., New York 1959.
5. Thring, M.W. and Essenhigh, R.H. "Chemistry of Coal Utilization": Supplementary Volume ch. 17, pp. 754-772, Wiley; New York, 1963.
6. Brunauer, S. "Adsorption of Gases and Vapors", p. 10, Oxford University Press, 1945.
7. Fischbeck, K.Z. *Electrochem* 39 (1933) 316; 40 (1934) 517.
8. Hottel, H.C. and Stewart, I.M. *Ind. Eng. Chem.* 32 (1940) 719.
9. Beer, J.M. and Thring, M.W. 1960 Anthracite Conference Proceedings: M. I. Experiment Station Bulletin No. 75 (Sept. 1961) p. 25 Pennsylvania State University.
10. Lee, K.B., Thring, M.W. and Beer, J.M. *Combustion and Flame* 6, (1962) 137.
11. Godsave, G.A.E. *Nat. Gas Turbine Estab. Report No. R.126* (1952).
12. Spalding, B.B. *Proc. Inst. Mech. Engrs. (Lond)* 168 (1954) 545.
13. Noyes, A. and Whitney, K. *Z. phys. Chem.* 23 (1897) 639.
14. Nusselt, W. *V.D.I.* 63 (1924) 124.
15. Essenhigh, R.H. and Thring, M.W. *Inst. Fuel Conference "Science in the Use of Coal"*, Sheffield, April 1958, Paper 28, p. D21. *Inst. Fuel (London)* 1958.
16. Essenhigh, R.H. *J. Engrg. for Power*, 85 (1963) 183.
17. Beeston, G. and Essenhigh, R.H. *J. Phys. Chem.* 67 (1963) 1349.

18. Sherwood, T.K. and Pigford, R.L. "Adsorption and Extraction", p.2, New York 1952.
19. International Critical Tables 5 (1929) 62.
20. Grober, H. and Erk, S. "Fundamentals of Heat Transfer", pp. 282, 283, 4.2, 3rd ed. (trans.) McGraw Hill 1961.
21. Frank-Kamenetskii, D.A. "Diffusion and Heat Exchange in Chemical Kinetics" Ch I and II: Princeton Univ. Press (Trans.) 1955
22. Ranz, W.E. and Marshall, W.R. Chem. Eng. Prog. 48 (1952) 403.
23. Predvoditelev, A.S., Khitrin, L.N., Tsukhanova, D.A., Colodtsev, H.L. and Grodzovski, M.K. Gorenio Ugleroda (1949), Izdatelstvo AN SSSR.
24. Golovina, E.S. and Khanstovich, G.P. 8th International Combustion Symposium (1960) Paper 84, p. 784, Williams and Wilkins Co., Baltimore 1962.
25. Graham, J.A., Brown, A.R.G., Hall, A.R. and Watt, W. Conf. on Ind. Carbon and Graphite, Soc. Chem. Ind. (Sept.) 1957.
26. Day, R.J. Ph.D. Thesis, The Pennsylvania State University, 1949.
27. Essenhigh, R.H. and Fells, I. Faraday Soc. Discussions "The Physical Chemistry of Aerosols" (Bristol 1960), p. 208, Faraday Soc. 1961.
28. Gadsby, J., Long, F.J., Sleightholm, P. and Sykes, K.W. Proc. Roy. Soc. A193 (1948) 357.
29. Gadsby, J., Hin shelwood, C.N. and Sykes, K.W. Proc. Roy. Soc. A187 (1946) 129.
30. Blyholder, G.D. and Eyring, H. U.S. Air Force: Office of Scientific Research Report (Technical Note) O.A. NoXX August 1956.
31. Trapnell, B.M.W. "Chemisorption", pp. 70,71, Butterworths Scientific Publications (London) 1955.
32. Barrer, R.M. J. Chem. Soc. (1936) 1261.
33. Parker, A.S. and Hottel, H.C. Ind. Eng. Chem. 28 (1936) 1334 - Analysis by D.A. Frank-Kamenetskii, (ref. 62 to 64).
34. Arthur, J.R. and Bleach, J.A. Ind. Eng. Chem. 44 (1952) 1028.
35. Barrer, R.M. and Rideal, E.K. Proc. Roy Soc. A149 (1935) 231, 253.
36. Wicke, E. 5th International Symposium on Combustion 1955, paper 17, p. 245 (Reinhold Pub. Corp. 1956).
37. Sherman, A. and Eying, H. J. Am. Chem. Soc. 54 (1932) 2661.
38. Laine, N.R., Vastola, F.J. and Walker, P.L. J. Phys. Chem. 67 (1963) 2030.
39. Gulbransen, E.A. and Andrew, K.F. Ind. Eng. Chem. 44 (1952) 1034, 1039, 1048.
40. Bannerjee, S. and Sarjant, R.J. Fuel 30 (1951) 130.
41. Beer, J. M. and Essenhigh, R.H. Nature (London) 187 (1960) 1106.
42. Essenhigh, R.H. J. Inst. Fuel, 34 (1961) 239.
43. Smith, D.F. and Gudmundsen, A. Ind. Eng. Chem. 23 (1931) 277.

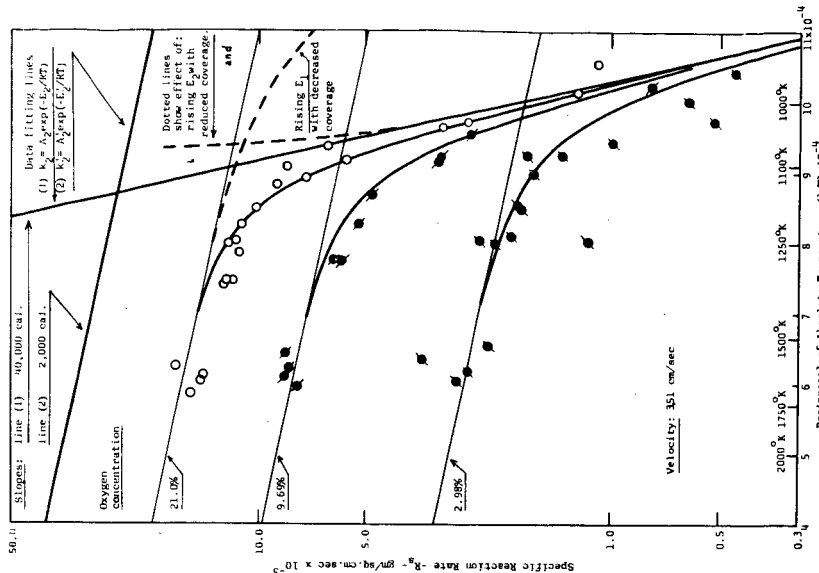


Figure 2 - Fitting Plot. Curves drawn according to equation: $1/R_p = (1/k_p) + (1/a_2) \cdot \ln(1 - \theta)$. Data from Tu, Davis, and Hottel (1)

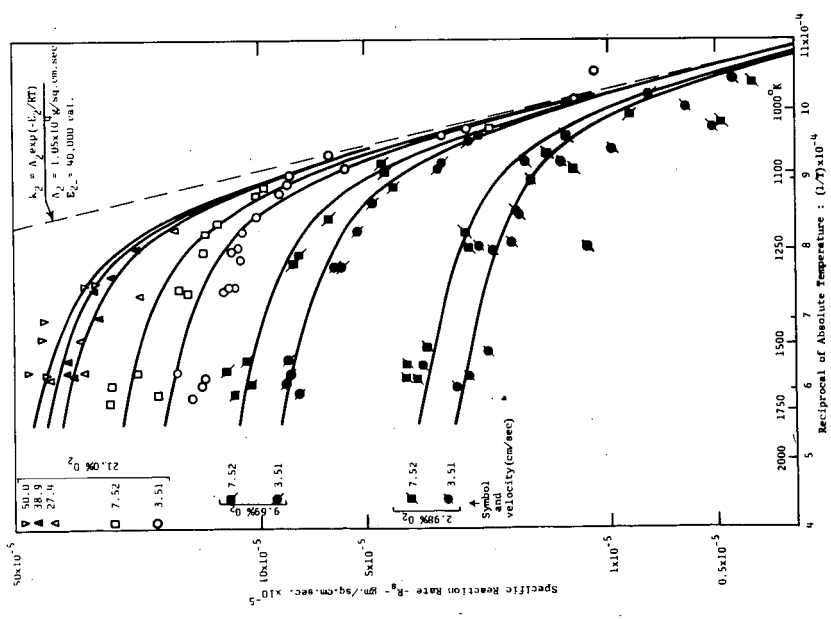


Figure 1 - Data Plot - Original data from Tu, Davis, and Hottel (1) Arrhenius plot, showing agreement with calculated curves (full lines) according to equation (9) (see text) of: Specific reaction rate (R_p) against reciprocal of temperature ($1/T$).

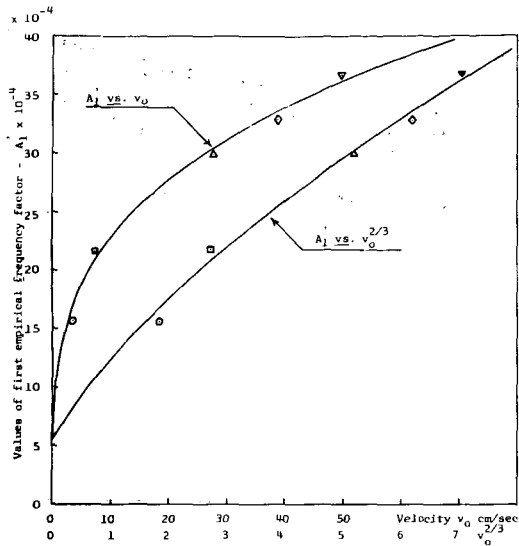


Figure 4 - Plot of first empirical frequency factor (A_1) against:
 (1) Velocity (v_0); (2) Square-root velocity ($v_0^{2/3}$)
 Data: Derived from Tu, Davis, and Hottel⁽¹⁾

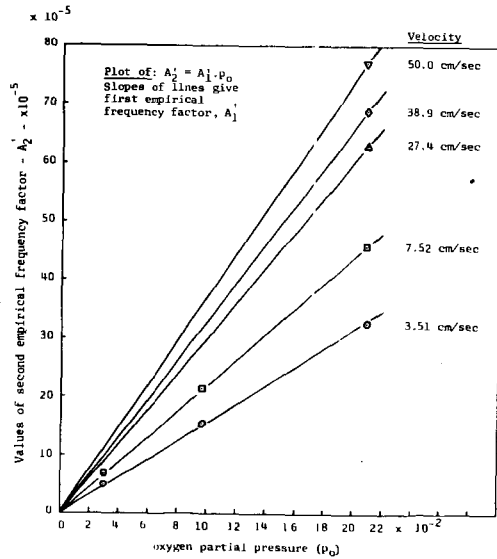


Figure 3 - Plot of second empirical frequency factor (A_2) against oxygen partial pressure (p_{O_2}), to show linear relationship - for two lower velocities. Three higher velocities (27.4, 38.9, and 50.0) added for comparison.
 Data: Derived from Tu, Davis, and Hottel⁽¹⁾

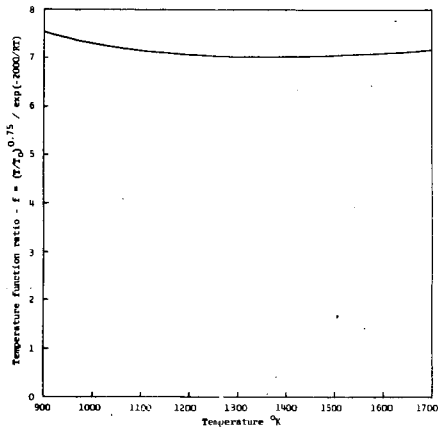


Figure 5 - Plot of temperature function ratio (f) against temperature (T) to show the consistency of ' f ' with ' T '.

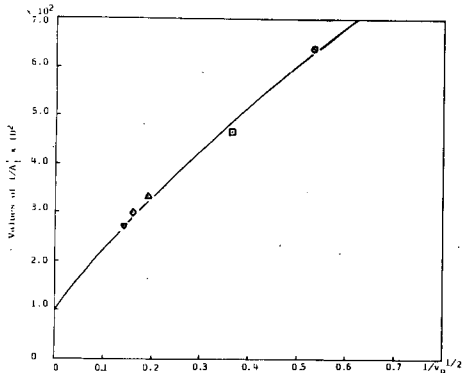


Figure 6 - Plot of reciprocal of first empirical frequency factor ($1/A_1$) against reciprocal of square-root of velocity ($1/V_0^{1/2}$)

Data: Derived from Tu, Davis, and Hottel (1)

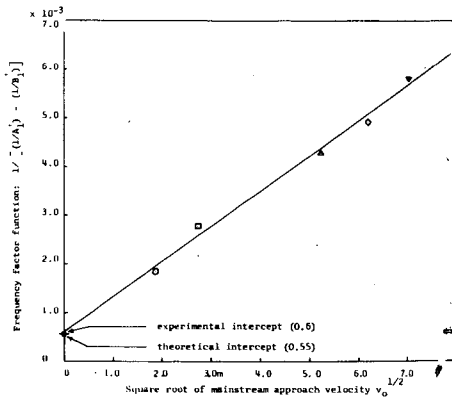


Figure 7 - Test of eq. (19c). Plot of frequency factor function against square root of velocity ($V_0^{1/2}$)

Data: Derived from Tu, Davis, and Hottel

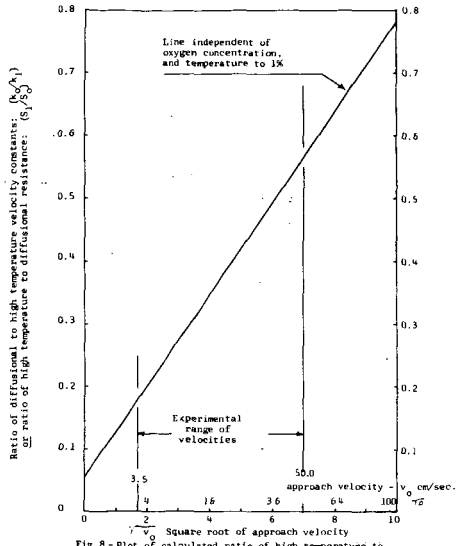


Fig. 8 - Plot of calculated ratio of high temperature to diffusional resistance $(S_1/S_2)^{1/2}$ against velocity $(v_0$ and $v_0^{1/2})$

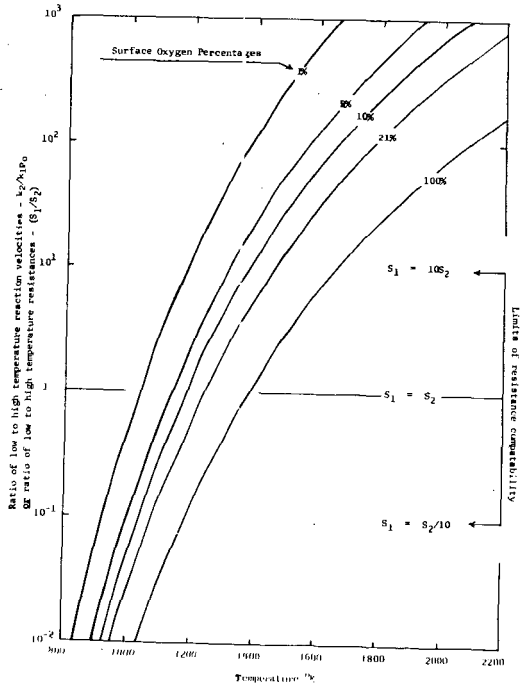


Figure 9 - Plot of calculated ratio of high to low temperature resistances (S_1/S_2) as a function of temperature, for 5 levels of oxygen concentration.

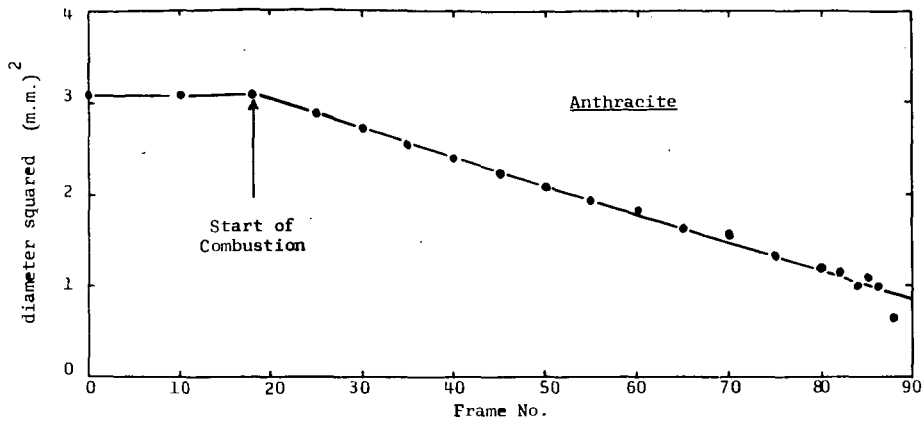


Figure 1 - Variation of diameter squared with time of burning anthracite particle (Stanlyd)

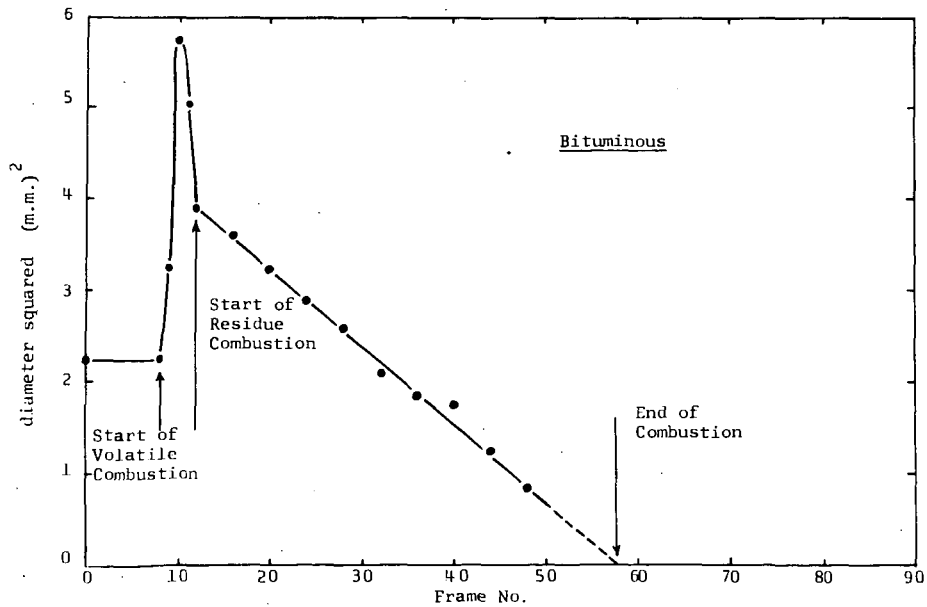


Figure 2 - Variation of diameter-squared with time of burning bituminous coal particle (Cowpen)